Influence of soil bulk density and matric potential on relative gas diffusivity and urea/nitrate-derived N_2O and N_2 losses.

A thesis

submitted in partial fulfilment

of the requirements for the Degree of

Doctor of Philosophy

at

Lincoln University

by

Nimlesh Balaine

Lincoln University

2012

Abstract of a thesis submitted in partial fulfilment of the requirements for the Degree of Doctor of Philosophy.

Influence of soil bulk density and matric potential on relative gas diffusivity and urea/nitrate-derived N_2O and N_2 losses.

by

Nimlesh Balaine

Soil compaction is a common problem, particularly when forages are grazed in winter. High animal stocking rates result in increased soil bulk density (ρ_b), increases in water-filled pore space (WFPS) and reduced gas diffusion into and out of the soil. These changes in soil physical properties increase the potential for N_2O emissions via denitrification from soil due to enhanced anaerobic conditions, especially in the presence of suitable substrates.

Nitrous oxide (N_2O) is a greenhouse gas whose production in soils is mediated by nitrifying and denitrifying organisms. It is also a significant precursor to compounds involved in the destruction of the stratospheric ozone. Agricultural practices, particularly ruminant urine deposited onto grazed pasture soils, are a significant source of agricultural N_2O emissions and under suitable conditions N_2O is completely denitrified to harmless dinitrogen (N_2) gas. This present study examined the fundamental effects of soil ρ_b on gas diffusivity and subsequent urea/nitrate derived N_2O and N_2 fluxes. The study also assessed which variables e.g. relative gas diffusivity (*Dp*/*Do*) or WFPS could be used as a suitable predictor of N_2O emissions.

The first laboratory experiment (Chapter 4) examined the effect of increasing soil ρ_b on urea-derived N_2O-N and N_2-N fluxes at a constant matric potential (ψ) of -10 kPa. *Dp*/*Do* decreased while WFPS increased with an increase in soil ρ_b. Mean cumulative N_2O-N and N_2-N fluxes after 35 days, as a percentage of applied N, ranged from 0.05 to 2.14% and 0.06 to 4.97%, respectively. There was a threshold *Dp*/*Do* value of 0.038 below which cumulative N_2-N fluxes increased significantly. Cumulative N_2-N: N_2O-N ratios were higher at soil ρ_b values of 1.3 and 1.4 Mg m^{-3}. Both *Dp*/*Do* and WFPS explained urea-derived cumulative N_2O-N and N_2-N fluxes equally well.

In Chapter 5, two laboratory experiments were performed using the same ρ_b levels as in chapter 4 but at different ψ levels, -6.0 kPa and -0.2 kPa, to provide wetter soil conditions. At both ψ levels (-0.2 and -6.0 kPa), soil N transformations, soil pH and DOC concentrations showed comparable trends to those observed in chapter 4 demonstrating that denitrification occurred in the soil. At -0.2 kPa, cumulative N_2-N fluxes were 20 to 25 times greater than the cumulative N_2O-N fluxes at all soil ρ_b treatments.

In Chapter 5, the maximum cumulative N_2O-N flux measured as a % of applied N was 16%, at -6.0 kPa at 1.3 Mg m^{-3} treatment and these N_2O-N fluxes decreased with further increases in soil ρ_b. Again both, *Dp*/*Do* and WFPS were equally good in explaining urea-derived cumulative N_2O-N and N_2-N fluxes. It was also demonstrated in this chapter that soil ρ_b has the potential to change the soil's pore size distribution. As soil ρ_b increased, macroporosity (% of total soil volume) decreased by 23% while soil mesoporosity and microporosity increased by 6 and 2%, respectively.

In Chapter 6, data from the previous experiments (Chapters 4 and 5) was compiled to assess the overall impact of increasing soil ρ_b on urea-derived cumulative N_2O-N and N_2-N fluxes at different levels of ψ. The maximum cumulative N_2O-N flux occurred at an intermediate ψ level (-6.0 kPa). *Dp*/*Do* showed better relationships than WFPS when these independent variables were plotted against cumulative N_2O-N and N_2-N fluxes and cumulative N_2-N: N_2O-N ratios.

In Chapter 7, a controlled experiment was performed where NO_3^- derived N_2O-N fluxes were measured at varying ρ_b and ψ levels. This experiment showed that N_2O-N fluxes peaked at a *Dp*/*Do* value that corresponded to the air entry value (ψ_a). This *Dp*/*Do* value, in the range of 0.006-0.0067, was where maximum N_2O-N fluxes occurred, regardless of changes in soil ρ_b. This critical value of *Dp*/*Do* was very similar to the *Dp*/*Do* value observed in chapter 6 where urea-derived cumulative N_2O-N fluxes peaked. At values of $\psi > \psi_a$, N_2O-N was either entrapped in the soil or was reduced to N_2, while at values of $\psi < \psi_a$, N_2O-N fluxes decreased, probably due to soil conditions becoming more aerobic. Soil entrapped N_2O concentrations measured in this experiment also support this finding since higher concentrations were measured at higher ψ levels. An equation was developed using data from this study to predict *Dp*/*Do*. It was better at predicting *Dp*/*Do* when compared to three other predictive *Dp*/*Do* models available in the literature. However, it requires further independent data sets for validation.

In summary

- At -10 kPa (field capacity) the soil conditions were not very conducive for N_2O production while at -0.2 kPa (saturated), soil conditions favoured complete denitrification resulting in more N_2-N than N_2O-N.

- At -6.0 kPa, the soil conditions were suited to N_2O production particularly at 1.3 Mg m^{-3} resulting in greater urea-derived cumulative N_2O-N fluxes.

- Even though, both *Dp*/*Do* and WFPS, were equally good in explaining variations in urea-derived cumulative N_2O-N and N_2-N fluxes at constant ψ levels (-10 and -6.0 kPa), it was *Dp*/*Do* that showed a better relationship with these fluxes when the data was combined across varying levels of soil ρ_b (Chapter 6).

- This study demonstrated, for the first time, the importance of ψ_a in determining the maximum N_2O-N flux via denitrification and showed that *Dp*/*Do* was better than WFPS in predicting this maximum flux when either soil ρ_b or ψ were varied.

- In terms of assessing the impacts of forage grazing on N_2O emissions from urine affected soils, emphasis needs to be placed on understanding changes in soil ρ_b and ψ with respect to their effects on *Dp*/*Do*.

Keywords: nitrous oxide, dinitrogen, ruminant urine, soil bulk density, soil matric potential, relative gas diffusivity, water-filled pore space , pore size distribution, air entry value

Acknowledgements

I extend my sincere thanks to my main supervisor, Professor Tim Clough, who provided me with the opportunity to learn and work under his excellent supervision. His encouragement, constructive advice and prompt feedback have helped me a lot during my research. It's difficult to express in words my gratitude towards him, for without his patience, support and continual motivation, this thesis would never have been possible.

I am deeply thankful to my other supervisors from Plant and Food, Dr Mike Beare and Dr Steve Thomas, for their helpful guidance and also for providing the stipend and funding to conduct this research.

I owe special thanks to Associate Professor Rob Sherlock for his helpful guidance and critiquing of my writing. I must also thank Associate Professor Graeme Buchan for his constructive guidance and discussions regarding soil physics.

Special thanks to Professor Keith Cameron, Professor Hong Di and Associate Professor Peter Almond for giving me further opportunities to work and learn new skills, which also helped me to earn some extra money. I am grateful to Dr Barbara Brown for patiently proof-reading my chapters and providing useful feedback. Special thanks to Neil Smith for helping me setup my experiments and for teaching me some of the necessary skills of plumbing. I really enjoyed talking to him, especially about different cultures and food. Many thanks to Roger McLenaghan, Janet Bertram and Alan Wise for allowing me work as demonstrator in their labs.

I would like to express my thanks to the whole Analytical Services team especially Manjula Premaratne, Roger Cresswell, and Qian Liang for carrying out large numbers of analyses for me, and to Leanne Hassall and Lynne Clucas for providing me with the necessary laboratory equipment. Thanks to Erin Lawrence (Plant and Food, Lincoln) for assisting me in soil sampling and collection. I am thankful to Kathryn Stillwell and Chris Dunlop, from Plant and Food, Lincoln, for analysing my samples. I would also like to express my thanks to Esther Meenken, Dr James Ross and Richard Sedcole for their assistance in statistical analysis.

Special thanks to Amal Torky who has always been there to support me. Her friendly smile and positive attitude are commendable. I have always enjoyed her company especially when out for a coffee. Many thanks to Brenda Lord for her help with formatting.

This journey was delightful due to the company of my fellow postgrads, Naomi Wells, Arezoo Taghizadeh Toosi, Fiona Shanhun, Diana Selbie, Janet Bertram, Andre Eger, Jack lee, Ivan Chirino Valle, Shabana Khan, Kelly Hamonts, Yoshi Uchida, Pranoy Pal, Brendon Malcolm and Dharini Paramschivam.

I am deeply indebted to my parents and grateful especially to my mother. She is my pillar of strength and courage. I am also very thankful to my sisters, brothers and brother in-law for their unconditional love and affection. Finally, I am grateful to God for giving me the understanding and patience to overcome obstacles and move ahead in life.

Nimlesh

October 2012

Table of Contents

Abstract ii

Acknowledgements v

Table of Contents vii

List of Tables x

List of Figures xii

List of Abbreviations xvii

Chapter 1 Introduction 1

1.1 Background 1

1.2 Research Objectives 2

1.3 Thesis structure 2

Chapter 2 Literature Review 4

2.1 Introduction 4

2.2 Global significance of N_2O and N_2 4

2.3 Ruminant urine derived N_2O and N_2 emissions 5

2.4 Mechanisms of nitrous oxide and dinitrogen production 6

2.4.1 Nitrification 7

2.4.2 Biological denitrification 9

2.4.3 Coupled nitrification-denitrification 10

2.4.4 Nitrifier-denitrification 10

2.4.5 Chemodenitrification 11

2.5 Factors affecting N_2O and N_2 production pathways in soil 12

2.5.1 Substrate N availability and concentration 12

2.5.2 Soil pH 12

2.5.3 Carbon supply 13

2.5.4 Soil physical conditions 14

2.6 Soil compaction and N_2O, N_2 emissions 14

2.6.1 Soil bulk density 15

2.6.2 Soil moisture 16

2.6.3 Soil relative gas diffusivity (*Dp*/*Do*) 22

2.7 Summary 27

Chapter 3 Materials and Methods 28

3.1 Determination of the soil gas diffusion coefficient (*Dp*) 28

3.1.1 Theory 28

3.1.2 Apparatus for determination of soil gas diffusion coefficient (*Dp*) 30

3.1.3 Description and calibration of O_2 sensors 33

3.1.4 Procedure for relative gas diffusivity (*Dp*/*Do*) determination 35

3.2 Soil core preparation 37

3.3 Head space gas sampling and analysis 38

3.3.1 Determination of N_2O by gas chromatography 38

3.4 Soil measurements 40

3.4.1 Soil pH 40

3.4.2 Gravimetric and volumetric soil moisture content and WFPS....40
3.4.3 Total porosity, Air-filled porosity and Pore continuity....41
3.4.4 Inorganic Nitrogen....41
3.4.5 Dissolved organic carbon (DOC)....42
3.5 Water retention curves and pore size distribution....42

Chapter 4 Effect of soil bulk density on relative gas diffusivity and urea-derived N_2O and N_2 fluxes measured under a constant matric potential....44
4.1 Introduction....44
4.2 Materials and Methods....45
4.2.1 Soil and treatments....45
4.2.2 Gas flux sampling and analyses....47
4.3 Statistical analysis....48
4.4 Results....49
4.4.1 Soil physical and chemical properties (first set of cores)....49
4.4.2 Second set of cores....50
4.5 Discussion....64
4.5.1 Substrate supply for N_2O and N_2 production....64
4.5.2 Gas diffusion, N_2O, N_2 emissions and N_2-N: N_2O-N ratios....65
4.6 Conclusions....67

Chapter 5 Effect of soil bulk density on relative gas diffusivity and urea-derived N_2O and N_2 fluxes measured under increased matric potential levels....68
5.1 Introduction....68
5.2 Materials and Methods....69
5.2.1 Experimental design....69
5.2.2 Gas flux sampling and analyses....70
5.2.3 Soil analysis....70
5.2.4 Statistical analyses....71
5.3 Results....71
5.3.1 Results from experiment 2a (-6.0 kPa)....71
5.3.2 Results from experiment 2b (-0.2 kPa)....88
5.3.3 Results from experiment 2c....102
5.4 Discussion....105
5.4.1 Soil surface pH, DOC, Inorganic N....105
5.4.2 N_2O-N, N_2-N fluxes and N_2-N:N_2O-N ratios....106
5.4.3 Soil relative gas diffusivity (*Dp*/*Do*), WFPS and cumulative N_2-N, N_2O-N fluxes....108
5.4.4 Effect of compaction on water retention curves and pore size distribution....109
5.5 Conclusions....109

Chapter 6 Synthesis of the data from previous chapters....110
6.1 Introduction....110
6.2 Results and Discussion....110

Chapter 7 Effect of soil bulk density and matric potential on relative gas diffusivity and nitrate-derived N_2O fluxes....116
7.1 Introduction....116
7.2 Hypotheses....117
7.3 Materials and Methods....117

7.3.1 Experimental approach adopted at each ψ 119
7.3.2 Gas sampling and analyses 120
7.3.3 Soil analyses 120
7.3.4 Entrapped N_2O in soil 120
7.3.5 Statistical analyses 122
7.4 Results 124
7.4.1 Results from the preliminary tests 124
7.4.2 Results from experiment 3 126
7.5 Discussion 169
7.5.1 Requirement for non-limiting substrates 169
7.5.2 Soil chemical characteristics 169
7.5.3 Soil physical characteristics 170
7.5.4 Relationship of N_2O-N fluxes with ψ, WFPS and *Dp*/*Do* 172
7.5.5 Entrapped N_2O in soil 175
7.5.6 N_2O-N fluxes after further substrate addition 175
7.5.7 *Dp*/*Do* predictive equation and comparisons with other predictive models 176
7.6 Conclusions 176

Chapter 8 Summary and Conclusions 178
8.1 Introduction 178
8.2 Why N_2O emissions and relative gas diffusivity? 178
8.3 Summary and conclusions 179
8.4 Recommendations for future research 182

Appendix A Results from -N soil cores (controls) 184
References 188

List of Tables

Table 2.1 Commonly used units for reporting soil ψ. 18
Table 2.2 Pore size terminology and pore size at equivalent matric potential (Luxmoore, 1981) ... 22
Table 4.1 Mean volumetric water content, Total porosity and WFPS of the compacted cores at -10 kPa, n = 4. Standard deviations are in brackets. 49
Table 4.2 Soil inorganic N and dissolved organic carbon (DOC) of the compacted cores at -10 kPa, n = 4. Standard deviations are in brackets. 49
Table 4.3 Mean soil physical characteristics of soil cores maintained at -10 kPa measured on day 1, n = 4. Standard deviations are in brackets. 50
Table 4.4 Mean soil physical characteristics of soil cores maintained at -10 kPa measured on day 35, n = 4. Standard deviations are in brackets. 51
Table 4.5 Effect of soil bulk density (ρ_b) on relative gas diffusivity (Dp/Do), ammonium (NH_4^+) depletion rates and nitrate (NO_3^-) accumulation rates. Standard deviations in brackets, n = 4. Values in a column that do not share a common letter are significantly different ($p < 0.05$, Tukey's test). 54
Table 5.1 Soil physical characteristics at -6.0 kPa. Values are the mean of 4 replicates with standard deviations in brackets. Values in rows that do not share a common letter are significantly different ($p < 0.05$, Tukey's test). 72
Table 5.2 Net rates of change in the soil NH_4^+-N and NO_3^--N concentrations in urea-treated cores (μg g^{-1}soil d^{-1}) affected by soil ρ_b at -6.0 kPa. Negative rates indicate decreasing concentrations. (n = 4). 77
Table 5.3 Pearson correlation between measured variables and N_2O-N and N_2-N fluxes at -6.0 kPa on day 1. Numerals in italics are p-values. 85
Table 5.4 Pearson correlation between measured variables and N_2O-N and N_2-N fluxes at -6.0 kPa on day 7. Numerals in italics are p-values. 85
Table 5.5 Pearson correlation between measured variables and N_2O-N and N_2-N fluxes at -6.0 kPa on day 14. Numerals in italics are p-values. 86
Table 5.6 Pearson correlation between measured variables and N_2O-N and N_2-N fluxes at -6.0 kPa on day 24. Numerals in italics are p-values. 86
Table 5.7 Pearson correlation between measured variables and N_2O-N and N_2-N fluxes at -6.0 kPa on day 35. Numerals in italics are p-values. 87
Table 5.8 Soil physical characteristics at -0.2 kPa. Values are the mean of 4 replicates with standard deviation in brackets. Values that do not share a common letter are significantly different ($p < 0.05$, Tukey's test). 88
Table 5.9 Net rates of change in the soil NH_4^+-N and NO_3^--N concentrations in urea treated cores (μg g^{-1}soil d^{-1}) affected by soil ρ_b at -0.2 kPa. Negative rates indicate decreasing concentrations (n = 4). 93
Table 5.10 Pearson correlation between measured variables and N_2O-N and N_2-N fluxes at -0.2 kPa on day 1. Numerals in italics are p-values. 99
Table 5.11 Pearson correlation between measured variables and N_2O-N and N_2-N fluxes at -0.2 kPa on day 7. Numerals in italics are p-values. 99
Table 5.12 Pearson correlation between measured variables and N_2O-N and N_2-N fluxes at -0.2 kPa on day 14. Numerals in italics are p-values. 100
Table 5.13 Pearson correlation between measured variables and N_2O-N and N_2-N fluxes at -0.2 kPa on day 24. Numerals in italics are p-values. 100
Table 5.14 Pearson correlation between measured variables and N_2O-N and N_2-N fluxes at -0.2 kPa on day 35. Numerals in italics are p-values. 101
Table 5.15 Total porosity of soil cores and % of total soil volume occupied by each given pore size. Note the sum of macroporosity, mesoporosity and microporosity equals total porosity. Values are means of four replicates. Standard deviations are in brackets. Values in a row that do not share a common letter are significantly different ($p < 0.01$, Tukey's test). 104

Table 7.1 Soil NO_3^--N concentrations at -1.0 kPa under varying soil ρ_b after saturation with NO_3^- solution and subsequent equilibration on tension tables. Values are means of 4 replicates with standard deviations in brackets. 124
Table 7.2 Soil DOC concentrations at -1.0 kPa under varying soil ρ_b after saturation with NO_3^- solution and subsequent equilibration on tension tables. Values are means of 4 replicates with standard deviations in brackets. 124
Table 7.3 Soil NO_3^--N concentrations at -10 kPa under varying soil ρ_b after saturation with NO_3^- solution and subsequent equilibration on tension tables. Values are means of 4 replicates with standard deviations in brackets. 125
Table 7.4 Soil DOC concentrations at -10 kPa under varying soil ρ_b after saturation with NO_3^- solution and subsequent equilibration on tension tables. Values are means of 4 replicates with standard deviations in brackets. 125
Table 7.5 Effect of soil ρ_b on the relationship between relative gas diffusivity (Dp/Do) and air-filled porosity (ε) measured at varying ψ. Equations are derived from fitting two parameter power functions ($Dp/Do = A(\varepsilon)^X$) to the data (Fig. 7.5) and the degree of variation and significances are shown as r^2 and p, respectively. 131
Table 7.6 Effect of matric potential (ψ) on the relationship between relative gas diffusivity (Dp/Do) and air-filled porosity (ε) measured under over a range of soil ρ_b. Equations are derived from fitting two parameter power functions ($Dp/Do = A'(\varepsilon)^{X'}$) to the data (Fig. 7.8) and the degree of variation and significances are shown as r^2 and p, respectively. 135
Table 7.7 Linear function fitted to the plots of mean DOC concentrations on y axis and mean NO_3^--N concentrations on x axis for each soil ρ_b treatment (Fig. 7.19). 147
Table 7.8 Means and standard deviation (in brackets) of variables measured when N_2O peaked (N_2Omax). Values in rows that do not share a common letter are significantly different ($p < 0.05$, Tukey's test). 153
Table 7.9 Soil water retention parameters (WRC) and ψ_{N2Omax} for different soil ρ_b treatments using the Campbell soil-water retention function (section 2.6.2) and a three parameter Gaussian function (section 7.3.5), respectively. Values represent individual replicates. 156
Table 7.10 The values are ^{15}N atom % enrichment of N_2O-N. Values are the averages of 4 replicates and standard deviations are in brackets. 163
Table 7.11 Mean values of Dp/Do_{N2Omax} (Dp/Do where N_2O-N flux was at maximum) measured and obtained by fitting a density-corrected model (Chamindu Deepagoda et al., 2011b) and the equation from this study. Standard deviations are in brackets. 168

List of Figures

Figure 2.1 Transformations of mineral nitrogen in soil. Adapted from Wrage et al. (2001) 8
Figure 2.2 Typical soil retention curve where matric potential on the X axis is depicted as suction expressed in positive values (Miller et al., 2002). 19
Figure 3.1 An example of boundary conditions when a soil core is placed above a diffusion chamber (Rolston and Moldrup, 2002) 30
Figure 3.2 Diffusion apparatus diagram (Rolston 1986).....31
Figure 3.3 (a) A diffusion chamber being made O_2 free (b) horizontal slide shifted to allow O_2 diffusion from atmosphere through the soil core into the chamber. Diffusion apparatus shown above is a modification of the apparatus used by Rolston (1986). 32
Figure 3.4 KE-25 O_2 sensors.....33
Figure 3.5 Calibration curve for KE-25 O_2 sensor. 34
Figure 3.6 The experimental set up comprising a diffusion chamber, datalogger and a computer for monitoring.....35
Figure 3.7 Example of ln (Cr) vs. time graph plotted for the diffusion coefficient measurements....36
Figure 4.1 Mean soil inorganic-N concentrations over time after urea application. Error bars = s.e.m, n = 4.....53
Figure 4.2 Mean surface soil pH over time after urea application. Error bars = s.e.m, n = 4.....55
Figure 4.3 Mean concentrations of dissolved organic carbon (DOC) over time after urea application. Error bars = s.e.m, n = 4. 56
Figure 4.4 Photographs of soil core increments showing penetration of Brilliant Blue dye at different soil bulk density (Mg m^{-3}) levels. 57
Figure 4.5 (a) Nitrous oxide emissions from different soil ρ_b treatments following urea application (b) Cumulative loss of N_2O from urea-treated soils, showing the amount of N emitted as N_2O-N as a percentage of the total N applied to the soil cores. Error bars = s.e.m, n = 4. 58
Figure 4.6 Mean ^{15}N atom % enrichment of N_2O-N. Error bars = s.e.m, n = 4. 59
Figure 4.7 (a) Mean N_2-N fluxes over days following urea application (b) Cumulative loss of N_2 from urea-treated soils, showing the amount of N emitted as N_2-N as a percentage of the total N applied to the cores. Error bars = s.e.m, n = 4. 60
Figure 4.8 Mean N_2-N: N_2O-N ratios over time. Error bars = s.e.m, n = 4. 61
Figure 4.9 Cumulative N_2-N: N_2O-N ratio plotted against soil ρ_b (Mg m^{-3}). Means that do not share a lower case letter are significantly different (Tukey's test, $p < 0.05$). Error bars = s.e.m, n = 4. 61
Figure 4.10 Scattergram of (a) cumulative N_2O-N fluxes and *Dp*/*Do* (day 35) (b) cumulative N_2-N fluxes and *Dp*/*Do* (day 35). Data points represent individual replicates. Exponential (three-parameter) and piecewise linear regression fitted to cumulative N_2O-N and cumulative N_2-N flux data, respectively. The intersection of the two lines in (b) is the breakpoint or trigger point which occurs at *Dp*/*Do* = 0.038 (s.e.m 0.003). 62
Figure 4.11 Scattergram of (a) cumulative N_2O-N fluxes with WFPS (b) cumulative N_2-N fluxes with WFPS. Data points represent individual replicates. Exponential (three-parameter) and piecewise linear regression fitted to cumulative N_2O-N and N_2-N flux data, respectively.....63
Figure 5.1 Soil surface pH of control and urea-treated cores over time. Error bars are generally < size of symbols. Numerals in the legend indicate ρ_b (Mg m^{-3}) applied. Error bars = s.e.m, n = 4.....73
Figure 5.2 Urea and soil ρ_b effects on DOC concentrations. Numerals in the legend indicate ρ_b (Mg m^{-3}) applied. Error bars = s.e.m, n = 4. 74
Figure 5.3 Soil NH_4^+-N (a) NO_3^--N (b) and NO_2^--N concentrations (c) in the control and urea-treated cores at -6.0 kPa. Numerals in the legend indicate ρ_b (Mg m^{-3}) applied. Error bars = s.e.m, n = 4. 76

Figure 5.4 (a) Mean N_2O-N fluxes measured in experiment 2a (-6.0 kPa) from the different ρ_b treatments over a period of 35 days. (b) Mean cumulative N_2O-N fluxes as % of applied N in experiment 2a (-6.0 kPa). Numerals in the legend indicate ρ_b (Mg m^{-3}) applied. Error bars = s.e.m, n = 4. 79
Figure 5.5 Mean atom % ^{15}N enrichment of the N_2O-N fluxes measured in experiment 2a (-6.0 kPa) under varying ρ_b treatments over a period of 35 days. Numerals in the legend indicate ρ_b applied. Error bars = s.e.m, n = 4. 80
Figure 5.6 (a) Mean N_2-N fluxes measured in experiment 2a (-6.0 kPa) under varying ρ_b treatments over a period of 35 days. (b) Mean cumulative N_2-N fluxes as % of applied N in experiment 2a (-6.0 kPa). Error bars = s.e.m, n = 4. 81
Figure 5.7 Soil N_2-N: N_2O-N ratio over time at -6.0 kPa following urea application. Error bars = s.e.m, n = 4. 82
Figure 5.8 Cumulative N_2-N: N_2O-N ratios versus soil ρ_b at -6.0 kPa. Values that do not share a common letter are significantly different ($p < 0.05$, Tukey's test). Error bars = s.e.m, n = 4. 82
Figure 5.9 Relationships between *Dp*/*Do* and (a) cumulative N_2-N fluxes (b) cumulative N_2O-N fluxes. Data represent individual replicates. 83
Figure 5.10 Relationships between WFPS and (a) cumulative N_2-N fluxes (b) cumulative N_2O-N fluxes. Data represent individual replicates. 84
Figure 5.11 Soil surface pH measured over time in experiment 2b (-0.2 kPa). Numerals in legend indicate ρ_b (Mg m^{-3}) applied. Error bars are generally < size of the symbols. Error bars = s.e.m, n = 4. 89
Figure 5.12 Soil DOC concentrations over time in experiment 2b (-0.2 kPa). Numerals in legend indicate ρ_b (Mg m^{-3}) applied. Error bars = s.e.m, n = 4. 90
Figure 5.13 Soil NH_4^--N (a) NO_3^--N (b) and NO_2^--N concentrations (c) over time from control and urea-treated cores in experiment 2b (-0.2 kPa). Numerals in the legend indicate ρ_b (Mg m^{-3}) applied. Error bars = s.e.m, n = 4. 92
Figure 5.14 (a) Mean N_2O-N fluxes measured over time in experiment 2b (-0.2 kPa) from different ρ_b treatments over a period of 35 days. (b) Mean cumulative N_2O-N fluxes as a % of applied N in experiment 2b (-0.2 kPa). Error bars = s.e.m, n = 4. 95
Figure 5.15 Mean atom % ^{15}N enrichment of N_2O-N measured over time in experiment 2b (-0.2 kPa) under different ρ_b treatments. Error bars = s.e.m, n = 4. 96
Figure 5.16 (a) Mean N_2-N fluxes measured in experiment 2b (-0.2 kPa) from different ρ_b treatments over a period of 35 days. (b) Mean cumulative N_2-N fluxes as a % of applied N at -0.2 kPa. Error bars = s.e.m, n = 4. 97
Figure 5.17 Soil N_2-N: N_2O-N ratio versus time measured in experiment 2b (-0.2 kPa). Numerals in the legend indicate ρ_b (Mg m^{-3}) applied. Error bars = s.e.m, n = 4. 98
Figure 5.18 Cumulative N_2-N: N_2O-N ratios versus soil ρ_b at -0.2 kPa. Values that do not share a common letter are significantly different ($p < 0.05$, Tukey's test). Error bars = s.e.m, n = 4. 98
Figure 5.19 Effect of soil ρ_b on water retention curve. Numerals in the legend indicate soil ρ_b (Mg m^{-3}) applied. Error bars are standard deviations, n = 4. 102
Figure 5.20 Mean soil porosities expressed as a % of total porosity under varying ρ_b (Mg m^{-3}) treatments. 103
Figure 6.1 Relationship of cumulative N_2O-N fluxes from a soil under varying ρ_b and ψ, with (a) *Dp*/*Do* (day 35) (b) WFPS. Data points represent individual replicates. 111
Figure 6.2 Relationship of cumulative N_2-N fluxes from a soil under varying ρ_b and ψ, with (a) *Dp*/*Do* (day 35) (b) WFPS. Data points represent individual replicates. 112
Figure 6.3 Relationship of cumulative N_2-N: N_2O-N ratios from a soil under varying ρ_b and ψ, with *Dp*/*Do* measured on day 35. Data points represent individual replicates. 113
Figure 6.4 Relationship of cumulative N_2-N: N_2O-N ratios from a soil under varying ρ_b and ψ, with WFPS. Data points represent individual replicates. 113
Figure 6.5 Effect of varying matric potential (ψ) on (a) cumulative N_2O-N fluxes (b) Cumulative N_2-N fluxes from a soil under varying soil ρ_b (Mg m^{-3}). Error bars = s.e.m, n = 4. 115

Figure 7.1 Effect of soil ρ_b on the relationship between air-filled porosity (ε) and matric potential (ψ) for +N soil cores. Numerals in the legend indicate ρ_b (Mg m^{-3}) applied. Error bars = s.e.m, n = 4. 126
Figure 7.2 Effect of soil ρ_b on the relationship between WFPS and matric potential (ψ) for +N soil cores. Numerals in the legend indicate ρ_b (Mg m^{-3}) applied. Error bars = s.e.m, n = 4. 127
Figure 7.3 Effect of soil ρ_b on the relationship between relative gas diffusivity (Dp/Do) and matric potential (ψ) for +N soil cores. Numerals in the legend indicate ρ_b (Mg m^{-3}) applied. Error bars = s.e.m, n = 4. 128
Figure 7.4 Mesh plot of relative gas diffusivity (Dp/Do) versus soil bulk density (ρ_b) and matric potential (ψ) for +N treated soil cores. 129
Figure 7.5 Effect of soil ρ_b on the relationship between relative gas diffusivity (Dp/Do) and air filled porosity (ε) obtained over a range of ψ applied. Numerals in the legend indicate ρ_b (Mg m^{-3}) applied. Data points indicate individual replicates. Equations for the fitted lines are shown in Table 7.5. 130
Figure 7.6 (a) Pore connectivity parameter (A) and (b) Water blockage factor (X) as a function of soil bulk density (Mg m^{-3}). Parameters A and X were obtained by fitting a two parameter power function to the relationship between Dp/Do and air-filled porosity (ε) observed at each level of ρ_b under varying ψ levels (Fig 7.5, Table 7.3). Regression lines are the modified single exponential decay function fitted to the data points. 132
Figure 7.7 Relationship between relative gas diffusivity (Dp/Do) and relative air filled porosity. Numerals in the legend indicate ρ_b applied. Data points are individual replicates. 133
Figure 7.8 Effect of matric potential (ψ) on the relationship between relative gas diffusivity (Dp/Do) and air filled porosity (ε) when data from varying ρ_b were pooled for each level of ψ. Numerals in the legend indicate ψ applied. Data points indicate individual replicates. Equations for the fitted lines are shown in Table 7.6. 134
Figure 7.9 (a) Water blockage factor (X'), and (b) Pore connectivity parameter (A') as a function of soil bulk density, ρ_b (Mg m^{-3}). Parameters A' and X' were obtained by fitting a power function to the relationship between Dp/Do and air-filled porosity (ε) observed at each level of ρ_b under varying ψ levels. Regression lines are split-line functions fitted to the data points. 136
Figure 7.10 Relationship between relative gas diffusivity (Dp/Do) and relative air filled porosity. Numerals in the legend indicate ψ applied. Data points are individual replicates. 137
Figure 7.11 Effect of soil ρ_b (Mg m^{-3}) on the relationship between pore continuity (C) and matric potential (ψ) for +N soil cores. Numerals in the legend indicate ρ_b (Mg m^{-3}) applied. Error bars = s.e.m, n = 4. 138
Figure 7.12 Mean bulk soil pH versus matric potential (ψ) from +N soil cores. Numerals in the legend indicate ρ_b (Mg m^{-3}) treatments applied. Error bars = s.e.m, n = 3. 139
Figure 7.13 Mean NO_3^--N concentrations from +N soil cores. Numerals in the legend indicate ρ_b (Mg m^{-3}) treatments applied. Error bars = s.e.m, n = 3. 140
Figure 7.14 Effect of soil bulk density (ρ_b) on the rate of change of NO_3^--N over matric potential (ψ). The data points are the mean slopes of the linear regression performed on the plot between NO_3^--N concentrations and ψ for each ρ_b replicate. Error bars = s.e.m, n = 3. 141
Figure 7.15 Mean NH_4^+-N concentrations from + N soil cores. Numerals in the legend indicate ρ_b (Mg m^{-3}) treatments applied. Error bars = s.e.m, n = 3. 142
Figure 7.16 Mean DOC concentrations from +N soil cores. Numerals in the legend indicate ρ_b (Mg m^{-3}) treatments applied. Error bars = s.e.m, n = 3. 143
Figure 7.17 Mean soil DOC concentrations from -N soil cores. Numerals in the legend indicate ρ_b (Mg m^{-3}) treatments applied. Error bars = s.e.m, n = 3. 144
Figure 7.18 Effect of soil bulk density (Mg m^{-3}) on the rate of change of DOC over matric potential (ψ). The data points are the mean slopes of the linear regression performed on the plot between DOC concentrations and ψ for each ρ_b replicate. Error bars = s.e.m, n = 3. 145

Figure 7.19 Plot of mean DOC versus mean NO_3^--N concentrations from +N soil cores for each ρ_b treatment across all levels of ψ. Numerals in the legend indicate ρ_b (Mg m^{-3}) treatments applied. Data points are means of 3 replicates. 146
Figure 7.20 Effect of soil ρ_b on the relationship between mean N_2O-N fluxes (+N cores) and matric potential (ψ). Plotted lines are derived from a three-parameter Gaussian model fitted to the N_2O and ψ data. Numerals in the legend indicate ρ_b (Mg m^{-3}) treatments applied. Error bars = s.e.m, n = 4. 148
Figure 7.21 Effect of soil ρ_b on the relationship between mean normalised N_2O-N fluxes (+N cores) and matric potential (ψ). Numerals in the legend indicate ρ_b (Mg m^{-3}) treatments applied. Error bars = s.e.m, n = 4. 148
Figure 7.22 Mesh plot of N_2O-N fluxes versus soil ρ_b (Mg m^{-3}) and matric potential (ψ) for +N treated soil cores. 149
Figure 7.23 Relationship between measured N_2O-N flux and relative soil gas diffusivity (Dp/Do) at varying soil ρ_b. Numerals in the legend indicate ρ_b (Mg m^{-3}) treatments applied. Error bars = s.e.m, n = 4. 150
Figure 7.24 Relationship of measured N_2O-N fluxes with (a) WFPS (%) (b) Volumetric water content (m^3 m^{-3}) at varying soil ρ_b (Mg m^{-3}). Numerals in the legend indicate ρ_b (Mg m^{-3}) treatments applied. Error bars = s.e.m, n = 4. 151
Figure 7.25 Relationship between measured N_2O-N flux and air-filled porosity (m^3 m^{-3}) at varying soil ρ_b (Mg m^{-3}). Numerals in the legend indicate ρ_b (Mg m^{-3}) treatments applied. Error bars = s.e.m, n = 4. 152
Figure 7.26 Log-log plot of WRC from soil compacted to varying ρ_b. Numerals in the legend indicate ρ_b (Mg m^{-3}) treatments applied. 154
Figure 7.27 Examples of the linear regressions performed on the log- log WRC plots for an individual replicate at (a) 1.1 Mg m^{-3} and (b) 1.5 Mg m^{-3} where the Campbell water retention parameter (-b) is equal to the slope and air entry value (ψ_a) was derived from the y intercept of the straight line fitted to a log-log plot of ψ and θ/θ_s (section 2.6.2). 155
Figure 7.28 Relationship between ψ_{N2Omax} (-kPa) and air entry value (ψ_a) (-kPa). Values represent individual replicates. The ψ_{N2Omax} was obtained by fitting a three parameter Gaussian function to N_2O-N and ψ. The values of ψ_a were obtained by fitting linear regressions to the log-log plot of WRC. The red dashed line is a 1:1 line. 157
Figure 7.29 Relationships between air entry value (ψ_a) and (a) Dp/Do_{N2Omax} (b) $WFPS_{N2Omax}$ (c) Macroporosity (d) Microporosity (e) Mesoporosity (f) C_{N2Omax}. Values represent individual replicates. 158
Figure 7.30 Relationship between ψ_{N2Omax} (-kPa) and macroporosity (% of total soil volume). Values represent individual replicates. 159
Figure 7.31 Mean N_2O entrapped in soil water from +N soil cores at varying ψ. Numerals in the legend indicate ρ_b (Mg m^{-3}) treatments applied. Error bars = s.e.m, n = 3. 160
Figure 7.32 Mean soil N_2O-N fluxes from +N soil cores at varying matric potential (-kPa) measured 6 h after the addition of 1 mL NO_3^- (solution 2) and 1 mL carbon (glucose). Numerals in the legend indicate ρ_b (Mg m^{-3}) treatments applied. Error bars = s.e.m, n = 4. A two parameter exponential curve was fitted to the N_2O-N and ψ data for each ρ_b level. 161
Figure 7.33 The relationship of N_2O-N obtained after further substrate addition and (a) Relative gas diffusivity (Dp/Do) (b) Water-filled pore space (WFPS) (c) Volumetric water content (m^3 m^{-3}). Numerals in the legend indicate ρ_b (Mg m^{-3}) treatments applied. Error bars = s.e.m, n = 4. 162
Figure 7.34 Relationship between relative gas diffusivity (Dp/Do) and relative air-filled porosity. Data points are individual replicates. 164
Figure 7.35 Scatter-plot comparison of model performance (a) density corrected model (b) WLR (Penman model) when tested against Dp/Do values (n = 220) measured at varying ρ_b over a range of ψ applied. 166

Figure 7.36 Scatter-plot comparison of model performance using the modified BBC model when tested against *Dp*/*Do* values (n = 220) measured at varying ρ_b over a range of ψ applied. 167
Figure 7.37 Scatter-plot comparison of model performance using the TPM model when tested against *Dp*/*Do* values (n = 220) measured at varying ρ_b over a range of ψ applied. 167
Figure 7.38 Scatter-plot comparison of model performance using the equation developed in this study when tested against *Dp*/*Do* values (n = 220) measured at varying ρ_b over a range of ψ applied. 168

List of Abbreviations

ρ_b	Soil bulk density (Mg m^{-3})
ψ	Matric potential (-kPa)
Dp	Gas diffusion coefficient in soil (m^3 soil air m^{-1} soil s^{-1})
Do	Gas diffusion coefficient in air (m^3 soil air m^{-1} soil s^{-1})
Dp/*Do*	Relative gas diffusivity
ϕ	Total porosity (m^3 air m^{-3} soil)
ε	Air-filled porosity (m^3 air m^{-3} soil)
ε/ϕ	Relative air-filled porosity
ρ_p	Soil particle density (Mg m^{-3})
θ_g	Gravimetric water content (g water g^{-1} dry soil)
θ_v	Volumetric water content (m^3 water m^{-3} soil)
ψ_a	Air entry value (-kPa)
AOB	Ammonia oxidising bacteria
AOA	Ammonia oxidising Archeae
A, *A*'	Pore connectivity parameter
b	Campbell water retention parameter
BBC	Buckingham Burdine Campbell
DI	Deionised water
DOC	Dissolved organic carbon
GC	Gas chromatograph
N_2O	Nitrous oxide
NO_3^-	Nitrate
NO_2^-	Nitrite
NH_4^+	Ammonium
N_2	Nitrogen gas
O_2	Oxygen gas
RMSE	Root mean square error
s.e.m	Standard error of mean
TPM	Three porosity model
WFPS	Water-filled pore space
WLR	Water-induced linear reduction
WRC	Water retention curve
X, *X*'	Water blockage factor

Chapter 1
Introduction

1.1 Background

Winter grazed forage crops are an integral part of New Zealand farm systems and are often used to supplement pastures in grazed animal production systems. When these forage crops are grazed *in situ* over winter, the high stocking rate results in considerable alteration of soil physical conditions because grazing normally coincides with a period of high soil moisture content (Singleton and Addison, 1999; Drewry and Paton, 2005; Houlbrooke et al., 2009). Increases in soil bulk density, ρ_b (Mg m^{-3}) have been routinely reported during *in situ* animal treading trials (Di et al., 2001; Menneer et al., 2005a; Thomas et al., 2008; Houlbrooke et al., 2009). Grazing also results in high deposition rates of animal excreta-N in the form of urine and dung (Haynes and Williams, 1993). Soil compacted by animal treading remains wet for a relatively longer time due to reduced drainage, a consequence of the decrease in soil macropores and reduced water usage by plants (Beare et al., 2006). For example, reductions in soil macroporosity by 7-10% have been observed under cattle grazing of a winter forage crop (Drewry and Paton, 2005; Houlbrooke et al., 2009). Increases in ρ_b (Mg m^{-3}) due to animal treading also increase water-filled pore space (WFPS) and decrease gas diffusion into and out of soils (Currie, 1984; Ball and Ritchie, 1999). This reduction in gas diffusion and increase in WFPS results in compacted soils becoming more anaerobic, and may result in high N_2O emissions from soils (Ball et al., 1999b; Sitaula et al., 2000; Ball et al., 2008). Thus changes in soil physical factors under forage crop grazing together with high rates of excreta-N returns, can make conditions conducive for the production of N_2O especially under saturated soil conditions.

However, there is a dearth of detailed research focusing on N_2O emissions from soil that is both compacted and affected by ruminant excreta, particularly urine. Furthermore, there is a lack of knowledge surrounding the emissions of N_2 that result under such conditions. Thus, this thesis focuses on assessing the influence of varying bulk density on N_2O and N_2 emissions with respect to changes in matric potential (ψ), and the ensuing changes in relative gas diffusivity (Dp/Do).

Emissions of N_2O are routinely related with WFPS in soil studies. However, the use of WFPS as a predictor for N_2O emissions from soil under varying bulk densities is debatable (Farquharson and Baldock, 2008). Therefore, the data compiled is also used to assess predictors of N_2O emissions and to fill gaps in our present understanding of N transformations in soils.

1.2 Research Objectives

- To assess the effect of varying soil ρ_b on *Dp*/*Do* and urea-derived N_2O and N_2 fluxes from a silt loam soil maintained at constant matric potential of -10 kPa, and examine the relationship of these fluxes with *Dp*/*Do* and WFPS (Chapter 4).

- To assess the effect of varying soil ρ_b on *Dp*/*Do* and urea-derived N_2O and N_2 fluxes under wetter conditions (-6.0 kPa and -0.2 kPa) and examine the relationship of these fluxes with *Dp*/*Do* and WFPS (Chapter 5).

- To combine the data obtained in the Chapters 4 and 5 and analyse which scalar, *Dp*/*Do* or WFPS, better described the urea-derived N_2O and N_2 fluxes from soil under varying ρ_b (Chapter 6).

- To determine the effect of varying soil ρ_b and ψ on nitrate-derived N_2O fluxes and *Dp*/*Do* and to develop an equation for predicting *Dp*/*Do* from soils under varying compaction and moisture levels and compare *Dp*/*Do* predictive models (Chapter 7).

1.3 Thesis structure

Chapter 1 This Chapter provides the thesis outline and objectives of the research performed.

Chapter 2 A review of the literature pertaining to the mechanisms involved in the production of N_2O and N_2 and the factors affecting these emissions is made. In particular, changes in soil physical properties are examined.

Chapter 3 This Chapter describes the materials and methods used during the experiments performed in this research.

Chapter 4 In Chapter 4 the potential effect of soil ρ_b on urea-derived N_2O and N_2 fluxes is examined at a constant matric potential of -10 kPa. This data is also examined in relation to *Dp*/*Do*.

Chapter 5 The effect of varying soil ρ_b on urea-derived N_2O and N_2 fluxes and their relationships to *Dp*/*Do* is studied under two levels of ψ i.e. -6.0 and -0.2 kPa.

Chapter 6 This Chapter combines and assesses the data obtained in the previous two chapters.

Chapter 7 This Chapter examines the effect of both the soil ρ_b and ψ on the nitrate-derived N_2O fluxes and *Dp*/*Do* in the absence of substrate induced nitrification.

Chapter 8 In Chapter 8, a summary of the results from previous chapters is presented and recommendations for future research are made.

Chapter 2

Literature Review

2.1 Introduction

The purpose of this literature review is to provide an overview of the nitrogen (N) cycling pathways and the factors relating to N cycling in agricultural soils that link to nitrous oxide (N_2O) and dinitrogen (N_2) emissions, with an emphasis on how soil physical conditions affect these processes.

2.2 Global significance of N_2O and N_2

Naturally occurring N compounds can be described as non-reactive or reactive. Non-reactive N occurs as N_2 while reactive N (Nr) comprises all the inorganic oxidised (NO_3^-, NO_x, N_2O) and reduced forms of N (NH_3, NH_4^+) as well as the organic N compounds (Galloway et al., 2003). The accumulation of Nr in the environment is of concern since several forms of Nr contribute directly or indirectly to global climate change or are precursors to stratospheric ozone depletion (Galloway et al., 2003). Reducing Nr accumulation is only possible by converting Nr to non-reactive N_2.

A very significant form of Nr is nitrous oxide (N_2O) which is the third most important greenhouse gas and it is also a precursor to compounds that deplete stratospheric ozone (Crutzen, 1981; Cicerone, 1987). It is currently the single most important ozone depleting emission and is expected to dominate throughout the 21st century (Ravishankara et al., 2009). It has a global warming potential (GWP) 298 times than that of carbon dioxide (CO_2) over a period of 100 yrs. and its concentration is increasing in the troposphere at rate of 0.26% yr^{-1} (Forster et al., 2007). The lifetime of N_2O in the stratosphere is 100 to 150 yr. (Galbally and Roy, 1983).

$$N_2O + h\nu \longrightarrow N_2 + O \quad \text{(for wavelengths < 260 nm)} \quad [2.1]$$

$$N_2O + O(^1D) \longrightarrow N_2 + O_2 \quad [2.2]$$

$$\longrightarrow 2NO$$

The only processes that remove N_2O from Earth's atmosphere are two photochemically initiated reactions (equations 2.1 and 2.2) in the stratosphere (Galbally and Roy, 1983) where O (^1D) is an electronically excited state of atomic oxygen. Subsequently, NO formed in equation 2.2 catalyses the destruction of ozone in the stratosphere (Crutzen, 1981).

2.3 Ruminant urine derived N_2O and N_2 emissions

Globally, agricultural soils are a major (over 40 %) source of anthropogenic N_2O emissions (Denman et al., 2007) and the ruminant grazing-derived N_2O emissions range from 0.2-9.9% of excreted N (Oenema et al., 1997). In grazed soils, one of the major sources of N substrate for N_2O production is ruminant excreted urine-N (Yamulki et al., 1998; Oenema et al., 2005; Clough et al., 2009). The N deposition rate in a urine patch usually ranges from 20-80 g m^{-2} (Oenema et al., 1997). Urine is randomly deposited onto pasture in 'patches' and the area under each patch is related to animal type and may range from 0.16 to 0.49 m^2 (Haynes and Williams, 1993). The rate of N deposited in a urine patch may be as high as 1000 kg N ha^{-1}, (Haynes and Williams, 1993). Typically over 70% of the nitrogen (N) in urine is present as urea (Doak, 1952; Haynes and Williams, 1993). Urea deposited on the soil surface undergoes rapid hydrolysis, catalysed by the enzyme urease which results in the formation of ammonium (NH_4^+) as shown below (Sherlock, 1984):

$$CO(NH_2)_2 + 2H_2O \longrightarrow 2NH_4^+ + CO_3^{2-} \qquad [2.3]$$

$$CO_3^{2-} + 2H_2O \longrightarrow HCO_3^- + OH^- \qquad [2.4]$$

The carbonate (CO_3^{2-}) ions formed in equation 2.3 then undergo hydrolysis (equation 2.4) resulting in a localized area of elevated pH (Sherlock, 1984; Haynes and Williams, 1992). Ammonium (NH_4^+) formed via urea hydrolysis is in equilibrium with ammonia (NH_3) in soil solution as shown in equation 2.5:

$$NH_4^+ \rightleftharpoons NH_3 + H^+ \qquad [2.5]$$

This equilibrium between NH_3 and NH_4^+ is affected by soil pH and temperature and results in net acidification of the soil with NH_3 being volatilized (Avnimelech and Laher, 1977). However, this loss of NH_3 does not depend on soil's original pH but it is related to the maximal pH values reached after complete urea hydrolysis in the soil (Sherlock, 1984).

Increases in soil pH during urea hydrolysis shift the equilibrium towards NH_3 and increases the potential for NH_3 volatilization (Haynes and Sherlock, 1986). One H^+ is released for each mole of NH_4^+ converted to NH_3, which subsequently results in a decrease in the soil pH and reduction in the fraction of NH_3 with the progress of the process (Avnimelech and Laher, 1977).

Under suitable conditions, ammonia (NH_3) may further undergo biological transformation via nitrification (section 2.4.1), resulting in the formation of nitrite, (NO_2^-) and nitrate (NO_3^-). These are Nr forms that may also be denitrified (section 2.4.2). Thus under a urine patch, there are dynamic changes in the concentration of NH_4^+, NO_2^-, and NO_3^-, with N_2O emissions potentially occurring during both processes (nitrification and denitrification) with N_2 being formed as the ultimate product from denitrification (Simpson and Steele, 1983). While N_2O is an obligate intermediate in the denitrification pathway (section 2.4.2), this is not the case with nitrification (section 2.4.1) (Firestone and Davidson, 1989). Nitrification and denitrification in soil are affected by a number of factors including O_2 supply, moisture content, N substrate, available soil C, temperature and pH (Tiedje, 1988) (section 2.5).

The proportion of ruminant urinary-N emitted as N_2O has been reported to vary from 0.1% to 3.8% according to Oenema et al. (1997). These findings were supported by (de Klein et al., 2003) who reported N_2O emissions from ruminant urine, following single urine application events onto five pastoral soils, ranging from 0.3 to 3.7% of the urine-N applied. However, Williams et al. (1999) reported 7% urinary-N lost as N_2O. The emissions of N_2O from soil affected by ruminant urine typically occur for longer than 30 days. For example, N_2O emissions following urine-N application have been reported to last for 42 days (Williams et al., 1999). The proportion of urinary-N evolved as N_2, in situ, especially under the effect of changing soil physical conditions, is not available in the literature and there is a dearth of such lab studies. The few studies performed, to date, have shown that the urine-induced N_2 emissions are higher from peat soils and that in a mineral soil they increase with increases in soil pH and moisture (Clough, 1994; Clough et al., 2004).

2.4 Mechanisms of nitrous oxide and dinitrogen production

Nitrous oxide is produced in soil by both biotic and abiotic mechanisms (Firestone and Davidson, 1989; Russow et al., 2009). Biotic mechanisms include nitrification, nitrifier-denitrification and denitrification, while abiotic mechanisms include chemodenitrification (Fig. 2.1).

2.4.1 Nitrification

Nitrification is an aerobic process in which NH_3 is oxidized to NO_2^- (equation 2.6) and then NO_2^- is further oxidized to NO_3^- (equation 2.7) (Schmidt, 1982). Nitrification is performed by archaea and bacteria including autotrophic bacteria, heterotrophs and methanotrophs (Schmidt, 1982). Autotrophic nitrifying bacteria gain energy to fix CO_2 into organic C compounds by oxidizing the N compounds NH_3 and NO_2^- as follows:

$$\begin{array}{l} NH_3 + 1.5\ O_2 \xrightarrow{6e^-} NO_2^- + H_2O + 2H^+ \\ \downarrow\uparrow \\ NH_4^+ \end{array} \qquad [2.6]$$

$$NO_2^- + 0.5\ O_2 \xrightarrow{2e^-} NO_3^- \qquad [2.7]$$

Two groups of organisms, namely NH_3 oxidising bacteria (AOB) e.g. *Nitrosomonas* and *Nitrospira*, and NH_3 oxidising archaea (AOA), perform the oxidation of NH_3 to NO_2^- (Leininger et al., 2006). Oxidation of NH_3 to NO_2^- decreases soil pH due to the production of hydrogen ions (equation 2.6). Conversion of NO_2^- to NO_3^- is performed by NO_2^- oxidizing bacteria (NOB) such as *Nitrobacter* (Haynes, 1986). While AOA are well recognized as nitrifiers, the significance of AOA in pasture ecosystems is not well researched. Di et al. (2009) found that AOA abundance and activity did not increase with the addition of an NH_3 substrate applied to six grassland soils, in New Zealand. Thus it was concluded that nitrification in New Zealand pasture soils was driven by AOB and not by AOA.

The rate of nitrification depends on various factors. Nitrification is influenced by substrate (NH_4^+, NO_2^-) concentrations in soil (Haynes, 1986). Addition of these substrates can increase autotrophic nitrifier numbers in soil (Ardakani et al., 1973).

The optimal pH for nitrification is in the range from 4.5 to 7.5 (Haynes, 1986). Park et al. (2007) found that the optimum pH for AOB and NOB lay in the range of 8.2 ± 0.3 and 7.9 ± 0.4, respectively. Soil pH not only influences the growth and metabolism of the nitrifying bacteria but also the availability and toxicity of the substrates and the products. For example, high pH (> 7.5) concomitant with the toxic levels of NH_3 may limit the activity of nitrifiers and may repress nitrification (Villaverde et al., 1997; Park et al., 2007). Aeration and moisture content also affect nitrification in soils.

The optimal soil matric potential (ψ) value for maximum nitrification rates ranges from -10 to -33 kPa. However at 0 kPa, nitrification is either absent or slow due to a lack of oxygen (O_2) (Malhi and McGill, 1982). Nitrification rates are reported to be optimal at a temperature range of 25 to 35^oC (Haynes, 1986).

During nitrification, N_2O is formed as a by-product of NH_3 oxidation due to the chemical decomposition of intermediates like hydroxylamine (NH_2OH), nitroxyl (NOH) or its dimer hyponitrite ($N_2O_2^{2-}$) or NO_2^- itself (Wrage et al., 2001). The amount of N_2O produced via nitrification is also affected by soil and environmental factors that affect nitrification such as pH, substrate supply, O_2, and moisture (section 2.5). It has been shown that N_2O evolved from soils that are well aerated and with a low moisture status correlate well with nitrifiable N compounds (NH_4^+ and NO_2^-) (Bremner and Blackmer, 1981).

In grazed soils, increases in the amount of NH_4^+ substrate and soil pH following urine application can enhance nitrification (Allison and Prosser, 1993) and contribute significantly to N_2O losses (Haynes and Williams, 1993). It has also been shown that under urine patches, nitrification may be inhibited by the urinary components, hippuric and benzoic acids (Bertram et al., 2009). However an *in situ* study showed no effect of hippuric /benzoic acid on nitrification (Clough et al., 2009).

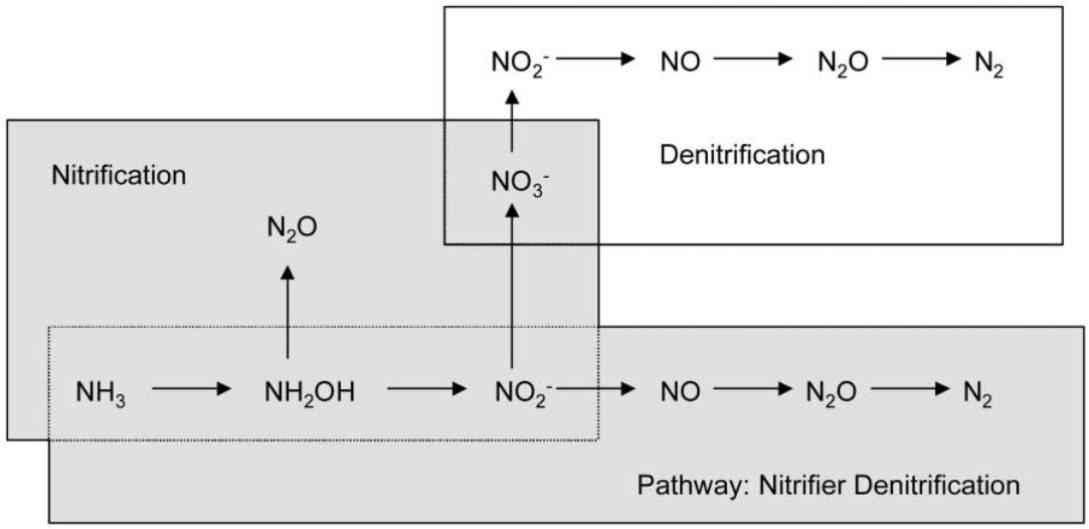

Figure 2.1 Transformations of mineral nitrogen in soil. Adapted from Wrage et al. (2001)

2.4.2 Biological denitrification

Denitrification is the anaerobic and stepwise reduction of NO_3^- to N_2 (Fig. 2.1). It is known to be dominantly performed by heterotrophic bacteria (Firestone, 1982; Knowles, 1982). Various reductase enzymes are involved in the denitrification process with each reductase catalysing a particular step in the denitrification sequence (equation 2.8).

$$\underset{}{NO_3^-} \xrightarrow[\text{reductase}]{\text{Nitrate}} \underset{}{NO_2^-} \xrightarrow[\text{reductase}]{\text{Nitrite}} \underset{}{NO} \xrightarrow[\text{reductase}]{\text{Nitric oxide}} \underset{}{N_2O} \xrightarrow[\text{reductase}]{\text{Nitrous oxide}} \underset{}{N_2} \qquad [2.8]$$

Denitrification occurs under low O_2 pressures when the facultative anaerobic bacteria use N-oxides as an electron acceptor in place of the O_2 molecule (Wrage et al., 2001). The requirements for denitrification to occur are the presence of microbes having the appropriate metabolic pathway, the availability of suitable reductants, a low level of O_2 and a supply of NO_3^- or other nitrogen oxides (Firestone, 1982; Knowles, 1982). It has also been found that denitrification can occur in aerobic soils due to the presence of anaerobic microsites (Müller et al., 2004). Denitrification plays a pivotal role in the N cycle since it serves as a sink for N_2O via reduction of N_2O to N_2 and returns N to the atmosphere (Firestone, 1982).

Not all N denitrified is converted to N_2 and both N_2O and N_2 may be produced. Sometimes nitric oxide (NO) is also produced and emitted to the atmosphere. The fraction of N_2O or N_2 evolved during denitrification is influenced by various soil and environmental factors as explained in section 2.5.

In grazed soils, denitrification is generally increased under urine patches due to the increased nitrogen (N) and carbon (C) substrate (Ambus et al., 2007). Thus urine patches are localised hot spots for denitrification to occur in grazed soils. Estimated denitrification losses from grazed grasslands in New Zealand range from 3-19 kg ha^{-1} (Ledgard et al., 1996). Clough (1994) showed that the denitrification losses of N applied from a silt loam soil ranged from 16-34% following urine application.

2.4.3 Coupled nitrification-denitrification

Coupled nitrification-denitrification is as the name suggests when NO_2^- or NO_3^-, derived from nitrification, is immediately available for denitrification (Kremen et al., 2005). In soils, coupled nitrification-denitrification can be a main source of N_2O when soil conditions are optimal for providing niches suitable for both nitrifiers and denitrifiers (Wrage et al., 2001; Kremen et al., 2005). Khdyer and Cho (1983) demonstrated that NO_3^- formed following oxidation of NH_3 in an aerobic soil layer was denitrified in the anaerobic layer with N_2O mainly produced at the aerobic-anaerobic interface in the soil columns amended with urea. However, the importance of coupled nitrification-denitrification is unknown especially in urine impacted grazed soils.

2.4.4 Nitrifier-denitrification

Nitrifier-denitrification is the process in which the oxidation of NH_3 to NO_2^- is followed by reduction of NO_2^- to N_2O and N_2 (Wrage et al., 2001) (Fig 2.1). It is a process performed by autotrophic NH_3 oxidisers (Kuai and Verstraete, 1998). Earlier reports on the significance of nitrifier-denitrification considered the process to be insignificant (Robertson and Tiedje, 1987) or comprising up to 30% of the total N_2O production in the drier soil (-1.0 kPa) and 3% of the total N_2O production in wetter soil (-0.1 kPa) (Webster and Hopkins, 1996). It is thought it is most likely to occur when soils have low carbon levels, high N contents and are under increased O_2 stress (Wrage et al., 2001).

Poth and Focht (1985) have proposed several reasons for the existence of nitrifier-denitrification including the conservation of O_2 for NH_3 oxidation or to remove toxic NO_2^-. Wrage et al. (2005) provided the first direct evidence of nitrifier-denitrification in soil and showed that it was a major source of N_2O, accounting for 44% of N_2O production in a 24 h period. Russow et al. (2009) incubated a black earth soil under varying O_2 partial pressures (0 to 20%) and demonstrated with the use of a ^{15}N enrichment technique that nitrifier-denitrification was significant at 5 to 2% O_2 while denitrification was dominant under more anaerobic conditions (< 0.3% O_2). Venterea (2007) while examining NO_2^- driven N_2O production from soil under aerobic conditions showed in an incubation study that nitrifier-denitrification occurred when the O_2 concentration was decreased from 21% to 5% and that biological denitrification occurred at < 5% O_2. Kool et al. (2011), in an incubation experiment, examined the contribution of nitrifier-denitrification to N_2O production from a sandy soil at different water-filled pore space (WFPS) levels (50%, 70% and 90%); finding that nitrifier-denitrification made a significant contribution (30-100%) to NH_4^+-derived N_2O production at all WFPS levels.

However, the contribution of nitrifier-denitrification to total N_2O was only significant at 50 and 70% WFPS while at WFPS 90%, its contribution to total N_2O was only 4-8%. In grazed soils, particularly under urine patches, the potential for nitrifier-denitrification occurring is relatively high due to the large substrate pools available (Koops et al., 1997).

2.4.5 Chemodenitrification

Chemodenitrification is the term used to describe abiotic reactions of NO_2^- in soils (Chalk and Smith, 1983; Wrage et al., 2001). It is a process that gains importance whenever NO_2^-, produced by nitrifying and denitrifying microorganisms, accumulates in soil and reacts chemically to form gaseous N compounds (Chalk and Smith, 1983). Nitrite (NO_2^-) exists in equilibrium with the protonated form of NO_2^-, nitrous acid (HNO_2) (pKa = 3.3). In soil solution low soil pH shifts the equilibrium towards HNO_2 (Van Cleemput and Samater, 1995) (equation 2.9).

$$NO_2^- + H^+ \longleftrightarrow HNO_2 \qquad [2.9]$$

Nitrous acid (HNO_2) subsequently undergoes self-decomposition to gaseous nitrogen oxides (van Cleemput, 1998) and is the main mechanism for NO production in soils (Nelson, 1982). The HNO_2 molecule may also undergo various non-enzymatic chemical reactions to form gaseous N compounds such as NO, N_2O, N_2 (Reuss and Smith, 1965; Nelson and Bremner, 1970; Smith and Chalk, 1980). Under acidic conditions HNO_2 reacts with free amino groups often resulting in the formation of N_2 which is known as the Van Slyke reaction (Van Slyke, 1911). Reaction of HNO_2 with phenolic groups of soil organic matter may also produce NO and N_2O (Blackmer and Cerrato, 1986). Venterea and Rolston (2000) showed that gross NO production rates in both sterile and non-sterile soils were highly correlated with HNO_2 concentrations but were not correlated with gross nitrification rates, NH_4^+ or NO_3^- levels which suggested that HNO_2-mediated reactions may have been the significant source of NO. Soil pH, organic matter content and soil NO_2^- concentrations are reported to be the most important factors that control abiotic production of NO in soil (Firestone and Davidson, 1989). Khan et al. (2011) determined the effect soil pH on urine-derived NO-N production and observed that the cumulative NO-N fluxes ranged from 0.02 to 0.05% of urine-N applied, and after 21 days the optimal pH for net NO-N flux was in the range of 5.7 to 6.0.

2.5 Factors affecting N_2O and N_2 production pathways in soil

2.5.1 Substrate N availability and concentration

The presence of mineral N substrate is the most important prerequisite for N_2O production in soil. The majority of the N available in soil after urine application is initially in the form of urea-N and this is hydrolysed to form NH_4^+-N (section 2.3). The NH_4^+-N concentration in soil may reach 270-370 mg N kg^{-1} following urine deposition (Haynes and Williams, 1992). This is too high for immediate utilisation by plants or soil microorganisms. Thus nitrification proceeds, resulting in relatively high concentrations of soil NO_3^- which is potentially available for denitrification. Thus, the urine patch is a substantial source of inorganic-N substrate for microbial transformation processes.

Denitrification may be limited by low concentrations of NO_3^- (< 5-10 mg N kg^{-1} soil) (Ryden, 1983) while, conversely, high concentrations of NO_3^- increase the denitrification rate in the presence of a carbon substrate (Weier et al., 1993). It has been shown that under anaerobic soil conditions, increasing NO_3^- concentrations to 5 µg g^{-1} soil stimulated the reduction of N_2O to N_2 while increasing NO_3^- concentrations to 50 µg g^{-1} inhibited the reduction of N_2O to N_2 (Blackmer and Bremner, 1979). Thus the proportion of NO_3^- emitted as N_2O increases as NO_3^- concentrations increase. The reason for this has been attributed to the inhibition of N_2O reductase activity (Blackmer and Bremner, 1978) and greater affinity of NO_3^-, compared to N_2O, for their respective reductase enzymes (Dendooven and Anderson, 1994).

2.5.2 Soil pH

Deposition of urine increases soil pH by 1-3 units (Doak, 1952; Haynes and Williams, 1992) as a consequence of the hydrolysis of carbonate ions formed during urea hydrolysis (Avnimelech and Laher, 1977; Sherlock, 1984). This increase in soil pH subsequently affects nitrification and denitrification rates and processes. Clough et al. (2004) showed that in the presence of urine, increasing the initial soil pH from 4.7 to 7.2 resulted in lower N_2O emissions at pH ≥ 5.9, under conditions suitable for nitrification. However, under conditions conducive for denitrification, both N_2 and N_2O emissions increased with an increase in initial soil pH, with the N_2: N_2O ratio increasing as soil pH increased. Increase in soil pH > 7.5 can cause repression of nitrification and result in accumulation of NO_2^- due to high levels of free ammonia (NH_3) (Monaghan and Barraclough, 1992; Park et al., 2007).

High denitrification reaction rates occur at pH 7.0-8.0 in the presence of a ready supply of NO_3^--N (Van Cleemput and Patrick Jr, 1974; Haynes and Sherlock, 1986). Simek et al. (2002) showed that the optimum pH for denitrification depends on the length of soil incubation with the optimum soil pH shifting towards a neutral pH, indicating either proliferation of new active denitrifiers or adaptation of the existing population to new conditions. They concluded that there was no optimum pH for denitrification and that an 'optimum' pH for denitrification should be annotated with the denitrification parameters to which it is being applied.

Soil pH affects denitrification rates and the product ratio of the gases evolved, i.e., N_2O and N_2 (Blackmer and Bremner, 1978; Firestone, 1982). Neutral and alkaline conditions in soil favour N_2 production while acidic conditions favour N_2O formation (Daum and Schenk, 1998). While increasing soil pH results in increasing denitrification rates, the percentage of N_2O formed declines due to the rate of N_2O reduction exceeding the rate of production (Focht, 1974; Arah and Smith, 1990).

2.5.3 Carbon supply

Metabolisable C sources are obligatory substrates for heterotrophic denitrifiers (Knowles, 1982). Increasing the C availability enhances the energy and electron supply to denitrifiers while also stimulating high O_2 consumption (Murray et al., 2004). This consequently increases denitrification in soil. It is the amount of microbially available C in the soil which is important. It is often measured as water soluble carbon (WSC) or dissolved organic carbon (DOC). It has been shown that WSC can correlate well with denitrification potentials of soils (Burford and Bremner, 1975). However, the quality (C:N ratio) of the soil carbon may also influence the transformation of N in soil with subsequent consequences for N_2O production (Aulakh et al., 1991b; Huang et al., 2004).

Several studies have observed relationships between soil organic C and denitrification (Firestone and Davidson, 1989; Luo et al., 1999; Azam et al., 2002). It is well known that increasing soil organic C can increase N_2O emissions and that C is often a limiting factor in denitrification (Haynes and Sherlock, 1986; Firestone and Davidson, 1989). Soil organic C also controls the relative proportions of N_2O and N_2 produced by denitrification (Firestone and Davidson, 1989). Increasing the availability of organic C in soil results in more complete reduction of NO_3^- consequently leading to more N_2 production (Rolston et al., 1978).

The C substrates that the denitrifiers require are assumed to be elevated under urine patches due to the increased soil pH and root scorching events (Carter et al., 2006). In grazed soils, elevated soil pH following urine application solubilises the organic matter in the soil (Monaghan and Barraclough, 1993; Shand et al., 2000; Clough et al., 2004) resulting in increases in DOC (Shand et al., 2002), and this is believed to promote denitrification.

2.5.4 Soil physical conditions

Soil physical conditions (e.g. bulk density and texture) influence soil water content, gas diffusion and pore size distribution of a soil. Changes in soil physical conditions ultimately affect gas transport within the soil profile. An event that completely disturbs the soil physical environment is soil compaction. It often occurs in grazed pastures and is induced by animal treading and farm machinery operations. Soil compaction can completely alter moisture-air characteristics and pore size distribution of soils (Stepniewski, 1981). Compaction is more prominent at the soil surface especially under high stocking rates (Greenwood and McKenzie, 2001). In the presence of animal excreta such as urine or dung, these changes in the soil physical characteristics potentially lead to formation of local hot spots for N_2O emissions from soils (van Groenigen et al., 2005; Bhandral et al., 2007). Soil compaction has been shown to increase emissions of urine-derived N_2O-N from 0.9% to 4.9% under moist conditions (van Groenigen et al., 2005). The reason for this five-fold increase in N_2O emissions was attributed to an increase in denitrification as a result of increasing anaerobic conditions. Uchida et al. (2008) also observed high N_2O fluxes from a compacted silt loam soil following urine application with N_2O emissions increasing from 0.3-9.6 % of urinary-N applied.

2.6 Soil compaction and N_2O, N_2 emissions

Soil compaction generally shows a cascade effect which ultimately leads to an increase in soil anaerobicity by changing soil physical properties such as soil bulk density (ρ_b), soil moisture and soil gas diffusivity (reviewed in detail below). Increases in soil ρ_b due to soil compaction results in decreases in soil total porosity and the volume of large sized pores (macropores). Furthermore it increases soil moisture retention and the volume of small sized pores (micropores) which consequently cause soil gas diffusion to cease, leading to anaerobic conditions suitable for denitrification. Thus to fully comprehend the effect of soil compaction on N_2O and N_2 emissions, an understanding of soil water characteristics and soil gas diffusion along with soil ρ_b is necessary.

2.6.1 Soil bulk density

Soil bulk density (ρ_b) is a good indicator of soil damage resulting from grazing of pastures and it is easy to measure (Greenwood and McKenzie, 2001). It is used as an indicator of soil compactness and porosity (Assouline, 2006). It is well documented that animal grazing results in an increase in soil ρ_b (Langlands and Bennett, 1973; Mulholland and Fullen, 1991; Greenwood et al., 1997). Soil ρ_b influences many aspects of the soil-water-atmosphere system, with increases often resulting in higher denitrification losses (Torbert and Wood, 1992; Menneer et al., 2005b).

Thomas et al. (2008) showed that animal treading increased the ρ_b of a silt loam soil under a winter forage crop from 1.17 to 1.32 Mg m^{-3}. The increase in soil ρ_b was more prominent when the soil moisture content was ≥ field capacity. It has also been reported that soil compaction enhanced N_2O emissions after ruminant urine application (800 kg N ha^{-1}) and that the cumulative N_2O flux ranged from 1.6 to 1.8 % of the N applied (Thomas et al., 2008). Increasing the soil ρ_b of a loamy sand from 1.4 to 1.8 Mg m^{-3}, at a WFPS of 60%, resulted in total ^{15}N losses increasing by a factor of 3.6 due to denitrification (Torbert and Wood, 1992). Ruser et al. (2006) observed the combined effects of soil moisture and compaction on N_2O and N_2 emissions from NO_3^- fertilised soil cores and found that these emissions increased with increasing soil moisture and compaction.

Thus, there are studies that have shown the effect of ρ_b on N_2O losses. But none of these studies have jointly examined the effects of matric potential (ψ) (section 2.6.2) and soil compaction on relative gas diffusivity (Dp/Do) (section 2.6.3) and its subsequent effect on urea- derived N_2O fluxes. There is also a lack of studies which have incorporated the effect of increasing soil ρ_b on urea-derived N_2 emissions.

2.6.2 Soil moisture

Changes in soil physical conditions resulting from increasing soil ρ_b often result in increases in soil moisture content making the soil conditions more conducive for denitrification (Ball et al., 2008; Beare et al., 2009).The proportion of the denitrification products (N_2O and N_2), actually emitted from the soil also depends on soil moisture since any increase in soil moisture often decreases soil aeration, which is conducive for both N_2O production and N_2O reduction (Focht, 1974; Weier et al., 1993; Rudaz et al., 1999). Increasing soil moisture also increases the likelihood that N_2O may get entrapped in soil water and be further reduced to N_2 gas (Letey et al., 1980; Smith et al., 2003; Clough et al., 2005).

Soil moisture is often expressed as gravimetric water (θ_g), volumetric water (θ_v), WFPS, or as a matric potential (ψ). However, N_2O emissions are routinely related with WFPS in soil studies (Dobbie et al., 1999; Dobbie and Smith, 2001; Beare et al., 2009). There has been debate over the suitability of using WFPS as a predictor for N_2O losses from soils varying in ρ_b and texture. According to Aulakh et al. (1991a), WFPS, which is derived from soil water content and ρ_b, is a better index for N_2O losses and microbial activity than either θ_g or θ_v. Linn and Doran (1984) stated that the use of WFPS allows direct comparison of microbial activities in soils differing in ρ_b.

Davidson and Schimel (1995) stated that because WFPS is directly related to diffusivity then soil water content should be noted in the case of gaseous fluxes. However, Farquharson and Baldock (2008) correctly pointed out that the use of total porosity in the calculation of WFPS (section 3.4.2) makes it inadequate for describing processes in soils with different ρ_b as it does not represent the fraction of the entire soil volume. Thus a single soil or soils with different ρ_b will have different air-filled porosities which may result in variation in relationships based on WFPS and N_2O fluxes. Thus for soils varying in physical properties the use of WFPS is questionable.

Many studies have also shown that ψ can be used to attempt to explain the observed variability in N_2O emissions from soil. Dobbie and Smith (2006) showed that increasing ψ from 35 to 45 cm in N fertilised grassland resulted in a 30% reduction in N_2O emissions. Smith et al. (1998) found that N_2O emissions, from the soil treated with ammonium nitrate (NH_4NO_3) peaked at -5.0 kPa and ceased at -2.5 kPa as soil became wetter.

Pilot and Patrick (1972) examined the effect of ψ on NO_3^- reduction in four soils with different textures and found that there was a critical value of ψ, specific for each soil type, above which no NO_3^- reduction occurred. Castellano et al. (2010) suggested that ψ could be a more suitable predictor of relative N_2O emissions across different soils since ψ showed less variation than other variables in explaining N_2O emissions from NO_3^- treated (100 kg N ha^{-1}) intact soil cores over a 96 h period. A study by van der Weerden et al. (2012) also showed that ψ and θ_v were better variables than WFPS for explaining N_2O emissions emitted from NO_3^- fertilised intact soil cores of two different soil types. They suggested that as θ_v has an advantage over ψ in being easily measured; it should be used as a proxy for modelling N_2O emissions from soils across different landscapes. They also recommended that future studies should include soils with varying ρ_b and pore size distributions when determining a suitable variable for N_2O emissions, as currently there is a lack of such studies in the literature. Therefore a complete understanding of a soil's water characteristics, as might be described by a water retention curve (WRC) and pore size distribution, and how they are affected by soil compaction becomes necessary.

2.6.2.1 Soil water retention curves and pore size distribution

Determination of soil water characteristics such as water retention curves (WRC) and associated soil pore size distributions are obtained by maintaining a soil at different matric potential (ψ) values. There are no studies which have examined the possible interaction of soil compaction i.e. increase in soil ρ_b and ψ on the resulting N_2O emissions. Matric potential (ψ) refers to the tension or suction (cm) applied to the soil to remove water from the pores. Matric potential is normally expressed in units of kPa with a negative value showing that energy must be exerted to extract water from the soil while suction or tension is generally in positive values. Different units have been used in the literature to express ψ (Table 2.1).

Table 2.1 Commonly used units for reporting soil ψ.

Soil matric potential (units)	Value				
Hydraulic head (cm H_2O)	0	10.2	102*	1020	15300**
Bar	0	0.01	0.1	1.00	15.00
kiloPascal (kPa)	0	-1	-10	-100	-1500
pF (log cm H_2O)	0	1	2	3	4.2

* Volumetric water content at -10 kPa is often taken as field capacity i.e. when water in the macropores has drained completely (Hillel, 2004).

** Volumetric water content at -1500 kPa is regarded as a permanent wilting point i.e. when soil water is unavailable to plants (Hillel, 2004).

A plot of a soil's θ_v and ψ values is known as a water retention curve (Assouline, 2006). It is an important and fundamental relationship often used to describe behaviour of an unsaturated soil (Miller et al., 2002). For a given soil, its WRC is determined experimentally either by draining the saturated soil (desorption) or by wetting the soil (sorption). A typical water retention curve is shown in Fig. 2.2 along with the defining parameters such as air entry value (ψ_a), residual water content (θ_r) and saturated water content (θ_s). A drainage curve normally starts from a water saturated soil (θ_s) at zero potential.

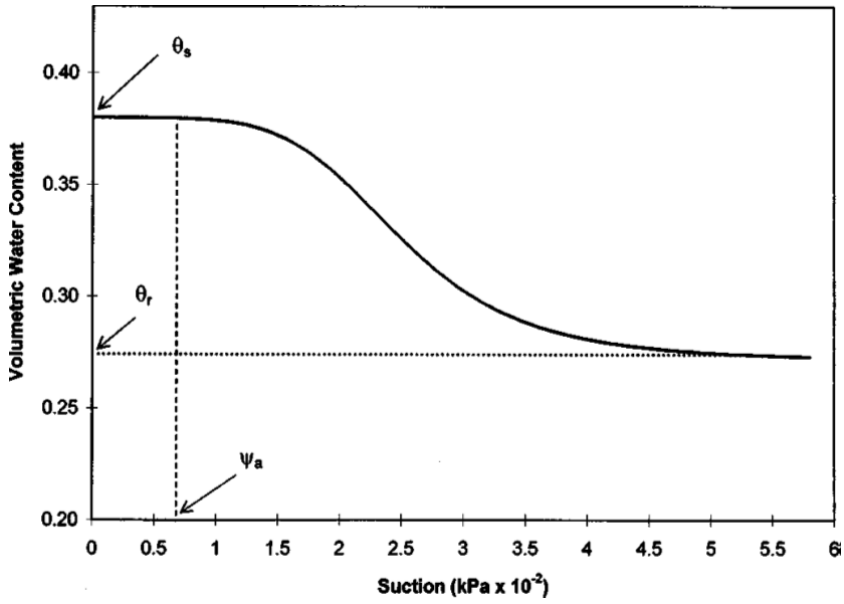

Figure 2.2 Typical soil retention curve where matric potential on the X axis is depicted as suction expressed in positive values (Miller et al., 2002).

When a matric potential is applied to the saturated soil with a volumetric water content, θ_s, no outflow of soil water takes place until a critical suction value is reached, whereupon the largest pores are drained. This value is the critical suction or air-entry value (ψ_a) (Hillel, 1998). The air-entry value is the threshold for the desaturation process. With further increases in ψ, θ_v content reaches a soil specific minimum which is known as the residual water content (θ_r). Determining a WRC is time consuming. However, it is an important parameter in soil hydrology studies. Thus many models have been designed to describe a soil's WRC. There are many expressions in the literature that relate ψ to θ_v (Hillel, 1998). Routinely used models that relate ψ with θ_v are given below:

$$\frac{\psi}{\psi_a} = \left(\frac{\theta_v}{\theta_s}\right)^{-b} \qquad \text{(Campbell, 1974)} \qquad [2.10]$$

equation 2.10 can be rewritten as:

$$\psi = \psi_a \left(\frac{\theta_v}{\theta_s}\right)^{-b} \qquad [2.11]$$

or as:

$$\log \psi = \log \psi_a - b \log \frac{\theta_v}{\theta_s} \qquad [2.12]$$

Therefore *b* (Campbell water retention parameter) and ψ_a can be estimated by fitting a straight line through a log-log plot of the WRC (equation 2.12) where *b* corresponds to slope and ψ_a is determined from the intercept of the straight line (Campbell, 1974; Arthur et al., 2012).

If the linear regression approach is used to fit the water retention data, then the points corresponding to $0 > \psi > \psi_a$ should be excluded from the regression (Cresswell and Paydar, 1996).

$$\frac{\theta_v - \theta_r}{\theta_s - \theta_r} = \left(\frac{\psi_a}{\psi}\right)^{\lambda} \qquad \text{(Brooks and Corey, 1964)} \qquad [2.13]$$

The *b* parameter in equations (2.10-2.12) is equal to -1/ λ where λ is dimensionless and is referred to as the pore size index in Brooks and Corey's equation (equation 2.13) (Miller et al., 2002).

Another commonly used equation for determining soil water retention parameters is:

$$\frac{\theta_v - \theta_r}{\theta_s - \theta_r} = \frac{1}{[1 + (\alpha\psi)^n]^m} \qquad \text{(van Genuchten, 1980)} \qquad [2.14]$$

where:

θ_s = saturated water content ($m^3\ m^{-3}$),

θ_r = residual water content ($m^3\ m^{-3}$),

α = inverse of air entry matric potential (m^{-1}),

n and *m* = dimensionless empirical curve shape parameter.

Different methods are used to apply ψ in a laboratory. Most commonly used are suction methods such as hanging water columns, tension tables and pressure plates. Water saturated soil is kept on a porous layer and is subjected to increasing negative suctions. When a static equilibrium is established at any given value of ψ, θ_v is determined. The process is repeated to obtain the WRC. Pressure plates are used to measure θ_v at higher matric potentials up to -1500 kPa.

The developed WRC also allows for the determination of pore size distribution (Klute, 1986). By using the capillary rise equation (equation 2.15) any given ψ value can be translated into an equivalent pore radius (*r*, in units of *m*) that remains full of water at that ψ value (Scott, 2000; Hillel, 2004). In equation 2.15, σ is the surface tension of water (kg s^{-2}) and θ is the angle of contact of water within the capillary tube. Capillary rise theory considers soil as a system of parallel cylindrical capillaries gradually decreasing in diameter (Scott, 2000).

$$\psi = \frac{-2\,\sigma\,cos(\theta)}{r} \qquad [2.15]$$

Assuming that the contact angle is zero, the above equation can be rewritten as:

$$h = \frac{2\sigma}{r\rho_w\,g} \qquad [2.16]$$

where:

h = matric potential expressed in suction (m H_2O),

ρ_w = density of water (1000 kg m^{-3}),

g = gravitational acceleration (9.8 m s^{-2}).

Substituting a value of σ at 25^{o}C (0.072 kg s^{-2}) into equation 2.17, an approximation (equation 2.17) arises which is often used in hydrological studies (Scott, 2000).

$$r = \frac{0.15}{h} \qquad [2.17]$$

where:

r = radius of pore (cm),

h = matric potential (cm H_2O).

Typical matric potentials and their equivalent pore sizes are shown in Table (2.2). Luxmoore (1981) divided soil pores in three categories on the basis of their sizes, macropores, mesopores and micropores with each class having its own relevant function (Table 2.2).

Table 2.2 Pore size terminology and pore size at equivalent matric potential (Luxmoore, 1981)

Pore name	Pore size (equivalent pore diameter in μm)	Pore function	Equivalent matric potential (kPa)
Macropore	> 1000	rapid drainage of water	< 0.3
Mesopore	1000-10	water storage and distribution	0.3-30
Micropore	< 10	retain water	> 30

2.6.2.2 Effect of soil compaction on soil water characteristics

Soil physical disturbances such as compaction may change the pore size distribution and consequently the WRC. This is because compaction alters soil total porosity and the relative volumes of large and small pores which decrease and increase respectively (Hill and Sumner, 1967; Richard et al., 2001; Assouline, 2006). At any given ψ, soil pores up to a fixed diameter are water-filled and any larger pores are air-filled. Soil compaction, at a more negative matric potential, reduces the proportion of larger pores. The volume of small pores then increases as a result, with the net effect being greater water retention in the soil, and hence the moisture content increases (Hill and Sumner, 1967; Assouline, 2006).

2.6.3 Soil relative gas diffusivity (*Dp*/*Do*)

Increasing both soil moisture content and soil ρ_b ultimately results in the decreased movement of gases both in and out of the soil (Stepniewski, 1981). The movement of gases within the soil profile occurs by two processes, by diffusion and convection. Diffusion depends on concentration gradients while convection depends on pressure gradients of the gases involved (Ball and Schjønning, 2002). However, movement of gases in and out of soil occurs mainly by diffusion (Penman, 1940). It occurs as a result of gas concentration gradients within the soil profile. Gas diffusion in soil, in one dimension, is described by Fick's law which states that the rate of diffusion is proportional to the concentration gradient (section 3.1).

However, Fick's law is strictly only applicable to equimolar and countercurrent diffusion of gases under isobaric and isothermal conditions. Soil gas diffusivity is generally represented as relative gas diffusivity (*Dp*/*Do*). This is the ratio of the gas diffusion coefficient in soil (*Dp*) to the gas diffusion coefficient in air (*Do*). It is generally very tedious to measure *Dp* as it requires special equipment either in laboratory or under *in situ* conditions (Rolston and Moldrup, 2002). Thus predictive models are often used to estimate *Dp*/*Do*. Buckingham (1904) pioneered the research on soil gas diffusion. Since then many models have been developed to relate soil relative gas diffusivity (*Dp*/*Do*), air-filled porosity (ε) and total porosity (ϕ) and are listed below.

$$\frac{D_p}{D_o} = \varepsilon^2 \qquad \text{(Buckingham, 1904)} \qquad [2.18]$$

$$\frac{D_p}{D_o} = 0.66\,\varepsilon \qquad \text{(Penman, 1940)} \qquad [2.19]$$

$$\frac{D_p}{D_o} = \varepsilon^{1.5} \qquad \text{(Marshall, 1959)} \qquad [2.20]$$

All the above models depend only on one parameter, ε, and were obtained by fitting different equations to the experimental data. The next generation of models included soil ϕ along with ε. The two-parameter model, which is most widely used, is:

$$\frac{D_p}{D_o} = \frac{\varepsilon^{\frac{10}{3}}}{\phi^2} \qquad \text{(Millington and Quirk, 1961)} \qquad [2.21]$$

Ball (1981) modeled soil gas diffusion through soil pores using two pore models. The first model considered pores as tortuous tubes of uniform radii while the second model considered pores as jointed tubes of different radii. However, it was suggested that the second model needed more refinement to increase its applicability to soils.

For the prediction of *Dp* in wet and repacked soil, Moldrup et al. (2000b) derived a water-induced linear reduction model (WLR) (equations 2.22-2.24) by modifying classical models to account for the effects of changes in pore shape in a wet soil as compared with a dry soil at the same value of *ε*.

$$\frac{D_p}{D_o} = 0.66\varepsilon \frac{\varepsilon}{\phi} \quad \text{WLR (Penman) model} \quad [2.22]$$

$$\frac{D_p}{D_o} = \varepsilon^{1.5}\left(\frac{\varepsilon}{\phi}\right) \quad \text{WLR (Marshall) model} \quad [2.23]$$

$$\frac{D_p}{D_o} = \varepsilon^{4/3}\left(\frac{\varepsilon}{\phi}\right) \quad \text{WLR (Millington) model} \quad [2.24]$$

However, the WLR model was not recommended for strongly compacted and intact soils (Moldrup et al., 2000b).

The effect of soil compaction on the relationship of *Dp*/*Do* and *ε* has been previously studied (Stepniewski, 1981; Currie, 1984; Fujikawa and Miyazaki, 2005). These studies showed that the relationship between *Dp*/*Do* and *ε* may be unaffected (Grable and Siemer, 1968; Stepniewski, 1981), or altered by soil ρ_b (Fujikawa and Miyazaki, 2005; Hamamoto et al., 2011).

Currie (1984) assessed the effect of compaction on soil gas diffusion and concluded that when changes in soil ρ_b occurs, no single relationship can describe the change in *Dp*/*Do* with *ε,* even for a single soil. Hamamoto et al. (2011) found that at any given value of *ε*, soil compaction resulted in an increase in *Dp*/*Do* due to a reduction in water blockage effects. But at any given value of ψ, lower *Dp*/*Do* values were reported from compacted soils since higher water retention occurred in extremely compacted soils. Previous use of soil ρ_b in the predictive models for *Dp*/*Do* is very limited. However, after considering the large variation in soil ρ_b that exists *in situ*, one recent study has developed a density-corrected predictive model (equation 2.25) for gas diffusivity for a range of soil types and levels of ρ_b (Chamindu Deepagoda et al., 2011b).

$$\frac{D_p}{D_o} = 0.2\left(\frac{\varepsilon}{\phi}\right)^3 + 0.004\left(\frac{\varepsilon}{\phi}\right) \quad [2.25]$$

Xu et al. (1992) found that *Dp*/*Do* decreased to zero at ε of 10%, suggesting the presence of isolated pores and discontinuity in pathways of the soil pores. Such pore space is termed as 'inactive' or 'residual' as it does not contribute to gas diffusion. It is also important to note that even though *Dp*/*Do* appears to be zero at this ε, it may in fact be 10^{-4} slower due to the reduced diffusivity of gas in water (Allaire et al., 2009). However, Hamamoto et al. (2011) showed that extremely compacted soil exhibited negligible inactive ε.

It is known that soil compaction influences water retention properties and the volume and distribution of pores (Assouline, 2006). However, few models have been developed which combine gas diffusivity with soil water retention parameters to take into account soil type effects. Freijer (1994) combined a gas flow pore model (Ball, 1981) and van Genuchten's model (section 2.6.2.1) and showed the air entry value (ψ_a) (section 2.6.2.1) of the soil's WRC to be an important parameter which indicates *a priori* the water content at which pore blocking becomes relevant .

Moldrup et al. (1996) introduced the Campbell *b* water retention parameter (section 2.6.2.1) into the gas diffusivity model as shown in the equation 2.26:

$$\frac{D_p}{D_o} = \phi^{\frac{4}{3}} \left(\frac{\varepsilon}{\phi}\right)^{1.5+\frac{3}{b}} \qquad [2.26]$$

Moldrup et al. (1999) developed a so-called BBC (Buckingham Burdine Campbell) model (equation 2.27) to predict gas diffusivity in undisturbed soils.

$$\frac{D_p}{D_o} = \phi^2 \left(\frac{\varepsilon}{\phi}\right)^{2+\frac{3}{b}} \qquad [2.27]$$

Moldrup et al. (2000a) modified the BBC model by introducing ε measured at -10 kPa (macroporosity, ε_{100}) to describe soil structure effects on gas diffusivity (equation 2.28).

$$\frac{D_p}{D_o} = (2{\varepsilon_{100}}^3 + 0.04\varepsilon_{100}) \left(\frac{\varepsilon}{\varepsilon_{100}}\right)^{2+3/b} \qquad [2.28]$$

Moldrup et al. (2004) further developed a three porosity model (TPM) (equation 2.29) to predict gas diffusivity for undisturbed soils when limited reduced water retention data is available.

$$\frac{D_p}{D_o} = \phi^2 \left(\frac{\varepsilon}{\phi}\right)^X \qquad [2.29]$$

where: *X* was referred to as the tortuosity-connectivity parameter.

Most of these models noted above for *Dp*/*Do* are modified power law functions of ε where the general equation can written as equation 2.30 (Troeh et al., 1982; Ball et al., 1988).

$$\frac{D_p}{D_o} = A\varepsilon^X \qquad [2.30]$$

where: *A* and *X* are empirical constants (dimensionless).

Hamamoto et al. (2011) described parameter *A* as the pore connectivity parameter and *X* as the water blockage parameter. The parameter *X* represents the resistance to gas diffusion due to the presence of water bridges between soil particles in the wet soil. The parameter *X* determines the curvature of the line representing the power law equation (equation 2.30) (Troeh et al., 1982).

2.6.3.1 Methods to measure *Dp*

There are various methods to determine *Dp* in soil. Taylor (1949) measured the diffusion of O_2 through soil using a Beckman O_2 analyzer and emphasized that O_2 diffusion through the soil might be important in determining soil aeration. Ball et al. (1981) measured gas diffusivity using radioactive krypton-85 as a trace gas. Currie (1983) measured the diffusion of hydrogen through the soil using a hot wire sensor. Rolston (1986) described the apparatus for measuring the diffusion of N_2 into a gas mixture of Ar and N_2 to determine the soil gas diffusion coefficient in the laboratory. Moldrup et al. (2000b) used O_2 as the experimental gas for diffusion measurements with the Rolston apparatus and assumed that O_2 consumption in soil did not induce significant error (< 1.5%).

2.6.3.2 *Dp*/*Do* and N_2O, N_2 emissions

The literature remains unclear as to whether *Dp*/*Do* is able to be used as a predictor of N_2O emissions when used as a variable in the predictive models. However, Andersen and Petersen (2009) suggested that *Dp*/*Do* could be a better predictor of N_2O emissions than WFPS after examining repacked soil, amended with nutrient solutions and adjusted to three matric potentials (-1.5 to -10 kPa).

There appear to have been only three studies that have attempted to relate N_2O emissions directly with measurements of *Dp*/*Do*. *In situ* N_2O emissions were found to increase from N-fertilized soil, when the diffusivity of freon-22 was reduced from 1.9 to 1.5 $mm^2\ s^{-1}$ following soil compaction (Sitaula et al., 2000). McTaggart et al. (2002) demonstrated a strong relationship between *Dp*/*Do* and cumulative N_2O emissions from intact, fertilized (120 kg N ha^{-1}), soil cores (four soil types) maintained at three different ψ levels. Van der Weerden et al. (2012) also demonstrated a strong linear relationship between *Dp*/*Do* and log N_2O emissions from NO_3^- applied to soil cores and found that there was a 4.8 fold decrease in N_2O emissions with a small increase in *Dp*/*Do*.

However, there is no study that relates both urine (urea) derived N_2O and N_2 emissions with *Dp*/*Do*. Moreover, data sets that examine the effects of soil ρ_b and ψ on *Dp*/*Do* are lacking, while such effects with respect to urea-derived N_2O and N_2 emissions do not exist.

2.7 Summary

This literature review has described the processes and factors affecting N_2O and N_2 emissions from soil. Soil compaction can potentially control and change the physical attributes of soil which in turn alter biological processes such as N_2O production and N_2O reduction. However, there are many gaps in our current knowledge and there is still a need to establish the relationships between soil physical conditions and ensuing N_2O emissions. In addition, remarkably few studies have measured N_2 emissions from compacted soils in association with N_2O. There is also a need to determine whether *Dp*/*Do* or WFPS is a better predictor for N_2O emissions since there is a lack of soil studies particularly under soil conditions varying in ρ_b. Therefore the focus of this study will be to link soil physical attributes with the N_2O and N_2 fluxes from soil treated with urea (the dominant N source in ruminant urine) or nitrate.

Chapter 3

Materials and Methods

This chapter describes the materials and methods used in the three experiments performed. Any materials or methods specific to an individual experiment are discussed in the relevant chapters.

3.1 Determination of the soil gas diffusion coefficient (D_p)

The method used in this current study relies on the accurate measurement of the concentration of O_2 within the diffusion chamber as a consequence of diffusion of atmospheric O_2 through the soil cores into the diffusion chamber. The method used to determine *Dp* is explained in detail in section 3.1.2.

3.1.1 Theory

The transport and emission of gas in or from the soil is predominantly governed by the process of diffusion. The soil gas diffusion coefficient (*Dp*) is the parameter governing gas diffusion under varying gas concentration gradients. According to Fick's law "The rate of diffusion in any direction is directly proportional to the concentration gradient in that direction". The unsteady diffusion of a non- reactive gas in one dimension is described by the combination of Fick's law and the continuity equation, yielding the following equation (Rolston and Moldrup, 2002):

$$\varepsilon\left(\frac{\partial C}{\partial t}\right) = D_p\left(\frac{\partial^2 C}{\partial x^2}\right) \qquad [3.1]$$

where:

ε = soil air-filled porosity (m^3 air m^{-3} soil),

C = gas concentration (g gas m^{-3} soil air),

Dp = gas diffusion coefficient (m^3 soil air m^{-1} soil s^{-1}),

t = time (s),

x = distance through soil, which in most cases is the height to the soil surface (m).

If the boundary and initial conditions are known, then the gas diffusivity of a soil core can be calculated by placing a soil core above a chamber as shown in Figure 3.1. If it is assumed that ε is constant in space and time, then the solution for the concentration in the chamber is given at any time > 0 by the following equation (Carslaw and Jaeger, 1959) (Fig 3.1):

$$C_r = \frac{C - C_s}{C_o - C_s} = \sum_{n=1}^{\infty} \frac{2h\, exp\left(\frac{-D_p\, \alpha_n^2\, t}{\varepsilon}\right)}{L(\alpha_n^2 + h^2) + h} \qquad [3.2]$$

where:

C_r = relative gas concentration (g m^{-3}) inside the diffusion chamber,

C = gas concentration at any time $t > 0$,

C_o = gas concentration (g m^{-3}) in the diffusion chamber at $t = 0$,

C_s = the gas concentration above the soil core (g m^{-3}),

α_n = positive roots of $\alpha L\, tan\, (\alpha\, L) = hL$, which can be obtained from the table provided by Rolston and Moldrup (2002),

$h = \varepsilon / a\varepsilon_c$,

ε_c = air content of the chamber (1.0 m^3 air m^{-3}),

a = Volume of chamber (V) (m^3) per area of soil core (A) (m^2).

After a period of time > 0, terms n ≥ 2 will be negligible and equation [3.2] reduces to equation [3.3] (Rolston, 1986) where α_1 is the first positive root of $\alpha L\, tan\, (\alpha\, L) = hL$ with $n = 1$

$$C_r = \frac{C - C_s}{C_o - C_s} = \frac{2h\, exp\left(\frac{-D_p\, \alpha_1^2\, t}{\varepsilon}\right)}{L\,(\alpha_1^2 + h^2) + h} \qquad [3.3]$$

The slope ($-Dp\, \alpha_1^2/\varepsilon$) of the plot of $ln\, (C - C_s / C_o - C_s)$ i.e. C_r vs. time (t), is used to determine Dp from the known values of ε and α_1.

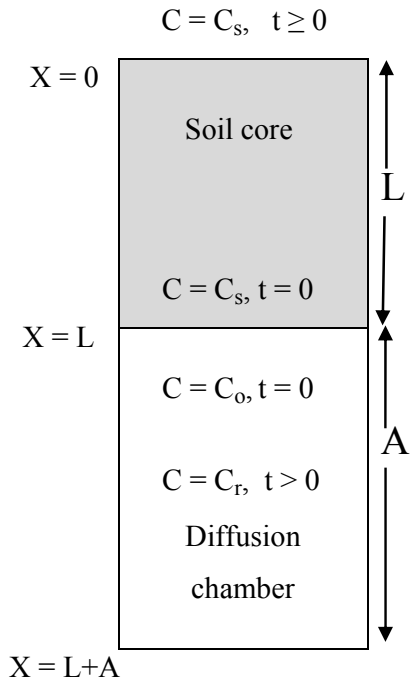

Figure 3.1 An example of boundary conditions when a soil core is placed above a diffusion chamber (Rolston and Moldrup, 2002)

3.1.2 Apparatus for determination of soil gas diffusion coefficient (*Dp*)

The gas diffusion coefficient (*Dp*) was measured on soil cores based on the method which uses changes in O_2 concentrations in the diffusion chamber to calculate gas diffusivities. Accurate determinations of the O_2 concentration in the chamber were critical to the success of the diffusion measurements. Professor Per Moldrup (Aarhus University, Denmark) and Professor Dennis Rolston (University of California, USA) were consulted on 'state of the art' methodologies for determining gas diffusion prior to constructing the apparatus.

The resulting apparatus was based on the design described by Rolston (1986) where a diffusion chamber (vessel) is sealed and conditions inside the chamber are stabilized, i.e. the chamber was purged with an appropriate gas mixture (position A, Fig. 3.2), prior to a horizontal slide being shifted (position B, Fig. 3.2) to expose the bottom of the soil surface to the diffusion chamber.

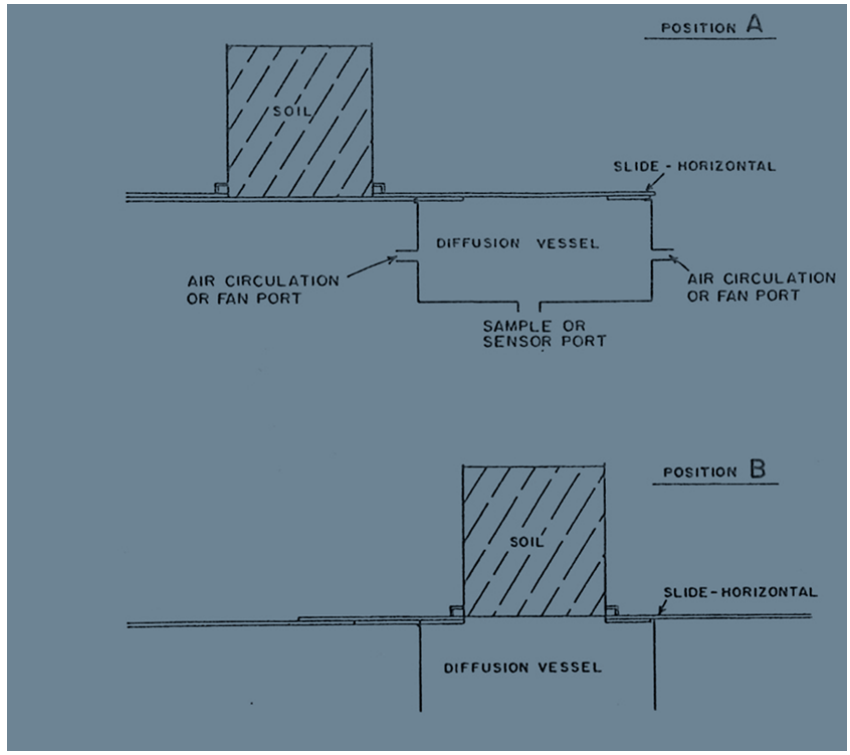

Figure 3.2 Diffusion apparatus diagram (Rolston 1986).

A picture of the constructed soil gas diffusion apparatus used in the following experiments is shown in Fig. 3.3. It consisted of an inert aluminium block machined to create a chamber (1.3 L) which has three ports sealed with rubber septa. One port was used for the gas inlet and the other one was used to check gas leakage, while the third port was used to connect O_2 sensors placed inside the diffusion chamber with the data logger and a computer. The perspex sliding plate on the diffusion chamber was lubricated with Vaseline to provide the required gas-tight seal. Two rubber-O rings, one at the base of the horizontal plate and other immediately below the soil core slot, provided gas-tight seals during the diffusion chamber operation. In this study five diffusion chambers were used simultaneously with each chamber attached to one O_2 sensor.

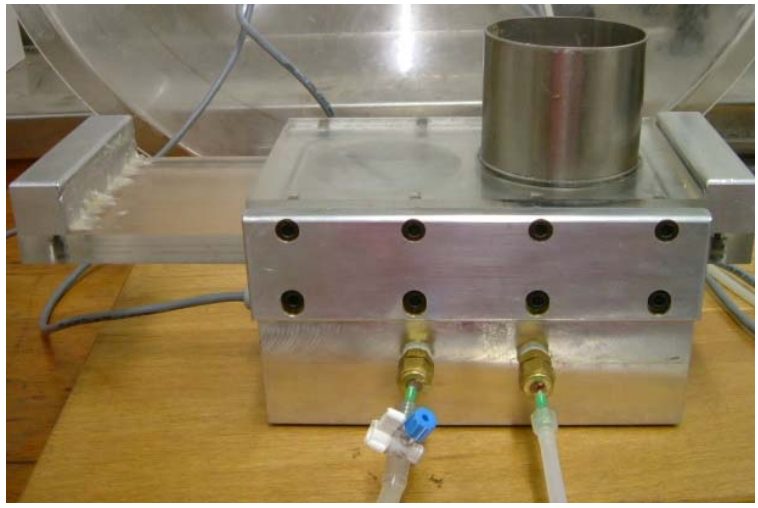

(a) Position A

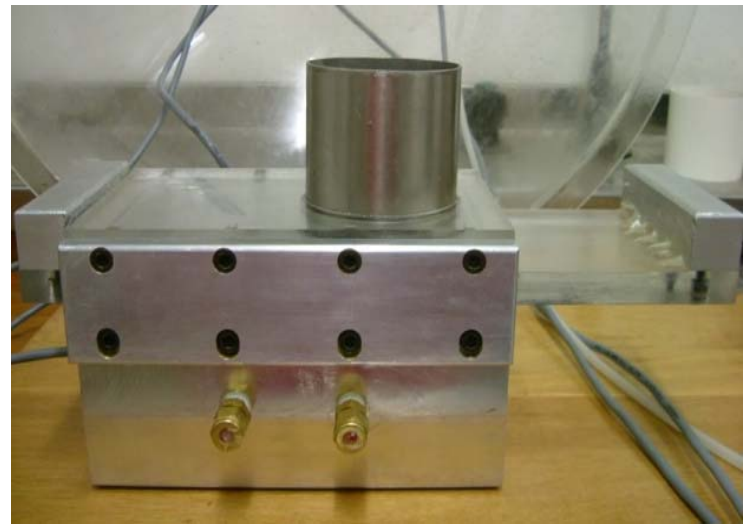

(b) Position B

Figure 3.3 **(a) A diffusion chamber being made O_2 free (b) horizontal slide shifted to allow O_2 diffusion from atmosphere through the soil core into the chamber. Diffusion apparatus shown above is a modification of the apparatus used by Rolston (1986).**

3.1.3 Description and calibration of O_2 sensors

The O_2 sensors, model KE-25 from Figaro engineering Inc. (Osaka, Japan) were used to measure O_2 concentrations in the diffusion chambers (Fig. 3.4). These sensors are galvanic cell type sensors with long life and excellent chemical durability. Each sensor consists of a lead O_2 cell with a lead anode and a gold cathode inside a specific acid electrolyte. The sensor works by allowing O_2 molecules to diffuse through a non-porous fluorine resin membrane into the electrochemical cell. The electrical current that flows between the electrodes is proportional to the O_2 concentration in the gas mixture being analysed. The signal is read as terminal voltages across the thermistor and resistor, with the change in output voltages representing the change in O_2 concentration.

The sensor provides a linear output voltage signal relative to O_2 concentration in the sample**.** The O_2 sensor is equipped with temperature compensation circuitry that uses a thermistor situated inside the sensor's body.

Figure 3.4 KE-25 O_2 sensors

Calibration of the O_2 sensors was undertaken according to the instructions provided by the sensor manufacturer (Figaro Engineering Inc.). Control, monitoring and automation of diffusion measurements were performed using a CR1000 data logger (Campbell Sci., Logan, UT).

The CRBasic Program was used for soil gas diffusion measurements. The accuracy of the measurements was critical and completely depended on the programming of the data logger, thus the CRBasic program was written carefully and specifically to calculate relative O_2 concentrations inside the diffusion chamber apparatus and to control the simultaneous working of all five diffusion chambers.

The O_2 sensors were calibrated in gas mixtures containing 0%, 30% and 99.9% O_2. To construct a standard curve (Fig 3.5) all the sensors were placed inside a diffusion chamber and then the chamber was purged with gas (90% Ar and 10% N_2) to remove all O_2. The system was left for 8 h to become stabilized and the output voltage represented the 0% O_2 condition. Similarly calibrations were performed at 30% and 99% O_2 by using standard gases (Southern Gas Services Ltd, Christchurch, NZ) containing 30% O_2 and 70% N_2 and 99.9% O_2 + 0.1% N_2, respectively. The standard curves established had a linear form ($y = mx + c$) where y was the output voltage in mV and x the standard gas concentration of O_2 (%). To calculate an unknown concentration (x) the linear equation was rearranged to get the multiplier and offset for each O_2 sensor and the values were incorporated in the CRBasic program.

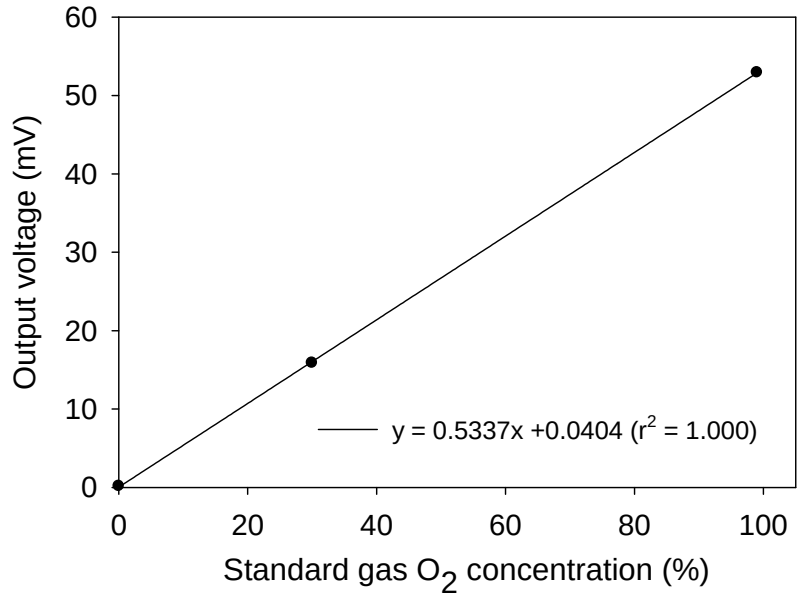

Figure 3.5 Calibration curve for KE-25 O_2 sensor.

3.1.4 Procedure for relative gas diffusivity (D_p/D_o) determination

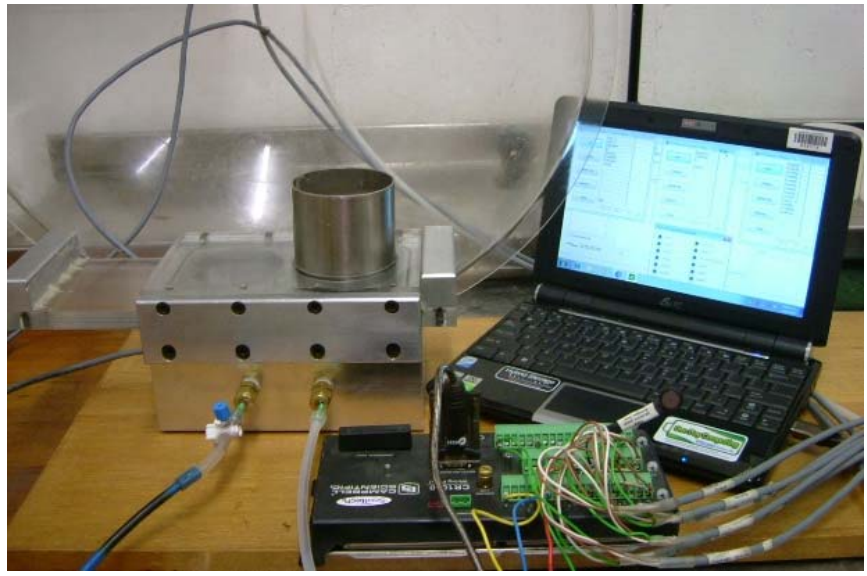

Figure 3.6 The experimental set up comprising a diffusion chamber, datalogger and a computer for monitoring.

The whole experimental set up for measuring relative gas diffusivity is shown in the Figure 3.6. At the start of a gas diffusivity determination the perspex slide was closed (Position A, Fig 3.3a), effectively sealing the chamber. Then a gas mixture comprising 90% Ar and 10% N_2 was used to purge the diffusion chamber until the O_2 content inside it was 0%. A gas mixture of Ar and N_2 was used as it has similar soil gas diffusivity to that of air (Rolston 1986). During this time the upper surface of the soil core was still exposed to the atmospheric O_2 concentration (21%, C_s). Then the Perspex slide was moved to position B (Fig. 3.3b) to permit the diffusion of O_2 through the soil core into the chamber and O_2 readings commenced and were taken every five minutes for a period of 2-3 h (Chamindu Deepagoda et al., 2011a). The O_2 concentration was measured as a function of time in the diffusion chamber. A graph of ln (C_r) vs. t was then plotted where C_r is the relative O_2 concentration inside the diffusion chamber. An example of a graph of ln (C_r) vs. t is shown in the Fig 3.7. Regression of the linear part of the plot was performed and the slope of this line corresponded to $-D_p \alpha_1^2/\varepsilon$. The value of Dp was then calculated from the value of α_1 found in Table 46-1 from Rolston and Moldrup (2002) and ε (m^3 air m^{-3} soil) was obtained from known soil core data (section 3.4).

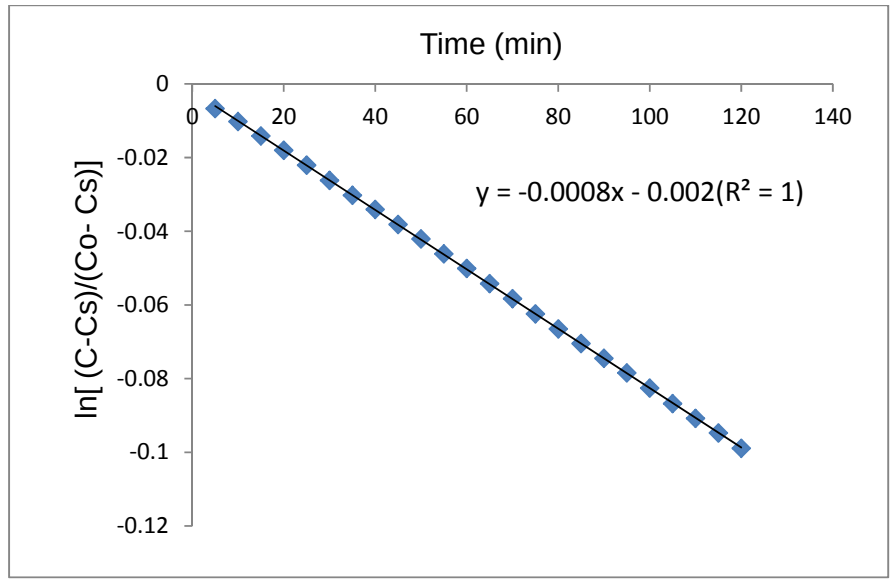

Figure 3.7 Example of ln (Cr) vs. time graph plotted for the diffusion coefficient measurements.

Diffusion chambers were routinely checked for gas leakage before and after experiments by observing the O_2 concentrations inside each closed chamber after it has been made O_2 free. Changes in the atmospheric pressure outside the diffusion chambers were negligible throughout the experiment being monitored continuously by a barometric pressure sensor (Apogee Instruments Inc.) attached to the datalogger. All diffusivity experiments were determined at 25°C. The relative gas diffusivity at 25°C was calculated as a ratio of *Dp* (O_2 diffusion coefficient in soil) to *Do* (O_2 diffusion coefficient in air) where *Do* at 25°C was 0.074 $m^2\ h^{-1}$, which was calculated based on the equation 3.4 given by Currie (1960).

$$D_{T2} = D_{T1}\left(\frac{T_2}{T_1}\right)^{1.72} \qquad [3.4]$$

where D_{T1} and D_{T2} are O_2 diffusion coefficients at temperatures 0°C (273K) and 25°C (298K), respectively. The value of the O_2 diffusion coefficient in air at 0°C was taken to be 0.178 $cm^2\ s^{-1}$ (Rolston and Moldrup, 2002) equivalent to 0.064 $m^2\ h^{-1}$. The diffusion coefficients were only measured for 120-180 minutes (2-3 h) and it is assumed using this method that error in the measured *Dp* value, due to O_2 consumption, in the repacked soil is insignificant (< 1.5%) (Moldrup et al., 2000b).

3.2 Soil core preparation

The soil used for making soil cores was obtained from the 0-15 cm depths where it had been under arable cropping. It was then air-dried and sieved to < 2 mm. The gravimetric water content of the soil (θ_g) was determined. In order to determine the amount of dry soil required (M_s) to obtain the required soil ρ_b (Mg m^{-3}) the following equation 3.5 was used,

$$M_s = \rho_b \,.\, V_s + \theta_g \,.\, \rho_b \,.\, V_s \qquad [3.5]$$

where:

M_s = mass of dry soil (g),

V_s = volume of the soil cores (m^3),

θ_g = gravimetric water content (g water g^{-1} dry soil).

A fixed amount of water was then added to the soil, prior to packing with the exact amount dependent on the resulting soil ρ_b and after that soil cores were prepared by packing the soil to a depth of 4.1 cm into stainless steel (SS) cylinders (7.3 cm internal diameter, 7.1 cm deep). A snug fitting tool was used to compress the soil uniaxially into the SS cylinders to ρ_b of 1.1, 1.2, 1.3, 1.4 and 1.5 Mg m^{-3}. To obtain uniform bulk densities, soil was compressed into the SS rings in four stages, 1 cm depth at a time. The bottom of each ring was covered with a fine nylon mesh to prevent any soil loss. To ensure that the required ρ_b had been obtained using the above method, some initially made soil cores (Chapter 4) were dried in oven at 105 ^{o}C for 24 h. Soil ρ_b was then calculated using the following equation 3.6:

$$\rho_b = \frac{M_s}{V_s} \qquad [3.6]$$

where:

ρ_b = soil bulk density (Mg m^{-3}),

M_s = Mass of dry soil (g),

V_s = Volume of soil core (m^3),

3.3 Head space gas sampling and analysis

Soil cores were placed in new 1 L paint tins equipped with pre-fitted gas tight rubber septa. It was assumed that there would be no loss of gases from below the soil cores as they were placed on the flat surface inside the paint tins. Thus only surface fluxes were measured. Ambient air samples were taken at time zero (t_0) and headspace gas samples (10 mL) for N_2O determination were taken at 15 (t_1) and 30 minutes (t_2) after sealing the headspace, using a 20 mL glass syringe fitted with a 3-way tap and 25 gauge 0.5 x 16 mm needles (Precision Glide, Becton- Dickinson, NJ). Each gas sample was transferred into a pre-evacuated (-1 atm.) 6 mL vial (Exetainer® tubes, Labco Ltd, UK) for N_2O determination by gas chromatography (section 3.3.1).

An isotope ratio mass spectrometer (PDZ Europa Ltd, Crewe, UK) interfaced to a TGII cryfocusing unit (PDZ-Europa Ltd 20-20) was used to determine the ^{15}N enrichment of the N_2O and N_2 in the gas sample (Stevens and Laughlin, 1998). Each gas sample (15 mL) was taken using a gas-tight syringe after the headspace of the tin in which soil core was placed, had been sealed for 3 h and was then transferred into a pre-evacuated 12 mL vial (Exetainer ® tubes, Labco Ltd, UK). Fluxes of N_2 were calculated using the equations of Mulvaney and Boast (1986) for triple collector mass spectrometers.

3.3.1 Determination of N_2O by gas chromatography

Nitrous oxide fluxes were determined using an automated GC (8610, SRI Instruments, Torrance, CA) interfaced to an autosampler (Gilson 222XL, Middleton, WI) as described by Clough et al. (2006). The autosampler had a purpose-built double concentric injection needle (PDZ Europa Ltd, Crewe, UK) which enabled rapid transfer of the entire gas sample from the Exetainer into the GC. The GC had two 3 mm OD SS columns; a 1 m long pre-column preceded a 6 m long analytical column, both packed with Haysep Q. An automated 10-port gas sampling valve on the GC sent the O_2-free N_2 carrier gas (40 ml min^{-1}) through both pre-column and analytical column in either 'inject' or 'back flush' modes. A 4-port gas sampling valve attached at the posterior of the analytical column was synchronized to send the gas stream to the detector.

Nitrous oxide concentrations were quantified with a ^{63}Ni electron capture detector (ECD) operated at 310^{o}C. The GC was calibrated by a series of standard gases interspersed with reference standards. The N_2O fluxes (equation 3.7) were calculated according to the equation given by Hutchinson and Mosier (1981).

$$F_{N2O} = \frac{V_c\,(C_1-C_o)^2}{(2C_1-C_2-C_o)}\; ln\left[\frac{C_1-C_o}{C_2-C_1}\right]\; \frac{P\,.\,M\,.\,C}{[G_c(T_k+T_c)]A_c t_1} \qquad [3.7]$$

where:

F_{N2O} = nitrous oxide flux (µg N_2O-N m^{-2} h^{-1}),

C_o = N_2O concentration at time t_o (µL L^{-1}),

C_1 = N_2O concentration at time t_1 (µL L^{-1}),

C_2 = N_2O concentration at time t_2 (µL L^{-1}),

P = atmospheric pressure (Pa) 101325,

V_c = chamber volume (m^3),

A_c = Chamber area (m^2),

G_c = Gas constant (JK^{-1} mol^{-1}) (8.314),

T_k = absolute temperature at 0^{o} (K) (273.15),

T_c = air temperature (^{o}C),

M = molecular weight of N_2O-N (g mol^{-1}) (28.0134),

C = minutes / hour (60),

t_o = start of cover period (min),

t_1 = t_2 / 2 (min),

t_2 = total cover period.

3.4 Soil measurements

Destructive sampling of repacked soil cores was performed at periodic intervals during the experiments. The soil from each core was extruded, mixed and then sub-sampled to determine changes in bulk soil pH, inorganic N concentrations and dissolved organic carbon (DOC).

3.4.1 Soil pH

When soil surface pH was measured, prior to core destruction, it was performed using a flat surface pH electrode (Broadley- James Corp, Irvine, CA.). If bulk soil pH was measured, it was performed by diluting soil samples at 2.5:1 by adding 25 mL of deionized water to 10 g of air-dried soil (Blakemore et al., 1987). The mixture was shaken for 30 s by hand and left to settle for a minimum of 12 h before measuring bulk soil pH with a pH meter (Mettler Toledo, USA). Buffer solutions of pH 4.0 and 7.0 were used for the calibration of the pH meter.

3.4.2 Gravimetric and volumetric soil moisture content and WFPS

Gravimetric soil moisture content (θ_g) was measured by weighing 10 g of sub-sampled soil from each soil core in a dish of known weight and then drying this in an oven at 105^{o}C for 24 h. The mass of wet soil and oven dry soil was recorded and θ_g was calculated using the following equation 3.8.

$$\theta_g = \frac{M_w - M}{M} \quad [3.8]$$

where:

θ_g = gravimetric soil content (g water g^{-1} oven dry soil),

M_w = mass of wet soil (g),

M = mass of oven dry soil (g).

Volumetric moisture (θ_v) content (m^3 water m^{-3} soil) was obtained by multiplying θ_g by the respective soil ρ_b (Mg m^{-3}).

Water-filled pore space (WFPS) was determined (%) using equation 3.9

$$WFPS = \frac{\theta_v}{\phi} \times \frac{100}{1} \quad [3.9]$$

where: ϕ is the soil total porosity (m^3 air m^{-3} soil).

3.4.3 Total porosity, Air-filled porosity and Pore continuity

Soil total porosity (ϕ) expressed in m^3 air m^{-3} soil was calculated using soil ρ_b and an assumed particle density (ρ_p) of 2.65 Mg m^{-3} (equation 3.10).

$$\phi = \frac{1-\rho_b}{\rho_p} \quad [3.10]$$

Air-filled porosity (ε) expressed in m^3 air m^{-3} soil was calculated by using ϕ and θ_v as follows:

$$\varepsilon = \phi - \theta_v \quad [3.11]$$

An index of pore continuity (C) (dimensionless ratio) was also derived as the ratio of *Dp/Do* to ε (Ball et al., 1988).

3.4.4 Inorganic Nitrogen

Soil inorganic N determinations were made by extracting the sub-sampled soil with 2M KCl at a 1:10 ratio. The extract was shaken for 1 h on a reciprocal shaker. The solution was then filtered into a 100 mL plastic bottle. All the samples were stored in a freezer at 4°C until analysis. The NH_4^+-N, NO_2^--N and NO_3^--N were analysed using Flow Injection Analysis (FIA) (Blakemore et al., 1987). The inorganic-N concentration of each sample was calculated using the following equation:

$$N = \frac{N_i \times V}{M} \quad [3.12]$$

where:

N = inorganic-N content (µg g^{-1} soil),

N_i = inorganic-N content of the extract (µg mL^{-1}),

V = volume of solution (mL),

M = weight of dry soil (g).

3.4.5 Dissolved organic carbon (DOC)

Dissolved organic carbon determinations were performed by adding 30 mL of DI water to 5 g of sub-sampled moist soil into a 50 mL centrifuge tube (Ghani et al., 2003). The tubes were placed on an end over end shaker for 30 min. The samples were then centrifuged for 20 min at 3500 rpm. The supernatant was then filtered through a pre-leached filter paper (Advantec 5C) into vials for analysis. DI water blanks were included in all runs and treated in a similar way. Values of TOC were determined on a Shimadzu TOC analyser TOC 5000A (Shimadzu Oceania Ltd, Sydney, Australia).

Equation (3.13) was used to calculate the dissolved organic carbon (DOC) concentration in each sample:

$$DOC = \frac{TOC \times V}{M} \qquad [3.13]$$

where:

DOC = Dissolved organic carbon (µg g^{-1} soil),

TOC = Total organic carbon in the extract (µg mL^{-1}),

V = volume of solution (mL),

M = weight of dry soil (g).

3.5 Water retention curves and pore size distribution

Water retention curves were used to determine the pore size distribution of the compacted soil. Soil was packed into SS cylinders at five ρ_b levels (1.1, 1.2, 1.3, 1.4 and 1.5 Mg m^{-3}) with each ρ_b replicated 4 times. All the cores were saturated from below for three days and subsequently drained at corresponding negative matric potentials of 0.5, 1, 1.5, 2, 3, 4, 5, 6, 7, 8, 9 and 10 kPa using tension tables. Soil cores were then weighed at each respective tension and then oven dried to determine θ_g values. Pressure plate apparatus was used to measure soil θ_g at negative water potentials of 20, 50, 100, 500 and 1500 kPa after draining at the respective potentials and drying in the oven. Volumetric water contents were determined using θ_g and ρ_b.

The diameter of the largest pore size filled with water at any given ψ was calculated using the modified form of the relation used by Schjønning et al. (2003):

$$d = \frac{300}{\psi} \quad [3.14]$$

where:

d = diameter of the largest pore size filled with water (µm),

ψ = matric potential (kPa).

The water retention curves for each ρ_b were then determined by plotting θ_v content against ψ. The volumes of the various pore size fractions were then calculated as the difference between θ_v at any two ψ. Following Walczak et al. (2002), the pore sizes were categorized as:

- Total pore space, i.e., θ_v at 0 kPa or saturation;
- Macroporosity, pores with diameter > 30 µm, i.e., difference in θ_v between 0 kPa and -10 kPa;
- Mesoporosity, pore with diameter between 30 to 0.2 µm, i.e., difference in θ_v between -10 kPa and -1500 kPa;
- Microporosity, pore with diameter < 0.2 µm, i.e., θ_v at -1500 kPa.

Chapter 4

Effect of soil bulk density on relative gas diffusivity and urea-derived N_2O and N_2 fluxes measured under a constant matric potential

4.1 Introduction

Soil compaction is known to increase soil bulk density (ρ_b) and soil water content. Soil ρ_b, a measure of soil compaction, has been reported to range from 0.77 to 1.32 Mg m^{-3} during *in situ* animal treading trials (Drewry et al., 2001; Thomas et al., 2008). In forage grazing systems intensive animal treading leads to compaction of wet soils (Menneer et al., 2005b; Thomas et al., 2008) creating anaerobic conditions that favour denitrification and higher N_2O emissions (van Groenigen et al., 2005; Bhandral et al., 2007; Uchida et al., 2008). Increasing the ρ_b of a loamy sand soil from 1.4 to 1.8 Mg m^{-3}, at a water-filled pore space (WFPS) of 60%, resulted in total ^{15}N losses increasing by a factor of 3.6 due to denitrification (Torbert and Wood, 1992).

Many studies have opted to use WFPS to report effects of water content on soil N_2O emissions (Smith et al., 1998; Abbasi and Adams, 2000; Ruser et al., 2006). However use of WFPS as a predictor of N_2O from a soil or soils under varying ρ_b has been questioned by Farquharson & Baldock (2008). They suggested using either air-filled porosity (ε) or volumetric water content (θ_v) from such soils. Since diffusion of gases in soil is controlled by ε (Farquharson and Baldock, 2008), the potential of *Dp*/*Do* to predict N_2O emission from soil or soils varying in ρ_b should be investigated.

Diffusion of a gas in the soil occurs through interconnected pores with diffusion rates decreasing as the proportion of water-filled pores increases, which further restricts O_2 diffusion into and within the soil profile, resulting in higher N_2O emissions (Ball et al., 1999) and also increasing its chances to be reduced to N_2. Few studies have attempted to relate direct measurements of *Dp*/*Do* with N_2O emissions. *In situ* N_2O emissions were found to increase from N-fertilized soil, when diffusivity of freon-22 was reduced from 1.9 to 1.5 mm^2 s^{-1} following soil compaction (Sitaula et al., 2000). McTaggart et al. (2002) demonstrated a strong relationship between *Dp*/*Do* and cumulative N_2O emissions from intact, fertilized (120 kg-N ha^{-1}), soil cores for four soil types, maintained at three different moisture tensions.

It has also been shown that soil gas diffusivity (*Dp*/*Do*) was a better predictor of N_2O emissions than WFPS in a study that examined repacked soil, amended with nutrient solutions and adjusted to three matric potential (ψ) levels (-1.5 to -10 kPa) (Andersen and Petersen, 2009). However, no studies have examined the role of increasing soil bulk density on *Dp*/*Do* and N_2O and N_2 emissions simultaneously following ruminant urine deposition to soil.

Therefore the aim of this controlled laboratory experiment was to measure *Dp*/*Do* of a soil following compaction and assess the relationships between *Dp*/*Do* and the ensuing gas fluxes (N_2O and N_2) and the N_2-N: N_2O-N ratios. It was hypothesised that at a constant ψ of -10 kPa, the subsequent urea deposition would lead to increases in both N_2O and N_2 fluxes with increasing soil ρ_b as a consequence of a decrease in *Dp*/*Do*.

4.2 Materials and Methods

4.2.1 Soil and treatments

Repacked soil cores were constructed using a silt-loam soil (Templeton silt loam, Typic Immature Pallic, NZ Soil Classification (Hewitt, 1998) collected (0-15 cm) from the Duncan Block, Lincoln University (43º 38' 0.7" S, 172º 29' 40" N), that had been air-dried and sieved to ≤ 2 mm. The soil texture comprised of 23% sand, 52% silt and 25% clay. Soil nitrogen (N), carbon (C), and organic matter contents were 2.6, 29.5 and 50 g kg^{-1} respectively, with a soil pH of 6.0. Soil was packed into stainless steel cylinders (section 3.3) to ρ_b of 1.1, 1.2, 1.3 and 1.4 Mg m^{-3}. The bottom of each cylinder was covered with a fine nylon mesh (0.1 mm) in order to prevent soil egress. To obtain uniform ρ_b during packing, the soil was carefully compressed uniaxially in four stages, 1 cm at a time, using a snug fitting compression tool.

An initial set of packed soil cores was made in order to determine the water content of the repacked soil cores, for each ρ_b treatment, at -10 kPa (field capacity). In order to achieve this, each ρ_b treatment was replicated 8 times (4 for WFPS and the other 4 for ρ_b) and then all cores were saturated with water for two days prior to being placed on tension tables at -10 kPa. After the soil cores had equilibrated at this tension for 1 week, half of the cores were removed to measure ρ_b and the other half were destructively analysed to determine gravimetric water content (θ_g), soil inorganic N and DOC. Soil cores for ρ_b were dried in an oven at 105°C for 24 h to ascertain whether the soil compacting method used in this experiment resulted in the desired ρ_b.

A second set of 100 cores was then made consisting of ρ_b treatments replicated four times in a randomized complete block design which allowed for five destructive samplings on days 7, 14, 21, 28 and 35. The five treatments were: no urea + ρ_b 1.1 Mg m^{-3} (control), urea + ρ_b 1.1 Mg m^{-3}, urea + ρ_b 1.2 Mg m^{-3}, urea + ρ_b 1.3 Mg m^{-3} and urea + ρ_b 1.4 Mg m^{-3}. The soil cores were packed with soil that had been wetted with deionised water to a moisture content that still allowed for the subsequent addition of the urea solution so that the final soil moisture content of the cores at the various bulk densities equalled the WFPS levels at field capacity (previously calculated using the first set of cores) at -10 kPa.

Two urea solutions (U1 and U2) with an N content of 10 g L^{-1} were used to simulate urine application. The urea N in the U1 solution had a ^{15}N enrichment of 50 atom% excess, relative to ambient air. The U2 solution was not enriched with ^{15}N (natural abundance). Urea solutions were applied (30 mL $core^{-1}$) at a conservative N rate of 700 kg ha^{-1} (Haynes and Williams, 1993). The U1 solution was applied to cores which were used to measure soil gas diffusion coefficients and the N_2O-^{15}N and N_2 -^{15}N fluxes throughout the experiment and which were destructively analysed on day 35 of the experiment. The U2 solution was applied to soil cores which were destructively analysed on days 7, 14, 21 and 28. Control cores were treated in an identical manner to those receiving urea solutions with the exception that they received 30 mL of distilled water, instead of urea. Resources did not permit a non-urea control for each level of ρ_b used (a further 60 cores). However, the use of the ^{15}N stable isotope permitted a direct measure of the treatment effects on the urea applied. The second set of 100 soil cores was then placed on tension tables set at -10 kPa during the 35 day period in a controlled temperature room (mean 24^{o}C, range 23^{o}C to 25^{o}C).

It is also recognised that artificial urine may not generate the same N_2O fluxes as ruminant urine (Kool et al., 2006). However, over 70% of the N in urine is present as urea (Bathurst, 1952; Haynes and Williams, 1993) and it is this major component of urine that undergoes hydrolysis, and subsequent N transformation. Since the aim of this study was not to derive relative N_2O emission factor data but to examine the relative effects of soil compaction and associated gas diffusivity on N_2O and N_2 fluxes under controlled conditions, urea was chosen over ruminant urine so as to have more control on the form of N input. This also enabled the use of a highly ^{15}N enriched substrate that facilitated N_2 flux measurement.

The reason for performing this experiment in controlled conditions was to minimize variability in N_2O and N_2 emissions by precisely controlling the ρ_b levels which is not possible *in situ*. This study was designed to run for 35 days only and not until the substrate was exhausted since there was no plant uptake or leaching of the soil NO_3^--N pool occurring.

4.2.2 Gas flux sampling and analyses

To measure N_2O and N_2 fluxes, the soil cores were taken off the tension tables and placed into 1 L stainless steel tins equipped with gas-tight lids pre-fitted with rubber septa. Ambient air samples were taken at time zero and headspace gas samples (10 mL) were taken at 15 and 30 minutes after sealing the headspace, using a 20 mL glass syringe fitted with a 3-way tap and 25 gauge 0.5 x16 mm needles (Precision Glide, Becton- Dickinson, NJ). Each gas sample was transferred into pre-evacuated (-1 atm) 6 mL vials (Exetainer® tubes, Labco Ltd, UK). Gas flux sampling was performed on days 1, 2, 3, 4, 5, 6, 7, 8, 10, 12, 14, 18, 21, 24, 28, 31 and 35.

Gas samples (15 mL) for the determination of ^{15}N enrichment of the N_2O and N_2 molecules were taken on days 4, 7, 20, 24, 31 and 35, after the headspace had been sealed for 3 h. These samples were again taken with a gas-tight syringe and transferred to a pre-evacuated 12 mL vial (Exetainer ® tubes, Labco Ltd, UK). An isotope ratio mass spectrometer (PDZ Europa Ltd, Crewe, UK) was used to determine the ^{15}N enrichment of the N_2O and N_2 (Stevens and Laughlin, 1998).

4.2.2.1 Soil analysis

Soil cores were destructively analysed for inorganic N and DOC on days 7, 14, 21, 28 and 35 (section 3.4). Soil surface pH was measured with a flat surface pH electrode after every 7 days (Section 3.4.1) (Broadley- James Corp, Irvine, CA.). Soil *Dp*/*Do* values were measured (section 3.1) on days 1 and 35. The net NH_4^+-N depletion rates and net NO_3^--N accumulation rates were calculated by regression of NH_4^+-N and NO_3^--N concentrations versus time (Venterea and Rolston, 2000).

4.2.2.2 Dye penetration method

A dye penetration experiment was also performed to assess the maximum penetration depth of the applied urea solution under varying ρ_b treatments. The low toxicity tracer dye 'Brilliant Blue FCF' is easily visible in a soil matrix (Flury and Fluhler, 1994). Air-dried and sieved soil (< 2mm) was packed into stainless steel cylinders at ρ_b of 1.1, 1.2, 1.3 and 1.4 Mg m^{-3} that had been brought to the same moisture content as the cores receiving urea solutions. Dye powder was mixed with water (6 g L^{-1}) and 30 mL was applied to repacked soil cores which were then placed on a tension table at -10 kPa. Then, 24 h later, the cores were excavated in 0.5 cm depth increments. Each 0.5 cm increment was carefully scraped clean of smeared dye and visually inspected for the presence of dye in each layer. A photographic record was also made (Fig. 4.4).

4.3 Statistical analysis

Data were tested for normality using the Anderson-Darling test (Anderson and Darling, 1952). Soil N_2 fluxes were log transformed using ln (flux+1) prior to analyses. Regression analyses were performed to assess the relationships of *Dp*/*Do* and WFPS with cumulative N_2O-N and N_2-N fluxes. Piecewise regression/split-line regression was performed to assess the relationship between cumulative N_2-N fluxes and other variables. The equation for piecewise linear regression continuous at x = c is explained as follows:

$$y_1 = a_1 + b_1 x \quad for\ x \leq c \qquad [4.1]$$

$$y_2 = a_2 + b_2 x \quad for\ x > c \qquad [4.2]$$

where:

a_1, a_2 = intercepts on y axis

b_1, b_2 = slope of the two straight lines

c = breakpoint

The two equations (4.1 and 4.2) are equal at breakpoint c and a_2 can be derived as

$$a_2 = a_1 + (b_1 - b_2)c \qquad [4.3]$$

Now the two equations (4.1 and 4.2) can be written as:

$$y_1 = a_1 + b_1 x \qquad for\ x \leq c \qquad [4.4]$$

$$y_2 = a_1 + (b_1 - b_2)c + b_2 x \qquad for\ x > c \qquad [4.5]$$

Pearson correlations were also performed. To test for differences between means, one-way ANOVA was performed on individual days. Tukey's test was used to determine which means were significantly different from one another. All statistics were performed using Minitab (Version 15).

4.4 Results

4.4.1 Soil physical and chemical properties (first set of cores)

Soil cores at high ρ_b had higher WFPS at -10 kPa even though there were only small differences in volumetric water content (θ_v) (Table 4.1). However, there were small differences in the inorganic N content and DOC due to ρ_b (Table 4.2). No statistical analysis was performed on this data. This preliminary and basic information about the effect of ρ_b in the absence of urea was gathered before the start of the experiment along with WFPS values for the second set of cores. Soil ρ_b obtained after soil compaction were similar to the desired ρ_b levels.

Table 4.1 Mean volumetric water content, Total porosity and WFPS of the compacted cores at -10 kPa, n = 4. Standard deviations are in brackets.

Desired Bulk density (Mg m^{-3})	Bulk density obtained (Mg m^{-3})	Volumetric water content (m^3 m^{-3})	Calculated total porosity (m^3 m^{-3})	WFPS (%)
1.1	1.12 (0.02)	0.25 (0.02)	0.58 (0.00)	42 (4.1)
1.2	1.20 (0.17)	0.28 (0.02)	0.55 (0.00)	51 (4.5)
1.3	1.28 (0.03)	0.30 (0.01)	0.51 (0.00)	58 (2.5)
1.4	1.41 (0.03)	0.31 (0.03)	0.47 (0.00)	66 (6.7)

Table 4.2 Soil inorganic N and dissolved organic carbon (DOC) of the compacted cores at -10 kPa, n = 4. Standard deviations are in brackets.

Bulk density (Mg m^{-3})	Nitrate (μg NO_3-N g^{-1} soil)	Ammonium (μg NH_4-N g^{-1} soil)	DOC (μg C g^{-1} soil)
1.1	4.89 (1.49)	9.68 (0.96)	38.93 (5.06)
1.2	5.44 (2.58)	8.38 (1.44)	45.55 (4.69)
1.3	5.60 (1.62)	8.64 (1.27)	43.45 (3.84)
1.4	5.23 (2.12)	11.43 (3.57)	44.23 (4.48)

4.4.2 Second set of cores

4.4.2.1 Soil physical characteristics

Since total porosity (ϕ) declined and WFPS increased with increasing ρ_b, ϵ declined with increasing ρ_b on days 1 and 35 (Tables 4.3 and 4.4), correlating positively with Dp/Do ($r = 0.95$, $p < 0.01$), and negatively with WFPS ($r = -0.99$, $p < 0.01$; Table 4.3). Pore continuity (C) declined as soil ρ_b increased on days 1 and 35 (Tables 4.3 and 4.4). The mean values of Dp/Do ranged from 0.07 to 0.008 on day 1 and 0.06 to 0.01 on day 35, decreasing with increasing ρ_b on both days (Tables 4.3 and 4.4).

Table 4.3 Mean soil physical characteristics of soil cores maintained at -10 kPa measured on day 1, n = 4. Standard deviations are in brackets.

	Soil ρ_b (Mg m^{-3})			
	1.1	**1.2**	**1.3**	**1.4**
Water-filled pore space WFPS (%)	44 (0.96)	51 (1.16)	61 (2.95)	70 (0.91)
Air-filled porosity (m^3 voids m^{-3} soil)	0.32 (0.006)	0.27 (0.006)	0.20 (0.016)	0.14 (0.004)
Calculated total porosity (m^3 voids m^{-3} soil)	0.58 (0.000)	0.55 (0.000)	0.51 (0.000)	0.47 (0.000)
Volumetric water content (m^3 water m^{-3} soil)	0.26 (0.006)	0.28 (0.006)	0.31 (0.016)	0.33 (0.004)
Relative diffusion coefficient (Dp/Do)	0.063 (0.008)	0.037 (0.012)	0.026 (0.007)	0.008 (0.005)
Pore continuity (C)	0.19 (0.03)	0.14 (0.04)	0.13 (0.03)	0.06 (0.04)

Table 4.4 Mean soil physical characteristics of soil cores maintained at -10 kPa measured on day 35, n = 4. Standard deviations are in brackets.

	Soil ρ_b (Mg m^{-3})			
	1.1	**1.2**	**1.3**	**1.4**
Water-filled pore space WFPS (%)	42 (1.61)	51 (2.17)	58 (1.80)	67 (1.4)
Air-filled porosity (m^3 voids m^{-3} soil)	0.33 (0.009)	0.27 (0.011)	0.21 (0.009)	0.15 (0.006)
Calculated total porosity (m^3 voids m^{-3} soil)	0.58 (0.000)	0.54 (0.000)	0.51 (0.000)	0.47 (0.000)
Volumetric water content (m^3 water m^{-3} soil)	0.25 (0.009)	0.28 (0.011)	0.30 (0.009)	0.31 (0.006)
Relative diffusion coefficient (*Dp/Do*)	0.061 (0.007)	0.039 (0.004)	0.026 (0.003)	0.013 (0.003)
Pore continuity (*C*)	0.18 (0.02)	0.14 (0.01)	0.12 (0.02)	0.08 (0.02)

4.4.2.2 Soil inorganic N

Ammonium (NH_4^+-N) concentrations ranged from 103 to 2.4 µg g^{-1}dry soil when urea was absent. Higher concentrations occurred ($p < 0.01$) under urea application and by day 7 mean values ranged from 1178 to 979 µg g^{-1}dry soil. In the presence of urea, lower NH_4^+-N concentrations occurred ($p > 0.05$) under the highest ρ_b except on day 35 (Fig. 4.1a). After day 14, soil NO_3^--N concentrations were lower ($p < 0.05$) in the control treatment (33.3 to 123.3 4 µg g^{-1}dry soil) than in the urea-treated cores where concentrations ranged from 295 to 329 µg g^{-1}dry soil by the end of the experiment (Fig. 4.1b). The effect of ρ_b on soil NO_3^--N was significant ($p < 0.05$) on days 7, 14 and 28 with higher concentrations at the highest ρ_b until day 14, after which the trend reversed. Soil NO_2^--N concentrations remained low in the control treatment (< 0.39 µg g^{-1}) but increased ($p < 0.05$) after urea application and on day 21 peak concentrations of 53 and 54 µg g^{-1} dry soil were observed in the 1.1 and 1.2 Mg m^{-3} ρ_b treatments respectively (Fig. 4.1c).

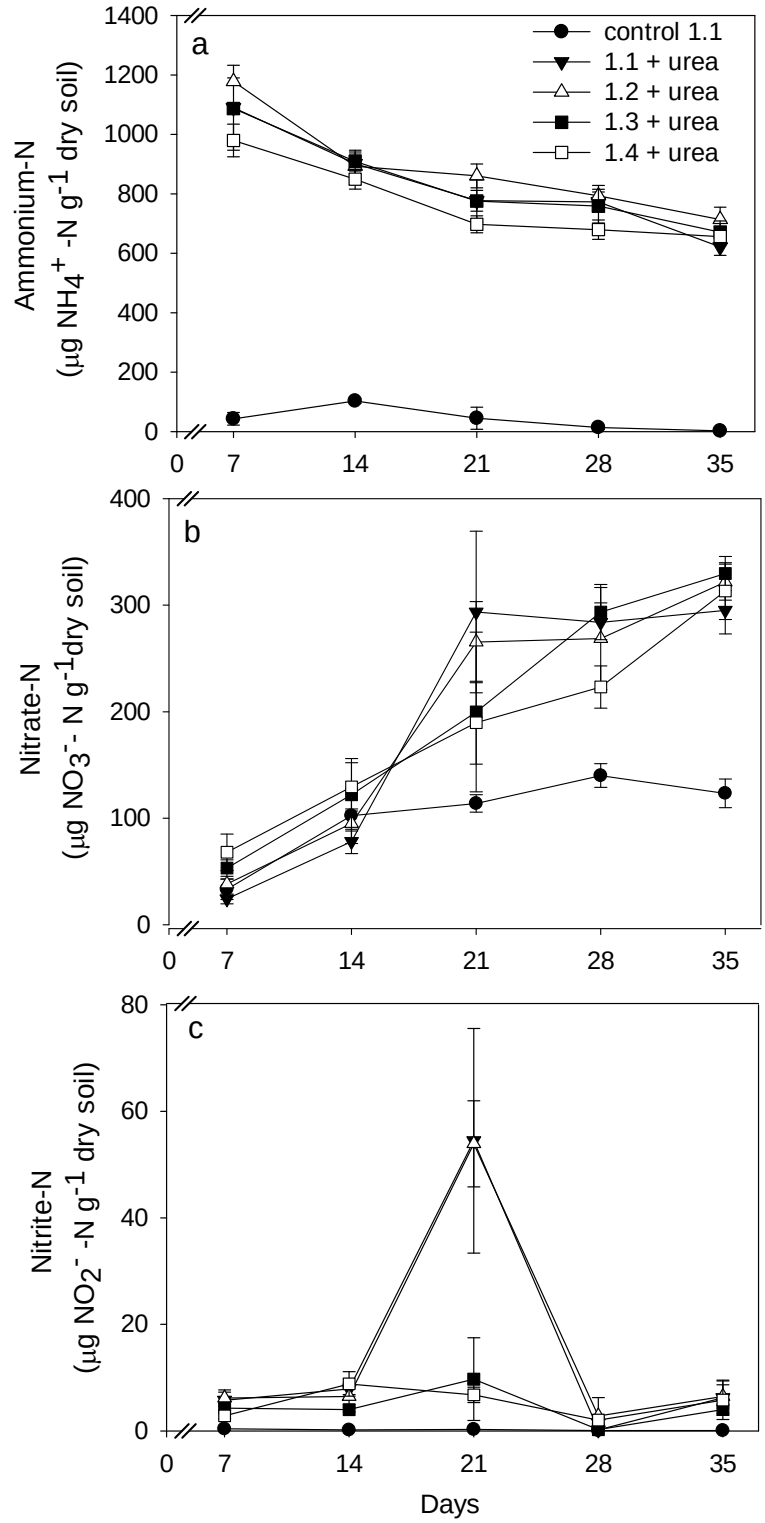

Figure 4.1 Mean soil inorganic-N concentrations over time after urea application. Error bars = s.e.m, n = 4.

As values of *Dp*/*Do* decreased with increases in ρ_b, both NH_4^+-N depletion rates and NO_3^--N accumulation rates decreased (Table. 4.5) with lower NO_3^--N accumulation rates ($p < 0.01$) and NH_4^+-N depletion rates ($p < 0.01$) at 1.4 Mg m^{-3} than at 1.1 Mg m^{-3}.

Table 4.5 Effect of soil bulk density (ρ_b) on relative gas diffusivity (*Dp*/*Do*), ammonium (NH_4^+) depletion rates and nitrate (NO_3^-) accumulation rates. Standard deviations in brackets, n = 4. Values in a column that do not share a common letter are significantly different ($p < 0.05$, Tukey's test).

Soil ρ_b (Mg m^{-3})	*Dp*/*Do* (day 35)	NH_4^+-N depletion rate (ng g^{-1} h^{-1})	NO_3^--N accumulation rate (ng g^{-1} h^{-1})
1.1	0.061 (0.007)**a**	702 (66.6)**a**	454 (31.1)**a**
1.2	0.039 (0.004)**b**	612 (50.1)**a**	441 (20.7)**a**
1.3	0.026 (0.003)**c**	584 (77.4)**ab**	426 (25.6)**a**
1.4	0.013 (0.003)**d**	466 (57.1)**b**	323 (27.9)**b**

4.4.2.3 Soil surface pH and DOC

In the control, the soil surface pH, as expected, was significantly lower than in the urea treatments. At day 7, soil surface pH was higher (8-9) in urea-treated soil, ($p < 0.01$) after which it declined to be in a range of 6.1 to 6.3 at day 35 with no differences due to ρ_b treatments at any time (Fig. 4.2). Pooling data over time showed soil NO_3^--N concentrations were negatively correlated with soil surface pH ($r = -0.62$, $p < 0.01$).

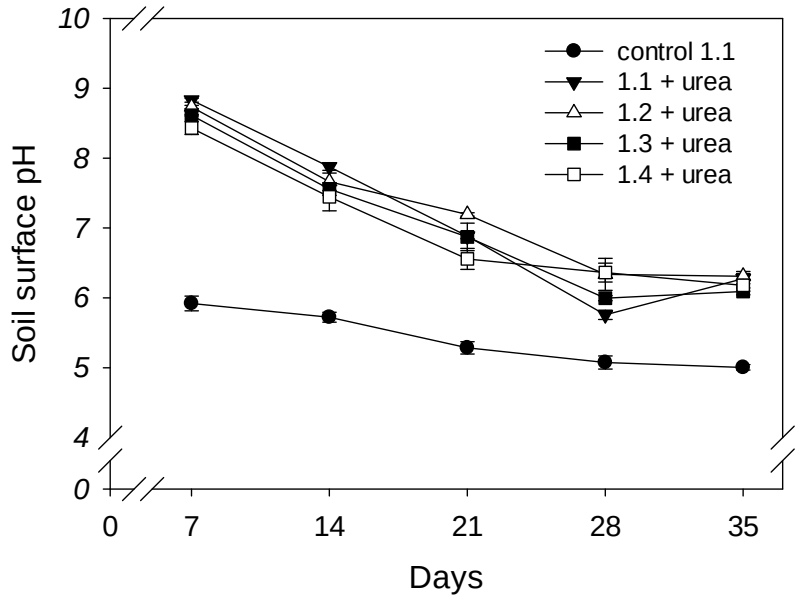

Figure 4.2 Mean surface soil pH over time after urea application. Error bars = s.e.m, n = 4.

In the control, soil DOC concentrations ranged from 21 to 44 μg g^{-1}dry soil. With urea application these concentrations increased (range 94 to 703 μg g^{-1}dry soil), peaking at day 7 and declining thereafter (Fig. 4.3). Mean DOC concentrations were lower ($p < 0.05$) under the higher ρ_b for all days except days 21 and 35 (Fig. 4.3). Soil surface pH was positively correlated with DOC on day 7 ($r = 0.86$, $p < 0.01$) and day 14 ($r = 0.85$, $p < 0.01$).

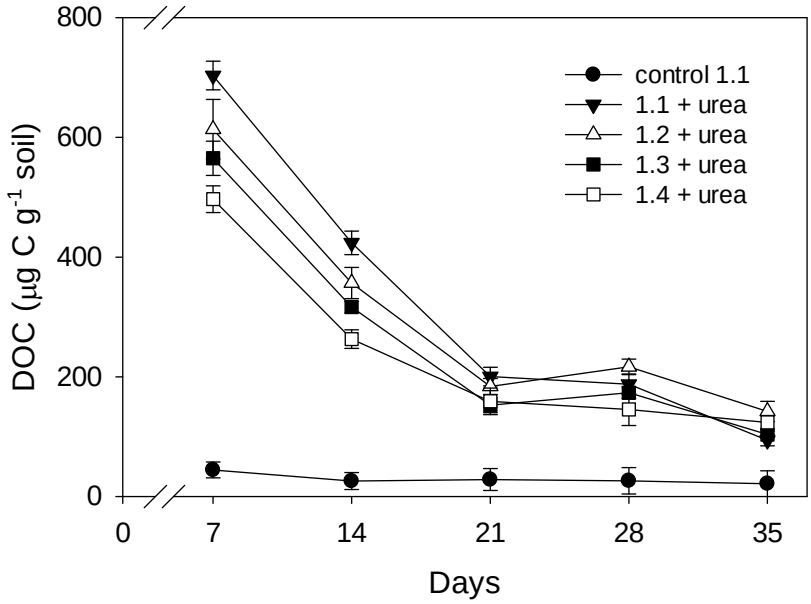

Figure 4.3 Mean concentrations of dissolved organic carbon (DOC) over time after urea application. Error bars = s.e.m, n = 4.

4.4.2.4 Brilliant Blue dye test

The average penetration depth of the 'Brilliant Blue' dye ranged from 4 to 3 cm for the 1.1 and 1.4 Mg m^{-3} ρ_b treatments, respectively (Fig. 4.4), with penetration depth decreasing with increasing ρ_b ($p < 0.01$). Soil DOC concentrations at day 7 and day 21 correlated with the depth of dye penetration ($r \geq 0.84$, $p < 0.01$, and $r \geq 0.61$, $p < 0.01$, respectively).

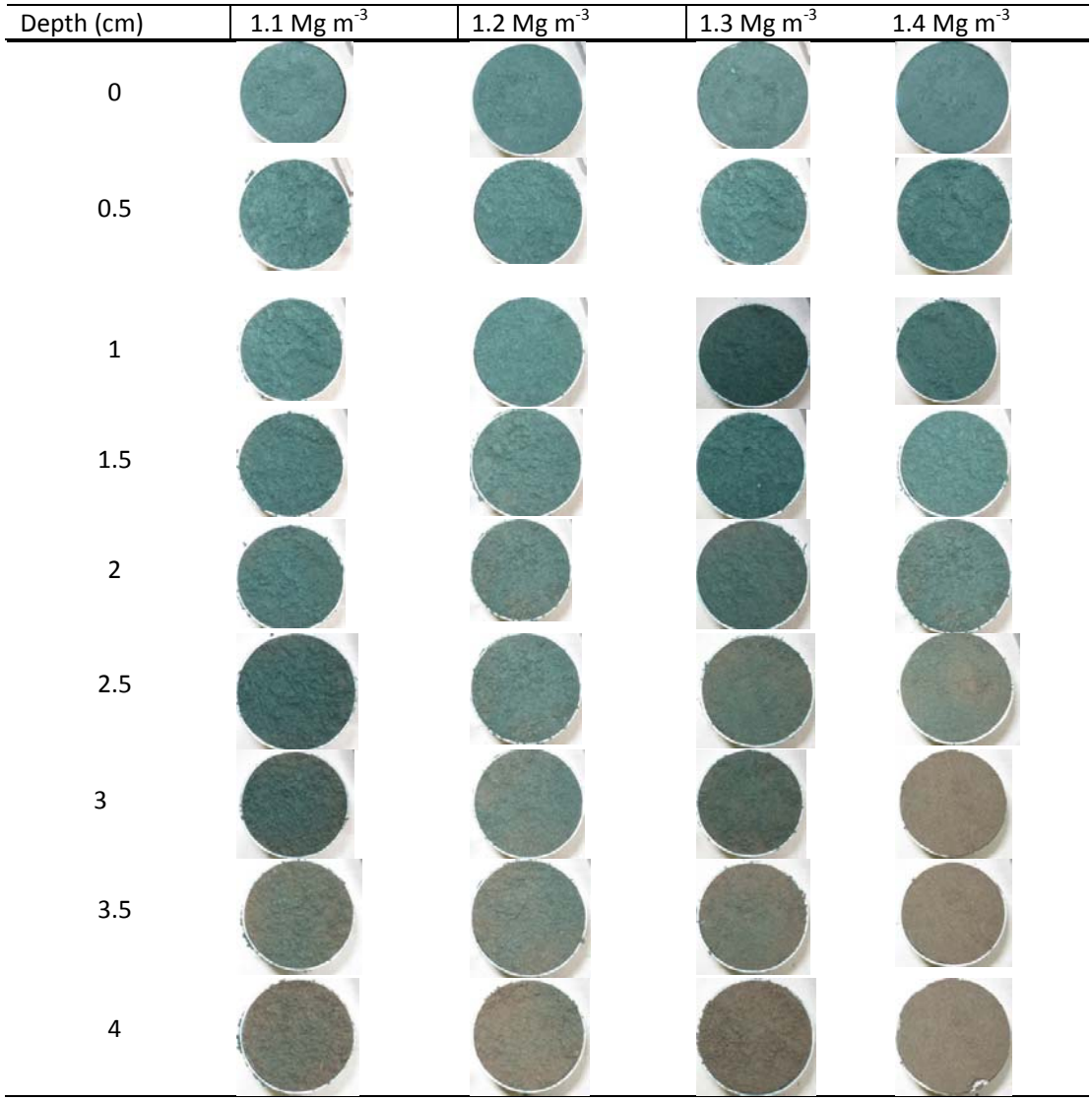

Figure 4.4 Photographs of soil core increments showing penetration of Brilliant Blue dye at different soil bulk density (Mg m^{-3}) levels.

4.4.2.5 N_2O and N_2 fluxes

Control treatment N_2O-N fluxes ranged from 0 to 128 µg N_2O-N m^{-2} h^{-1}. The mean N_2O-N fluxes from urea-treated cores varied ($p < 0.01$) with ρ_b (10-10,300 µg N_2O-N m^{-2} h^{-1}) with higher fluxes at 1.4 Mg m^{-3} (Fig. 4.5a). After 35 d mean cumulative N_2O-N emissions, as a percentage of N applied, ranged from 0.05 to 2.14% (Fig. 4.5b), increasing with increasing ρ_b ($p < 0.01$). The atom % ^{15}N enrichments of the N_2O fluxes ranged from 2.3 to 45 atom% ^{15}N, increasing rapidly until day 12 whereupon they remained constant at ca. 45 atom %. The ^{15}N enrichment of the N_2O-N flux was higher ($p < 0.01$) in the 1.4 Mg m^{-3} treatment than in the other treatments on all sampling occasions prior to day 12 (Fig. 4.6).

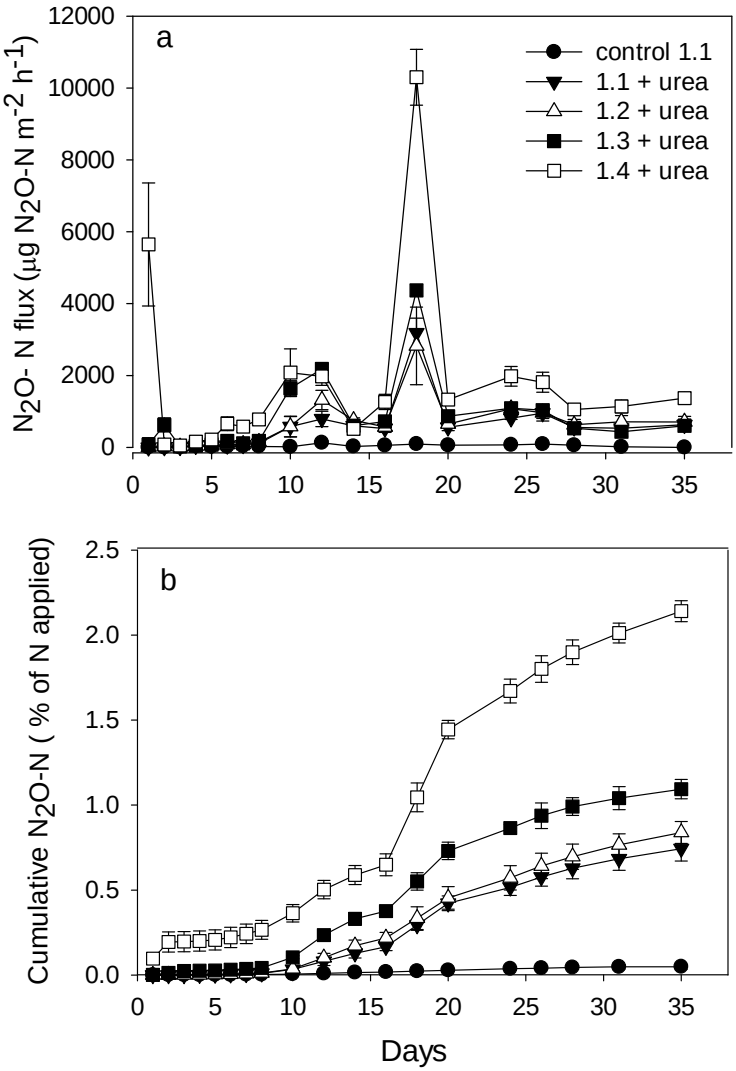

Figure 4.5 (a) Nitrous oxide emissions from different soil ρ_b treatments following urea application (b) Cumulative loss of N_2O from urea-treated soils, showing the amount of N emitted as N_2O-N as a percentage of the total N applied to the soil cores. Error bars = s.e.m, n = 4.

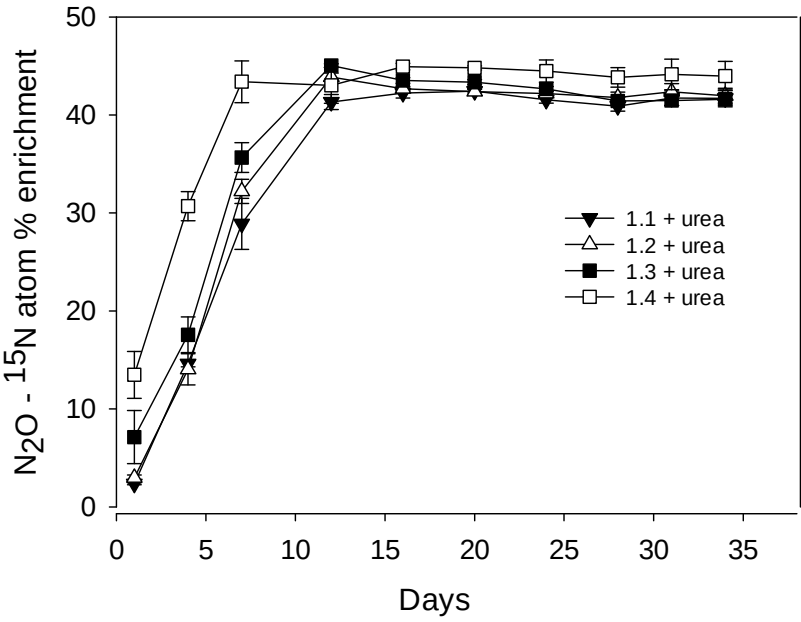

Figure 4.6 Mean ^{15}N atom % enrichment of N_2O-N. Error bars = s.e.m, n = 4.

Mean N_2-N fluxes ranged from 552 to 4,950 µg m^{-2} h^{-1} (Fig. 4.7a) and were generally higher ($p < 0.01$) at ≥ 1.3 Mg m^{-3}. Cumulative N_2-N emissions as a percentage of N applied, also increased with increasing ρ_b ($p < 0.01$), ranging from 0.06 to 4.97% after 35 days (Fig. 4.7b). Mean values of $^{15}X_N$ (the mole fraction of ^{15}N in the N pool from which the N_2 or N_2O was derived) were 0.29 (0.02), 0.32 (0.03), 0.43 (0.02), 0.43 (0.01) for the 1.1, 1.2, 1.3 and 1.4 Mg m^{-3} ρ_b treatments, respectively (standard deviations in brackets).

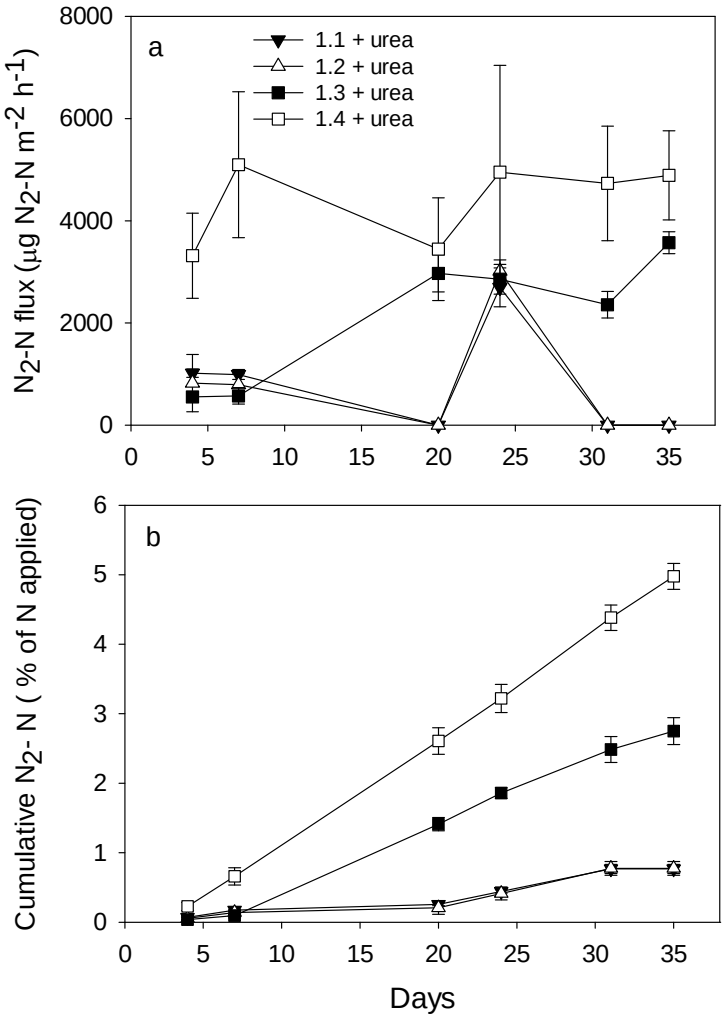

Figure 4.7 (a) Mean N_2-N fluxes over days following urea application (b) Cumulative loss of N_2 from urea-treated soils, showing the amount of N emitted as N_2-N as a percentage of the total N applied to the cores. Error bars = s.e.m, n = 4.

The mean N_2-N: N_2O-N ratio was 27 at day 4 and declined thereafter, with no significant effect of ρ_b treatments on the ratio at any sampling occasion while no N_2-N: N_2O-N ratios were obtained from ρ_b 1.1 and 1.2 Mg m^{-3} on days 31 and 35 (Fig. 4.8). The cumulative N_2-N: N_2O-N ratio increased significantly ($p < 0.01$) at 1.3 and 1.4 Mg m^{-3} (Fig. 4.9).

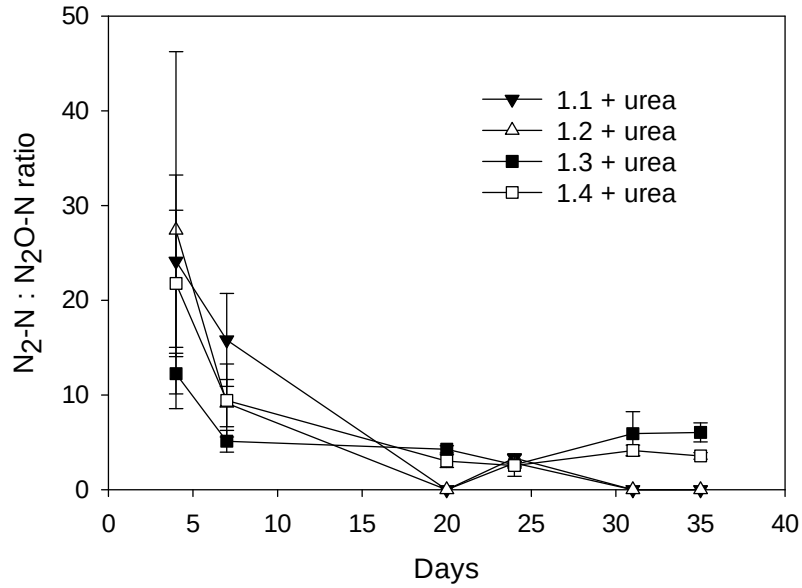

Figure 4.8 Mean N_2-N: N_2O-N ratios over time. Error bars = s.e.m, n = 4.

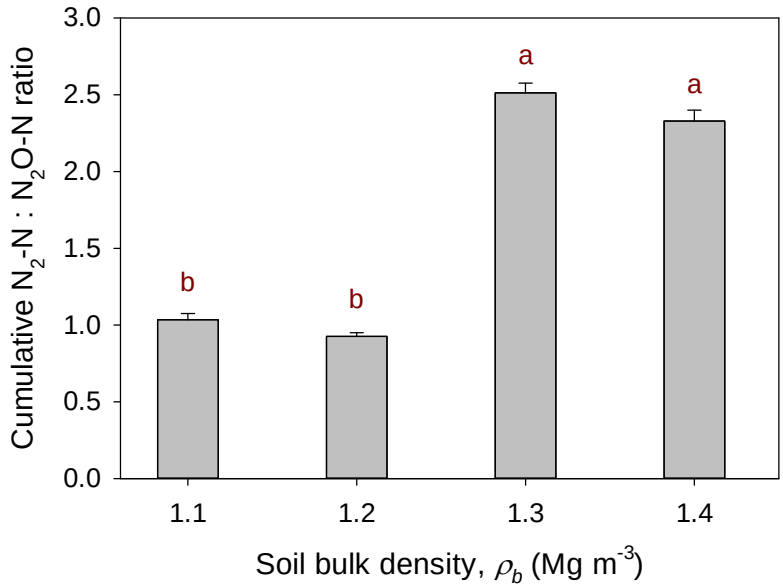

Figure 4.9 Cumulative N_2-N: N_2O-N ratio plotted against soil ρ_b (Mg m^{-3}). Means that do not share a lower case letter are significantly different (Tukey's test, $p < 0.05$). Error bars = s.e.m, n = 4.

4.4.2.6 Relationship of cumulative N_2O-N and N_2-N fluxes with *Dp*/*Do* and WFPS

Negative exponential relationships were derived when cumulative N_2O fluxes were plotted against *Dp*/*Do* (Fig. 4.10a) while a positive exponential relationship was observed with WFPS (Fig. 4.11a). A piecewise linear regression satisfactorily described the relationship between cumulative N_2-N fluxes and *Dp*/*Do* with the break point in the cumulative fluxes of N_2-N occurring when *Dp*/*Do* equalled 0.038 (Fig 4.10b). Similar piecewise regressions described the relationship between cumulative N_2-N fluxes and WFPS with the breakpoint occurring at WFPS equalled 52.5 % (Fig. 4.11b).

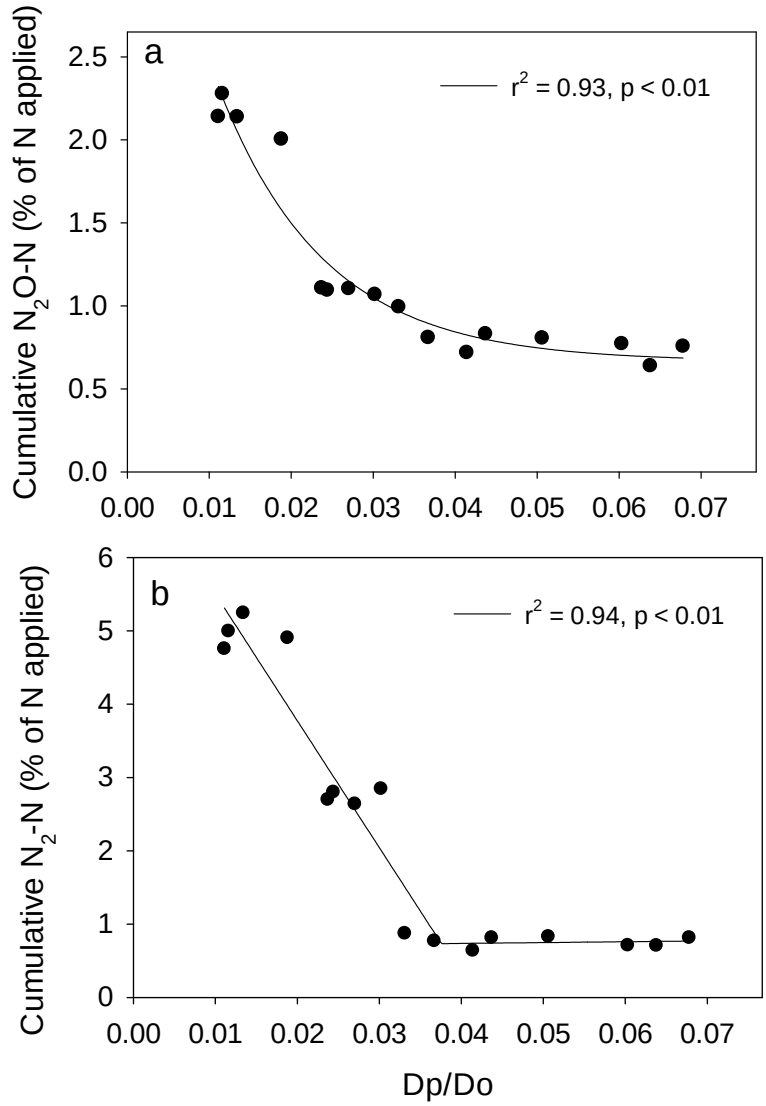

Figure 4.10 Scattergram of (a) cumulative N_2O-N fluxes and *Dp*/*Do* (day 35) (b) cumulative N_2-N fluxes and *Dp*/*Do* (day 35). Data points represent individual replicates. Exponential (three-parameter) and piecewise linear regression fitted to cumulative N_2O-N and cumulative N_2-N flux data, respectively. The intersection of the two lines in (b) is the breakpoint or trigger point which occurs at *Dp*/*Do* = 0.038 (s.e.m 0.003).

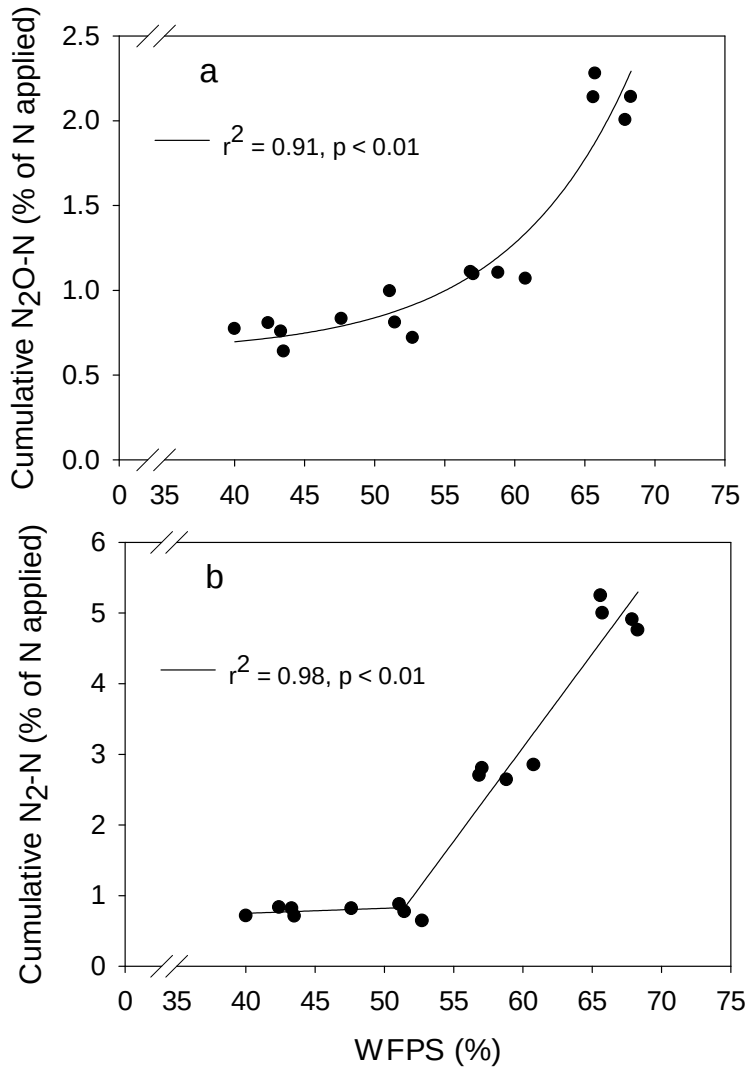

Figure 4.11 Scattergram of (a) cumulative N_2O-N fluxes with WFPS (b) cumulative N_2-N fluxes with WFPS. Data points represent individual replicates. Exponential (three-parameter) and piecewise linear regression fitted to cumulative N_2O-N and N_2-N flux data, respectively.

4.5 Discussion

4.5.1 Substrate supply for N_2O and N_2 production

Dominant pathways for N_2O production include nitrification, nitrifier-denitrification and denitrification, with the latter two processes also able to form N_2 (Wrage et al., 2001; Kool et al., 2011). Nitrifiers, utilise ammonia (NH_3) sourced from NH_4^+ (Suzuki et al., 1974), while denitrifiers, are capable of reducing NO_3^-, NO_2^-, nitric oxide (NO) or N_2O, ultimately to N_2. The concentrations of NH_4^+ were sufficient for nitrification to occur. The observed decrease in the NH_4^+-N depletion rate, with increasing soil ρ_b, was almost certainly due to a progressive limitation of O_2 as *Dp*/*Do* decreased. Russow et al. (2009) clearly demonstrated the sensitivity of nitrification to O_2 concentration by showing that NH_4^+-N contributions to the NO_2^--N pool progressively decreased from 88, 33, 2 and 0%, as O_2 concentrations were reduced to 20, 2, 0.3 and 0%, respectively. Despite progressive reductions in NO_3^--N accumulation with increasing ρ_b there was sufficient NO_3^--N present for denitrification (> 5μg g^{-1} soil) in all treatments (Ryden, 1982). However, this decline in the rate of NO_3^--N accumulation was only statistically significant at 1.4 Mg m^{-3}. The decline in the rate of NO_3^--N accumulation as *Dp*/*Do* decreased was likely the net result of decreasing NH_4^+-N oxidation rates and enhanced denitrification rates. The latter is a consequence of reduced soil aeration as *Dp*/*Do* decreased with increased ρ_b.

Again, the study of Russow et al. (2009) provides an example of how the contribution of denitrification to the NO_2^- pool increases rapidly as soil O_2 levels decrease, with contributions equalling 12, 67, 98 and 100% at O_2 concentrations of 20, 2, 0.3 and 0%, respectively.

Increases in DOC concentrations following urea addition can be attributed to solubilisation of soil organic matter (Monaghan and Barraclough, 1993) due to the high soil pH that ensues as a consequence of urea hydrolysis (Doak, 1952; Sherlock and Goh, 1984). The subsequent decline in the surface soil pH over time occurs as a consequence of H^+ release during NH_3 volatilization and nitrification (Bremner and Blackmer, 1981).The progressively lower DOC concentrations observed, as ρ_b increased, possibly occurred because the depth of penetration of the urea solution declined as ρ_b increased, as indicated by the dye test performed (Fig. 4.4). Therefore the soil volume exposed to the high pH was reduced and thus the amount of C solubilised was also reduced as ρ_b increased. The lower DOC values at higher ρ_b potentially have implications for the rate of denitrification, a heterotrophic process, and the ratio of N_2-N: N_2O-N which increases as C supply increases (Firestone and Davidson, 1989).

4.5.2 Gas diffusion, N_2O, N_2 emissions and N_2-N: N_2O-N ratios

The increase in N_2O emissions following soil compaction is consistent with previous studies (van Groenigen et al., 2005; Uchida et al., 2008; Beare et al., 2009) and the cumulative losses of N_2O-N after 35 d, as a percentage of N applied were of a typical magnitude to those observed in the field from ruminant urine studies (Clough et al., 1996; Oenema et al., 1997; Yamulki et al., 1998; de Klein et al., 2003).

The relatively high N_2O fluxes that occurred under urea with the reduced gas diffusivity and restricted soil aeration in the 1.3 and 1.4 Mg m^{-3} treatments follow the trend previously observed *in situ* under tillage systems by Ball et al. (1999b), who found N_2O fluxes increased as both *Dp*/*Do* and air-filled pore space decreased, as a consequence of increasing ρ_b and heavy rainfall influencing WFPS. McTaggart et al. (2002) also found a negative exponential relationship between cumulative N_2O flux and either air-filled pore space or *Dp*/*Do* (r^2 range 0.53-0.55) in intact soil cores of different soil types. In the current study regression analysis explained more of the variation between cumulative N_2O flux and *Dp*/*Do* (Fig. 4.10a) than that observed by McTaggart et al. (2002), possibly due to the use of repacked soil cores.

However, direct comparisons are not valid due to difference in the experimental conditions and duration. The study by McTaggart et al. (2002) also found a rapid increase in N_2O fluxes when air-filled porosity fell below 10-15% corresponding to a WFPS of > 80%. A similar effect is seen in the current study with cumulative fluxes of N_2O increasing significantly at an air-filled porosity of ~ 20% (Table 4.3).

In the current study WFPS or *Dp*/*Do*, were both able to explain equally well the variability in cumulative N_2O-N fluxes (Fig. 4.10a and 4.11a). However, given previous questioning of the suitability of WFPS to describe N_2O fluxes across a range of soil ρ_b it was not expected that WFPS would be as effective at explaining the variation in cumulative N_2O emissions.

Increasing ρ_b reduces total porosity and alters pore size distribution, increasing the proportion of smaller pores. Thus at a constant matric potential (ψ), WFPS will increase with ρ_b due to the increasing amounts of soil water being retained by the increasing proportion of smaller pores. While WFPS and *Dp*/*Do* were equally effective at predicting N_2O emissions in this study this may not hold for soils of varying texture or at varying ψ and this needs to be investigated further.

The author is not aware of any previous studies that have examined the relationship between cumulative N_2-N fluxes and *Dp*/*Do*. The significant increase in the cumulative N_2-N flux at a ρ_b ≥ 1.3Mg m^{-3}, when *Dp*/*Do* was ≤ 0.026, possibly indicates that a 'trigger or break' point (Fig. 4.10b) was reached with respect to N_2 production. Statistically, piecewise linear regression showed this break point occurred at a *Dp*/*Do* value of 0.038. The 'trigger' for increasing N_2 fluxes occurs, as shown by Russow et al. (2009), when soil O_2 consumption exceeds diffusive supply, leading to anaerobic conditions. Production of N_2 increases at this trigger point because O_2 inhibition of N_2O reductase, the enzyme controlling N_2O reduction to N_2, decreases. Inhibition of N_2O reductase at O_2 concentrations of >5% has been previously reported (Tiedje, 1988; Zumft, 1997; Murray and Knowles, 2003) and variation in critical O_2 concentrations may be due to the fact that microbial taxa may vary in terms of their N_2O reductase response (Cavigelli and Robertson, 2001). The activity of N_2O reductase generally increases with rising pH values, decreasing NO_3^--N concentrations and decreasing O_2 diffusion rates (Chapuis-Lardy et al., 2007). Since there were few differences between ρ_b treatments in terms of surface soil pH values and NO_3^--N concentrations, the factor that most likely triggered the sharp increase in the N_2 flux at ≥ 1.3 Mg m^{-3} was the decrease in the diffusion of O_2 into the soil. Like this study, the ^{15}N tracing approach used by Russow et al. (2009) also showed non-linear increases in denitrification as O_2 concentration decreased.

Stepniewski (1981) stated that the onset of soil anaerobiosis occurs within the *Dp*/*Do* range of 0.005-0.02 which coincides with the sharp increase in N_2 fluxes observed at ≥ 1.3 Mg m^{-3} in the current study where *Dp*/*Do* was ≤ 0.026, respectively. Thus in order to explain the abrupt increase in N_2 at ≥ 1.3 Mg m^{-3} it is proposed that *Dp*/*Do* was such that O_2 consumption exceeded supply, enhancing anaerobic conditions to a point where inhibition of N_2O reductase, by O_2, ceased to be significant.

Soil compaction treatments affected the cumulative N_2-N: N_2O-N ratio which resulted in the significant increases in this ratio particularly at ≥ 1.3 Mg m^{-3}, *Dp*/*Do* ≤ 0.026. As *Dp*/*Do* declines as a result of increasing soil water content and a soil becomes more anaerobic, the ratio of cumulative N_2-N: N_2O-N should tend to infinity all other things being equal but not necessarily at a linear rate. However, when soil ρ_b increased from 1.3 to 1.4 Mg m^{-3}, *Dp*/*Do* decreased with soil ρ_b but the cumulative N_2-N: N_2O-N ratio did not increase. The lack of such a trend in the current study may have been due to a maximum N_2 flux rate being attained or N_2 becoming entrapped in the soil cores as WFPS increased (Letey et al., 1980; Clough et al., 2001).

The study by Letey et al. (1980) calculated that under saturated conditions only about 30% of the N_2 produced was evolved. A similar scenario applies to N_2O which leads to a greater opportunity for further reduction to N_2 (Chapuis-Lardy et al., 2007). Alternatively the lack of an increase in the N_2 flux may have been due to other precursors becoming rate limited such as NO_2^--N and N_2O. The net nitrification rate was lower at the highest ρ_b and its contribution to the soil NO_2^--N pool would have been reduced, potentially limiting denitrification substrate.

4.6 Conclusions

At -10 kPa increases in soil ρ_b affected net rates of NH_4^+-N depletion and NO_3^--N accumulation. Decreases in DOC concentrations with increasing ρ_b were due to ρ_b affecting the penetration of urea solution into the soil cores. There was a sharp increase in the cumulative N_2 fluxes when *Dp*/*Do* was below the threshold value. The variability in cumulative fluxes of both N_2O-N and N_2-N could be explained equally well by changes in *Dp*/*Do* and WFPS. The cumulative N_2-N: N_2O-N ratio at 1.3 and 1.4 Mg m^{-3} was nearly two times higher than at 1.1 and 1.2 Mg m^{-3}. Future work should involve experiments with similar ρ_b levels but covering the range of ψ which provide wetter soil conditions.

Chapter 5

Effect of soil bulk density on relative gas diffusivity and urea-derived N_2O and N_2 fluxes measured under increased matric potential levels

5.1 Introduction

The soil matric potential (ψ) value influences soil aeration by determining which pore size fractions are water-filled. Soil compaction results in decreases in total porosity (ϕ) and the volume of large pores, particularly pore sizes > 150 µm, with a subsequent increase in the volume of small pores and decreased soil gas diffusivity (Hill and Sumner, 1967; Stepniewski, 1981; Ball et al., 1999b; Assouline, 2006). It is also known that the magnitude of relative gas diffusivity (*Dp*/*Do*), which is dependent on air-filled porosity (ε) and ψ, controls the transport and emission of gases into, within and from the soil profile (Moldrup et al., 2005; Resurreccion et al., 2008). Thus increasing ψ (from more negative to less negative) and decreasing ϕ as a result of soil compaction can make soil anaerobic and provide conditions that are conducive to both N_2O production and N_2O reduction to N_2, which may result in a higher N_2: N_2O ratios. This ratio denotes the extent to which N_2O is reduced to N_2 and is crucial in understanding and regulating denitrification in soils (Davidson and Seitzinger, 2006).

There is a dearth of studies which have quantified the effect of varying ρ_b on both N_2O and N_2 emissions and *Dp*/*Do* at different ψ. The results from the first experiment (Chapter 4) were derived from a soil maintained at field capacity (-10 kPa). These results suggested that decreasing the value of *Dp*/*Do*, as a result of increasing ρ_b, caused N_2 emissions to rise significantly below a threshold *Dp*/*Do* value. Therefore, in this chapter two further experiments were performed as an extension of experiment 1 (Chapter 4). The experimental design was repeated but soil cores were maintained at -6.0 kPa (experiment 2a) and at-0.2 kPa (experiment 2b).The rationale for these two experiments was to extend the data sets in order to further explore the relationships between soil ψ, ρ_b and *Dp*/*Do* and their effects on N_2O and N_2 fluxes. It was hypothesised that increases in soil ρ_b with ψ increasing from -6.0 to -0.2 would make conditions more suitable for N_2O reduction to N_2 resulting in an increase in N_2-N: N_2O-N ratios.

5.2 Materials and Methods

5.2.1 Experimental design

A silt-loam soil (Templeton silt loam, Typic Immature Pallic) was collected (0-15 cm) from the Duncan Block, Lincoln University and air-dried prior to sieving to ≤ 2 mm. Two experiments were performed, one at -6.0 kPa (experiment 2a) and the other at -0.2 kPa (experiment 2b). Both experiments had five identical ρ_b treatments replicated four times. The ρ_b treatments were 1.1, 1.2, 1.3, 1.4 and 1.5 Mg m^{-3}. There were five destructive sampling times on days 1, 7, 14, 24 and 35. Controls for 1.1 and 1.5 Mg m^{-3} were also run. For each experiment, a set of 140 cores consisting of all ρ_b treatments and controls was placed on tension tables set at either -6.0 kPa (experiment 2a) or at -0.2 kPa (experiment 2b). Air temperature in the room housing the tension tables ranged from 23 to 25^{o}C (mean 24.2^{o}C).

Sieved soil was packed into SS rings (section 3.2). To obtain uniform ρ_b during packing, the soil was carefully compressed uniaxially in four stages, using a snug compression tool. The bottom of each cylinder was covered with a fine nylon mesh (0.1 mm) in order to prevent any soil loss. The soil cores were packed with soil that had been previously wetted with deionised water to a moisture content that still allowed for the subsequent addition of a urea solution to bring the soil moisture to the required WFPS level. The purpose of having soil cores, post urea application, at the pre-determined WFPS values was so that no drainage of urea solution occurred during application or after placement on the tension tables.

In order to determine the required WFPS at -0.2 kPa and -6.0 kPa, a completely separate set of soil cores was initially made where each ρ_b was replicated four times and all the cores were then saturated with water for two days prior to being placed on tension tables at -0.2 kPa and -6.0 kPa and left for one week to equilibrate. They were removed and then destructively analysed to determine gravimetric water content (θ_g) and WFPS was calculated.

For each experiment, urea solutions (A1 and A2) with an N content of 10 g L^{-1} were used to simulate urine application. The urea N in the A1 urea solution had a ^{15}N enrichment of 40 atom % excess, relative to ambient air. The A2 urea solution was not enriched with ^{15}N (natural abundance). Urea solutions were applied at a conservative rate of 700 kg-N ha^{-1} by pipetting them onto the soil surface, 30 mL per core at time zero.

The A1 solution was applied to soil cores which were used to measure the N_2O-^{15}N and N_2 -^{15}N fluxes throughout the experiment and which were destructively analysed on day 35 of the experiment. The A2 solution was applied to the soil cores which were to be destructively analysed on days 1, 7, 14 and 24. Control cores received 30 mL of distilled water.

5.2.2 Gas flux sampling and analyses

For each experiment, gas flux sampling for N_2O was performed on days 1, 2, 3, 4, 5, 6, 7, 8, 10, 12, 14, 16, 20, 24, 28, 31 and 35. Each soil core was placed in a new paint tin (1 L) equipped with a gas-tight rubber septum. For N_2O concentrations a 10 mL gas sample was taken as described in section 3.3 with a syringe and transferred into a pre-evacuated 6 mL vial (Exetainer ® tubes, Labco Ltd, UK). Gas samples (15 mL) for N_2 were taken on days 1, 3, 7, 10, 12, 14, 24, 28 and 35 using a gas-tight syringe, after the headspace had been sealed for 3 h, and samples were transferred into pre-evacuated 12 mL vials (Exetainer ® tubes, Labco Ltd, UK). Nitrous oxide and N_2 analyses and flux calculations were performed as described in section 3.3.

5.2.3 Soil analysis

Soil destructive analyses were performed on a weekly basis with DOC and inorganic N measurements made (section 3.4). Soil surface pH was measured weekly with a flat surface pH electrode (Broadley-James Corp, Irvine, CA. Values of *Dp*/*Do* (section 3.1) were also measured from urea treated cores and controls on day 7 and 35.

To determine the effect of compaction on soil water characteristics, soil water retention curves and pore size distributions were determined separately in a further experiment (2c) after experiments 2a and 2b were finished. To determine the soil water retention curve, soil cores for each ρ_b level (mentioned in section 5.2.1) were made in an identical fashion as described in the section 3.2. Four replicates were prepared giving a total of 20 soil cores. These soil cores were then used to determine water retention curves and pore size distribution as described in the section 3.5.

5.2.4 Statistical analyses

All statistical analyses were performed using Minitab (version 15). Each data set was tested for normality (Anderson and Darling, 1952). Fluxes of N_2O and N_2 concentrations were not distributed normally so were log-transformed using ln (value+1) prior to analyses (Tiedje et al., 1989). One-way ANOVA was used to determine differences among treatments on individual days with soil ρ_b as a factor and where differences occurred, Tukey's test was used to determine which means were significantly different from one another. A Repeated Measures ANOVA (General linear model, Minitab) was used to determine the interaction of time x ρ_b on N_2O and N_2 data. Regression analyses were performed using Sigmaplot (version 12) to assess the relationship between cumulative N_2-N and N_2O-N fluxes with *Dp*/*Do* and WFPS. Pearson correlation coefficients were also calculated to determine the relationships between soil variables on individual days. Least significant differences (LSD) were calculated at the 1% level of significance for net rates of change in the NH_4^+-N and NO_3^--N concentrations. The two experiments, 2a at -6.0 kPa and 2b at -0.2 kPa were performed separately, each as an individual experiment. Therefore, it was not statistically valid to analyse ρ_b x ψ interaction effects. However, the data from experiments 1, 2a and 2b are compiled and discussed in the following Chapter 6.

5.3 Results

The results are divided into two parts, experiment 2a performed at -6.0 kPa and experiment 2b performed at -0.2 kPa.

5.3.1 Results from experiment 2a (-6.0 kPa)

5.3.1.1 Soil physical conditions (-6.0 kPa)

The soil volumetric water content (θ_v) increased with increase in the ρ_b ($p < 0.01$) up to 1.4 Mg m^{-3} with no significant differences between the 1.4 and 1.5 Mg m^{-3} ρ_b treatments. The WFPS increased with increasing ρ_b ($p < 0.01$) while ε declined with increasing ρ_b ($p < 0.01$). Soil *Dp*/*Do* decreased with increasing soil ρ_b ($p < 0.01$) on both day 7 and 35 (Table 5.1). There was no effect of urea treatment on the *Dp*/*Do* values when controls at 1.1 and 1.5 Mg m^{-3} were compared with the urea-treated 1.1 and 1.5 Mg m^{-3} ρ_b treatments, repectively.

Table 5.1 Soil physical characteristics at -6.0 kPa. Values are the mean of 4 replicates with standard deviations in brackets. Values in rows that do not share a common letter are significantly different ($p < 0.05$, Tukey's test).

Soil physical characteristics	Soil bulk density (Mg m^{-3})				
	1.1	1.2	1.3	1.4	1.5
Volumetric water content (m^3 m^{-3})	0.32**d**	0.35**c**	0.37**b**	0.39**a**	0.38**ab**
	(0.006)	(0.009)	(0.006)	(0.008)	(0.005)
Water-filled pore space WFPS (%)	54**a**	64**b**	73**c**	85**d**	89**e**
	(0.98)	(1.66)	(1.21)	(1.77)	(1.24)
Air-filled porosity (m^3 m^{-3})	0.27**a**	0.19**b**	0.14**c**	0.07**d**	0.06**e**
	(0.005)	(0.009)	(0.006)	(0.008)	(0.005)
Total Porosity (m^3 m^{-3})	0.58**a**	0.55**b**	0.51**c**	0.47**d**	0.43**e**
	(0.000)	(0.000)	(0.000)	(0.000)	(0.000)
Dp/Do (day 7)	0.014**a**	0.01**b**	0.007**c**	0.004**d**	0.002**e**
	(0.002)	(0.001)	(0.0004)	(0.0002)	(0.0002)
Dp/Do (day 35)	0.01**a**	0.007**b**	0.005**c**	0.004**d**	0.0014**e**
	(0.001)	(0.0002)	(0.0001)	(0.0002)	(0.0002)

5.3.1.2 Soil surface pH (-6.0 kPa)

Mean surface pH of the controls, which received no urea, were 6.09 and 6.07 for the 1.1 and 1.5 Mg m^{-3} ρ_b treatments, respectively when averaged over the experimental period, and they did not differ significantly ($p > 0.05$) from each other (Fig. 5.1).

Soil pH increased immediately after urea application in all urea-treated cores and varied ($p < 0.01$) between treatments on all days with the highest values occurring in the lowest ρ_b treatment except on day 35 where the surface pH of the 1.5 Mg m^{-3} ρ_b was higher than at other soil ρ_b values ($p < 0.01$) (Fig. 5.1). In the presence of urea, the mean surface pH values on day 1 and day 35 for 1.1 Mg m^{-3} were 8.65 and 5.79, respectively, while in the 1.5 Mg m^{-3} treatment the values were 8.27 and 6.14, respectively. There was also a *time* x ρ_b interaction on soil surface pH ($p < 0.01$) with a slower decline in soil surface pH in the 1.1 Mg m^{-3} ρ_b treatment than in the other ρ_b treatments till day 24.

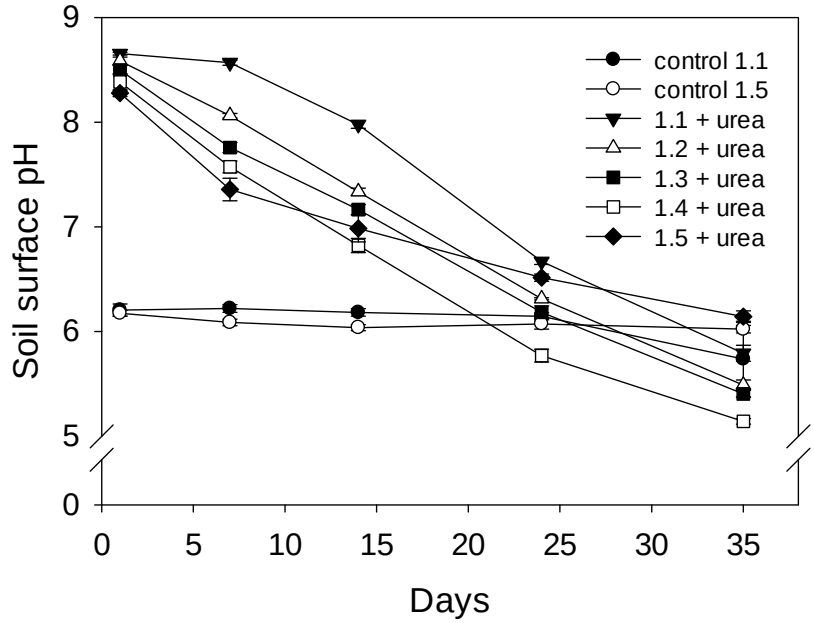

Figure 5.1 Soil surface pH of control and urea-treated cores over time. Error bars are generally < size of symbols. Numerals in the legend indicate ρ_b (Mg m^{-3}) applied. Error bars = s.e.m, n = 4.

5.3.1.3 Dissolved organic carbon (DOC) (-6.0 kPa)

Mean soil DOC concentrations of the control treatments (1.1 and 1.5 Mg m^{-3}), averaged over the experimental period did not differ significantly ($p > 0.05$) from each other and were ≤ 27 µg g^{-1} soil (Fig. 5.2). Soil DOC concentrations increased by day 1 in response to urea application (Fig. 5.2) and ranged from 566 to 80 µg g^{-1} soil at 1.1 Mg m^{-3} and from 321 to 49 µg g^{-1} soil for 1.5 Mg m^{-3} (Fig. 5.2). On days 1, 7, 14 and 35 the DOC concentrations in the urea treatments were highest at the lowest soil ρ_b ($p < 0.01$). Decreases in the DOC concentrations with time showed that there was a strong time effect on these concentrations ($p < 0.01$). There was also a *time* x ρ_b effect as the decline in DOC concentrations in the urea-treated 1.1 Mg m^{-3} ρ_b treatment was slower than in the other urea-treated ρ_b treatment till day 7. After this time DOC concentrations declined further, but at a faster rate in the 1.1 Mg m^{-3} ρ_b treatment, until day 14. After this time DOC continued to decline further. Soil DOC concentrations were positively correlated with soil surface pH at -6.0 kPa on days 1, 7, 14 and 24 (Tables 5.3-5.6).

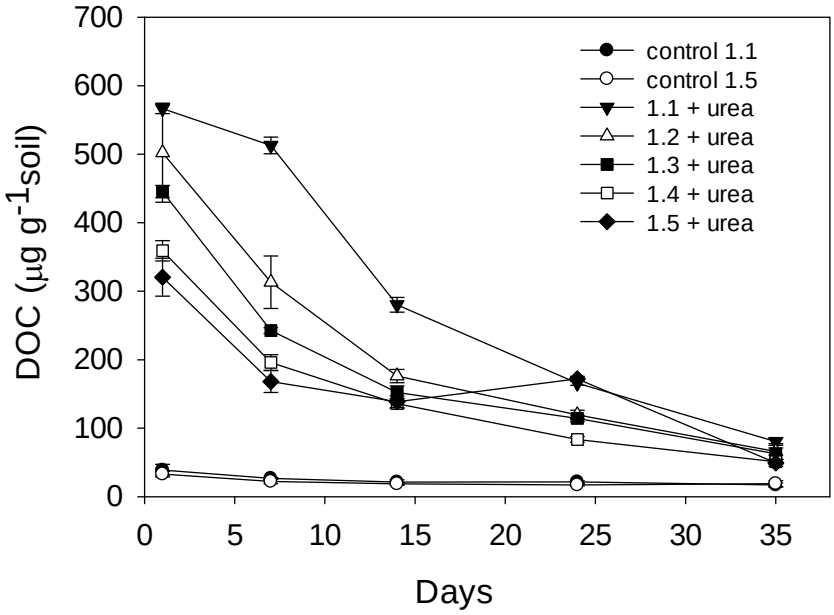

Figure 5.2 Urea and soil ρ_b effects on DOC concentrations. Numerals in the legend indicate ρ_b (Mg m^{-3}) applied. Error bars = s.e.m, n = 4.

5.3.1.4 Soil inorganic N (-6.0 kPa)

Data from the destructive sampling of the control cores at 1.1 and 1.5 Mg m^{-3} showed that ρ_b treatment did not affect soil NH_4^+-N concentrations ($p > 0.05$) with concentrations ≤ 12 µg g^{-1} soil at all times (Fig. 5.3a). However, immediately following urea application soil NH_4^+-N concentrations became elevated, peaking at day 1, before declining over time. Mean NH_4^+-N concentrations in these urea treated cores ranged from 1400 to 1055 µg g^{-1} soil on day 1 and 776 to 430 µg g^{-1} dry soil by day 35 (Fig. 5.3a). Soil NH_4^+-N concentrations under urea were higher at 1.1 Mg m^{-3} when compared to other urea-ρ_b treatments, on all days of observation ($p < 0.05$). While soil NH_4^+-N concentrations decreased with time ($p < 0.01$) there was no *time* x ρ_b interaction. Soil NH_4^+-N concentrations correlated positively with soil surface pH at -6.0 kPa on days 1, 7 and 14 (Tables 5.3-5.5).

Soil NO_3^- -N concentrations in the controls at 1.1 and 1.5 Mg m^{-3} did not differ due to soil ρ_b ($p < 0.05$) and were ≤ 25 µg g^{-1} soil (Fig. 5.3b). Following urea application, soil NO_3^--N concentrations ranged from 15 to 20 µg g^{-1} soil on day 1 and increased steadily over time in almost all soil ρ_b treatments to ca. 400 µg g^{-1} soil on day 35 (Fig. 5.3b). The increase in the soil NO_3^--N concentrations was initially not as fast in the 1.1 Mg m^{-3} treatment on days 7 and 14 (Fig. 5.3b).

The exception was the 1.5 Mg m^{-3} treatment, in which, NO_3^--N concentrations did not continue to increase after day 14 and remained at 200 µg g^{-1} soil until day 35 (Fig.5.3b). As a consequence there was a strong *time* x ρ_b effect ($p < 0.01$) for soil NO_3^--N in the urea treated cores. Soil NO_3^--N concentrations correlated negatively with soil surface pH on all days (Tables 5.3-5.7).

Soil NO_2^--N concentrations in the controls at 1.1 and 1.5 Mg m^{-3} did not differ due to soil ρ_b when averaged over time ($p < 0.05$) and were ≤ 0.1 µg g^{-1} soil (Fig. 5.3c). Under urea, soil NO_2^--N concentrations were affected by soil ρ_b treatments ($p < 0.01$) and concentrations increased on day 7 under all ρ_b treatments. They remained elevated at 1.1 Mg m^{-3} on days 7 and 14 ($p < 0.01$) ranging between 8.4 to 10.6 µg g^{-1} soil while on day 24 significantly higher concentrations occurred at 1.5 Mg m^{-3} with a maximum concentration of 13.8 µg g^{-1} soil ($p < 0.01$) (Fig 5.3c). Consequently a *time* x ρ_b interaction occurred ($p < 0.01$) (Fig. 5.3c).

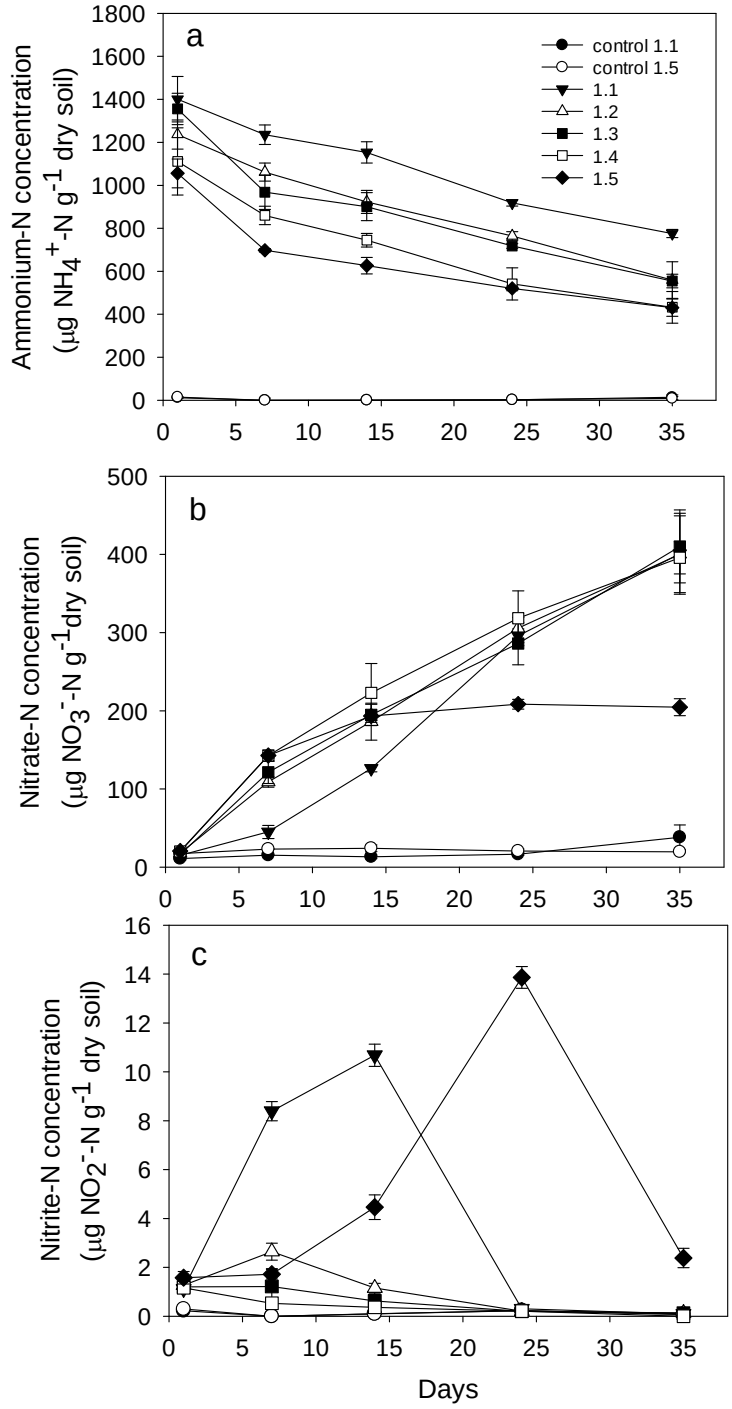

Figure 5.3 **Soil NH_4^+-N (a) NO_3^--N (b) and NO_2^--N concentrations (c) in the control and urea-treated cores at -6.0 kPa. Numerals in the legend indicate ρ_b (Mg m^{-3}) applied. Error bars = s.e.m, n = 4.**

5.3.1.5 Net rates of change in NH_4^+-N and NO_3^--N concentrations (-6.0 kPa)

Net rates of change in NH_4^+-N and NO_3^--N concentrations were calculated as the difference in the concentrations over time. In the urea-treated cores the net rates of depletion in the soil NH_4^+-N concentrations were not influenced by soil ρ_b at any time (Table 5.2). Net NO_3^--N accumulation rates differed with ρ_b on days 0-7 with the net NO_3^--N accumulation rate in the 1.4 and 1.5 Mg m^{-3} treatments being higher than in the other ρ_b treatments ($p < 0.01$) while the trend was reversed on days 14-24 (Table 5.2). By day 35 the net rate of change in the NO_3^--N concentration was only negative in the highest ρ_b treatment.

Table 5.2 Net rates of change in the soil NH_4^+-N and NO_3^--N concentrations in urea-treated cores (µg g^{-1}soil d^{-1}) affected by soil ρ_b at -6.0 kPa. Negative rates indicate decreasing concentrations. (n = 4).

	Time (days)				
	NH_4^+-N (µg g^{-1} soil d^{-1})				
Soil ρ_b	**0-1**	**1-7**	**7-14**	**14-24**	**24-35**
1.1	1400	-27	-12	-24	-13
1.2	1236	-29	-20	-16	-19
1.3	1356	-65	-10	-18	-15
1.4	1111	-42	-16	-20	-10
1.5	1056	-60	-10	-11	-8
significance	NS	NS	NS	NS	NS
LSD (0.01) df=15, n= 4	305	54	21	15	12
	NO_3^--N (µg g^{-1} soil d^{-1})				
Soil ρ_b	**0-1**	**1-7**	**7-14**	**14-24**	**24-35**
1.1	15	5	12	16	10
1.2	18	15	11	12	9
1.3	16	18	10	9	11
1.4	20	20	11	10	7
1.5	21	20	7	2	-0.3
significance	*	**	NS	**	NS
LSD (0.01) df = 15, n = 4	6	4	8	7	12

** $p < 0.01$, * $p < 0.05$, NS = not significant

5.3.1.6 Soil N_2O-N Fluxes (-6.0 kPa)

Mean N_2O-N fluxes from control soil cores in experiment 2a (-6.0 kPa) ranged from 0 to 0.3 mg m^{-2} h^{-1} and were higher at 1.1 Mg m^{-3} ($p < 0.01$) when compared with the 1.5 Mg m^{-3} treatment (Fig. 5.4a).

Following urea application, soil N_2O-N fluxes were affected by soil ρ_b ($p < 0.01$) peaking sharply on days 7 to 8 for soil ρ_b treatments 1.1 to 1.3 Mg m^{-3}, after which N_2O-N fluxes declined until day 16 whereupon they proceeded to increase again. Meanwhile, under urea at 1.4 and 1.5 Mg m^{-3} N_2O-N fluxes remained relatively low throughout the experiment (Fig. 5.4a). Under the urea treatments there was also a *time* x ρ_b interaction ($p < 0.01$) with lower N_2O-N fluxes from the 1.1 Mg m^{-3} treatment during days 1 to 3 while from days 16 to 35 N_2O-N fluxes in the 1.4 and 1.5 Mg m^{-3} treatments were relatively lower but constant while they generally increased in the ρ_b treatments ≤ 1.3 Mg m^{-3}.

Consequently, cumulative N_2O-N fluxes in this experiment (-6.0 kPa) differed with soil ρ_b from day 7 onwards with lower cumulative fluxes in the urea-treated 1.4 and 1.5 Mg m^{-3} ρ_b treatments when compared with other soil ρ_b treatments (Fig. 5.4 b). Within the 1.1, 1.2 and 1.3 Mg m^{-3} ρ_b treatments, the cumulative N_2O-N fluxes were lowest in the 1.1 Mg m^{-3} ρ_b treatment ($p < 0.01$). At the end of the experiment mean cumulative N_2O-N fluxes, as a percentage of N applied, were highest in the urea-treated 1.3 Mg m^{-3} treatment ($p < 0.01$) with a value of 16.3% and lowest in the urea-treated 1.4 and 1.5 Mg m^{-3} treatments with values of 2.2 and 2.1%, respectively (Fig. 5.4b).

Mean N_2O-N fluxes were positively correlated with DOC, NO_3^--N and NH_4^+-N concentrations on days 7 and 35 (Tables 5.3 and 5.7). A positive correlation of mean daily N_2O-N fluxes with NO_2^--N was observed on day 7 (Table 5.4) while a negative correlation occurred on day 35 (Table 5.7).

The atom % ^{15}N enrichment of the N_2O-N fluxes from urea treated cores ranged from 21 to 32% on day 1 and 32 to 36% on day 35 (Fig. 5.5). On days 1, 3 and 35, the ^{15}N enrichment of the N_2O-N flux was higher in the 1.4 and 1.5 Mg m^{-3} urea-treated ρ_b treatments than in the lower soil ρ_b treatments ($p < 0.01$) while on day 24, it was only higher at 1.5 Mg m^{-3} ($p < 0.01$) (Fig. 5.5).

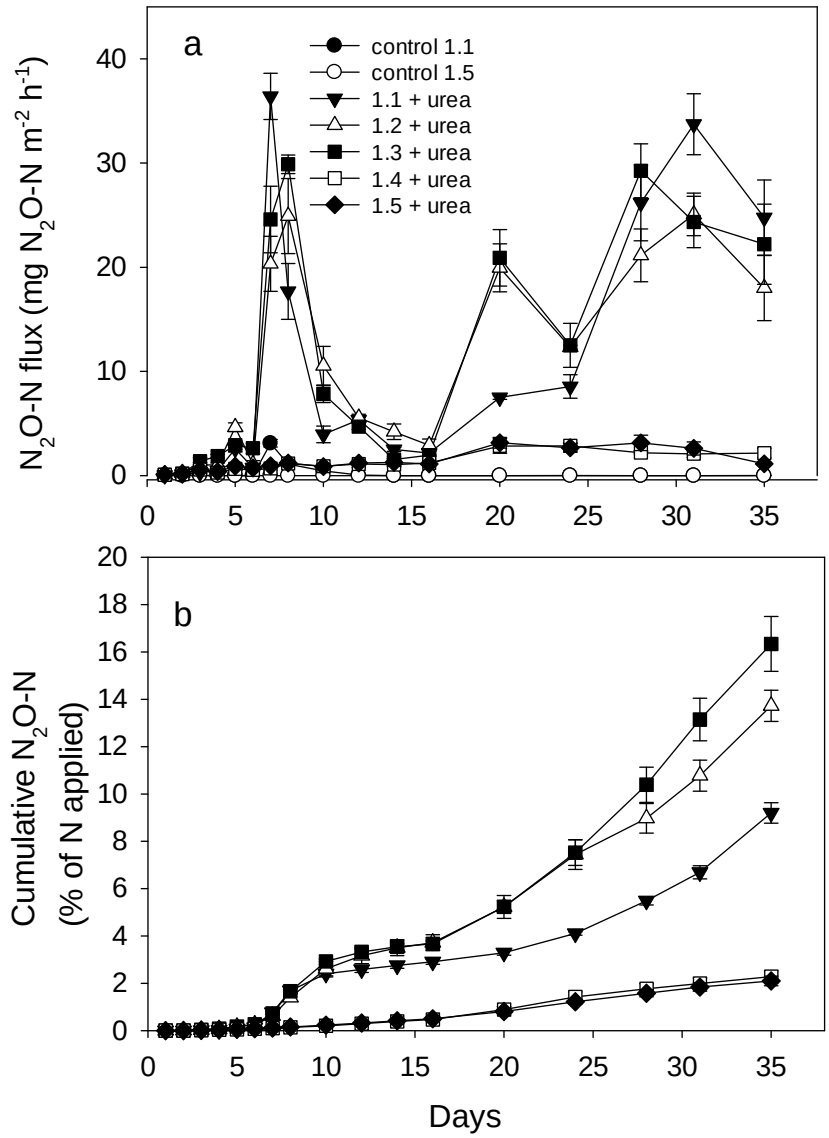

Figure 5.4 **(a) Mean N_2O-N fluxes measured in experiment 2a (-6.0 kPa) from the different ρ_b treatments over a period of 35 days. (b) Mean cumulative N_2O-N fluxes as % of applied N in experiment 2a (-6.0 kPa). Numerals in the legend indicate ρ_b (Mg m^{-3}) applied. Error bars = s.e.m, n = 4.**

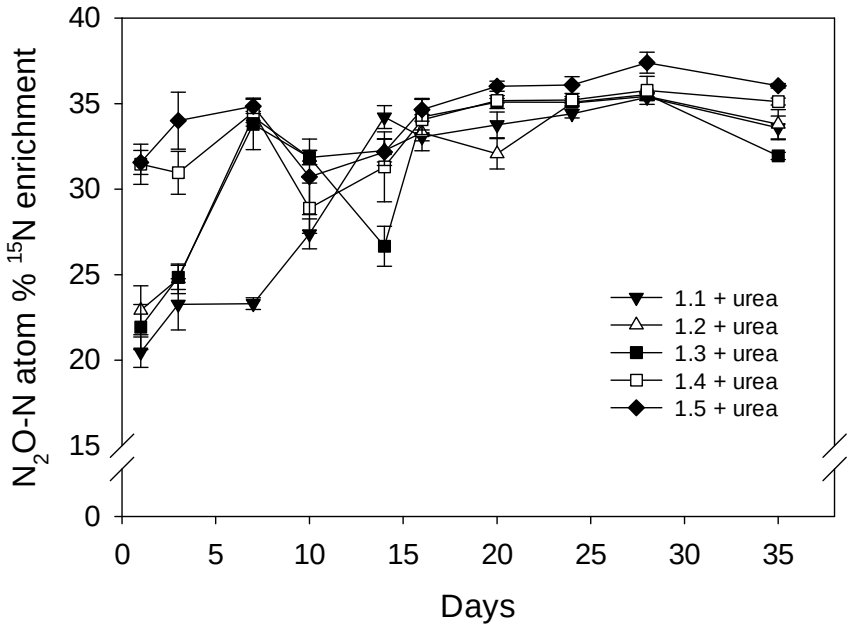

Figure 5.5 Mean atom % ^{15}N enrichment of the N_2O-N fluxes measured in experiment 2a (-6.0 kPa) under varying ρ_b treatments over a period of 35 days. Numerals in the legend indicate ρ_b applied. Error bars = s.e.m, n = 4.

5.3.1.7 Soil N_2-N fluxes and the N_2-N: N_2O-N ratios from urea treated cores (-6.0 kPa)

Increasing soil ρ_b ($p < 0.01$) increased N_2-N fluxes at -6.0 kPa. Maximum N_2-N fluxes occurred on days 14, 24, 28 and 35 at 1.5 Mg m^{-3} with values ranging from 38 to 64 mg m^{-2} h^{-1} (Fig. 5.6a). Mean values of $^{15}X_N$ (the mole fraction of ^{15}N in the N pool from which N_2 or N_2O was derived) were 0.29 (0.005), 0.28 (0.008), 0.28 (0.02), 0.28 (0.02) and 0.32 (0.01) for the 1.1, 1.2, 1.3, 1.4 and 1.5 Mg m^{-3} treatments, respectively (standard deviations in brackets) over the experimental period. The significant increase in N_2-N fluxes at 1.5 Mg m^{-3} beyond day 14 meant that there was also a *time* x ρ_b interaction ($p < 0.01$).

Mean cumulative N_2-N fluxes increased with increases in soil ρ_b on all days of observations ($p < 0.01$) after day 5 (Fig. 5.6b). After 35 days the mean cumulative N_2-N fluxes ranged from 8.3 to 50.0% of the applied N for the 1.1 and 1.5 Mg m^{-3} ρ_b treatments, respectively. The N_2-N fluxes correlated positively with NO_3^--N concentrations on days 1, 7 and 14 while the trend reversed on days 24 and 35 (Tables 5.3-5.7). There was a significant negative correlation between N_2-N fluxes and NH_4^+-N concentrations on all days (Tables 5.3-5.7).

Under a ψ of -6.0 kPa the effect of soil ρ_b on N_2-N: N_2O-N ratios was to produce higher ratios at 1.4 and 1.5 Mg m^{-3} throughout the experiment ($p < 0.01$) (Fig. 5.7). This trend was reflected in the cumulative N_2-N: N_2O-Nratios which were higher in the 1.4 and 1.5 Mg m^{-3} ρ_b treatments ($p < 0.01$) (Fig. 5.8).

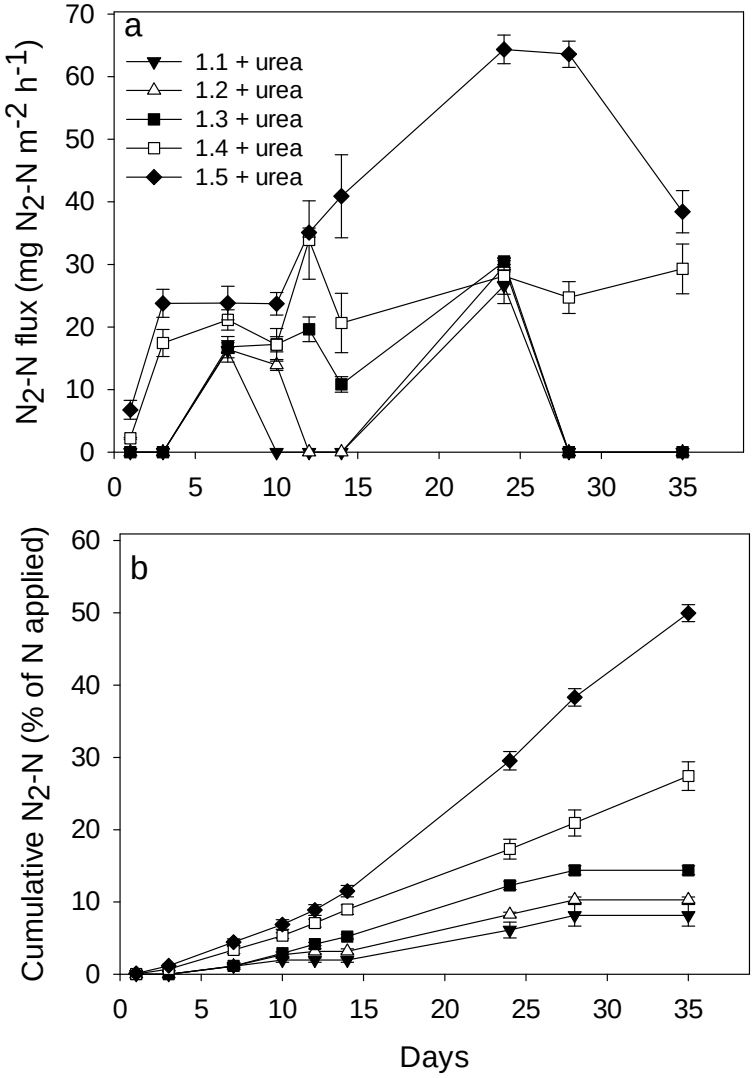

Figure 5.6 (a) Mean N_2-N fluxes measured in experiment 2a (-6.0 kPa) under varying ρ_b treatments over a period of 35 days. (b) Mean cumulative N_2-N fluxes as % of applied N in experiment 2a (-6.0 kPa). Error bars = s.e.m, n = 4.

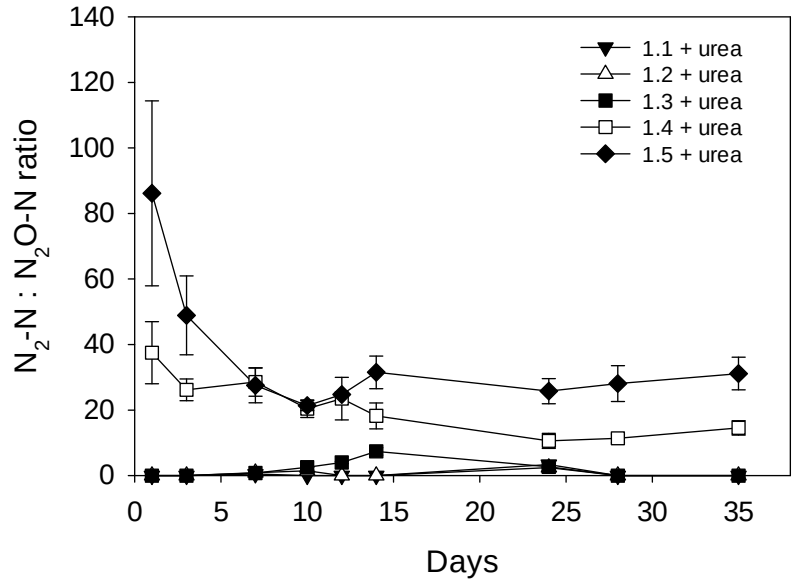

Figure 5.7 **Soil N_2-N: N_2O-N ratio over time at -6.0 kPa following urea application. Error bars = s.e.m, n = 4.**

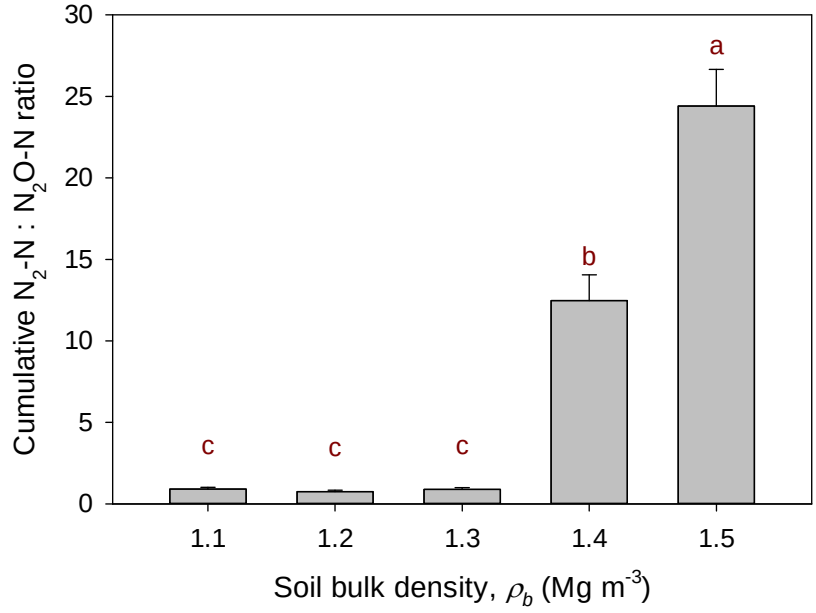

Figure 5.8 **Cumulative N_2-N: N_2O-N ratios versus soil ρ_b at -6.0 kPa. Values that do not share a common letter are significantly different ($p < 0.05$, Tukey's test). Error bars = s.e.m, n = 4.**

5.3.1.8 Relationships of *Dp*/*Do* and WFPS with cumulative-N_2-N and cumulative N_2O-N fluxes at -6.0 kPa.

When the cumulative N_2-N fluxes from all the replicates of ρ_b treatments from experiment 2a (-0.6 kPa) were plotted against *Dp*/*Do* measured on day 35 (Fig. 5.9a) and WFPS (Fig. 5.10a), strong exponential relationships emerged which explained 98% and 92% of the variability in the cumulative N_2-N fluxes, respectively (Fig. 5.9a). No single relationship was derived between cumulative N_2O-N fluxes and *Dp*/*Do* (Fig. 5.9b) or WFPS (Fig. 5.10b). However cumulative N_2O-N fluxes decreased sharply when *Dp*/*Do* was < 0.005 (Fig. 5.9b) and WFPS was > 80% (Fig. 5.10b).

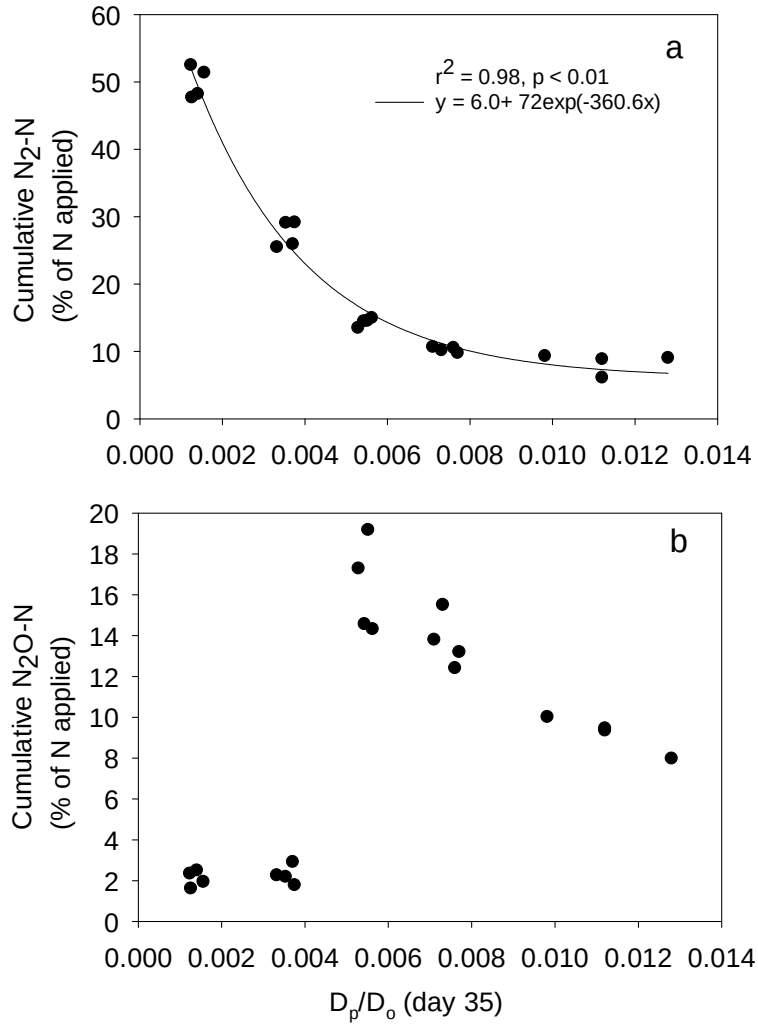

Figure 5.9 Relationships between *Dp*/*Do* and (a) cumulative N_2-N fluxes (b) cumulative N_2O-N fluxes. Data represent individual replicates.

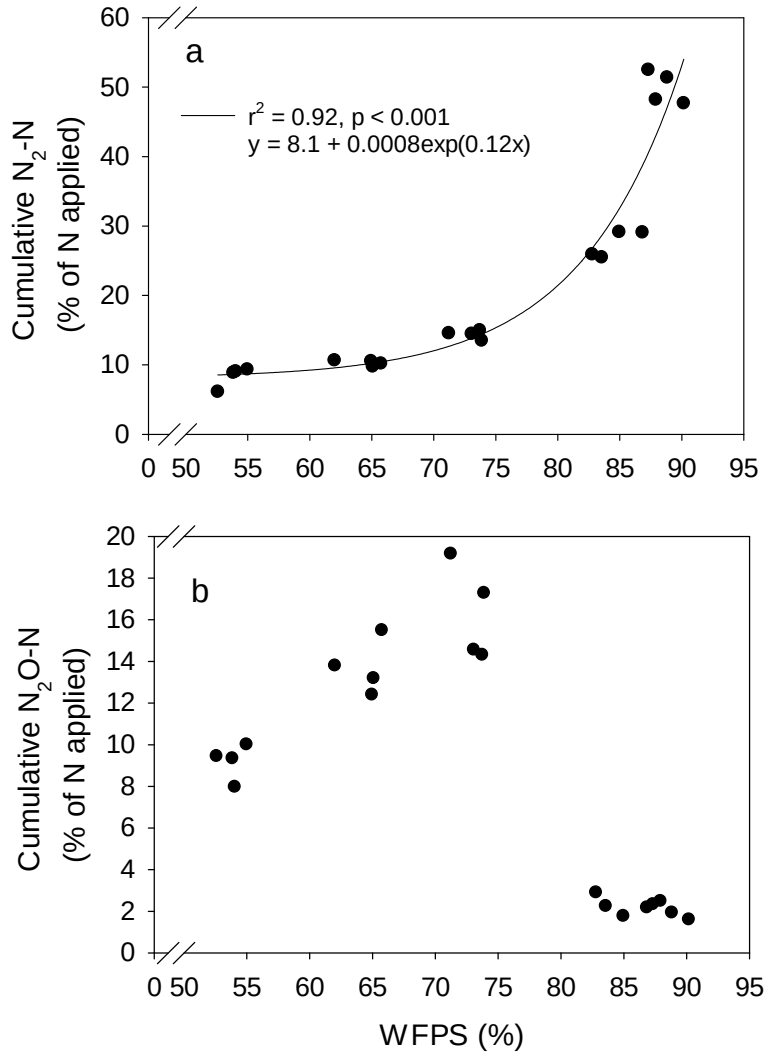

Figure 5.10 Relationships between WFPS and (a) cumulative N_2-N fluxes (b) cumulative N_2O-N fluxes. Data represent individual replicates.

Table 5.3 **Pearson correlation between measured variables and N_2O-N and N_2-N fluxes at -6.0 kPa on day 1. Numerals in italics are p-values.**

	N_2O-N	N_2-N	pH	DOC	NH_4^+-N	NO_3^--N
N_2-N	0.05 *0.83*					
pH	-0.31 *0.18*	-0.75 *0.00*				
DOC	-0.29 *0.20*	-0.71 *0.00*	0.96 *0.00*			
NH_4^+-N	-0.19 *0.41*	-0.54 *0.01*	0.67 *0.00*	0.57 *0.00*		
NO_3^--N	0.18 *0.43*	0.46 *0.04*	-0.66 *0.00*	-0.61 *0.00*	-0.80 *0.00*	
NO_2^--N	0.27 *0.25*	0.51 *0.02*	-0.45 *0.05*	-0.48 *0.03*	0.09 *0.699*	0.11 *0.65*

Table 5.4 **Pearson correlation between measured variables and N_2O-N and N_2-N fluxes at -6.0 kPa on day 7. Numerals in italics are p-values.**

	N_2O-N	N_2-N	pH	DOC	NH_4^+-N	NO_3^--N
N_2-N	-0.66 *0.00*					
pH	0.86 *0.00*	-0.58 *0.00*				
DOC	0.86 *0.00*	-0.51 *0.02*	0.98 *0.00*			
NH_4^+-N	0.87 *0.00*	-0.54 *0.01*	0.94 *0.00*	0.93 *0.00*		
NO_3^--N	-0.84 *0.00*	0.57 *0.01*	-0.94 *0.00*	-0.93 *0.00*	-0.82 *0.00*	
NO_2^--N	0.74 *0.00*	-0.34 *0.13*	0.87 *0.05*	0.87 *0.00*	0.76 *0.00*	-0.93 *0.00*

Table 5.5 Pearson correlation between measured variables and N_2O-N and N_2-N fluxes at -6.0 kPa on day 14. Numerals in italics are p-values.

	N_2O-N	N_2-N	pH	DOC	NH_4^+-N	NO_3^--N
N_2-N	-0.49					
	0.02					
pH	0.43	-0.65				
	0.05	*0.00*				
DOC	0.41	-0.64	0.95			
	0.07	*0.00*	*0.00*			
NH_4^+-N	0.42	-0.74	0.86	0.83		
	0.07	*0.00*	*0.00*	*0.00*		
NO_3^--N	-0.36	0.42	-0.79	-0.78	-0.60	
	0.12	*0.06*	*0.00*	*0.00*	*0.00*	
NO_2^--N	0.06	-0.17	0.79	0.82	0.56	-0.75
	0.77	*0.49*	*0.00*	*0.00*	*0.01*	*0.00*

Table 5.6 Pearson correlation between measured variables and N_2O-N and N_2-N fluxes at -6.0 kPa on day 24. Numerals in italics are p-values.

	N_2O-N	N_2-N	pH	DOC	NH_4^+-N	NO_3^--N
N_2-N	-0.51					
	0.02					
pH	0.19	0.32				
	0.42	*0.16*				
DOC	-0.01	0.53	0.95			
	0.97	*0.02*	*0.00*			
NH_4^+-N	0.61	-0.54	0.53	0.32		
	0.00	*0.02*	*0.02*	*0.17*		
NO_3^--N	0.34	-0.80	-0.44	-0.63	0.44	
	0.15	*0.00*	*0.05*	*0.00*	*0.05*	
NO_2^--N	-0.54	0.96	0.36	0.58	-0.56	-0.86
	0.15	*0.00*	*0.11*	*0.01*	*0.01*	*0.00*

Table 5.7 Pearson correlation between measured variables and N_2O-N and N_2-N fluxes at -6.0 kPa on day 35. Numerals in italics are p-values.

	N_2O-N	N_2-N	pH	DOC	NH_4^+-N	NO_3^--N
N_2-N	-0.84					
	0.00					
pH	-0.08	0.26				
	0.72	*0.25*				
DOC	0.77	-0.72	0.04			
	0.00	*0.00*	*0.88*			
NH_4^+-N	0.72	-0.69	0.13	0.78		
	0.00	*0.00*	*0.59*	*0.00*		
NO_3^--N	0.55	-0.61	-0.65	0.53	0.39	
	0.11	*0.00*	*0.00*	*0.02*	*0.08*	
NO_2^--N	-0.49	0.62	0.75	-0.47	-0.33	-0.78
	0.03	*0.00*	*0.00*	*0.04*	*0.16*	*0.00*

5.3.2 Results from experiment 2b (-0.2 kPa)

5.3.2.1 Soil physical conditions (-0.2 kPa)

The effect of soil ρ_b on soil physical properties is depicted in Table 5.8. Values of θ_v at -0.2 kPa differed with soil ρ_b ($p < 0.01$) with the lowest θ_v at the highest ρ_b treatment. There was no effect ($p > 0.05$) of soil ρ_b on WFPS or ε at -0.2 kPa. Values of *Dp*/*Do* at -0.2 kPa were equal to zero for all values of soil ρ_b due to almost saturated conditions.

Table 5.8 Soil physical characteristics at -0.2 kPa. Values are the mean of 4 replicates with standard deviation in brackets. Values that do not share a common letter are significantly different ($p < 0.05$, Tukey's test).

	Soil bulk density (Mg m^{-3})				
-0.2 kPa	**1.1**	**1.2**	**1.3**	**1.4**	**1.5**
Volumetric water content (m^3 m^{-3})	0.57**a** (0.008)	0.54**b** (0.002)	0.50**c** (0.006)	0.46**d** (0.009)	0.43**e** (0.006)
Water-filled pore space WFPS (%)	98**a** (1.37)	99**a** (0.44)	98**a** (1.32)	98**a** (1.90)	99**a** (1.38)
Air-filled porosity (m^3 m^{-3})	0.01**a** (0.008)	0.006**a** (0.002)	0.01**a** (0.007)	0.007**a** (0.009)	0.005**a** (0.006)
Total Porosity (m^3 m^{-3})	0.58**a** (0.00)	0.55**b** (0.00)	0.51**c** (0.00)	0.47**d** (0.00)	0.43**e** (0.00)
Dp/Do	0	0	0	0	0

5.3.2.2 Soil surface pH (-0.2 kPa)

At -0.2 kPa, mean soil surface pH of the control 1.1 Mg m^{-3} soil ρ_b treatment averaged over 35 days, was lower than in the control 1.5 Mg m^{-3} ρ_b treatment ($p < 0.01$) with values of 6.20 and 6.30 respectively (Fig. 5.11). Soil surface pH increased immediately after urea application in all ρ_b treatments (Fig. 5.11). In urea-treated cores soil surface pH on day 1 ranged from 8.25 to 8.65 and decreased to a range of 6.24 to 6.68 by day 35. Soil surface pH was higher ($p < 0.01$) in the lower ρ_b treatments on days 1 and 7 with the trend reversing on days 14 and 35 (Fig. 5.11). Soil surface pH was influenced by soil ρ_b ($p < 0.01$) when data were pooled over time with a more rapid decline till day 14 ($p < 0.01$) at lowest levels of ρ_b which lead to a *time* x ρ_b interaction effect on soil surface pH ($p < 0.01$). In urea-treated cores soil surface pH was positively correlated with DOC and NH_4^+-N concentrations on days 1 and 7 (Tables 5.10-5.11).

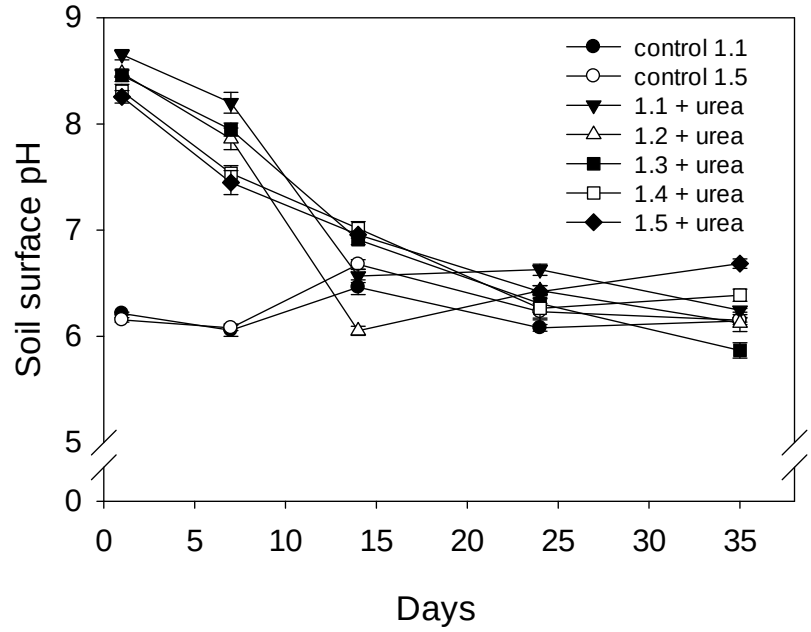

Figure 5.11 Soil surface pH measured over time in experiment 2b (-0.2 kPa). Numerals in legend indicate ρ_b (Mg m^{-3}) applied. Error bars are generally < size of the symbols. Error bars = s.e.m, n = 4.

5.3.2.3 Dissolved organic carbon (DOC) (-0.2 kPa)

Mean DOC concentrations averaged over 35 days were higher in the control 1.5 Mg m^{-3} soil ρ_b treatment ($p < 0.01$) than in the control 1.1.Mg m^{-3} ρ_b treatment. Soil DOC concentrations increased after urea application on day 1 and decreased thereafter. Under urea, mean soil DOC concentrations decreased from 710 to 221 µg g^{-1} soil at 1.1 Mg m^{-3} and from 370 to 131 µg g^{-1} soil at 1.5 Mg m^{-3} over the 35 day period (Fig. 5.12), with significant soil ρ_b effects on DOC concentrations on days 1, 7and 35, with higher concentrations in the lowest ρ_b treatment ($p < 0.01$) on these days. There was a *time* x ρ_b effect on DOC up to day 14, with a greater rate of decline in DOC concentrations in the lower ρ_b treatments.

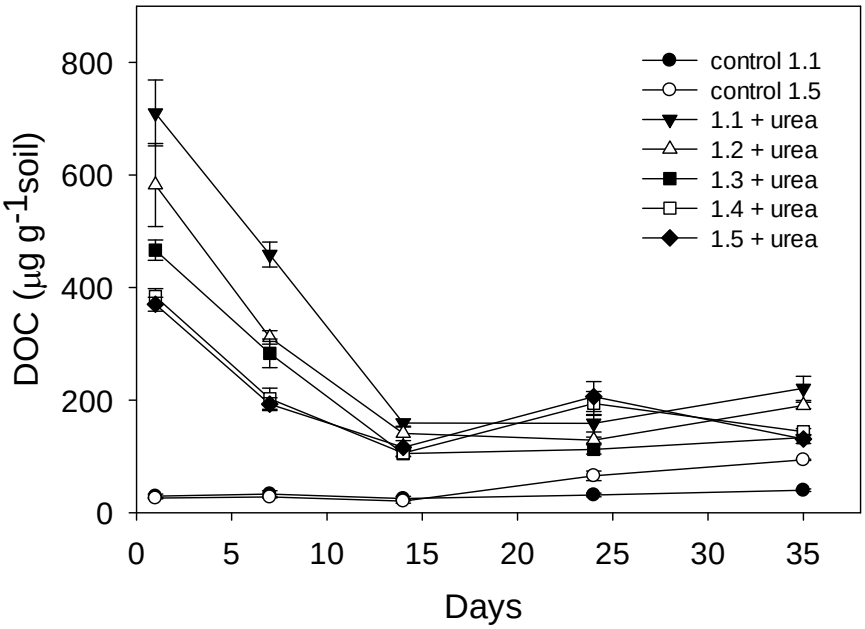

Figure 5.12 Soil DOC concentrations over time in experiment 2b (-0.2 kPa). Numerals in legend indicate ρ_b (Mg m^{-3}) applied. Error bars = s.e.m, n = 4.

5.3.2.4 Soil inorganic N (-0.2 kPa)

Soil ρ_b did not affect NH_4^+-N concentrations in the controls which averaged ≤ 12 µg NH_4^+-N g^{-1} soil over the experimental period ($p > 0.05$). Soil NH_4^+-N concentrations were elevated by day 1 after urea application and then declined as the experiment progressed. Under urea, mean NH_4^+-N concentrations ranged from 1490 to 994 on day 1 and by day 35 they were 539 to 419 µg g^{-1} soil (Fig. 5.13a). Both time and soil ρ_b affected ($p < 0.01$) NH_4^+-N concentrations, with higher concentrations of NH_4^+-N occurring at 1.1 and 1.2 Mg m^{-3} ρ_b treatments on all days, while significant ($p < 0.01$) lower NH_4^+-N concentrations occurred on day 7 at 1.5 Mg m^{-3} and at 1.4 Mg m^{-3} on days 1 and 14.

Soil NO_3^- -N concentrations (Fig. 5.13b) in the controls at 1.1 and 1.5 Mg m^{-3}, when averaged over 35 days, were higher in the 1.1 Mg m^{-3} ($p < 0.01$) with mean values of 12 and 9 µg g^{-1} soil respectively. Under urea, soil NO_3^--N concentrations increased from day 1 at ≤ 21 µg g^{-1} soil, where no ρ_b effect occurred, and peaked on day 14 with a maximum value of 243 µg g^{-1} soil at 1.3 Mg m^{-3} ρ_b treatment (Fig 5.13b). However, there were no significant differences due to soil ρ_b on days 7 and 14 ($p > 0.05$). After day 14, under urea, soil NO_3^- -N concentrations decreased with lower values in both the 1.4 and 1.5 Mg m^{-3} ρ_b treatments ($p < 0.01$) on days 24 and 35. There was a significant effect of time on soil NO_3^--N concentrations since the concentrations increased till day 14 and then declined. The slower decline in NO_3^--N, under urea, at 1.1, 1.2 and 1.3 Mg m^{-3} when compared with 1.4 and 1.5 Mg m^{-3} after day 14 produced an interaction ($p < 0.01$) between time and soil ρ_b.

Soil NO_2^- -N concentrations in the controls at 1.1 and 1.5 Mg m^{-3}, did not differ due to soil ρ_b when averaged over time ($p < 0.05$) and were ≤ 0.1 µg g^{-1} soil (Fig. 5.13c). Soil NO_2^--N concentrations, under urea, (Fig. 5.13c) had increased by day 7 with the highest NO_2^--N concentrations at 1.1 and the lowest at 1.5 Mg m^{-3} ($p < 0.01$). However, the NO_2^--N concentrations at 1.1, 1.2 and 1.3 Mg m^{-3} were lower than in the 1.4 and 1.5 Mg m^{-3} ρ_b treatments by day 14 ($p < 0.01$). By 35 days, the situation was reversed with NO_2^--N concentrations at 1.4 and 1.5 Mg m^{-3} ranging from 0.8 to 0.9 µg g^{-1} soil while at 1.1, 1.2 and 1.3 Mg m^{-3} NO_2^--N concentrations still ranged from 13 to 21 µg g^{-1} soil ($p < 0.01$). Thus a *time* x ρ_b interaction effect ($p < 0.01$) on soil NO_2^--N concentrations occurred.

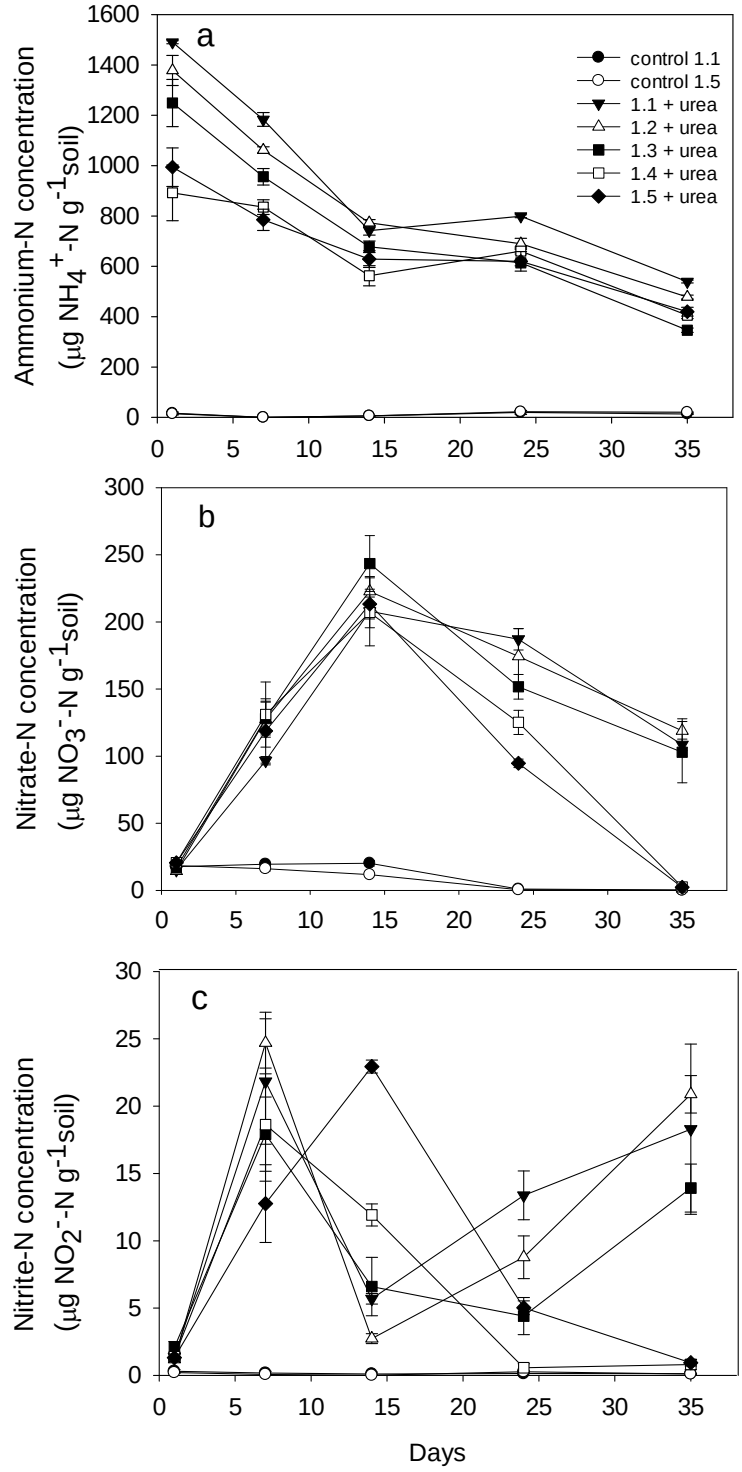

Figure 5.13 Soil NH_4^--N (a) NO_3^--N (b) and NO_2^--N concentrations (c) over time from control and urea-treated cores in experiment 2b (-0.2 kPa). Numerals in the legend indicate ρ_b (Mg m^{-3}) applied. Error bars = s.e.m, n = 4.

5.3.2.5 Net rates of change in NH_4^+-N and NO_3^--N concentrations (-0.2 kPa)

The net rates of increase in NH_4^+-N concentrations were only influenced by soil ρ_b on days 0-1 with greater rates at 1.1, 1.2 and 1.3 Mg m^{-3} ρ_b treatments when compared with 1.4 and 1.5 Mg m^{-3} ($p < 0.01$) with no difference between 1.4 and 1.5 Mg m^{-3} treatments (Table 5.9). Net rates of NH_4^+-N depletion differed with ρ_b treatments between 7-24 days with higher depletion rates at lower ρ_b treatments ($p < 0.01$). Net NO_3^--N accumulation rates only differed due to ρ_b on days 0-1 where the NO_3^--N accumulation rates in the 1.4 and 1.5 Mg m^{-3} ρ_b treatments were higher than in other ρ_b treatments ($p < 0.01$). Net NO_3^--N depletion rates were also influenced by soil ρ_b with greater NO_3^--N depletion rates at ≥ 1.4 Mg m^{-3}.

Table 5.9 Net rates of change in the soil NH_4^+-N and NO_3^--N concentrations in urea treated cores (µg g^{-1}soil d^{-1}) affected by soil ρ_b at -0.2 kPa. Negative rates indicate decreasing concentrations (n = 4).

	Time (days)				
	NH_4^+-N (µg g^{-1} soil d^{-1})				
Soil ρ_b	**0-1**	**1-7**	**7-14**	**14-24**	**24-35**
1.1	1491	-51	-63	6	-24
1.2	1378	-52	-41	-8	-19
1.3	1249	-48	-39	-6	-24
1.4	892	-9	-39	9	-23
1.5	994	-35	-22	-1	-18
significance	**	NS	**	**	NS
LSD (0.01) df = 15, n = 4	240	54	23	13	7
	NO_3^--N (µg g^{-1}soil d^{-1})				
Soil ρ_b	**0-1**	**1-7**	**7-14**	**14-24**	**24-35**
1.1	15	14	16	-2	-7
1.2	14	19	14	-4	-5
1.3	16	19	16	-9	-4
1.4	20	18	11	-8	-11
1.5	21	16	14	-12	-9
significance	**	NS	NS	**	**
LSD (0.01) df = 15, n = 4	3	6	7	4	3

** $p < 0.01$, NS = not significant

5.3.2.6 Soil N_2O-N Fluxes (-0.2 kPa)

Mean N_2O-N fluxes from controls at 1.1 and 1.5 Mg m^{-3} ranged from 0 to 2 mg m^{-2} h^{-1} when averaged over 35 days with greater N_2O-N emissions at 1.5 Mgm^{-3} ($p < 0.01$). Under urea application, daily mean N_2O-N emissions were generally much higher ($p < 0.01$) in the 1.5 Mg m^{-3} ρ_b treatment throughout the experimental period. Maximum N_2O-N fluxes of 9.5 mg m^{-2} h^{-1} occurred at 1.5 Mg m^{-3} on day 7 (Fig. 5.14a). The N_2O-N flux was influenced by a *time* x ρ_b interaction ($p < 0.01$) since the N_2O flux at 1.5 Mg m^{-3} peaked twice on days 7 and 20, while at 1.4 Mg m^{-3} the N_2O-N fluxes increased on day 7 but then decreased as the time progressed.

Under urea, cumulative N_2O-N fluxes reflected daily fluxes and were higher in the 1.4 and 1.5 Mg m^{-3} ρ_b treatments when compared with other ρ_b treatments with significant increases observed in all ρ_b treatments from day 7 onwards but especially at 1.5 Mg m^{-3} ($p < 0.01$) (Fig. 5.14b). After 35 days, mean cumulative N_2O-N fluxes, as a percentage of N applied, ranged from 0.8 to 2.3% at ρ_b values of 1.1 and 1.5 Mg m^{-3}, respectively.

Mean N_2O-N fluxes were negatively correlated with pH, DOC and NH_4^+-N concentrations on days 1 and 7 (Tables 5.10-5.11). A significant negative correlation of mean N_2O-N fluxes with NO_2^--N was observed on days 7, 24 and 35 while a positive correlation occurred on day 14 (Tables 5.11-5.14).

The atom % ^{15}N enrichments of the N_2O-N produced ranged from mean values of 13.0 to 23.4% on day 1 and 32 to 34% on day 35 (Fig. 5.15). The ^{15}N enrichment of the N_2O-N flux only differed with ρ_b until day 16, with higher mean values at 1.5 Mg m^{-3} than in other ρ_b treatments on days 1, 7, 10 and 16 ($p < 0.01$).

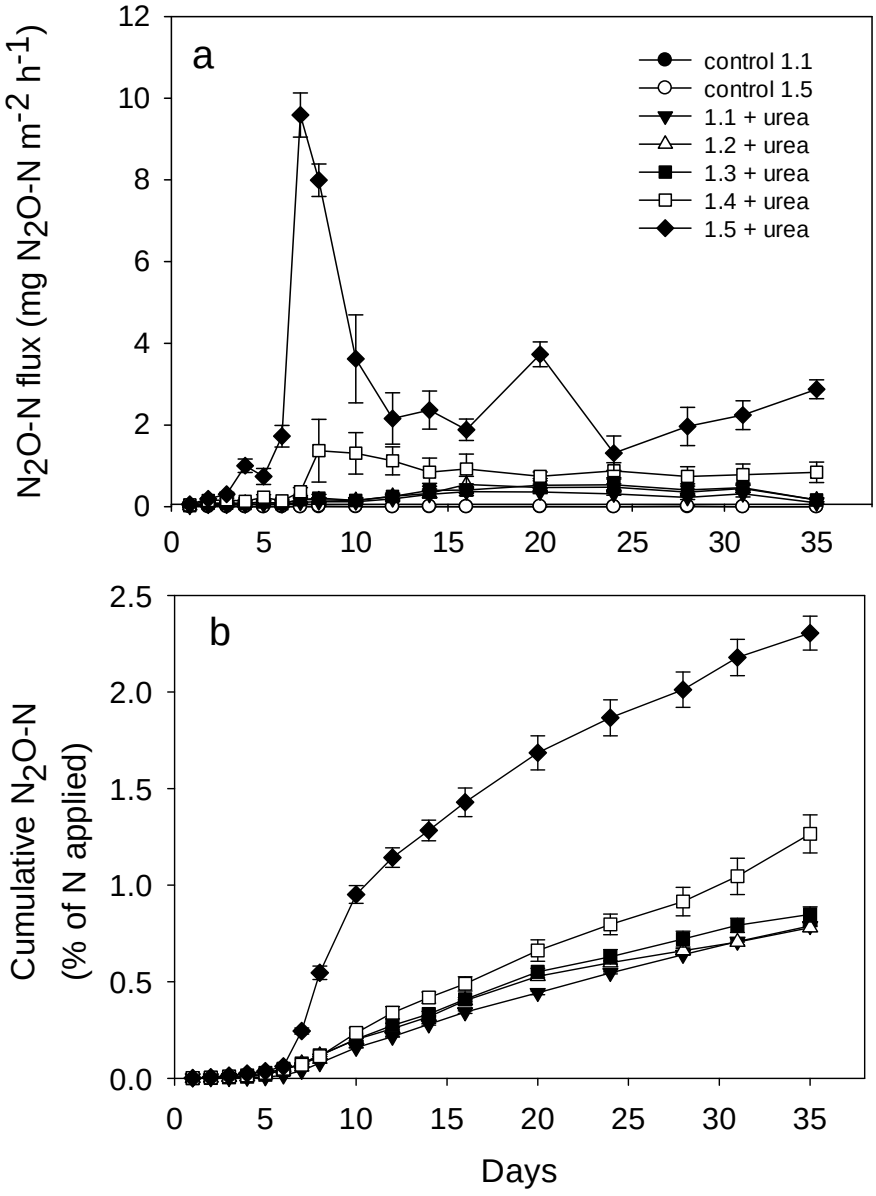

Figure 5.14 (a) Mean N_2O-N fluxes measured over time in experiment 2b (-0.2 kPa) from different ρ_b treatments over a period of 35 days. (b) Mean cumulative N_2O-N fluxes as a % of applied N in experiment 2b (-0.2 kPa). Error bars = s.e.m, n = 4.

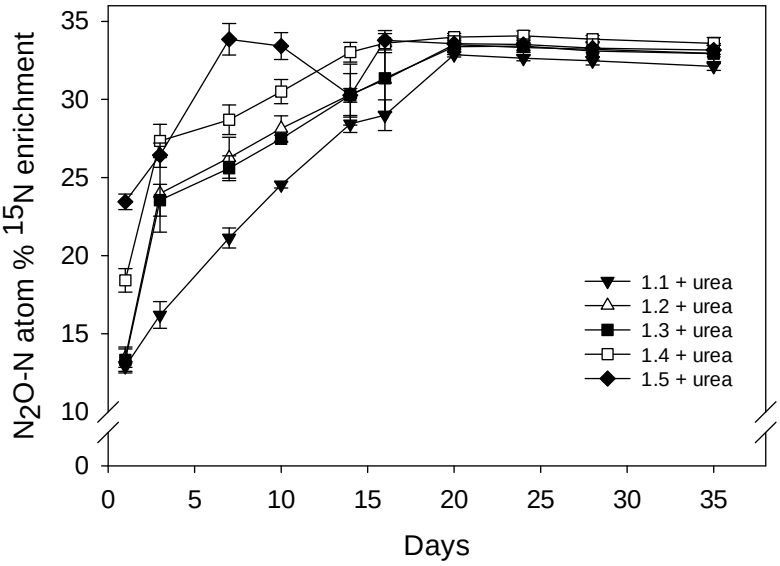

Figure 5.15 Mean atom % ^{15}N enrichment of N_2O-N measured over time in experiment 2b (-0.2 kPa) under different ρ_b treatments. Error bars = s.e.m, n = 4.

5.3.2.7 Soil N_2-N fluxes and the N_2-N: N_2O-N ratios from urea treated cores (-0.2 kPa)

Mean N_2-N fluxes were greater ($p < 0.01$) at 1.4 and 1.5 Mg m^{-3} on days 14, 28 and 35. Maximum fluxes of N_2-N occurred on days 24 and 35 in the 1.5 Mg m^{-3} treatment with values of 63 mg m^{-2} h^{-1} (Fig. 5.16a). The mean enrichments of the NO_3^--N pool undergoing denitrification, $^{15}X_N$, from which N_2 was derived, were 0.30 (0.02), 0.32 (0.02), 0.32 (0.01), 0.32 (0.01) and 0.31 (0.01) for the 1.1, 1.2, 1.3, 1.4 and 1.5 Mg m^{-3} ρ_b treatments, respectively (standard deviations in brackets).

Soil N_2-N emissions were also influenced by a *time* x ρ_b interaction ($p < 0.01$) with fluxes increasing significantly after day 10 and remaining high till the end of the experiment particularly in the 1.4 and 1.5 Mg m^{-3} ρ_b treatments. Cumulative N_2-N fluxes, as a % of N applied, reflected trends in daily fluxes, with cumulative fluxes increasing with soil ρ_b, and with higher fluxes ($p < 0.01$) from the 1.4 and 1.5 Mg m^{-3} ρ_b treatments (Fig. 5.16b).

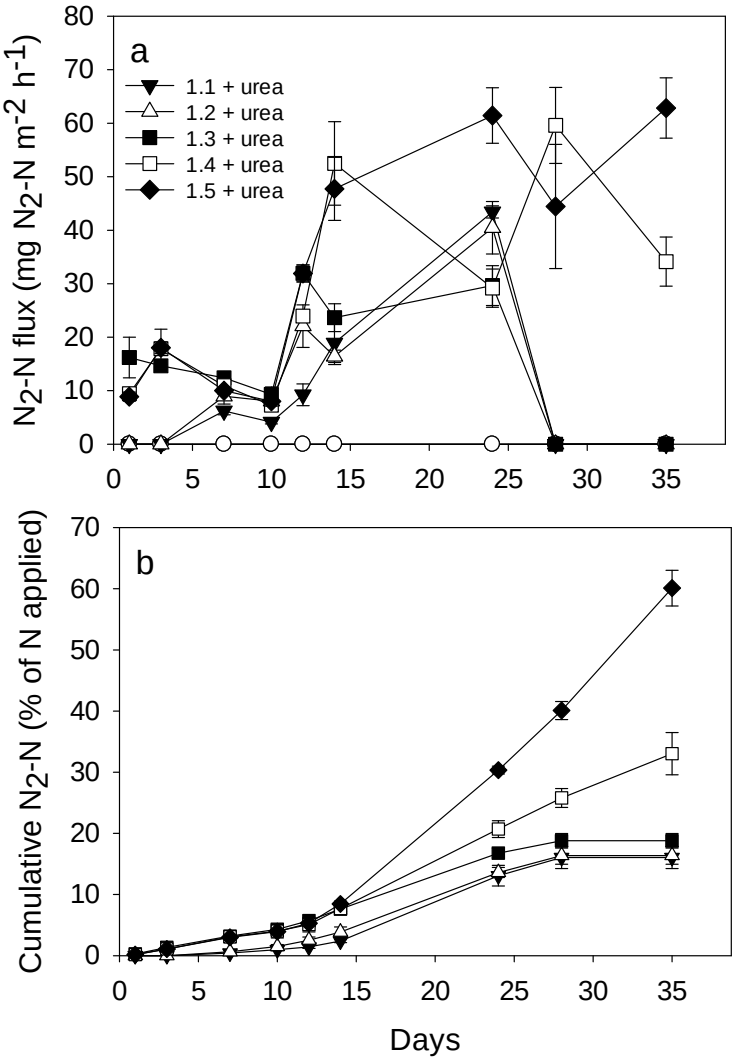

Figure 5.16 (a) Mean N_2-N fluxes measured in experiment 2b (-0.2 kPa) from different ρ_b treatments over a period of 35 days. (b) Mean cumulative N_2-N fluxes as a % of applied N at -0.2 kPa. Error bars = s.e.m, n = 4.

After 35 days, mean cumulative N_2-N emissions, as a percentage of N applied, ranged from 16.0 to 60.0% at 1.1 and 1.5 Mg m^{-3} ρ_b, respectively (Fig. 5.16b). A significant negative correlation occurred between daily N_2-N fluxes and DOC on days 1, 7, 14, and 35 (Tables 5.10-5.14). Daily N_2-N fluxes on day 14, correlated positively with soil NO_2^--N concentrations (Table 5.12).

Mean N_2-N: N_2O-N ratios ranged from 0 to 624 with higher ($p < 0.01$) ratios at ≥ 1.3 Mg m^{-3} on days 1 and 3 after which the ratio declined with little difference due to soil ρ_b (Fig. 5.17). Cumulative N_2-N: N_2O-N ratios differed significantly with ρ_b with higher ratios at 1.4 and 1.5 Mg m^{-3} ($p < 0.01$) (Fig. 5.18). Soil gas diffusivity measured at -0.2 kPa was equal to zero in all the ρ_b treatments as a consequence of the saturated soil conditions. Thus no relationship between gas fluxes could be derived using *Dp*/*Do* as an independent variable.

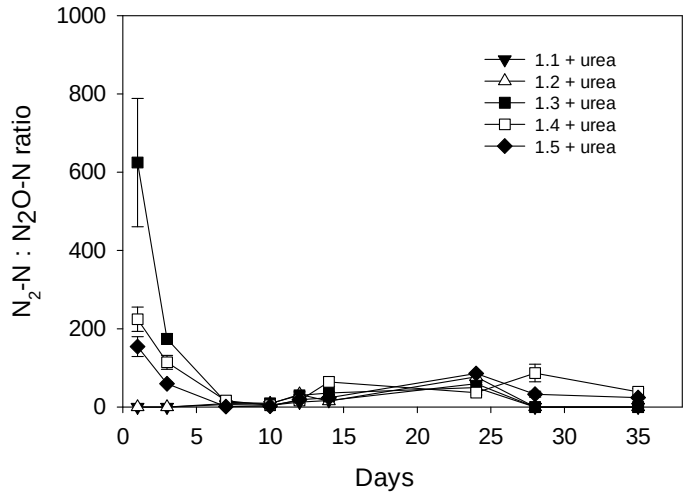

Figure 5.17 Soil N_2-N: N_2O-N ratio versus time measured in experiment 2b (-0.2 kPa). Numerals in the legend indicate ρ_b (Mg m^{-3}) applied. Error bars = s.e.m, n = 4.

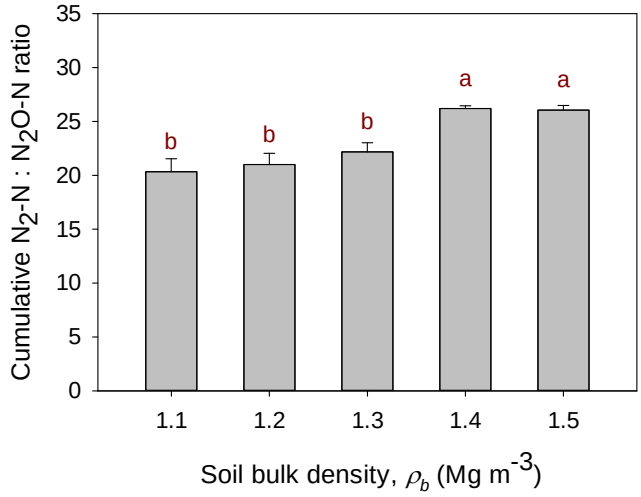

Figure 5.18 Cumulative N_2-N: N_2O-N ratios versus soil ρ_b at -0.2 kPa. Values that do not share a common letter are significantly different ($p < 0.05$, Tukey's test). Error bars = s.e.m, n = 4.

Table 5.10 Pearson correlation between measured variables and N_2O-N and N_2-N fluxes at -0.2 kPa on day 1. Numerals in italics are p-values.

	N_2O-N	N_2-N	pH	DOC	NH_4^+-N	NO_3^--N
N_2-N	0.36 *0.11*					
pH	-0.83 *0.00*	-0.38 *0.09*				
DOC	-0.76 *0.00*	-0.59 *0.00*	0.84 *0.00*			
NH_4^+-N	-0.76 *0.00*	-0.46 *0.05*	0.84 *0.00*	0.82 *0.00*		
NO_3^--N	0.71 *0.00*	0.40 *0.08*	-0.77 *0.00*	-0.71 *0.00*	-0.91 *0.00*	
NO_2^--N	-0.23 *0.32*	0.44 *0.05*	0.04 *0.85*	-0.11 *0.66*	0.05 *0.82*	0.07 *0.76*

Table 5.11 Pearson correlation between measured variables and N_2O-N and N_2-N fluxes at -0.2 kPa on day 7. Numerals in italics are p-values.

	N_2O-N	N_2-N	pH	DOC	NH_4^+-N	NO_3^--N
N_2-N	0.06 *0.79*					
pH	-0.62 *0.00*	-0.36 *0.12*				
DOC	-0.57 *0.00*	-0.53 *0.02*	0.93 *0.00*			
NH_4^+-N	-0.59 *0.00*	-0.44 *0.05*	0.89 *0.00*	0.94 *0.00*		
NO_3^--N	-0.08 *0.72*	0.43 *0.05*	-0.35 *0.12*	-0.45 *0.04*	-0.43 *0.06*	
NO_2^--N	-0.53 *0.02*	-0.32 *0.17*	0.41 *0.07*	0.45 *0.05*	0.54 *0.01*	-0.33 *0.15*

Table 5.12 Pearson correlation between measured variables and N_2O-N and N_2-N fluxes at -0.2 kPa on day 14. Numerals in italics are p-values.

	N_2O-N	N_2-N	pH	DOC	NH_4^+-N	NO_3^--N
N_2-N	0.51					
	0.02					
pH	0.45	0.65				
	0.04	*0.00*				
DOC	-0.29	-0.56	-0.70			
	0.20	*0.01*	*0.00*			
NH_4^+-N	-0.41	-0.70	-0.77	0.62		
	0.07	*0.00*	*0.00*	*0.00*		
NO_3^--N	-0.17	-0.27	-0.05	-0.25	0.31	
	0.47	*0.47*	*0.82*	*0.27*	*0.19*	
NO_2^--N	0.87	0.70	0.65	-0.43	-0.57	-0.22
	0.00	*0.00*	*0.00*	*0.06*	*0.01*	*0.36*

Table 5.13 Pearson correlation between measured variables and N_2O-N and N_2-N fluxes at -0.2 kPa on day 24. Numerals in italics are p-values.

	N_2O-N	N_2-N	pH	DOC	NH_4^+-N	NO_3^--N
N_2-N	0.39					
	0.08					
pH	-0.36	0.39				
	0.11	*0.08*				
DOC	0.68	0.43	0.04			
	0.00	*0.06*	*0.86*			
NH_4^+-N	-0.44	0.03	0.68	0.07		
	0.00	*0.89*	*0.00*	*0.75*		
NO_3^--N	-0.81	-0.33	0.47	-0.55	0.63	
	0.00	*0.15*	*0.03*	*0.01*	*0.00*	
NO_2^--N	-0.49	0.26	0.82	-0.21	0.78	0.67
	0.02	*0.27*	*0.00*	*0.36*	*0.01*	*0.00*

Table 5.14 Pearson correlation between measured variables and N_2O-N and N_2-N fluxes at -0.2 kPa on day 35. Numerals in italics are p-values.

	N_2O-N	N_2-N	pH	DOC	NH_4^+-N	NO_3^--N
N_2-N	0.86 *0.00*					
pH	0.81 *0.00*	0.84 *0.00*				
DOC	-0.51 *0.02*	-0.59 *0.01*	-0.19 *0.41*			
NH_4^+-N	-0.17 *0.46*	-0.27 *0.25*	0.19 *0.40*	0.87 *0.00*		
NO_3^--N	-0.69 *0.00*	-0.89 *0.00*	-0.78 *0.00*	0.62 *0.00*	0.33 *0.15*	
NO_2^--N	-0.65 *0.00*	-0.83 *0.00*	-0.65 *0.00*	0.64 *0.00*	0.45 *0.04*	0.93 *0.00*

5.3.3 Results from experiment 2c

Soil ρ_b affected soil water retention (Fig. 5.19). The amount of water retained at -0.5 kPa decreased with an increase in the soil ρ_b ($p < 0.01$). However, the trend reversed when ψ decreased and became more negative, < -1.0 kPa, with more water retained as ρ_b increased ($p < 0.01$). At -10 kPa, soil water retention at a ρ_b value of 1.1 Mg m^{-3} was significantly ($p < 0.01$) lower than in the other ρ_b treatments. Increasing ρ_b also changed the soil pore size distribution, when soil porosity fractions were expressed as a % of total porosity (Fig. 5.20) and as a % of total soil volume (Table 5.15). ANOVA performed on soil porosities expressed as a % of total soil volume showed that as the soil ρ_b increased, macroporosity (volume of pores with diameter > 30 µm) decreased by up to 23% at 1.5 Mg m^{-3} ($p < 0.01$) (Table 5.15). Increasing soil ρ_b led to an increase in soil mesoporosity (volumes of pores with diameter 30-0.2 µm) by 6% and an increase in microporosity (volumes of pores with diameter < 0.2 µm) by 2.0% (Table 5.15). Thus, increasing soil ρ_b resulted in an increase in the soil volume occupied by mesopores and micropores and a decrease in the soil volume occupied by macropores.

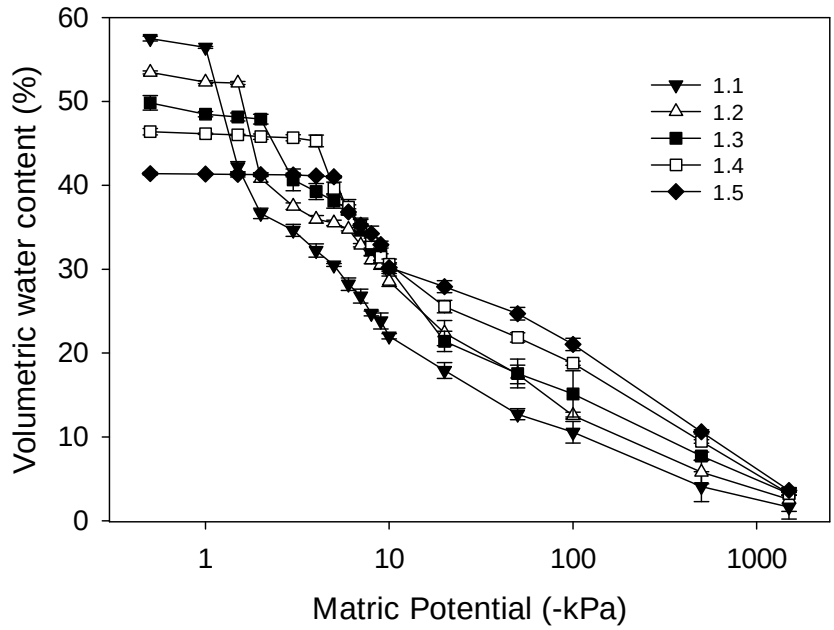

Figure 5.19 Effect of soil ρ_b on water retention curve. Numerals in the legend indicate soil ρ_b (Mg m^{-3}) applied. Error bars are standard deviations, n = 4.

ANOVA performed on soil porosities expressed as a % total porosity showed that with the increase in soil ρ_b, macroporosity decreased ($p < 0.01$) from 62% at 1.1 Mg m^{-3} to 30% at 1.5 Mg m^{-3} while both mesoporosity and microporosity increased by a factor of 27% and 6%, respectively.

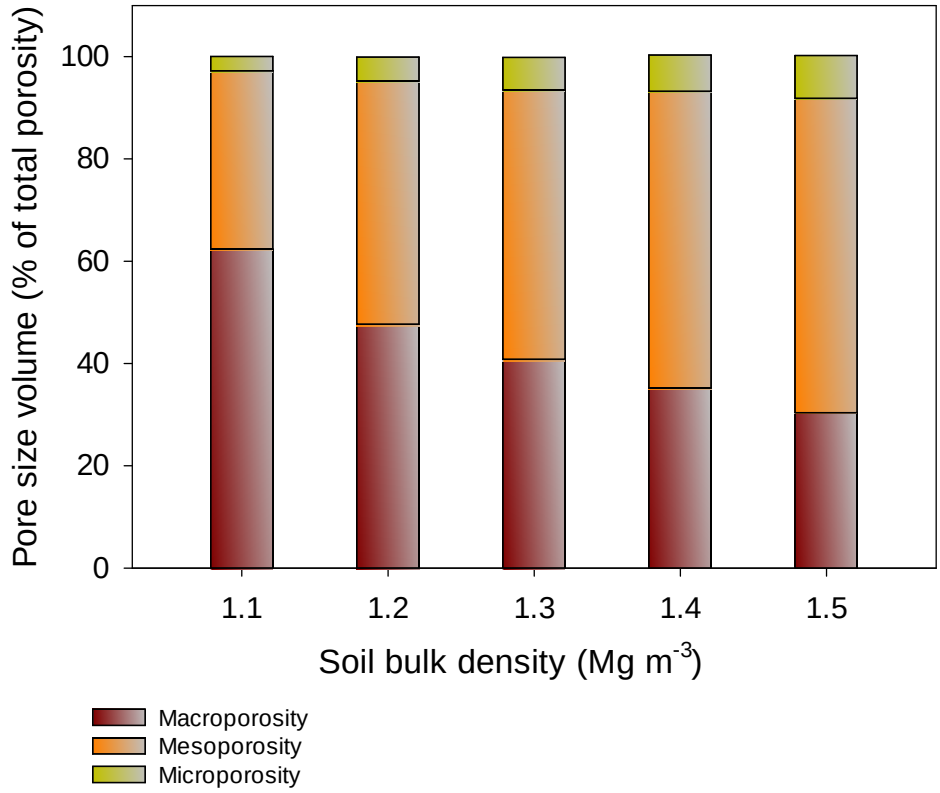

Figure 5.20 Mean soil porosities expressed as a % of total porosity under varying ρ_b (Mg m^{-3}) treatments.

Table 5.15 **Total porosity of soil cores and % of total soil volume occupied by each given pore size. Note the sum of macroporosity, mesoporosity and microporosity equals total porosity. Values are means of four replicates. Standard deviations are in brackets. Values in a row that do not share a common letter are significantly different ($p < 0.01$, Tukey's test).**

% of soil volume	Matric potential (-kPa)	Soil bulk density (Mg m^{-3})					
		1.1	1.2	1.3	1.4	1.5	
Total Porosity		**58.5**	**54.7**	**50.9**	**47.1**	**43.3**	
Macroporosity > 30µm	**< 10**	**36.4a**	**26.1b**	**20.8c**	**16.6d**	**13.2e**	**
		(0.32)	**(0.62)**	**(0.64)**	**(0.62)**	**(0.43)**	
Pores > 600 µm	<0.5	0.99a	1.24a	1.1a	0.77a	2.00a	NS
		(0.27)	(0.17)	(0.87)	(0.38)	(0.15)	
Pores 600-300 µm	0.5-1.0	1.04abc	1.16ab	1.35a	0.24bc	0.05c	**
		(0.20)	(0.11)	(0.69)	(0.31)	(0.08)	
Pores 300-200 µm	1.0-1.5	14.24a	0.103b	0.332b	0.14b	0b	**
		(0.68)	(0.08)	(0.16)	(0.11)	(0.00)	
Pores 200-150 µm	1.5-2.0	5.55a	11.4b	0.265c	0.206c	0.11c	**
		(0.29)	(0.52)	(0.15)	(0.25)	(0.09)	
Pores 150-100 µm	2.0-3.0	2.01a	3.31a	7.24b	0.12c	0.04c	**
		(0.11)	(0.71)	(0.83)	(0.19)	(0.01)	
Pores 100-50 µm	3-6	6.4b	2.8c	3.5c	8.2a	4.4c	**
		(0.57)	(0.21)	(0.86)	(0.77)	(0.50)	
Pores 50-30 µm	6-10	6.2a	6.2a	7.0a	6.8a	6.63a	NS
		(0.19)	(0.46)	(0.33)	(0.55)	(0.44)	
Mesoporosity 30-0.2 µm	**10-1500**	**20.4b**	**26.0a**	**26.8a**	**27.3a**	**26.6a**	**
		(0.65)	**(0.86)**	**(0.82)**	**(0.61)**	**(0.52)**	
Pore 30-3 µm	10-100	11.4c	16.0a	15.0ab	11.7bc	9.2c	**
		(1.35)	(0.81)	(2.24)	(0.40)	(0.57)	
Pores 3 -0.2 µm	100-1500	8.9c	10.0c	11.8bc	15.5ab	17.4a	**
		(1.36)	(0.17)	(2.9)	(0.3)	(0.9)	
Microporosity < 0.2 µm	**< 1500**	**1.6c**	**2.5b**	**3.2ab**	**3.3ab**	**3.6a**	**
		(0.42)	**(0.42)**	**(0.19)**	**(0.21)**	**(0.22)**	
Meso + Microporosity	**> 10**	**22.0c**	**28.5b**	**30.1a**	**30.6a**	**30.2a**	**
		(0.32)	**(0.62)**	**(0.64)**	**(0.62)**	**(0.43)**	

** $p < 0.01$, NS = not significant

5.4 Discussion

5.4.1 Soil surface pH, DOC, Inorganic N

In experiments 2a (-6.0 kPa) and 2b (-0.2 kPa), the surface soil pH data provides evidence of rapid urea hydrolysis i.e. the dramatic increase in soil surface pH following urea application. Increases in soil surface pH and NH_4^+-N concentrations immediately after urine application occurs due to rapid hydrolysis of urea in soil (Sherlock and Goh, 1984). The reason for the increase in soil pH has been described as resulting from the hydrolysis of carbonate ions formed during urea hydrolysis (Sherlock, 1984).

The increase in soil DOC concentrations immediately after urine application generally occurs as a result of solubilisation of soil organic matter due to high soil pH (Monaghan and Barraclough, 1993; Shand et al., 2000). The DOC data here are explained by this effect while the differences due to soil ρ_b were a consequence of differing depths of penetration by the urea solution, as discussed in Chapter 4.

The decrease in soil pH and NH_4^+-N concentrations occur as a consequence of NH_3 volatilization and nitrification; both processes generate H^+ ions (Sherlock, 1984; Wrage et al., 2001). After urea application, changes in the NH_4^+-N concentrations followed similar patterns in both experiments 2a (-6.0 kPa) and 2b (-0.2 kPa) with comparable and high NH_4^+-N concentrations on day 1 and then decreasing thereafter. Decreases in NH_4^+-N concentrations from day 1 to day 35 and increases in soil NO_3^--N concentrations from days 1 to 14 in both experiments 2a (-6.0 kPa) and 2b (-0.2 kPa) indicate that nitrification had occurred.

In experiment 2a (-6.0 kPa) NO_3^--N concentrations continued to increase over the 35 day period in all soil ρ_b treatments except at 1.5 Mg m^{-3} indicating production of NO_3^--N was still exceeding its consumption via denitrification but not at 1.5 Mg m^{-3} where the NO_3^--N concentrations remained static after day 14 indicating that denitrification was balancing NO_3^--N production in this ρ_b treatment. In fact, soil NO_3^--N in the ρ_b treatments 1.1 to 1.4 Mg m^{-3}, with an exception of the 1.5 Mg m^{-3} ρ_b treatment, were on average 2-3 times higher than in experiment 2b (-0.2 kPa) indicating that conditions were not as suitable for NO_3^--N reduction as in experiment 2b (-0.2 kPa).

At -6.0 kPa, soil NO_2^--N concentrations were generally low except in the 1.1 and in the 1.5 Mg m^{-3} ρ_b treatments. The possible reason for the delayed peaking in NO_2^--N at 1.1 Mgm^{-3} (-6.0 kPa) might be due to the retardation of NO_2^--N oxidation within a few days of urine application, potentially caused by high NH_3 levels in the presence of high pH and high NH_4^+-N concentrations (Monaghan and Barraclough, 1992). Delayed nitrification was also supported by the prolonged higher pH and the slower rate of NO_3^--N accumulation from days 1 to 7 with soil surface pH remaining high till day 14 in this ρ_b treatment. However, inhibition of NO_2^--N oxidation does not explain the delayed NO_2^--N peak in the 1.5 Mg m^{-3} ρ_b treatment at -6.0 kPa. In this ρ_b treatment it is unlikely that the delayed NO_2^--N peak was due to a lag in the synthesis of the NO_2^- reductase enzyme under anaerobic conditions, since studies have shown the synthesis of *de novo* NO_2^--N reductase enzyme commences 3-6 h after the onset of anoxic conditions (Smith and Tiedje, 1979; Dendooven and Anderson, 1994). The most likely reason was enhanced NO_3^--N reduction as evident from the static soil NO_3^--N concentration during that same time period, promoting NO_2^--N production via denitrification. Similar explanations could be invoked for NO_2^--N dynamics in the experiment 2b (-0.2 kPa) where NO_2^--N peaked at day 7 as nitrification proceeded rapidly following the initial retardation by NH_3. Then in the 1.1 to 1.3 Mg m^{-3} ρ_b treatments NO_2^--N again built up slowly due to denitrification and /or continuing denitrification but at 1.4 and 1.5 Mg m^{-3}, due to more intense denitrifying conditions, NO_2^--N was significantly reduced. The decrease in NO_3^--N concentrations in the experiment 2b (-0.2 kPa), after day 14, in all ρ_b treatments, suggests that denitrification occurred in these treatments.

5.4.2 N_2O-N, N_2-N fluxes and N_2-N:N_2O-N ratios

In soil, N_2O is predominately produced by nitrification, denitrification and nitrifier-denitrification (Wrage et al., 2001; Wrage et al., 2005) while N_2 is produced by reduction of N_2O formed during these processes by the enzyme N_2O reductase (Firestone, 1982; Knowles, 1982). Since equal amounts of urea were applied to the ρ_b cores in both experiments, 2a (-6.0 kPa) and 2b (-0.2kPa), it was anticipated that the fluxes of N_2O and N_2 would be different depending upon the complex interaction of substrates and changes in physical properties due to soil compaction and ψ. The relatively high ^{15}N enrichment of N_2O-N from day 15 onwards in both experiments, 2a and 2b, indicated that these fluxes, after this time were predominantly sourced from the labelled urea ^{15}N applied.

Soil NO_2^- is the gateway to N_2O production regardless of the production mechanism (Stevens et al., 1998; Wrage et al., 2001). For NO_2^--N to be present in sufficient quantities for N_2O production it must be delivered via the nitrification or denitrification processes. In both experiments 2a and 2b, N_2O-N fluxes were seen to increase dramatically at approximately day 7 and this was particularly evident when observing the cumulative N_2O-N fluxes. The rate of increase in N_2O-N fluxes was dependent on soil ρ_b as discussed below but with respect to soil NO_2^--N concentrations, the increase in N_2O fluxes in experiment 2b (-0.2 kPa) and the elevations in concentrations of soil NO_2^--N occurred on the same day i.e. day 7. However, this was not evident in experiment 2a (-6.0 kPa) indicating other factors were also influencing N_2O fluxes.

In experiment 2a (-6.0 kPa), there was a clearly defined peak in N_2O-N fluxes on day 7 in the 1.1, 1.2 and 1.3 Mg m^{-3} ρ_b treatments possibly due to high nitrifier activity during this time. Increases in N_2O fluxes (-6.0 kPa) again after day 16 in these ρ_b treatments were possibly due to the coupling of nitrification and denitrification as NO_3^--N concentrations were still increasing in these ρ_b treatments during this time. Nitrous oxide fluxes have been reported to be highest between a WFPS of 60 to 80% as aerobic and anaerobic conditions have been known to coexist in soil permitting both nitrification and denitrification simultaneously (Wrage et al., 2001; Rafique et al., 2011). This is consistent with the results in the experiment 2a (-6.0 kPa) where cumulative fluxes of N_2O-N increased from 8% to 16%, as a percentage of applied N, when soil ρ_b was increased from 1.1 to 1.3 Mg m^{-3} along with the increase in WFPS from 54% to 73% as expected. Soil compaction increases WFPS due to greater water retention, as a result of an increasing % of small sized pores, and decreases in air-filled porosity and soil diffusivity, which in this experiment might have created O_2 deficient conditions (anoxic) suitable for denitrification (Ball et al., 1999a; Smith et al., 2003).

In experiment 2a (-6.0 kPa), daily and cumulative N_2O-N fluxes at 1.4 and 1.5 Mg m^{-3} were low, coinciding with higher N_2-N fluxes especially at 1.5 Mg m^{-3}, which indicated that at 1.4 and 1.5 Mg m^{-3}, conditions were conducive for N_2O reduction to N_2. Daily and cumulativeN_2-N: N_2O-N ratios were also higher at 1.4 and 1.5 Mg m^{-3} which also indicated that N_2-N was the main product of denitrification. This was possibly due to soil compaction as an increase in soil compaction decreases the potential transport of N_2O through the soil and hence increases the residence time of N_2O in soil while increasing the time for potential reduction of N_2O to N_2 (Clough et al., 2005).

In experiment 2b (-0.2 kPa), daily and cumulative N_2O-N fluxes were greater in the 1.4 and 1.5 Mg m^{-3} ρ_b treatments although there was little difference in the WFPS levels (98 to 99%) among the soil ρ_b treatments. Cumulative N_2-N fluxes were 20 to 25 times greater than cumulative N_2O-N fluxes in all the ρ_b treatments at -0.2 kPa which showed that denitrification was the dominant process in all the ρ_b treatments with N_2 as the main product. Ruser et al. (2006) also observed high N_2: N_2O ratios while assessing the combined effects of soil compaction and soil moisture on N_2 and N_2O emissions from NO_3^- fertilised intact soil cores.

It is well documented that N_2O fluxes via denitrification increase dramatically when WFPS exceeds ca. 60% (Linn and Doran, 1984; Clough et al., 2004) and at a WFPS > 80% denitrification becomes the dominant process with N_2 as the main end product (Veldkamp et al., 1998). The WFPS levels obtained following soil compaction in this study are similar to those earlier studies and support the view that denitrification resulting in N_2 production was the dominant process at ρ_b values of 1.4 and 1.5 Mg m^{-3} in experiment 2a (-6.0 kPa) and in all the ρ_b treatments in experiment 2b (-0.2 kPa).

5.4.3 Soil relative gas diffusivity (*Dp*/*Do*), WFPS and cumulative N_2-N, N_2O-N fluxes

At -6.0 kPa (experiment 2a), cumulative N_2O-N and N_2-N fluxes produced similar relationships with both, *Dp*/*Do* and WFPS, suggesting that at this ψ level both WFPS and *Dp*/*Do* are equally important in predicting these fluxes. A similar result was also seen in Chapter 4.

In experiment 2a (-6.0 kPa), the value of *Dp*/*Do* was 0.004 and 0.0014 for the 1.4 and 1.5 Mg m^{-3} ρ_b treatments, respectively. This is below the previously reported limit (range of 0.005-0.02) where anaerobic conditions begin to develop in the soil (Stepniewski, 1981). Thus at -6.0 kPa, a decrease in *Dp*/*Do* below 0.005 provided conditions suited for N_2O-N reduction to N_2-N (Fig. 5.9b). The increase in WFPS from 85 to 89% at 1.4 and 1.5 Mg m^{-3} ρ_b treatments in experiment 2a (-6.0 kPa) was 4% (Table 5.1) while the decrease in *Dp*/*Do* was very small (0.002-0.0026) which resulted in an increase in the cumulative N_2-N fluxes by approximately 20% at the end of the experiment. This shows that denitrification is very sensitive to small changes in *Dp*/*Do*.

In experiment 2b (-0.2 kPa), *Dp*/*Do* was zero in all the ρ_b treatments. The reason for this was attributed to the low ε resulting from soil compaction and saturated soil conditions. It is known that at $\varepsilon < 10\%$, soil gas diffusion is near zero due to the presence of air as isolated pockets and discontinuity of pores in the gas diffusion pathways (Xu et al., 1992).

5.4.4 Effect of compaction on water retention curves and pore size distribution

Soil compaction increases ρ_b, decreases ϕ and alters pore size distribution and soil water retention capabilities (Assouline, 2006; Beare et al., 2009). Compaction of soil at more negative ψ causes larger pores to be reduced to a size smaller or equal to those at that ψ. The volume of small pores then increases and they retain more water and hence the moisture content increases (Hill and Sumner, 1967). However, at near saturation (less negative ψ) the dominance of reduction in total porosity due to loss of larger pores increases over the relative increase in volume of small pores which subsequently results in a decrease in soil moisture content with increasing soil ρ_b. This explains the findings in the current experiment where more water was retained at higher ρ_b between -10 and -1000 kPa where there was an increase in the volume of pores with an equivalent diameter between 300 and 0.3 µm, while there was a decrease in the water retained between saturation and -1 kPa as soil ρ_b increased, which corresponded to a reduction of the volumes of pores with diameter > 300 µm.

Data gained from the soil moisture curves showed that increases in the soil ρ_b resulted in increases in the proportion of mesopores and micropores and decreases in the proportion of macropores. The results are consistent with those of Cui et al. (2010) who showed on a sieved loamy soil, by mercury porosimetry, that mechanical compression caused larger pores to decrease in size and new small pores were created. In one study by Shestak and Busse (2005), it was shown that soil compaction increased the proportion of small pores (mesopores) (0.2 -30 µm) in a sandy loam soil by 39% while macropores (> 30 µm) decreased by 50-90%.

5.5 Conclusions

The inorganic-N dynamics, changes in soil pH and DOC concentrations after urea application and the pattern of decrease in soil *Dp*/*Do* were similar to the first experiment (Chapter 4) and consistent with previous studies. Significantly higher cumulative N_2-N: N_2O-N ratios were observed in experiment 2a (-6.0 kPa) in the 1.4 and 1.5 Mg m^{-3} ρ_b treatments. In experiment 2b (-0.2 kPa), cumulative N_2-N fluxes were 20 to 25 times greater than the cumulative N_2O-N fluxes at all ρ_b treatments. However, in both experiments 2a and 2b, cumulative N_2-N: N_2O-N ratios were very comparable in the 1.5 Mg m^{-3} ρ_b treatments. Soil porosities varied with soil ρ_b. As soil macroporosity decreased, soil mesoporosity and microporosity increased. The data sets gathered in experiments 1, 2a and 2b are unique and when combined they present an opportunity to assess the effect of soil compaction and ψ on N_2O-N and N_2-N fluxes and their associated relationships with *Dp*/*Do* and WFPS. These relationships are discussed in the following Chapter 6.

Chapter 6

Synthesis of the data from previous chapters

6.1 Introduction

This chapter is the synthesis of all the data from experiment 1 (Chapter 4) and experiment 2 (2a and 2b, Chapter 5). There is no comparable data in the literature. It is acknowledged that direct comparisons of the results from these experiments are not valid statistically as these experiments were performed as individual experiments at different times. Nevertheless, the compilation of data from these experiments was conducted in order to determine which variable, water filled pore space (WFPS) or relative gas diffusivity (*Dp*/*Do*), relates better to cumulative N_2O-N and N_2-N fluxes and also to cumulative N_2-N: N_2O-N ratios. Another purpose was to evaluate the effect of increasing matric potential (ψ) from -10 kPa (experiment 1) to -6.0 kPa (experiment 2a) and then to -0.2 kPa (experiment 2b) on ruminant urine (i.e. urea)-derived cumulative N_2O-N and N_2-N fluxes from a soil under varying bulk density (ρ_b) treatments.

6.2 Results and Discussion

In Chapters 4 and 5 it was shown that both *Dp*/*Do* and WFPS were similar in predicting cumulative N_2O-N and N_2-N fluxes from varying ρ_b treatments at a given ψ. However, it is apparent from the complied data that *Dp*/*Do* (Fig. 6.1a) produced a better relationship than WFPS (Fig. 6.1b) and could be a better predictor of urine-derived N_2O from the soil varying in ρ_b and ψ. This holds true for cumulative N_2-N fluxes as well (Fig. 6.2). This complied data supports the view suggested by Farquharson and Baldock (2008) that WFPS should not be used to construct predictive measures for predicting N_2O emissions from soil varying in ρ_b.

Maximum cumulative N_2O-N fluxes occurred at a mean *Dp*/*Do* value of 0.005. A decrease in cumulative N_2O-N fluxes with a further decreases in *Dp*/*Do* to < 0.005 suggests N_2O entrapment in soil (Clough et al., 2005) increasing the probability of complete reduction of N_2O-N to N_2-N which was also supported by high cumulative N_2-N fluxes at *Dp*/*Do* values of < 0.005.

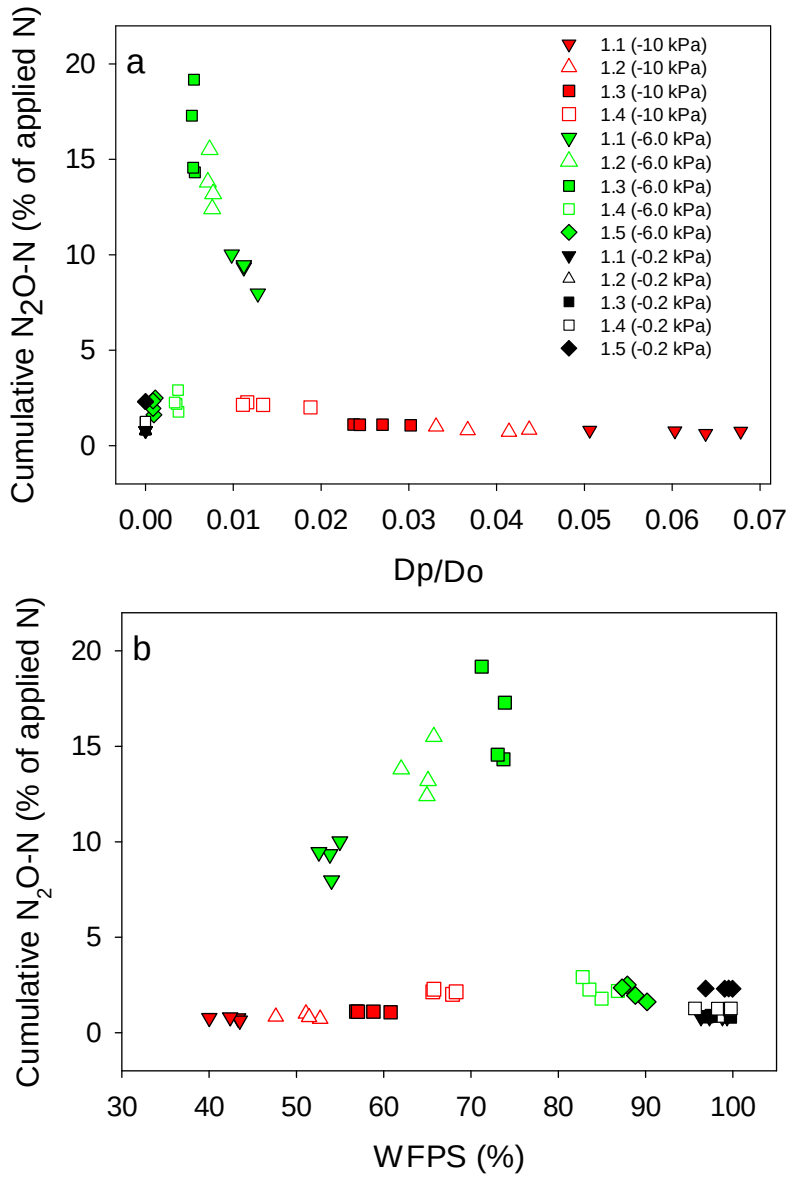

Figure 6.1 **Relationship of cumulative N_2O-N fluxes from a soil under varying ρ_b and ψ, with (a) *Dp/Do* (day 35) (b) WFPS. Data points represent individual replicates.**

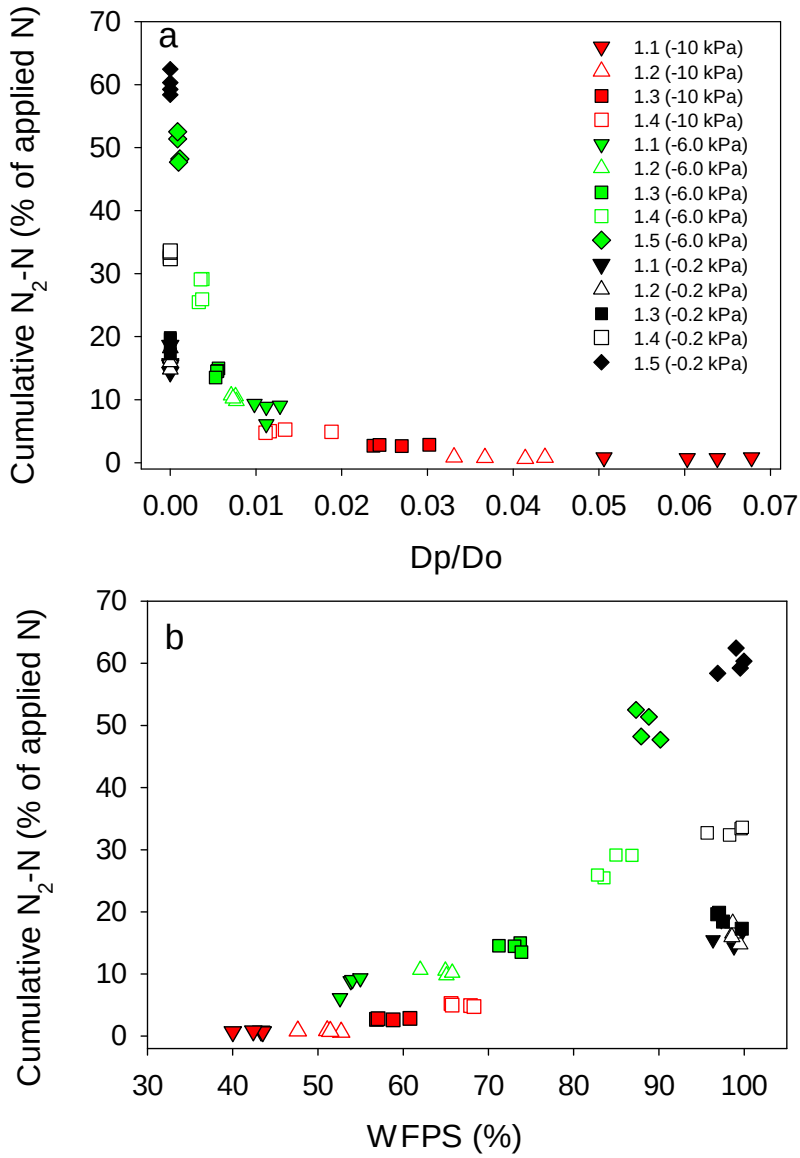

Figure 6.2 **Relationship of cumulative N_2-N fluxes from a soil under varying ρ_b and ψ, with (a) *Dp/Do* (day 35) (b) WFPS. Data points represent individual replicates.**

When cumulative N_2-N: N_2O-N ratios were plotted against both *Dp*/*Do* (Fig. 6.3) and WFPS (Fig. 6.4), the resulting plots were similar but *Dp*/*Do* produced least scatter which suggest that *Dp*/*Do* could be more sensitive in predicting cumulative N_2O-N, N_2-N fluxes and N_2-N: N_2O-N ratios. The N_2: N_2O ratios are crucial to the studies relating to denitrification from urine affected soils. Thus, future studies should explore the ability of *Dp*/*Do* as a potential predictor of N_2O fluxes via nitrification and denitrification from soils varying in physical characteristics.

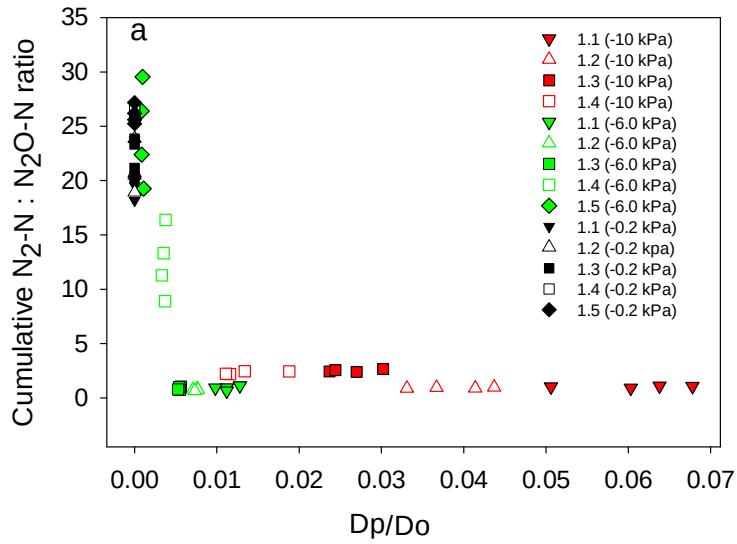

Figure 6.3 Relationship of cumulative N_2-N: N_2O-N ratios from a soil under varying ρ_b and ψ, with *Dp*/*Do* measured on day 35. Data points represent individual replicates.

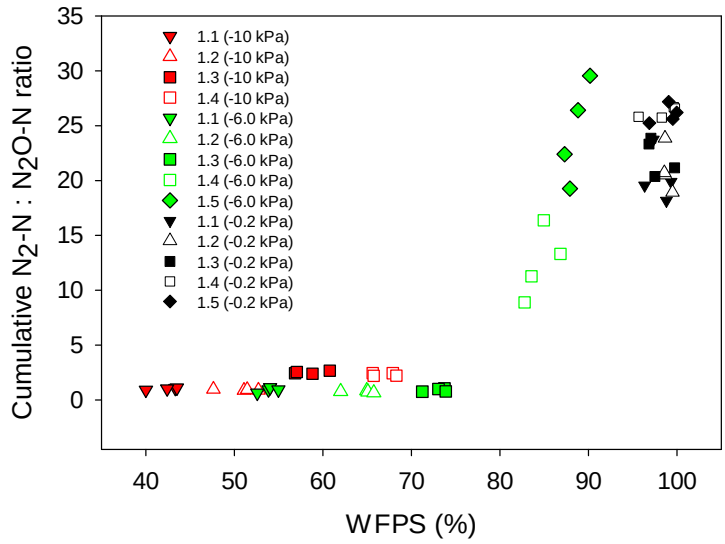

Figure 6.4 Relationship of cumulative N_2-N: N_2O-N ratios from a soil under varying ρ_b and ψ, with WFPS. Data points represent individual replicates.

The combined effects of increasing ψ from -10 to -0.2 kPa and increasing soil compaction is evident from the Fig. 6.5a. It is also interesting to note that the cumulative N_2O-N fluxes from these ρ_b treatments were highest at -6.0 kPa, which was the intermediate ψ level. This is similar to the results shown by Andersen and Petersen (2009), although they did not use varying compaction levels in their study. In that particular study, the highest potential for N_2O evolution was observed at the intermediate ψ level i.e. -3.0 kPa. From this current compiled data it is also very apparent that at -10 kPa (field capacity) the soil conditions were not entirely conducive for N_2O production (Fig. 6.5a) while at -0.2 kPa (saturated), soil conditions favoured complete denitrification resulting in more N_2-N than N_2O-N (Fig. 6.5b). This demonstrates that concurrent effects of changes in ψ and soil compaction need to be considered when determining ruminant urine-derived N_2O emissions.

All the above data and relationships were derived from ruminant urine (i.e. urea) affected soils where effects of both nitrification and denitrification were included. Thus, it would be interesting to obtain N_2O-N flux values solely via denitrification from varying ρ_b treatments after applying NO_3^- as a source of N to the same soil maintained at differing ψ levels (Chapter 7).

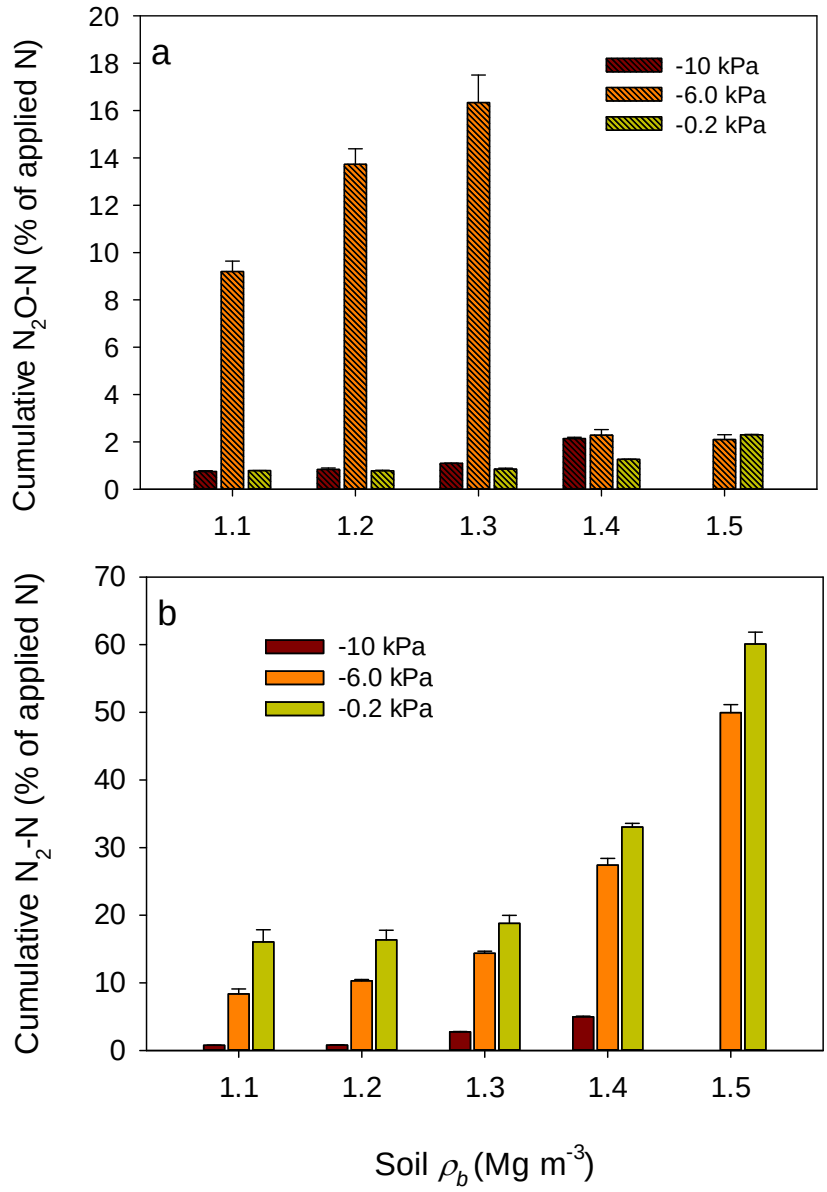

Figure 6.5 **Effect of varying matric potential (ψ) on (a) cumulative N_2O-N fluxes (b) Cumulative N_2-N fluxes from a soil under varying soil ρ_b (Mg m^{-3}). Error bars = s.e.m, n = 4.**

Chapter 7

Effect of soil bulk density and matric potential on relative gas diffusivity and nitrate-derived N_2O fluxes

7.1 Introduction

Chapter 4 showed that both N_2O-N and N_2-N fluxes increased with increases in soil bulk density (ρ_b) at a given matric potential (ψ). This increase in N_2O-N and N_2-N emissions was due to the negative effect that increasing soil ρ_b had on relative gas diffusivity (Dp/Do), a consequence of increasing WFPS. Previous chapters demonstrated that as ψ increased, soil conditions became more conducive for N_2O reduction in soil. Moreover, the water retention curve (WRC) and pore size distribution data obtained in Chapter 5 (experiment 2c) showed that ρ_b significantly affected soil water retention. The previous experiments were performed at only 3 different ψ levels (-10, -6.0 and -0.2 kPa) using urea as an N source to simulate ruminant urine. However, since urea was used in these experiments, there were simultaneously occurring processes i.e. nitrification of NH_4^+ and denitrification of NO_3^-, both of which contribute to N_2O production. There was also a rapid and substantial change in the soil pH during urea hydrolysis. While these processes do occur simultaneously in a urine patch due to dominance of urea-N, there is a need to further distil the relationship between ψ, Dp/Do and N_2O fluxes when only a NO_3^- substrate is present. Thus, in this chapter, it was decided to use NO_3^- as an N source instead of urea in order to obtain NO_3^- derived N_2O (via denitrification) fluxes over a range of ψ applied. This ensured the absence of substrate induced nitrification and other effects associated with urea hydrolysis e.g. significant increases in soil pH (Sherlock, 1984).

The relationship between ψ (independent variable) and N_2O fluxes (dependent variable) has been shown to vary from Gaussian (peak)(Castellano et al., 2010) to exponential (Dobbie and Smith, 2006). Castellano et al. (2010) showed that maximum N_2O emissions occurred at a matric potential which corresponded to a mean pore radius of 39.6 µm for varying soils within a landscape. They also emphasised that the relationship between N_2O and ψ was independent of the effect of soil type and proposed that water-filled pore size was an important factor affecting N_2O emissions. Smith et al. (1998) also demonstrated a similar response with an optimum ψ for N_2O fluxes from a single gleysol soil. Dobbie and Smith (2006) demonstrated, in a field study on a grassland soil, that N_2O emissions from a single soil decreased exponentially with decreasing ψ.

Van der Weerden et al. (2012), in a laboratory study, examined the effect of varying ψ on NO_3^- derived N_2O emissions from soils, of different textures and demonstrated that ψ and θ_v were the best variables for predicting N_2O emissions. However, there are no published studies that have examined the interaction between soil compaction and ψ on NO_3^- derived N_2O despite it being known that soil compaction has the potential to change pore size distribution, ultimately creating anaerobic conditions leading to high N_2O emissions (Chapter 5 and 6).

Therefore in this experiment soil was compressed in SS cores to similar ρ_b levels as in the previous experiments (Chapters 4 and 5) where urea had been applied to simulate urine application. However, in this experiment, soil cores at varying ρ_b levels were saturated with a NO_3^- solution and then further de-saturated to designated ψ to assess the effect of ρ_b on the relationship between ψ and N_2O fluxes from soil.

7.2 Hypotheses

As ψ decreases (becomes more negative), a higher percentage of pores drain and *Dp*/*Do* increases (Chapters 4 and 5). Thus, based on the previous experiments, it was hypothesised that in the presence of unlimited denitrification substrates, N_2O production via denitrification would be driven by the size of pores drained and *Dp*/*Do*, both of which would subsequently depend on the interaction of ψ and ρ_b. It was also hypothesised that *Dp*/*Do* would be better than either WFPS or ψ in explaining N_2O emissions from a soil varying in ρ_b.

7.3 Materials and Methods

A silt loam soil was randomly sampled (0-15 cm depth) from the Duncan Block, Lincoln University. It was air dried and sieved to ≤ 2 mm. Treatments included ρ_b at five levels (1.1, 1.2, 1.3, 1.4, and 1.5 Mg m^{-3}), each replicated four times with NO_3^--N at two levels (±N) and 11 levels of ψ (-1.0, -1.5, -2.0, -3.0, -4.0, -5.0, -6.0, -7.0, -8.0, -9.0 and -10.0 kPa). At each level of ψ, 2 sets of cores were made, A and B. Set A and set B included 40 cores each, both comprising all the ρ_b levels with ±N treatments. Set A was used to measure N_2O and *Dp*/*Do* while set B was used to measure soil physical and chemical characteristics (section 7.3.1)**.** All the soil cores were subjected to similar conditions during the course of the experiment. The temperature of the room in which the tension tables and soil cores were housed was in the range of 21.8-24.2^oC (mean 23.1^oC) throughout the experimental period.

A preliminary test was performed prior to performing the main experiment to observe the changes in NO_3^--N and DOC levels over a period of 6 days following soil core saturation. Measurements were made of inorganic N and DOC on day 2 (following 2 days of saturation), on day 4 (2 days after placing cores on tension tables), and on day 6 (after 4 days of equilibration on tension tables) as it was thought that soil native carbon (C) might get depleted during this period. For this test, 4 replicates of each ρ_b were made (section 3.2) and soaked in a KNO_3 solution (NO_3^--N, 1800 µg mL^{-1}) for 2 days and then drained at -1.0 kPa for a further 4 days. After which NO_3^--N and DOC were measured by destructive analysis. This process was also performed at -10 kPa. After observing the results from the preliminary test it was confirmed that both NO_3^--N and DOC were present in sufficient quantities to support denitrification (section 7.4.1).

Finally, experiment 3 was performed where soil cores were made by compacting the soil to a depth of 4.1 cm into SS rings (7.3 cm internal diameter, 7.4 cm deep)(section 3.2) and then all soil cores were pre-soaked in a KNO_3 solution 1 (1800 µg mL^{-1} NO_3^--N) for 2 days. After this soil cores were placed on a tension table to equilibrate for another 4 days at designated ψ levels, whereupon *Dp*/*Do* and N_2O readings were taken. The concentration of the NO_3^--N in KNO_3 solution 1 was calculated so that each ρ_b soil core attained a NO_3^--N concentration of at least 400 µg NO_3^--N g^{-1} soil upon saturation. This minimum value of NO_3^--N was used because it was similar to the highest NO_3^--N concentrations reached in previous experiments (Chapters 4 and 5). This was done to ensure NO_3^--N was non-limiting. All the -N cores (controls) were treated in a similar way except DI water was used in place of the NO_3^- solution to saturate the cores.

Tension tables were prepared by pouring 10 mL of the KNO_3 solution 1 evenly across the tension tables before placing the soil cores on in order to provide a good connection between the soil cores and the tension table.

It took 1.5 days to finish N_2O and *Dp*/*Do* measurements as *Dp*/*Do* was measured immediately following the N_2O flux measurements. After these measurements were completed, 1 mL of KNO_3 solution 2 (600 µg mL^{-1} NO_3-N) and 1 mL of a C solution (600 µg mL^{-1} C) were added to the +N cores and they were again placed on a tension table set at the same ψ for a period of 6 h after which a second set of N_2O measurements was taken. This was done to assess whether adding more substrate to the soil would further affect the N_2O fluxes and to try and determine N_2: N_2O ratios. In the ρ_b 1.1 and 1.5 Mg m^{-3} treatments, the NO_3^--N (KNO_3 solution 2) was ^{15}N enriched at 40 atom %.

Rather than running all the 880 soil cores at once (5 levels of ρ_b x 11 levels of ψ x 4 replicates x 2 N levels x 2 sets i.e. Set A and Set B), which was physically impossible, sets of 80 soil cores, 40 for Set A (± N x 5 levels of ρ_b x 4 replicates) and 40 for Set B (± N x 5 levels of ρ_b x 4 replicates) (section 7.3.1) were made each time and then used to evaluate the effect of a given level of ψ. The process from soil core saturation to completion of the measurements including N_2O and *Dp*/*Do* and destructive analysis from 80 soil cores at each ψ level took 8 days. A new set of cores for each ψ level ensured that similar native soil DOC concentrations were available at each ψ level which would not have been possible if the same set of cores had been drained stepwise to different ψ.

7.3.1 Experimental approach adopted at each ψ

Set A (±N)

was used to measure N_2O and *Dp*/*Do*

↓

Saturated with KNO_3 solution 1 (+ N cores) or DI water (-N cores) for 2 days and drained at X* on tension tables

↓

Soil cores equilibrated on tension tables for 4 days. After that N_2O and *Dp*/*Do* were measured as described in sections 3.3 and 3.1, respectively.

↓

Following N_2O and *Dp*/*Do* measurements, 1 mL of carbon (glucose solution) + 1 mL of KNO_3 (solution 2) were added to +N cores (section 7.3)

↓

N_2O measured after 6 h

Note: X* was the level of ψ applied.

Set B (±N)

was used to measure soil physical and chemical characteristics.

↓

Saturated with KNO_3 solution 1 (+ N cores) or DI water (-N cores) for 2 days and drained at X* on tension tables

↓

Soil cores equilibrated on tension tables for 4 days. After that soil cores were destructively sampled to determine entrapped N_2O (section 7.3.4), inorganic-N, DOC, bulk soil pH, WFPS and air-filled porosity (ε) (section 3.4).

7.3.2 Gas sampling and analyses

'Set A' soil cores were used for N_2O flux determination. Gas flux sampling for N_2O fluxes was performed by placing each soil core in a paint tin (1 L) and sealing it with an air-tight lid (section 3.3). Gas samples were taken at 0, 15 and 30 min after sealing the paint tin and were analysed by gas chromatography (SRI- 8610, CA, USA) equipped with a ^{63}Ni electron capture detector (section 3.3.1). A 15 mL gas sample was also taken from 'set A' cores 3 h after closing the tin and these were analysed by isotope ratio mass spectrometry (PDZ Europa Ltd, Crewe, UK) to determine the ^{15}N enrichment of the N_2O.

7.3.3 Soil analyses

Soil destructive analyses were performed on 'set B' soil cores on 11 occasions to measure entrapped N_2O (section 7.3.4),WFPS, ε, bulk soil pH, soil inorganic N concentrations and soil DOC concentrations (section 3.4). Soil WFPS and ε were determined only on +N soil cores from 'Set B' soil cores. Bulk soil pH was measured by diluting soil samples to a 2.5:1 ratio by adding 25 mL of deionized water to 10 g of air dried soil. After shaking the soil solution for 30 seconds by hand, it was left to settle for a minimum of 12 h before measuring the pH with a calibrated pH meter (Mettler Toledo, USA) (section 3.4.1). Soil surface pH was not measured in this experiment. Soil inorganic-N and DOC concentrations were measured as described previously (section 3.4). However, as the measurements at each ψ level were to be finished within 1.5 days, only 3 replicates at each ρ_b were analyzed for entrapped N_2O and further subsampled for bulk soil pH, inorganic N and DOC analyses. Values of Dp/Do at each ρ_b were measured on 'Set A' cores to investigate the response to varying ψ. Pore continuity (C) was also calculated as the ratio of Dp/Do to ε from individual measurements (section 3.4.3).

7.3.4 Entrapped N_2O in soil

Soil entrapped N_2O was measured by placing each soil core from 'Set B' into a Ziploc® plastic bag (30 x 25.5 cm) and sealing it. The soil from the core was then pushed out into the bag and rapidly spread inside the plastic bag to release the entrapped N_2O. A 10 mL gas sample was then removed from the plastic bag using a gas-tight syringe and placed into a 6-mL Exetainer® which was then analysed for N_2O (section 3.3). After this the whole bag was immersed into a container filled with water and the volume of water displaced by the bag and its contents was determined. The volume of gas (V_g) inside the plastic bag was then calculated by subtracting the volumes of the soil, soil water and soil ring.

The concentration of N_2O in soil solution was calculated using the following equation (Davidson and Firestone, 1988):

$$(N_2O)_{liquid} = (N_2O)_{gas} \times \alpha \quad [7.1]$$

Where α is the Bunsen coefficient (mL of gas mL^{-1} water at standard temperature and pressure). The Bunsen coefficient of N_2O at 25°C was taken to be 0.544 (Davidson and Firestone, 1988). The soil Bunsen coefficient accounts for N_2O dissolved in the liquid phase of the soil cores by assuming equilibrium between headspace and liquid phases.

The total N_2O in the Ziploc® plastic bag was then calculated as follows:

$$N = C \times \left(V_g + [V_l \times \alpha]\right) \quad [7.2]$$

where:

N = total N_2O in the plastic bag (µL),

C = headspace N_2O concentration (µL L^{-1}),

V_g = volume of gas inside plastic bag (L),

V_l = volume of liquid in soil (L),

α = Bunsen coefficient for N_2O (mL of gas mL^{-1} water).

The concentration of N_2O in soil water was calculated using the following equation:

$$C_{N2O} = \frac{N}{V_l} \quad [7.3]$$

where:

C_{N2O} = N_2O concentration in soil water (µL L^{-1}),

N = total N_2O in the plastic bag (µL),

V_l = volume of liquid in soil (L).

7.3.5 Statistical analyses

All the statistical analyses were performed using Minitab (version 16). Data were tested for normality using the Anderson-Darling test. The N_2O-N flux data was ln (value +1) transformed while *Dp*/*Do* was $\log_{10}$ transformed before analyses. The effect of ρ_b at each level of ψ on inorganic N, DOC, bulk soil pH, WFPS, *C*, *Dp*/*Do*, N_2O-N emissions and entrapped N_2O-N from soil cores was performed using one way ANOVA with $p < 0.05$ to indicate level of significance of the differences. Tukey's test was performed to detect the differences between the means. Effects of interaction between soil ρ_b and ψ on N_2O-N fluxes, inorganic N, bulk soil pH, DOC, entrapped N_2O and soil physical characteristics measured from +N soil cores were assessed using two-way ANOVA. Graphing and non-linear curve fitting were performed using Sigmaplot (version 12) while split-line regression (section 4.3) was performed using GenStat (version 14).

One way ANOVA and Tukey's test were also used to assess the effect of ρ_b on the values of WFPS, θ_v, *Dp*/*Do*, and soil pore continuity (C) and pore size drained where maximum N_2O-N flux occurred. These indices are subsequently referred as $WFPS_{N2Omax}$, $\theta_{vN2Omax}$, Dp/Do_{N2Omax}, C_{N2Omax} and $pore\ size_{N2Omax}$. A three-parameter Gaussian function described by equation 7.4 was fitted to the N_2O-N fluxes and ψ data to identify ψ_{N2Omax}, i.e. ψ at which maximum N_2O occurred for each ρ_b.

$$y = ae^{\left[-0.5\left(\frac{x-x_o}{b}\right)^2\right]} \qquad [7.4]$$

where:

y = N_2O-N (mg m^2 h^{-1}),

x = ψ (-kPa),

x_o= ψ_{N2Omax}(-kPa).

a and b are fitting parameters (dimensionless)

Soil water retention curves (WRC) obtained in Chapter 5 were used to calculate the air entry value (ψ_a) (section 2.6.2.1) using the Campbell equation (section 2.6.2.1). Data points that showed deviation from a linear fit were not included in fitting a linear line to the log-log plot of the water retention data for each level of ρ_b. The slope and the intercept of the straight line corresponded to the Campbell water retention parameter (-b) and air entry value (ψ_a), respectively (section 2.6.2.1). One way ANOVA was used to compare the means of -b and ψ_a obtained under varying ρ_b treatments.

The values for bulk soil pH, NO_3^--N, NH_4^+-N and N_2O-N fluxes obtained from -N cores are provided in Appendix A.

A scatter plot comparison was also performed between the measured *Dp*/*Do* data and *Dp*/*Do* values obtained using predictive models. Diffusivity models were compared using the root mean square (RMSE) of prediction for overall best fit compared with the measured data (Moldrup et al., 2004).

$$RMSE = \sqrt{\frac{1}{n}\sum_{i=1}^{n}(d_i)^2} \quad [7.5]$$

where:

d_i = difference between the predicted and the measured value of *Dp/Do* at a given ψ,

n = total number of measurements.

Bias was also used to determine the model's overestimation (positive bias) or underestimation (negative bias) of the measured data (Moldrup et al., 2004).

$$Bias = \frac{1}{n}\sum_{i=1}^{n}(d_i) \quad [7.6]$$

7.4 Results

7.4.1 Results from the preliminary tests

Following saturation, high NO_3^--N (≥ 400 μg g^{-1} soil) and DOC concentrations were obtained at both -1.0 kPa (Tables 7.1, 7.2) and -10 kPa (Tables 7.3, 7.4). This ensured non-limiting substrate concentrations for denitrification. However, both NO_3^--N and DOC concentrations decreased with time. No further statistical analysis was performed on the preliminary data.

Table 7.1 Soil NO_3^--N concentrations at -1.0 kPa under varying soil ρ_b after saturation with NO_3^- solution and subsequent equilibration on tension tables. Values are means of 4 replicates with standard deviations in brackets.

	NO_3^--N (μg g^{-1} soil) at -1.0 kPa		
Soil bulk density (Mg m^{-3})	**After saturation (day 2)**	**After 2 days of equilibration on tension tables (day 4)**	**After 4 days of equilibration on tension tables (day 6)**
1.1	607 (16)	432 (21)	167 (13)
1.3	657 (27)	412 (16)	122 (16)
1.5	505 (16)	489 (17)	104 (14)

Table 7.2 Soil DOC concentrations at -1.0 kPa under varying soil ρ_b after saturation with NO_3^- solution and subsequent equilibration on tension tables. Values are means of 4 replicates with standard deviations in brackets.

	DOC (μg C g^{-1} soil) at -1.0 kPa		
Soil bulk density (Mg m^{-3})	**After saturation (day 2)**	**After 2 days of equilibration on tension tables (day 4)**	**After 4 days of equilibration on tension tables (day 6)**
1.1	120 (18)	115 (15)	38 (6)
1.3	139 (12)	128 (11)	42 (9)
1.5	158 (14)	124 (17)	35 (7)

Table 7.3 **Soil NO_3^--N concentrations at -10 kPa under varying soil ρ_b after saturation with NO_3^- solution and subsequent equilibration on tension tables. Values are means of 4 replicates with standard deviations in brackets.**

	NO_3^--N (μg g^{-1} soil) at -10 kPa		
Soil bulk density (Mg m^{-3})	**After saturation (day 2)**	**After 2 days of equilibration on tension tables (day 4)**	**After 4 days of equilibration on tension tables (day 6)**
1.1	611 (21)	400 (20)	313 (11)
1.3	632 (22)	458 (11)	323 (14)
1.5	513 (15)	301 (13)	218 (12)

Table 7.4 **Soil DOC concentrations at -10 kPa under varying soil ρ_b after saturation with NO_3^- solution and subsequent equilibration on tension tables. Values are means of 4 replicates with standard deviations in brackets.**

	DOC (μg C g^{-1} soil) at -10 kPa		
Soil bulk density (Mg m^{-3})	**After saturation (day 2)**	**After 2 days of equilibration on tension tables (day 4)**	**After 4 days of equilibration on tension tables (day 6)**
1.1	113 (18)	108 (5)	103 (14)
1.3	131 (17)	112 (11)	96 (17)
1.5	142 (15)	98 (13)	89 (28)

7.4.2 Results from experiment 3

7.4.2.1 Soil physical conditions

There was a significant ($p < 0.01$) effect of soil ρ_b on soil ε at all levels of ψ except at -1.0 kPa with ε being higher in lower ρ_b treatments (Fig. 7.1). The mean values of ε ranged from 0.06 to 0.34 $m^3\ m^{-3}$ for 1.1 Mg m^{-3} and 0.05 to 0.16 $m^3\ m^{-3}$ for 1.5 Mg m^{-3} with the decrease in ψ from -1.0 to -10 kPa. A strong interaction ($p < 0.01$) between ρ_b and ψ also existed with the rate of increase in ε higher at -1.5, -2.0 and -5.0 kPa for 1.1, 1.2 and 1.4 Mg m^{-3} treatments, respectively (Fig. 7.1).

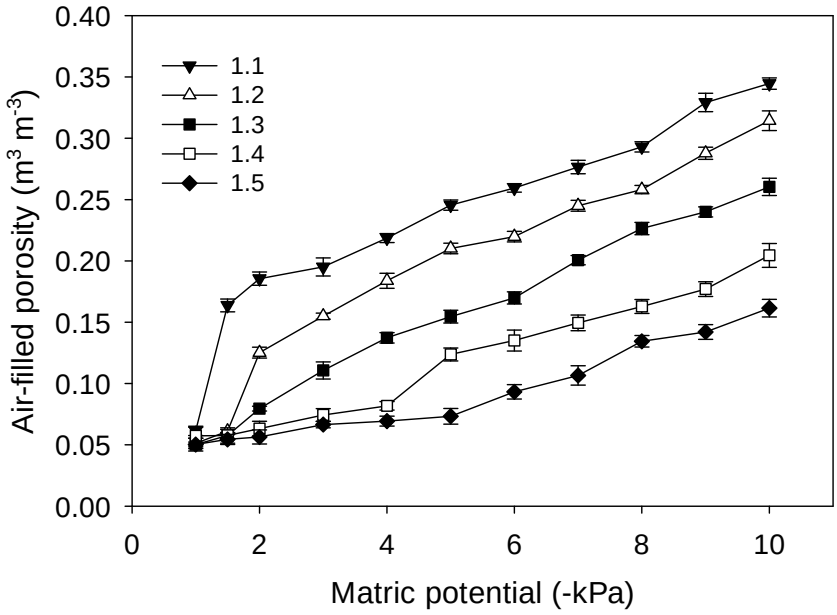

Figure 7.1 Effect of soil ρ_b on the relationship between air-filled porosity (ε) and matric potential (ψ) for +N soil cores. Numerals in the legend indicate ρ_b (Mg m^{-3}) applied. Error bars = s.e.m, n = 4.

Soil ρ_b significantly ($p < 0.01$) affected WFPS with higher WFPS values in the higher ρ_b treatments except at -1.0 kPa (Fig. 7.2). The mean values of WFPS ranged from 89 to 41% for 1.1 Mg m^{-3} and 88 to 65% for 1.5 Mg m^{-3} with the decrease in ψ from -1.0 to -10 kPa. A strong interaction ($p < 0.01$) between ρ_b and ψ was due to a greater rate of decrease in WFPS at -1.5, -2.0 and -5.0 kPa for the 1.1, 1.2 and 1.4 Mg m^{-3} treatments, respectively (Fig. 7.2).

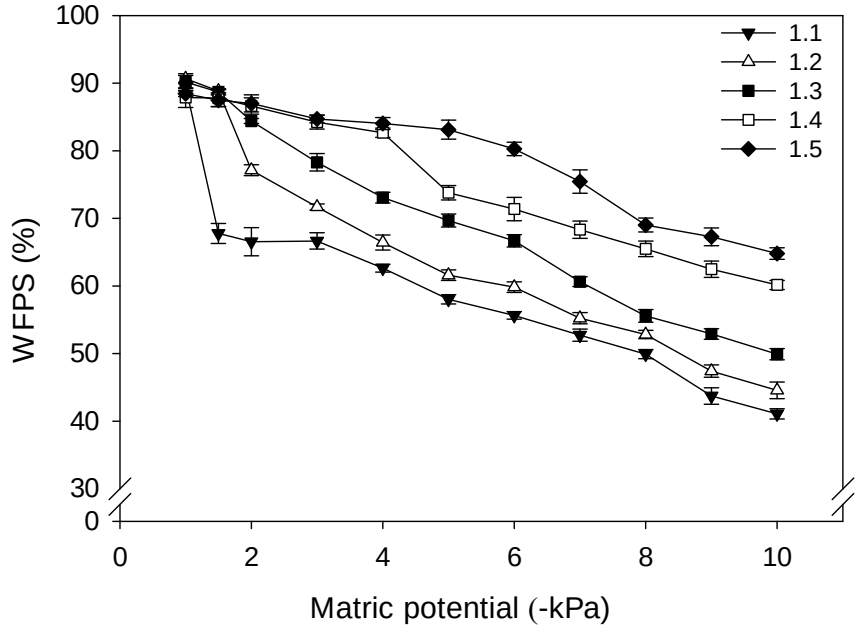

Figure 7.2 Effect of soil ρ_b on the relationship between WFPS and matric potential (ψ) for +N soil cores. Numerals in the legend indicate ρ_b (Mg m^{-3}) applied. Error bars = s.e.m, n = 4.

Soil ρ_b also significantly ($p < 0.01$) affected log-transformed *Dp*/*Do* with higher *Dp*/*Do* values in the lower ρ_b treatments. The mean values of *Dp*/*Do* ranged from 0 to 0.077 at 1.1 Mg $m^{-3}$and 0 to 0.015 for 1.5 Mg m^{-3} with the decrease in ψ from -1.0 to -10 kPa (Fig. 7.3). Values of *Dp*/*Do* were zero at -1.0 kPa at all levels of soil ρ_b. A strong interaction ($p < 0.01$) between ρ_b and ψ occurred with rates of increase in *Dp*/*Do* greater at 1.1 and 1.2 Mg m^{-3} when ψ decreased from -7.0 to -10.0 kPa. The interaction between ψ and soil ρ_b and the effect on *Dp*/*Do* is depicted by a 3D mesh plot in the Fig.7.4.

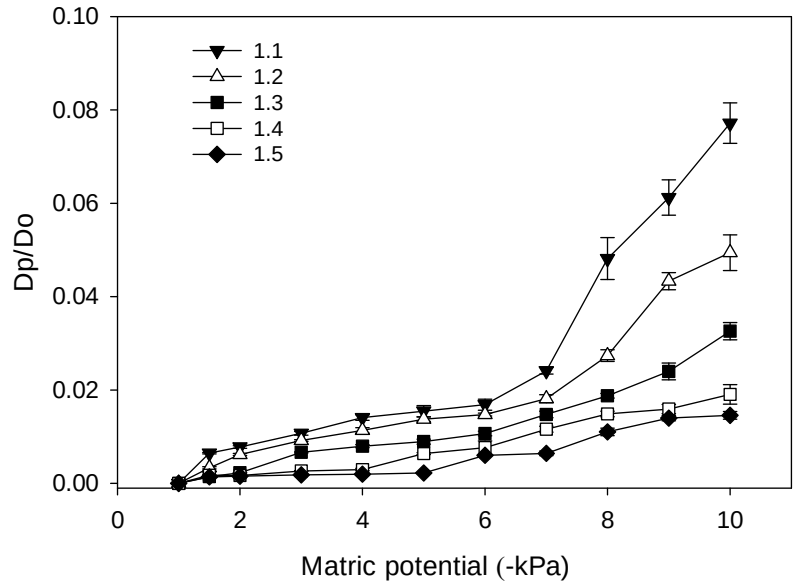

Figure 7.3 Effect of soil ρ_b on the relationship between relative gas diffusivity (*Dp*/*Do*) and matric potential (ψ) for +N soil cores. Numerals in the legend indicate ρ_b (Mg m^{-3}) applied. Error bars = s.e.m, n = 4.

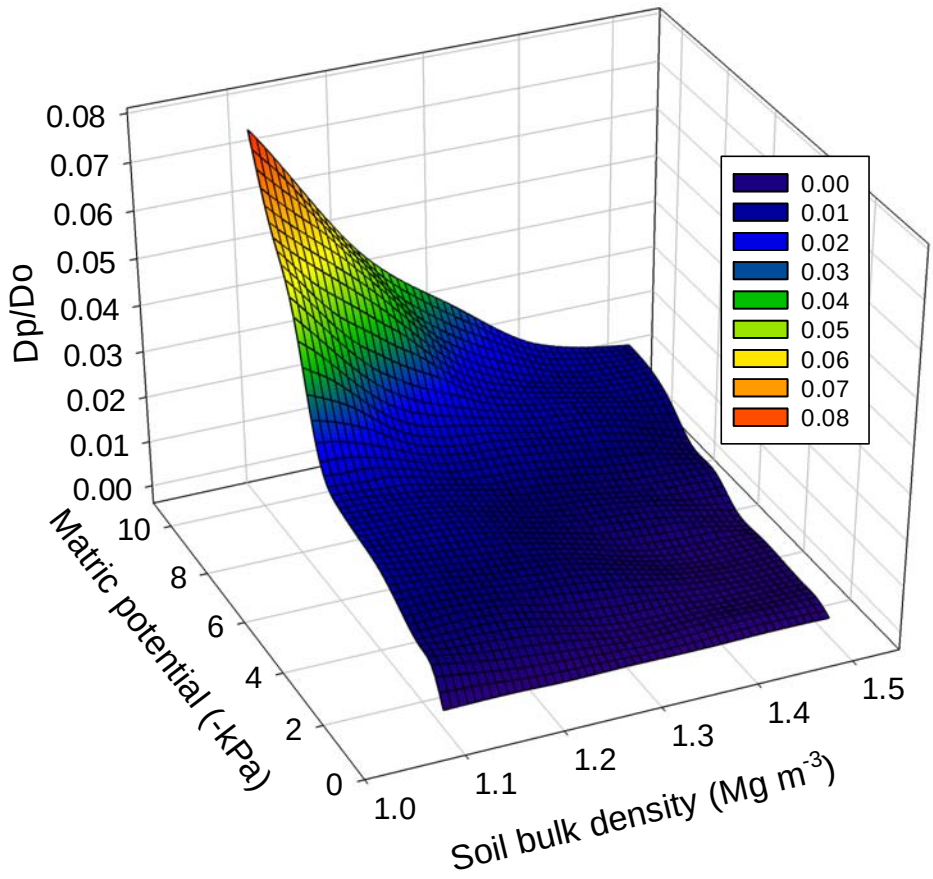

Figure 7.4 **Mesh plot of relative gas diffusivity (*Dp*/*Do*) versus soil bulk density (ρ_b) and matric potential (ψ) for +N treated soil cores.**

When *Dp*/*Do* values measured over a range of ψ from each ρ_b treatment were plotted against ε, significant ($p < 0.01$) relationships emerged (Fig. 7.5). At a given ε value, there was an increase in *Dp*/*Do* with increases in soil ρ_b when ε was < 0.3. For each soil ρ_b, the relationship between the measured *Dp*/*Do* and ε was well described by a two parameter power function (section 2.6.3) (Ball et al., 1988; Hamamoto et al., 2011) depicted by the following equation:

$$\frac{Dp}{Do} = A(\varepsilon)^X \qquad [7.7]$$

where:

A = pore connectivity parameter (dimensionless),

X= water blockage factor (dimensionless).

The equations for the fitted two parameter power curves are presented in the Table 7.5.

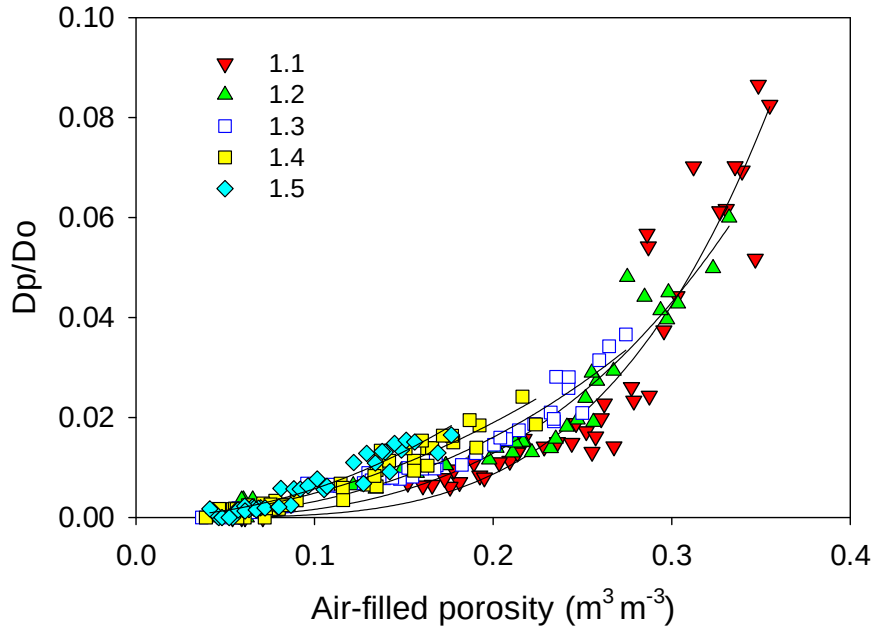

Figure 7.5 Effect of soil ρ_b on the relationship between relative gas diffusivity (*Dp*/*Do*) and air filled porosity (ε) obtained over a range of ψ applied. Numerals in the legend indicate ρ_b (Mg m^{-3}) applied. Data points indicate individual replicates. Equations for the fitted lines are shown in Table 7.5.

Table 7.5 **Effect of soil ρ_b on the relationship between relative gas diffusivity (Dp/Do) and air-filled porosity (ε) measured at varying ψ. Equations are derived from fitting two parameter power functions ($Dp/Do = A(\varepsilon)^X$) to the data (Fig. 7.5) and the degree of variation and significances are shown as r^2 and p, respectively.**

Soil bulk density (Mg m^{-3})	Equation	r^2, p value
1.1	$Dp/Do = 4.78(\varepsilon)^{3.92}$	0.90, $p < 0.01$
1.2	$Dp/Do = 1.55(\varepsilon)^{2.98}$	0.94, $p < 0.01$
1.3	$Dp/Do = 0.67(\varepsilon)^{2.33}$	0.95, $p < 0.01$
1.4	$Dp/Do = 0.44(\varepsilon)^{2.0}$	0.92, $p < 0.01$
1.5	$Dp/Do = 0.63(\varepsilon)^{2.0}$	0.91, $p < 0.01$

When both, *A* and *X* were plotted versus soil ρ_b, strong exponential relationships emerged (Fig. 7.6a and 7.6b) which showed that these parameters decreased with an increase in soil ρ_b.

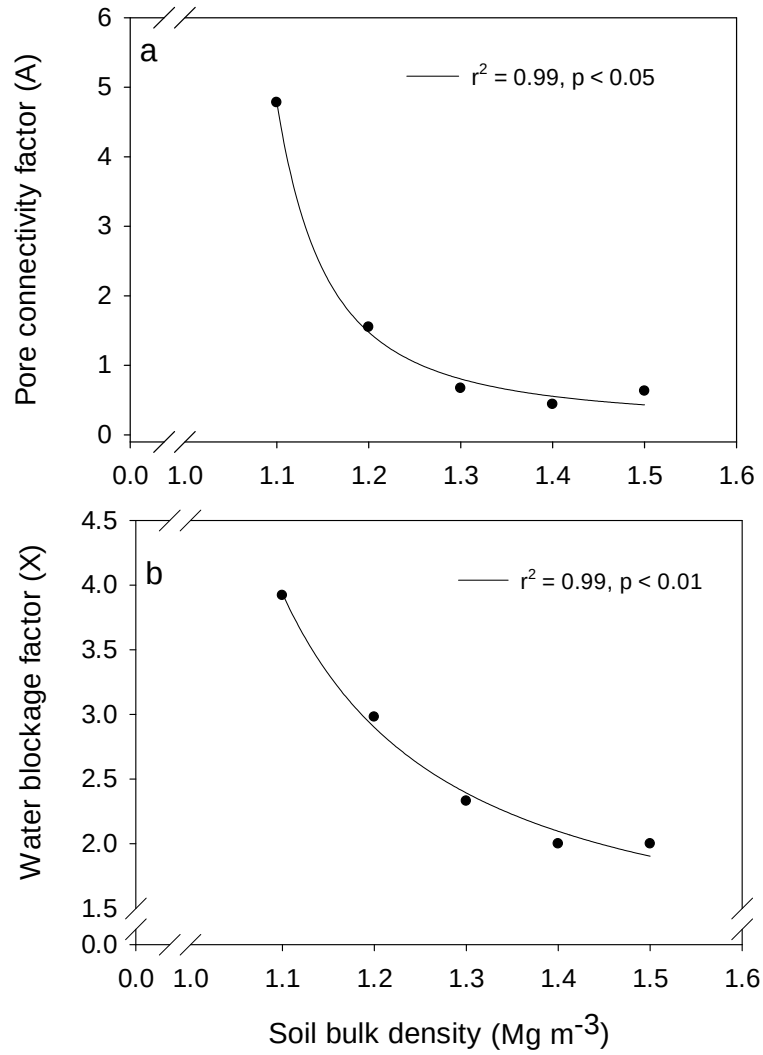

Figure 7.6 (a) Pore connectivity parameter (*A*) and (b) Water blockage factor (*X*) as a function of soil bulk density (Mg m^{-3}). Parameters *A* and *X* were obtained by fitting a two parameter power function to the relationship between *Dp*/*Do* and air-filled porosity (ε) observed at each level of ρ_b under varying ψ levels (Fig 7.5, Table 7.3). Regression lines are the modified single exponential decay function fitted to the data points.

When *Dp*/*Do* was plotted against relative air-filled porosity (ε/ϕ), soil ρ_b induced differences were reduced (Fig. 7.7).

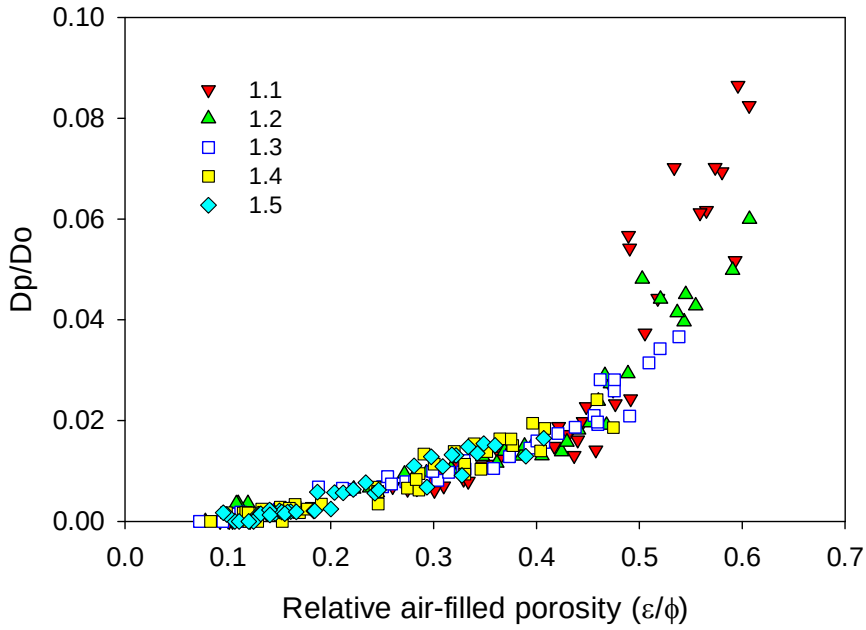

Figure 7.7 Relationship between relative gas diffusivity (*Dp*/*Do*) and relative air filled porosity. Numerals in the legend indicate ρ_b applied. Data points are individual replicates.

When *Dp*/*Do* values were plotted against ε for each ψ, with data pooled across varying ρ_b treatments, significant ($p < 0.01$) relationships emerged (Fig. 7.8). There was an increase in *Dp*/*Do* at more negative ψ levels across the ε interval (0.15- 0.27) At each ψ level, the measured *Dp*/*Do* data was well described by a power function depicted by the following equation:

$$\frac{Dp}{Do} = A'(\varepsilon)^{X'} \qquad [7.8]$$

where:

A' = pore connectivity parameter (dimensionless),

X' = water blockage factor (dimensionless).

The fitted equations and the parameters are shown in Table 7.6.

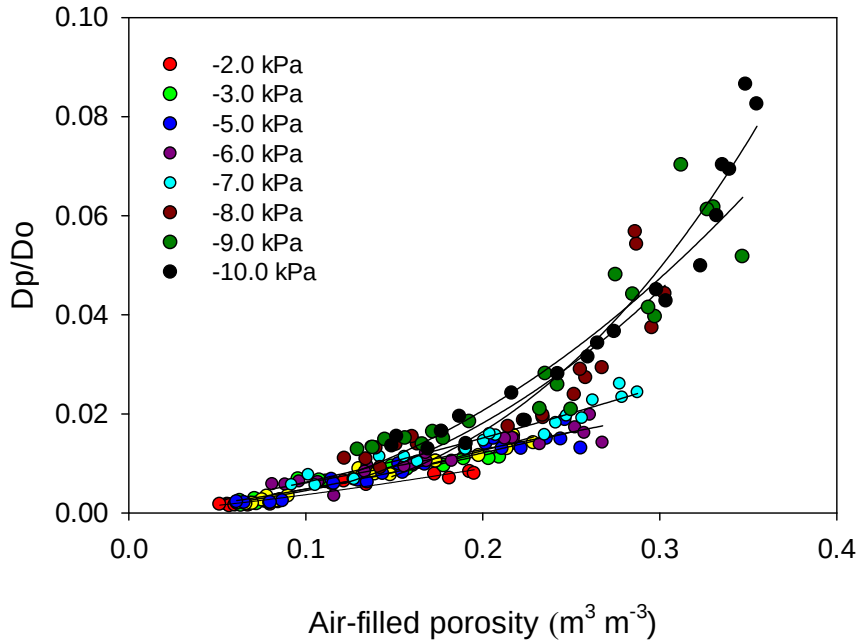

Figure 7.8 **Effect of matric potential (ψ) on the relationship between relative gas diffusivity (*Dp/Do*) and air filled porosity (ε) when data from varying ρ_b were pooled for each level of ψ. Numerals in the legend indicate ψ applied. Data points indicate individual replicates. Equations for the fitted lines are shown in Table 7.6.**

Table 7.6 **Effect of matric potential (ψ) on the relationship between relative gas diffusivity (Dp/Do) and air-filled porosity (ε) measured under over a range of soil ρ_b. Equations are derived from fitting two parameter power functions ($Dp/Do = A'(\varepsilon)^{X'}$) to the data (Fig. 7.8) and the degree of variation and significances are shown as r^2 and p, respectively.**

Matric potential (-kPa)	Parameter A'	Parameter X'	r^2, p value
2.0	0.07	1.27	0.91, $p < 0.001$
3.0	0.09	1.27	0.92, $p < 0.001$
4.0	0.13	1.48	0.96, $p < 0.001$
5.0	0.10	1.33	0.92, $p < 0.001$
6.0	0.07	1.08	0.88, $p < 0.001$
7.0	0.12	1.28	0.93, $p < 0.001$
8.0	0.66	2.24	0.80, $p < 0.001$
9.0	0.55	2.04	0.86, $p < 0.001$
10.0	1.30	2.70	0.94, $p < 0.001$

When *X'* and *A'* were plotted against ψ strong relationships emerged (Fig. 7.9a and 7.9b) which showed that these parameters varied when ψ decreased from -2.0 to -10 kPa. A split-line regression (section 7.3.5) performed on the data showed that both, *A'* and *X'* increased linearly ($p < 0.01$) when ψ ranged from -7.0 to -10.0 kPa. When *Dp*/*Do* was plotted against relative air-filled porosity (ε/ϕ), ψ induced differences were also reduced (Fig. 7.10).

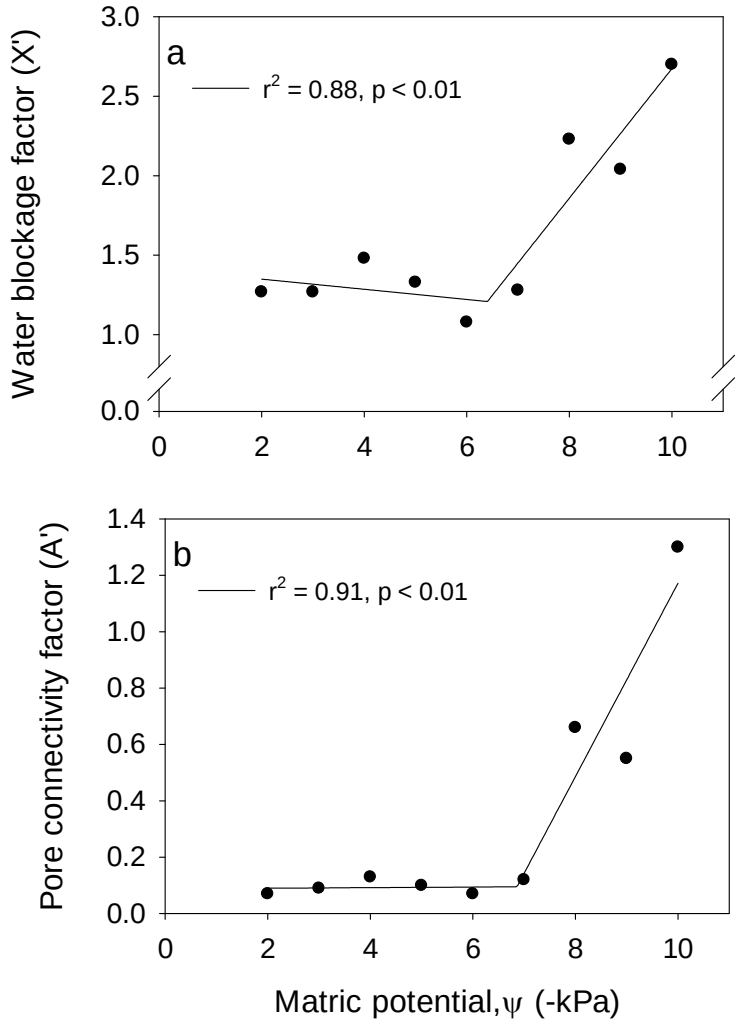

Figure 7.9 (a) Water blockage factor (*X'*), and (b) Pore connectivity parameter (*A'*) as a function of soil bulk density, ρ_b (Mg m^{-3}). Parameters *A'* and *X'* were obtained by fitting a power function to the relationship between *Dp*/*Do* and air-filled porosity (ε) observed at each level of ρ_b under varying ψ levels. Regression lines are split-line functions fitted to the data points.

.

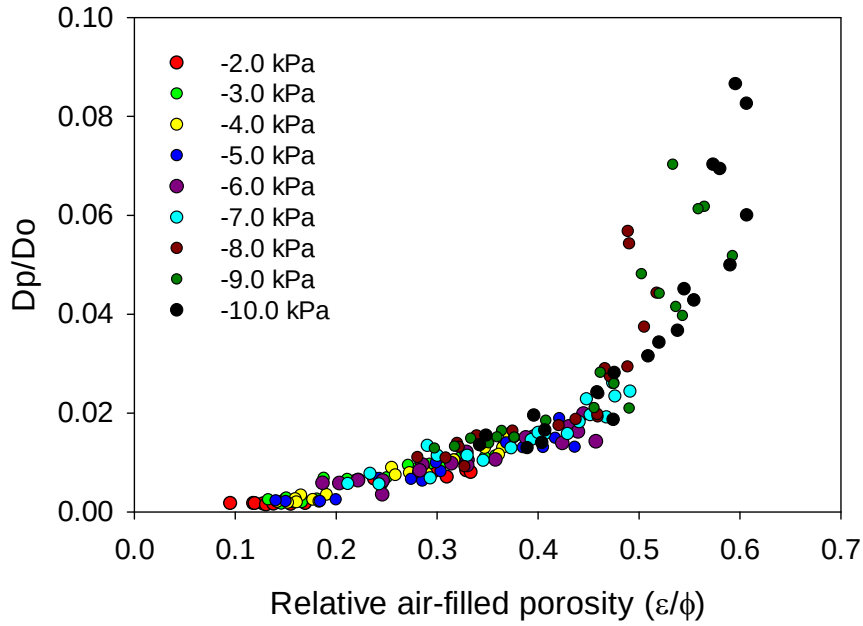

Figure 7.10 Relationship between relative gas diffusivity (*Dp*/*Do*) and relative air filled porosity. Numerals in the legend indicate ψ applied. Data points are individual replicates.

Soil pore continuity (*C*), the ratio of *Dp*/*Do* to ε, was also affected by soil ρ_b with higher *C* values in the lower ρ_b treatments except at -1.0 and -6.0 kPa (Fig. 7.11). The mean values of *C* ranged from 0 to 0.22 for 1.1 Mg m^{-3} and 0 to 0.09 for 1.5 Mg m^{-3} when ψ went from -1.0 to -10 kPa. A strong ($p < 0.01$) interaction between ρ_b and ψ also occurred with *C* increasing at a faster rate at 1.1 Mg m^{-3} from -7.0 to -10.0 kPa.

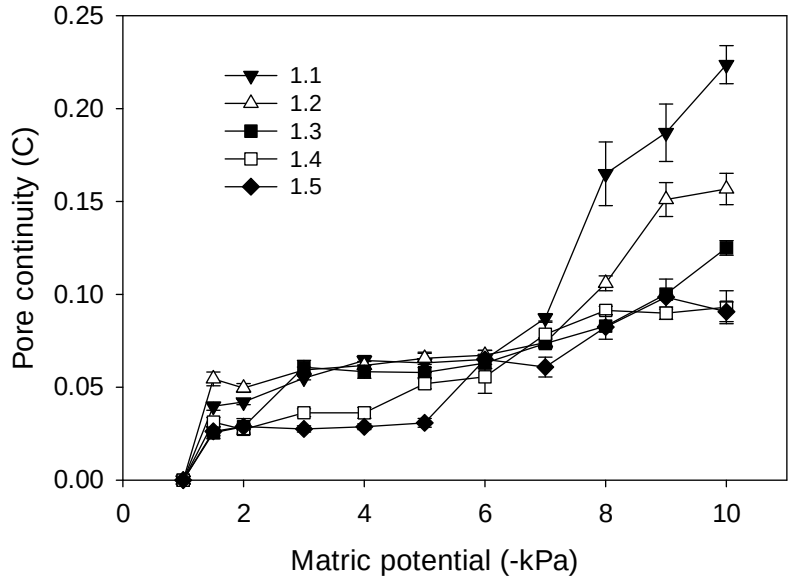

Figure 7.11 Effect of soil ρ_b (Mg m^{-3}) on the relationship between pore continuity (*C*) and matric potential (ψ) for +N soil cores. Numerals in the legend indicate ρ_b (Mg m^{-3}) applied. Error bars = s.e.m, n = 4.

7.4.2.2 Bulk soil pH, inorganic N, DOC

Bulk soil pH in +N soil cores ranged from 6.60 to 6.97 at -1.0 kPa and decreased, thereafter, with further decreases in ψ, reaching values of 5.3 to 5.65 at -10 kPa, respectively (Fig.7.12). Soil ρ_b significantly ($p < 0.01$) affected bulk soil pH in +N cores with higher bulk soil pH in the 1.4 and 1.5 Mg m^{-3} treatments when compared with ≤ 1.3 Mg m^{-3} ρ_b treatments at all levels of ψ (Fig. 7.12). There was no significant interaction between ρ_b and ψ on bulk soil pH in +N soil cores. In control cores (-N), however, no effect of soil ρ_b was seen on bulk soil pH at most ψ levels except at -4.0, -5.0 and -9.0 kPa where higher ($p < 0.01$) bulk soil pH was observed at higher ρ_b treatments. When comparing ± N treatments, it was found that the bulk soil pH in +N cores was higher ($p < 0.01$) than in the -N cores from -1.0 to -7.0 kPa.

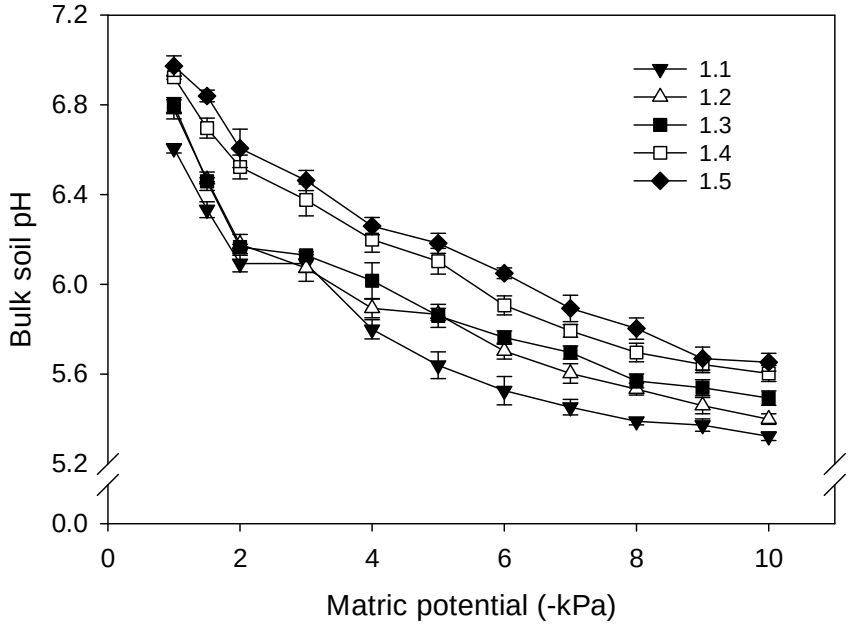

Figure 7.12 Mean bulk soil pH versus matric potential (ψ) from +N soil cores. Numerals in the legend indicate ρ_b (Mg m^{-3}) treatments applied. Error bars = s.e.m, n = 3.

After 4 days of equilibration on tension tables, mean soil NO_3^--N concentrations in the +N soil cores ranged from 126 to 84 µg g^{-1} soil at 1.1 and 1.5 Mg m^{-3}, respectively, at -1.0 kPa. At -10 kPa, mean soil NO_3^--N concentrations at ρ_b values of 1.1 and 1.5 Mg m^{-3} were 389 and 286 µg g^{-1} soil, respectively (Fig. 7.13). Mean soil NO_3^--N concentrations in -N soil cores were in the range of 0.3 to 0.4 µg g^{-1} soil at -1.0 kPa and 15.1 to 18.0 at -10 kPa, respectively and were significantly lower than in + N cores at all levels of ψ. There was a significant ($p < 0.01$) effect of soil ρ_b on soil NO_3^--N concentrations in +N cores at a given ψ with lower NO_3^--N concentrations at higher ρ_b. Soil NO_3^--N concentrations in the +N soil cores increased significantly ($p < 0.01$) with the change in ψ from -1.0 to -10 kPa in all the ρ_b treatments with a significant interaction ($p < 0.01$) (Fig. 7.13) between ρ_b and ψ where within the $\rho_b \leq 1.3$ Mg m^{-3}treatments, higher NO_3^--N concentrations occurred in 1.3 Mg m^{-3} at -1.5 kPa than at 1.2 Mg m^{-3} but the trend reversed at -4.0 kPa with no significant differences between these two ρ_b treatments from -6.0 to -10 kPa.

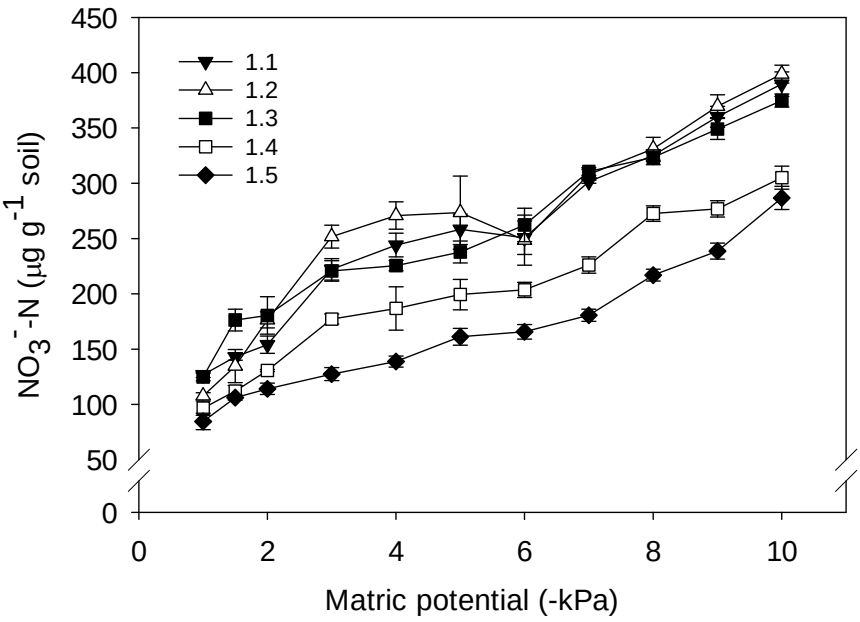

Figure 7.13 Mean NO_3^--N concentrations from +N soil cores. Numerals in the legend indicate ρ_b (Mg m^{-3}) treatments applied. Error bars = s.e.m, n = 3.

The net rate of change of NO_3^--N over ψ was calculated for each ρ_b level by performing a linear regression on the plot of NO_3^--N concentrations versus ψ for each replicate obtained from +N soil cores. The slopes of these linear regressions were then plotted against ρ_b (Fig. 7.14) which showed that the rate of change in NO_3^--N over ψ varied with soil ρ_b.

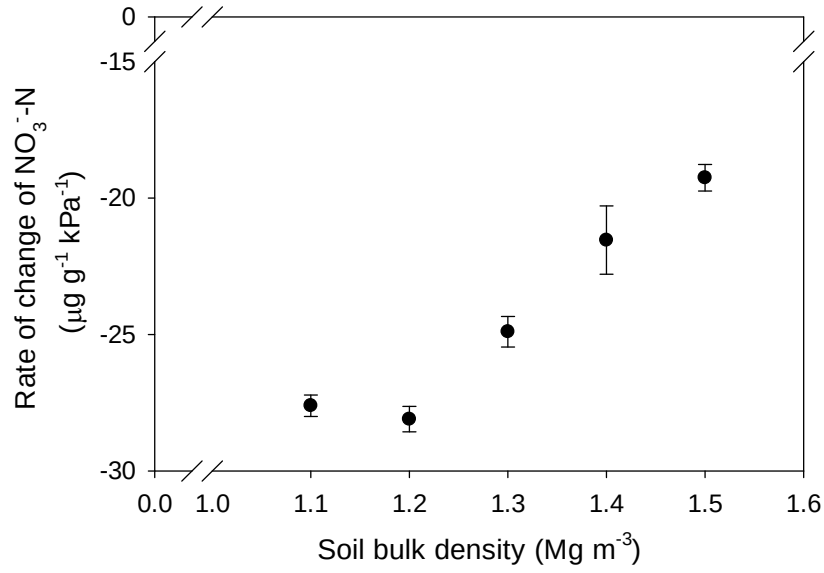

Figure 7.14 Effect of soil bulk density (ρ_b) on the rate of change of NO_3^--N over matric potential (ψ). The data points are the mean slopes of the linear regression performed on the plot between NO_3^--N concentrations and ψ for each ρ_b replicate. Error bars = s.e.m, n = 3.

Mean soil NH_4^+-N concentrations in +N cores at -1.0 kPa were 20 µg g^{-1} soil in all ρ_b treatments except at 1.4 Mg m^{-3} where it was 22 µg g^{-1} soil (Fig. 7.15). At -10 kPa, mean soil NH_4^+-N concentrations at 1.1 and 1.5 Mg m^{-3} were 1.1 and 0.9 µg g^{-1} soil, respectively (Fig. 7.15). There was no significant effect of soil ρ_b on soil NH_4^+-N concentrations in +N soil cores except at -2.0 kPa where the NH_4^+-N concentrations were higher ($p < 0.05$) in lower ρ_b treatments and also at -5.0 kPa where the trend reversed ($p < 0.01$) which led to a significant ($p < 0.01$) interaction between ρ_b and ψ.

Mean soil NH_4^+-N concentrations in -N soil cores were in the range of 15 to 20 µg g^{-1} soil at -1.0 kPa and 0.8 to 2.1 µg g^{-1} soil at -10 kPa and there was no significant effect of N addition on NH_4^+-N concentrations at any given level of ψ. However, NH_4^+-N concentrations in both +N and -N soil cores decreased significantly with the decrease in ψ from -1.0 to -10 kPa. The NO_2^--N concentrations were below the detection limit.

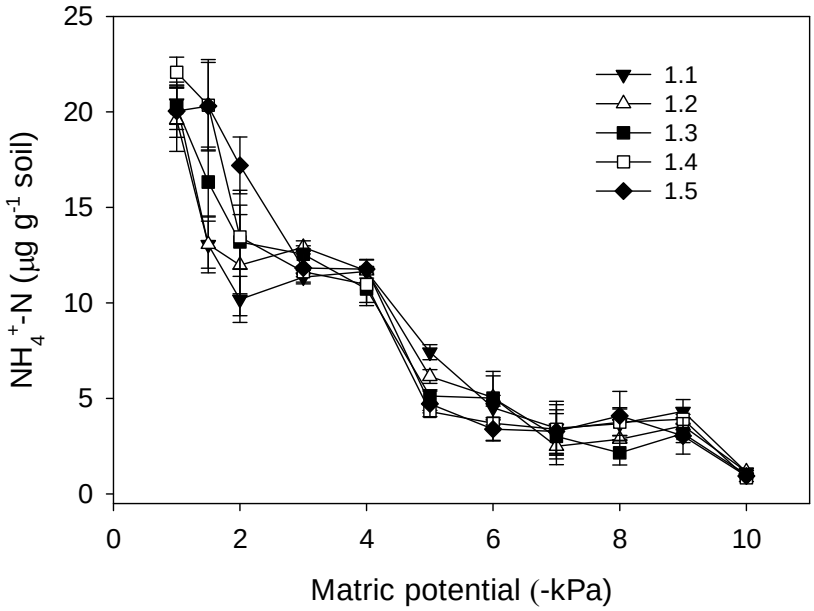

Figure 7.15 Mean NH_4^+-N concentrations from + N soil cores. Numerals in the legend indicate ρ_b (Mg m^{-3}) treatments applied. Error bars = s.e.m, n = 3.

After 4 days of equilibration on tension tables, mean soil DOC concentrations in the +N soil cores ranged from 37.5 to 15.4 µg C g^{-1} soil at 1.1 to 1.5 Mg m^{-3}, respectively at -1.0 kPa while at -10 kPa mean soil DOC concentrations at 1.1 and 1.5 Mg m^{-3}ranged from 94 to 68 µg C g^{-1} soil, respectively (Fig. 7.16). Within +N cores, soil DOC concentrations were lower ($p < 0.01$) at higher ρ_b values for any given level of ψ (Fig. 7.16) and DOC concentrations increased ($p < 0.01$) as ψ went from -1.0 to -10 kPa. There was no significant interaction between ρ_b and ψ on soil DOC concentrations in +N soil cores.

A significant ($p < 0.01$) effect of N addition on DOC concentrations was observed with higher DOC concentrations in -N soil cores when compared with +N soil cores from -1.0 to -9.0 kPa. Mean soil DOC concentrations in -N soil cores at 1.1 and 1.5 Mg m^{-3} ranged from 132 and 148 µg C g^{-1} soil at -1.0 kPa while at -10 kPa, mean soil DOC concentrations at 1.1 and 1.5 Mg m^{-3} were 95 and 82 µg C g^{-1} soil, respectively (Fig. 7.17). There was no effect of soil ρ_b on DOC concentrations in -N soil cores at most levels of ψ except at -4.0, -7.0 and -8.0 kPa where mean DOC concentrations at 1.5 Mg m^{-3} were significantly lower than at 1.1 Mg m^{-3}. Mean DOC concentrations in -N soil cores decreased as ψ went from -1.0 to -10.0 kPa (Fig. 7.17).

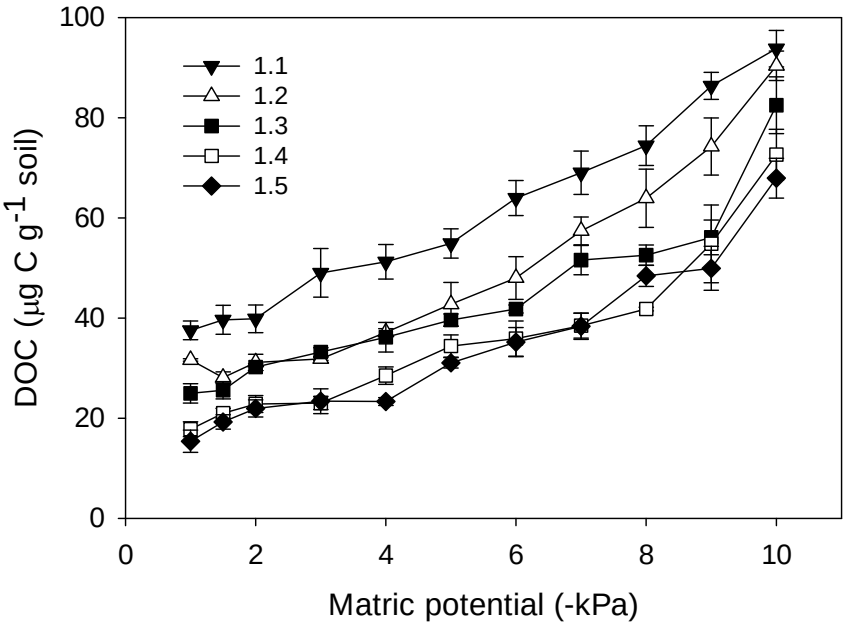

Figure 7.16 Mean DOC concentrations from +N soil cores. Numerals in the legend indicate ρ_b (Mg m^{-3}) treatments applied. Error bars = s.e.m, n = 3.

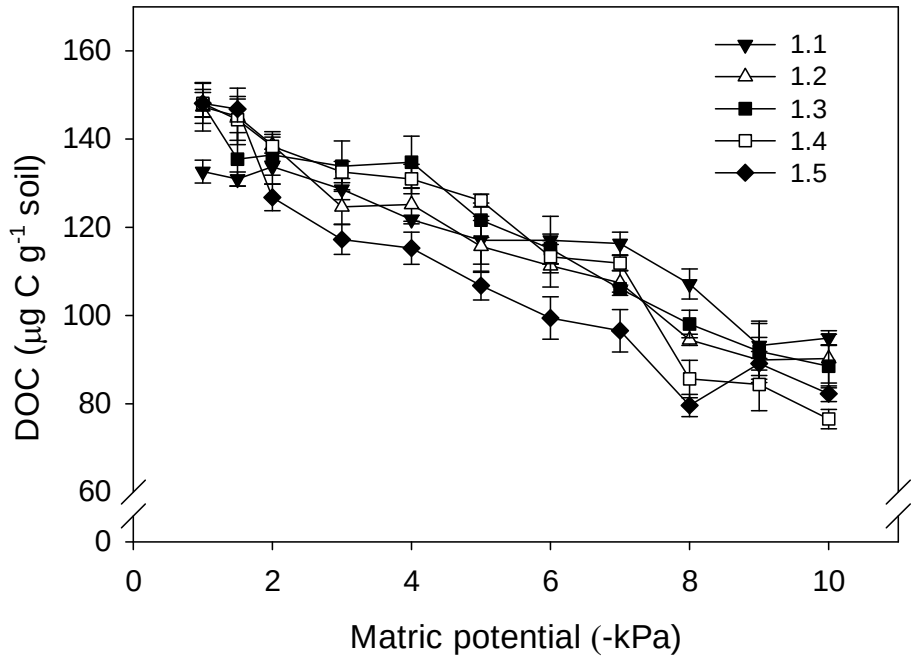

Figure 7.17 Mean soil DOC concentrations from -N soil cores. Numerals in the legend indicate ρ_b (Mg m^{-3}) treatments applied. Error bars = s.e.m, n = 3.

The net rate of change of DOC over ψ was calculated for each ρ_b level by performing a linear regression on the plot of DOC concentrations and ψ for each replicate obtained from +N soil cores. The slopes of these linear regressions were then plotted against ρ_b (Fig. 7.18) which showed that there the rate of change in DOC over ψ varied with soil ρ_b.

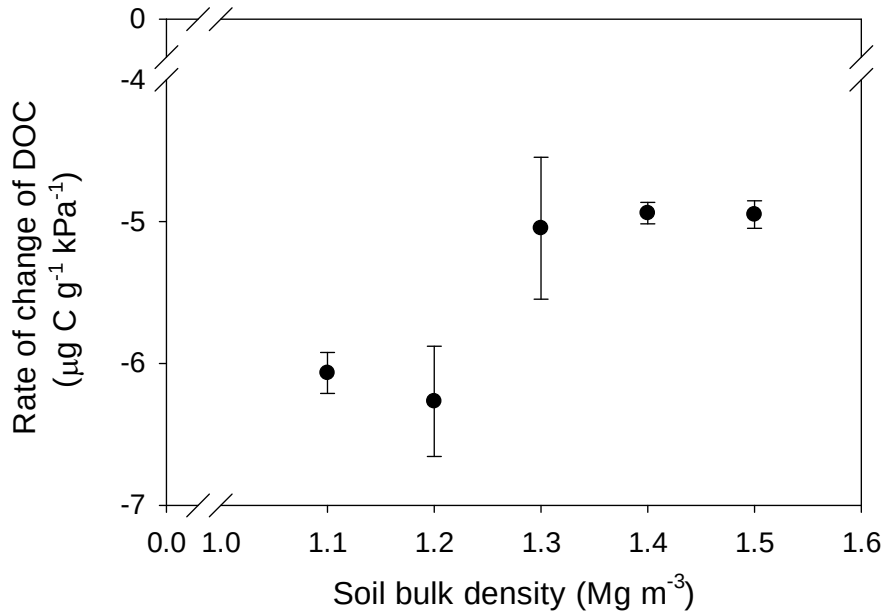

Figure 7.18 Effect of soil bulk density (Mg m^{-3}) on the rate of change of DOC over matric potential (ψ). The data points are the mean slopes of the linear regression performed on the plot between DOC concentrations and ψ for each ρ_b replicate. Error bars = s.e.m, n = 3.

Figure 7.19 shows the relationship between mean soil DOC concentrations and mean soil NO_3^--N concentrations from each ρ_b treatment measured over all ψ levels in the +N treatment. The DOC concentrations decreased with the decrease in soil NO_3^--N concentrations and remained higher in the 1.1 Mg m^{-3} ρ_b treatment. Regression analysis performed on the data showed that there was a linear relationship (Table 7.7) between mean DOC concentrations and mean NO_3^--N concentrations for each ρ_b treatment.

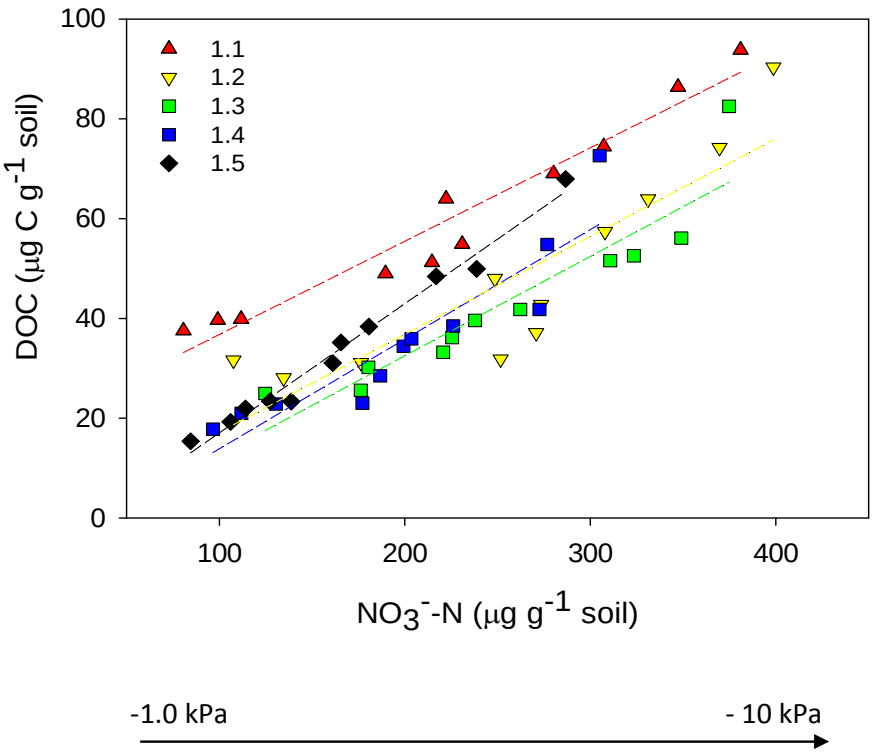

Figure 7.19 Plot of mean DOC versus mean NO_3^--N concentrations from +N soil cores for each ρ_b treatment across all levels of ψ. Numerals in the legend indicate ρ_b (Mg m^{-3}) treatments applied. Data points are means of 3 replicates.

Table 7.7 Linear function fitted to the plots of mean DOC concentrations on y axis and mean NO_3^--N concentrations on x axis for each soil ρ_b treatment (Fig. 7.19).

Soil bulk density (Mg m^{-3})	Fitted equation	r^2, p value
1.1	y = 0.21x + 6.0	0.95, p < 0.01
1.2	y = 0.20x - 2.4	0.78, p < 0.01
1.3	y = 0.20x - 7.3	0.86, p < 0.01
1.4	y = 0.22x - 8.1	0.84, p < 0.01
1.5	y = 0.25x - 8.8	0.98, p < 0.01

7.4.2.3 Soil N_2O-N fluxes and relationship of N_2O-N fluxes with ψ, Dp/Do, WFPS and ε

Mean nitrous oxide fluxes from +N soil cores ranged from 0.01 to 71 mg m^{-2} h^{-1} (Fig. 7.20) and 0.002 to 0.03 mg m^{-2} h^{-1} from -N soil cores during the course of the experiment. When the log-transformed N_2O-N fluxes were analysed by one way ANOVA, there was a significant ($p < 0.01$) effect of soil ρ_b on N_2O-N fluxes measured in +N cores. Within +N soil cores, N_2O-N fluxes at 1.4 and 1.5 Mg m^{-3} were higher than at lower ρ_b treatments, except at -1.0, -1.5 and -2.0 kPa with maxima at -5.0 and -6.0 kPa, respectively (Fig. 7.20). An interaction ($p < 0.01$) between ρ_b and ψ within +N soil cores resulted in N_2O-N peaking at different levels of ψ depending on ρ_b. Maximum N_2O-N fluxes occurred at -1.5 and -6.0 kPa for 1.1 and 1.5 Mg m^{-3} ρ_b treatments, respectively (Fig. 7.20). The levels of ψ where the N_2O-N flux was at a maximum, hereafter called ψ_{N2Omax} were determined by fitting a Gaussian function to the data (section 7.3.5). Values of ψ_{N2Omax} are presented in the Table 7.9. There was also a significant ($p < 0.01$) effect of N addition on the N_2O-N fluxes as the N_2O-N fluxes from +N cores were significantly ($p < 0.01$) higher than in -N cores. However, no effect of ρ_b was seen on N_2O-N fluxes in the -N soil cores. The N_2O-N fluxes were also normalised by dividing each individual N_2O-N flux (mg m^{-2} h^{-1}) value by the highest N_2O-N flux (mg m^{-2} h^{-1}) value attained in the experiment (Fig. 7.21). When normalised N_2O-N fluxes were plotted versus ψ, relationships similar to those shown in Fig. 7.21 were obtained at each ρ_b level. A three dimensional relationship between N_2O-N, soil ρ_b and ψ is shown in the Fig. 7.22.

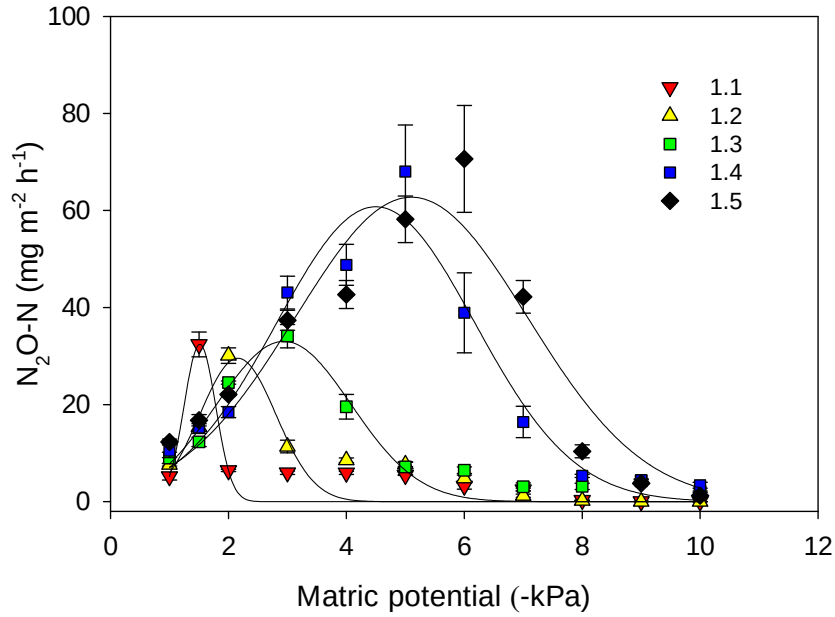

Figure 7.20 **Effect of soil ρ_b on the relationship between mean N_2O-N fluxes (+N cores) and matric potential (ψ). Plotted lines are derived from a three-parameter Gaussian model fitted to the N_2O and ψ data. Numerals in the legend indicate ρ_b (Mg m^{-3}) treatments applied. Error bars = s.e.m, n = 4.**

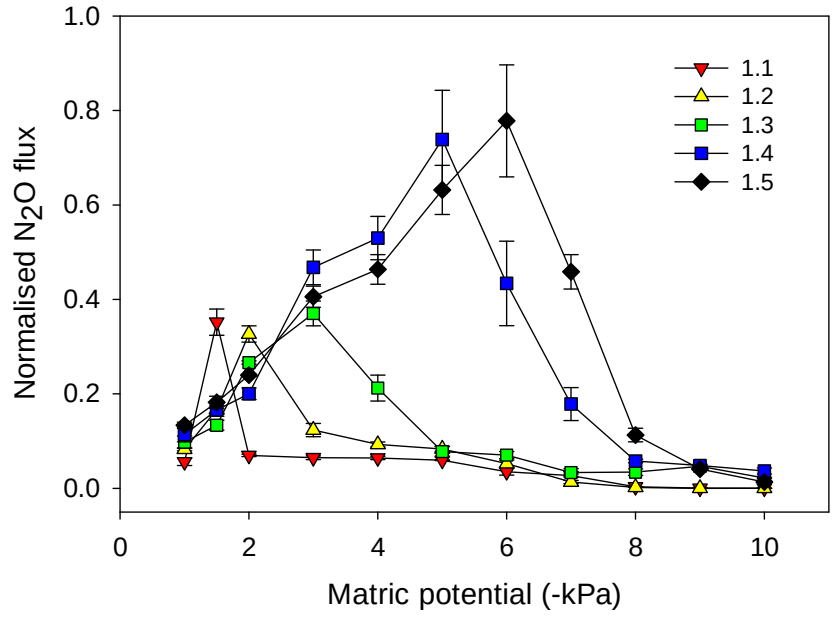

Figure 7.21 **Effect of soil ρ_b on the relationship between mean normalised N_2O-N fluxes (+N cores) and matric potential (ψ). Numerals in the legend indicate ρ_b (Mg m^{-3}) treatments applied. Error bars = s.e.m, n = 4.**

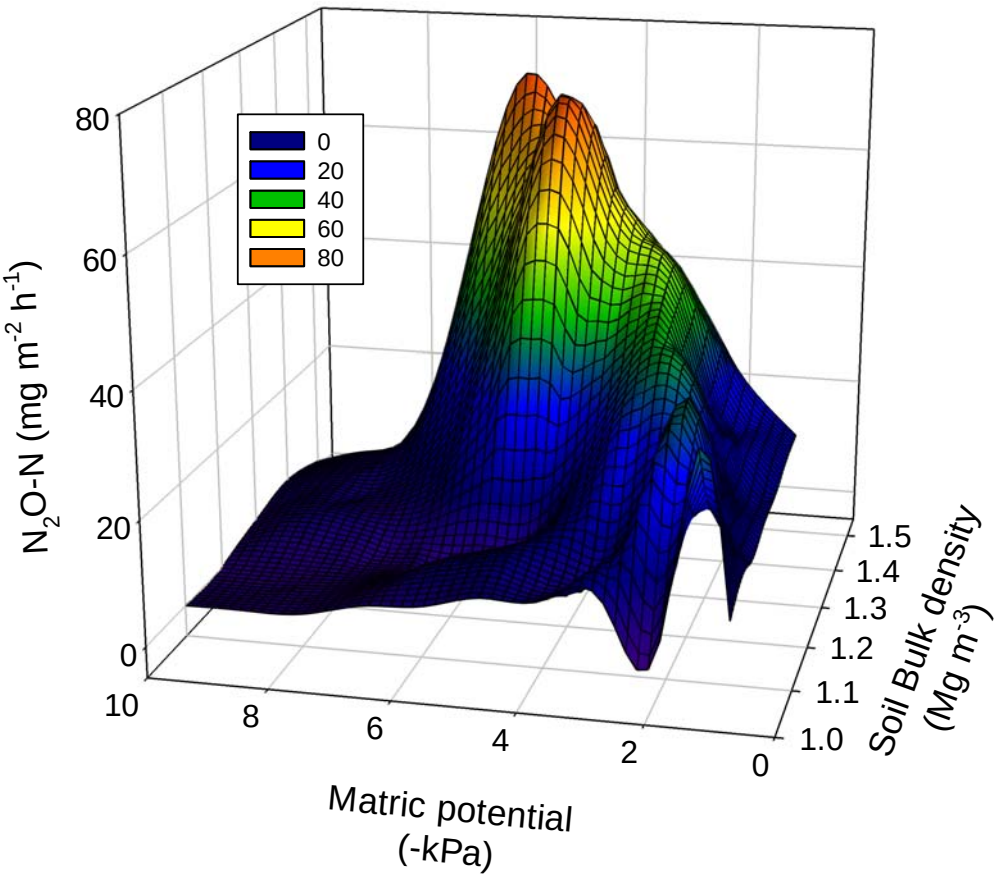

Figure 7.22 Mesh plot of N_2O-N fluxes versus soil ρ_b (Mg m^{-3}) and matric potential (ψ) for +N treated soil cores.

When the measured mean N_2O-N fluxes for each ρ_b treatment were plotted against the corresponding *Dp*/*Do* values, it was found that the peak N_2O-N fluxes all occurred at very similar *Dp*/*Do* values (Fig. 7.23). However, these same peak N_2O-N fluxes occurred at varying WFPS and volumetric water contents (θ_v) (Fig. 7.24a and 7.24b) ranging from 67 to 80% and 0.42 to 0.34 $m^3\ m^{-3}$, repectively. Similarly, these measured peaks of N_2O-N fluxes occurred at varying values of ε ranging from 0.09 to 1.16 m^3 air m^{-3} soil (Fig. 7.25). However, *Dp*/*Do* consistently provided a critical value where maximum measured N_2O-N fluxes occurred regardless of ρ_b treatment and ψ level (Fig. 7.23, Table 7.8)

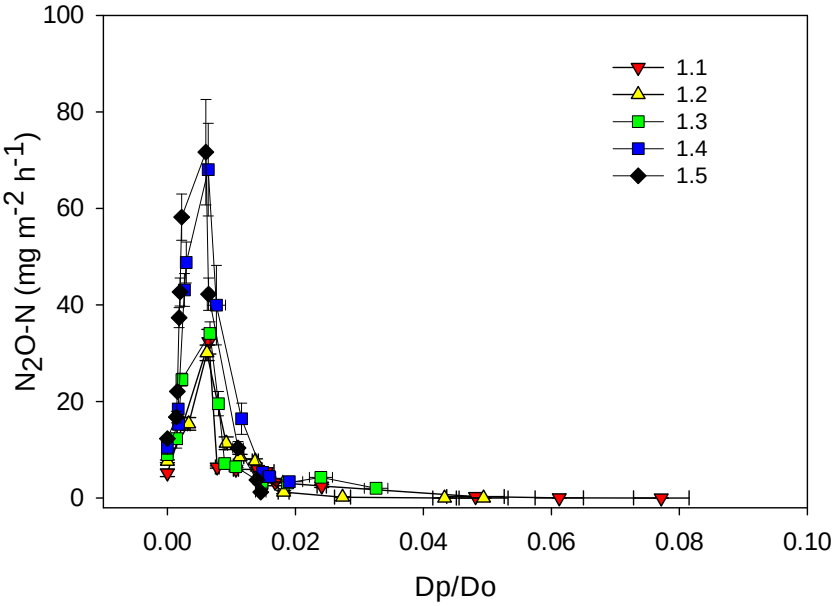

Figure 7.23 Relationship between measured N_2O-N flux and relative soil gas diffusivity (*Dp*/*Do*) at varying soil ρ_b. Numerals in the legend indicate ρ_b (Mg m^{-3}) treatments applied. Error bars = s.e.m, n = 4.

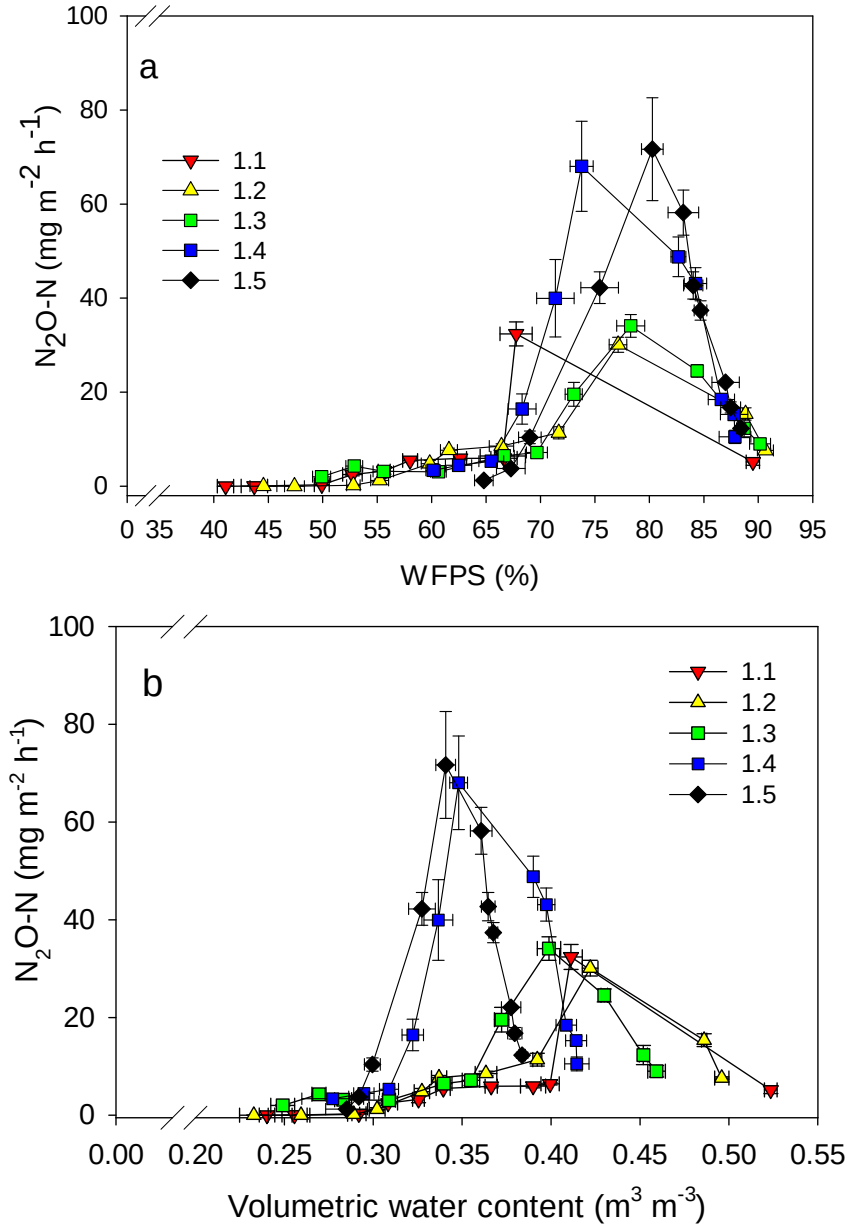

Figure 7.24 Relationship of measured N_2O-N fluxes with (a) WFPS (%) (b) Volumetric water content (m^3 m^{-3}) at varying soil ρ_b (Mg m^{-3}). Numerals in the legend indicate ρ_b (Mg m^{-3}) treatments applied. Error bars = s.e.m, n = 4.

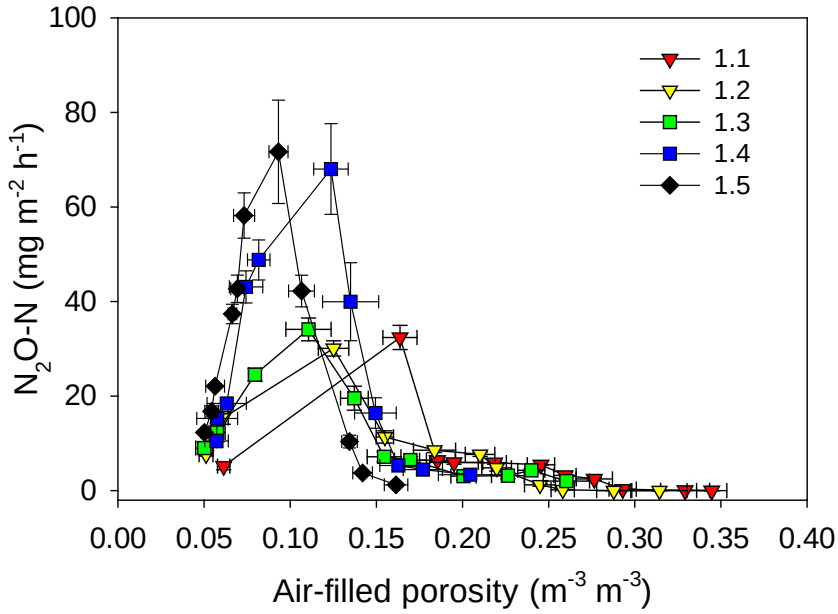

Figure 7.25 Relationship between measured N_2O-N flux and air-filled porosity (m^3 m^{-3}) at varying soil ρ_b (Mg m^{-3}). Numerals in the legend indicate ρ_b (Mg m^{-3}) treatments applied. Error bars = s.e.m, n = 4.

The values of WFPS and θ_v where the maximum N_2O-N fluxes occurred are subsequently defined $WFPS_{N2Omax}$ and $\theta_{vN2Omax}$ and other variables were also defined accordingly as Dp/Do_{N2Omax}, C_{N2Omax}, ε_{N2Omax} and *pore size*$_{N2Omax}$. When the values of these variables were determined, it was found that only Dp/Do_{N2Omax} was the variable unaffected ($p = 0.316$) by soil ρ_b (Table 7.8)**.** In contrast, the other variables differed with ρ_b ($p < 0.01$). The measured N_2O-N flux values were at a maximum when a specific pore size was drained and these ranged from 197 to 57 µm for the 1.1 and 1.5 Mg m^{-3} treatments, corresponding to a ψ of approximately -1.5 and -6.0 kPa, respectively (Table 7.8).

Table 7.8 **Means and standard deviation (in brackets) of variables measured when N_2O peaked (N_2Omax). Values in rows that do not share a common letter are significantly different ($p < 0.05$, Tukey's test).**

Variables	Bulk density (Mg m^{-3})					
	1.1	**1.2**	**1.3**	**1.4**	**1.5**	
Relative gas diffusivity Dp/Do_{N2Omax}	0.0065**a** (0.0003)	0.0062**a** (0.0004)	0.0067**a** (0.0002)	0.0064**a** (0.0004)	0.0060**a** (0.0003)	NS
Water-filled pore space $WPFS_{N2Omax}$ (%)	67.76**c** (2.95)	77.12**ab** (1.61)	78.28**ab** (2.57)	73.77**b** (2.12)	80.27**a** (1.99)	**
Volumetric water content $\theta_{vN2Omax}$ (cm^3 cm^{-3})	0.41**a** (0.013)	0.42**a** (0.008)	0.39**a** (0.013)	0.35**b** (0.010)	0.34**b** (0.011)	**
Pore continuity C_{N2Omax}	0.04**c** (0.004)	0.05**bc** (0.004)	0.06**ab** (0.007)	0.05**bc** (0.005)	0.07**a** (0.005)	**
Air-filled porosity ε_{N2Omax} (m^3 m^{-3})	0.16**a** (0.01)	0.13**b** (0.008)	0.11**bc** (0.01)	0.12**c** (0.01)	0.09**c** (0.01)	**
Pore size drained *pore size*$_{N2Omax}$ (µm)	197**a** (6.25)	146**b** (4.12)	106**c** (3.7)	67**d** (2.2)	57**e** (2.7)	**

NS = not significant, ** $p < 0.01$

7.4.2.4 Air entry values (ψ_a) and their relationship with ψ, *Dp*/*Do*, macroporosity, meso porosity, microporosity, *C* and WFPS.

The water retention curves (WRC) (section 2.6.2) obtained for each ρ_b in Chapter 5 demonstrated a distinct ψ value at which there was a significant decrease in θ_v following saturation. This is known as the air entry value (ψ_a) (section 2.6.2). After determining that the maximum N_2O-N fluxes were related to a specific ψ value ($\psi_{N2O\ max}$), it was decided to calculate the air entry value (ψ_a) at each level of ρ_b from the WRC curves using the Campbell equation (section 2.6.2) and then to relate these ψ_a values with ψ_{N2Omax}.

Air entry values (ψ_a) calculated from the log-log plot of the WRC (Fig. 7.26) obtained from chapter 5, showed that ψ_a values were significantly ($p < 0.01$) affected by soil ρ_b, decreasing (becoming more negative) with an increase in soil ρ_b. Campbell water retention parameter (-*b*) is the slope, while ψ_a was derived from the y intercept of the linear regression performed on the log-log plot of the WRC (Fig. 7.26). In the 1.1 and 1.5 Mg m^{-3} treatments the mean value of ψ_a was -1.3 kPa and -5.7 kPa, respectively. Examples of the linear regression performed on the log-log plots of WRC are depicted in Fig 7.27. Table 7.9 shows all the values of the Campbell water retention parameter (-*b*) and ψ_a values from each replicate. The values of -*b* were also significantly ($p < 0.01$) affected by soil ρ_b, increasing with an increase in soil ρ_b (Table 7.9).

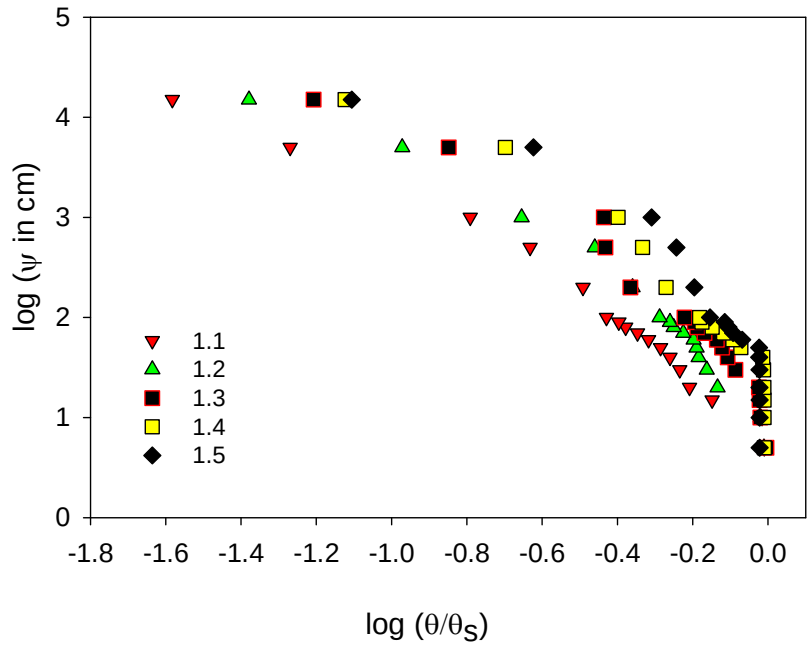

Figure 7.26 Log-log plot of WRC from soil compacted to varying ρ_b. Numerals in the legend indicate ρ_b (Mg m^{-3}) treatments applied.

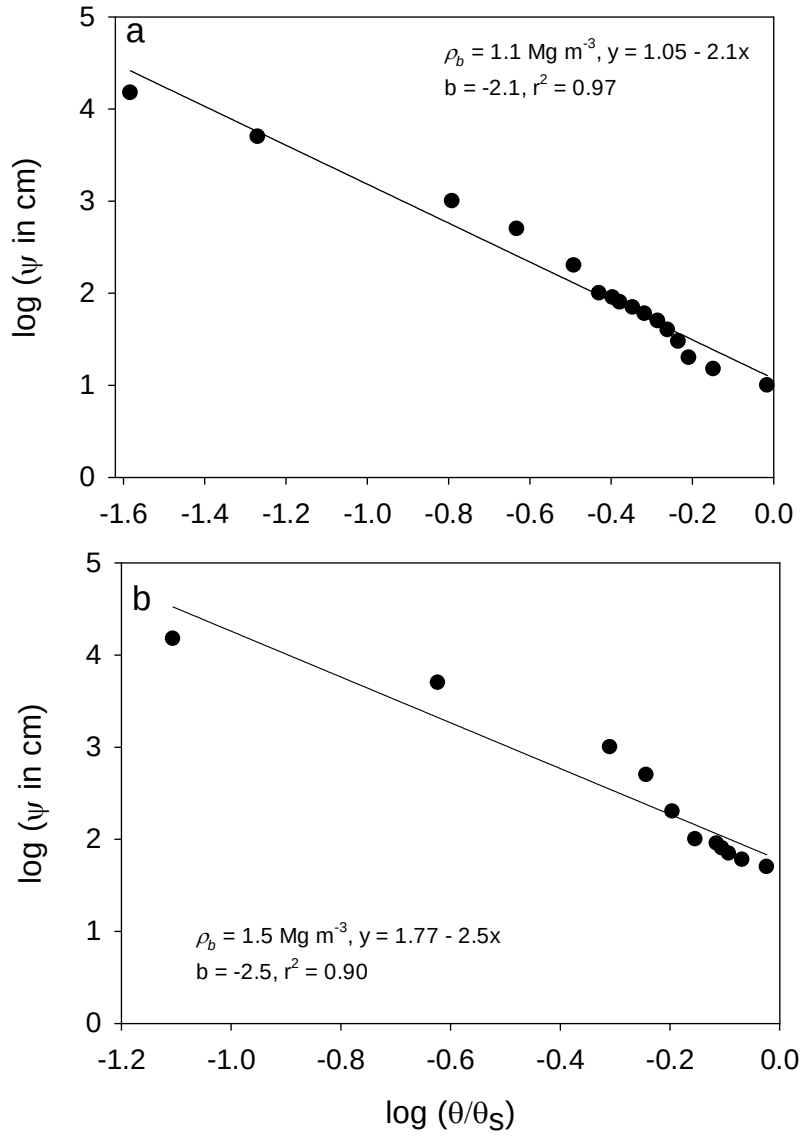

Figure 7.27 Examples of the linear regressions performed on the log- log WRC plots for an individual replicate at (a) 1.1 Mg m^{-3} and (b) 1.5 Mg m^{-3} where the Campbell water retention parameter (-*b*) is equal to the slope and air entry value (ψ_a) was derived from the y intercept of the straight line fitted to a log-log plot of ψ and θ/θ_s (section 2.6.2).

Table 7.9 Soil water retention parameters (WRC) and ψ_{N2Omax} for different soil ρ_b treatments using the Campbell soil-water retention function (section 2.6.2) and a three parameter Gaussian function (section 7.3.5), respectively. Values represent individual replicates.

Bulk density (Mg m^{-3})	Replicate	ψ_a (-kPa)	-b	**r^2	ψ_{N2Omax} (-kPa)	*r^2
1.1	1	1.3	2.04	0.97	1.50	0.90
1.1	2	1.2	2.14	0.98	1.60	0.91
1.1	3	1.5	1.95	0.94	1.52	0.89
1.1	4	1.1	2.10	0.98	1.45	0.88
1.2	1	1.9	2.30	0.95	2.08	0.78
1.2	2	2.2	2.23	0.96	2.15	0.82
1.2	3	2.0	2.32	0.97	2.07	0.85
1.2	4	1.9	2.40	0.97	2.12	0.77
1.3	1	3.0	2.43	0.96	2.71	0.90
1.3	2	3.1	2.42	0.96	2.85	0.93
1.3	3	2.5	2.51	0.98	2.81	0.95
1.3	4	2.4	2.53	0.98	2.92	0.89
1.4	1	4.0	2.56	0.94	4.50	0.93
1.4	2	4.3	2.53	0.92	4.66	0.91
1.4	3	4.0	2.50	0.93	4.36	0.89
1.4	4	4.4	2.54	0.93	4.62	0.93
1.5	1	5.7	2.50	0.90	5.01	0.85
1.5	2	5.4	2.58	0.90	5.22	0.80
1.5	3	5.5	2.64	0.92	5.35	0.81
1.5	4	6.0	2.52	0.90	5.60	0.82

**r^2 was obtained by fitting linear regression of a log-log plot of the WRC obtained in Chapter 5.

*r^2 was obtained by fitting a 3-parameter Gaussian curve to the plot between N_2O-N fluxes and ψ.

When ψ_{N2Omax}, which was obtained by fitting a three parameter Gaussian curve to measured N_2O-N fluxes, was plotted against ψ_a, a significant linear relationship was observed (Fig.7.28). However, when ψ_a values were plotted against other measured variables, it was found that only macroporosity was significantly related to ψ_a with 99% of the variation in ψ_a explained and a strong ($p < 0.01$) exponential relationship emerging between macroporosity and ψ_a (Fig. 7.29). No relationship was obtained between ψ_a and Dp/Do_{N2Omax} or ψ_a and mesoporosity (Fig. 7.29). Soil microporosity, C_{N2Omax} and $WFPS_{N2Omax}$ showed weaker relationships with ψ_a (Fig. 7.29).

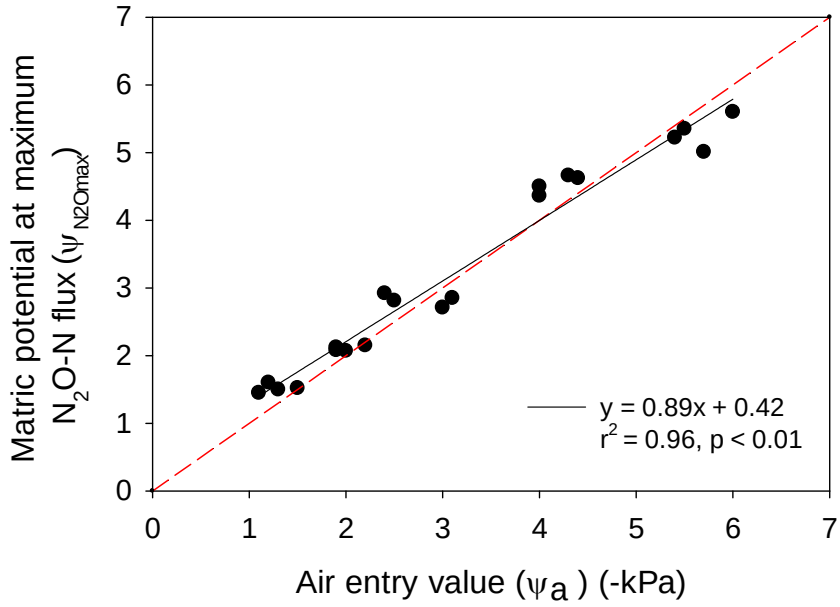

Figure 7.28 Relationship between ψ_{N2Omax} (-kPa) and air entry value (ψ_a) (-kPa). Values represent individual replicates. The ψ_{N2Omax} was obtained by fitting a three parameter Gaussian function to N_2O-N and ψ. The values of ψ_a were obtained by fitting linear regressions to the log-log plot of WRC. The red dashed line is a 1:1 line.

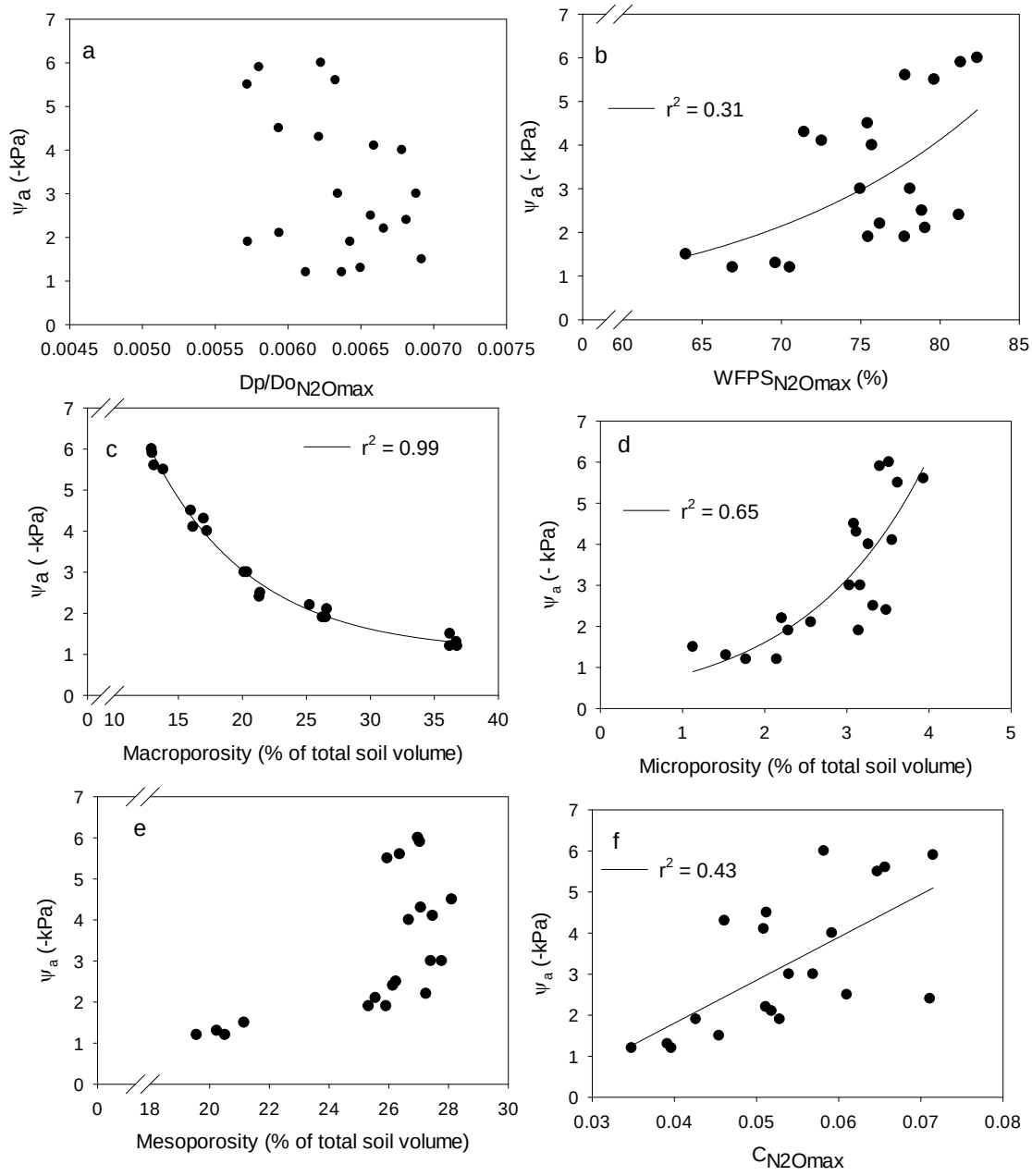

Figure 7.29 Relationships between air entry value (ψ_a) and (a) Dp/Do_{N2Omax} (b) $WFPS_{N2Omax}$ (c) Macroporosity (d) Microporosity (e) Mesoporosity (f) C_{N2Omax}. Values represent individual replicates.

Since ψ_a was exponentially related to macroporosity (Fig 7.29c) and ψ_{N2Omax} was linearly related to ψ_a (Fig. 7.28), it was expected that ψ_{N2Omax} would also relate to macroporosity (% of total soil volume) as shown in the Fig. 7.30.

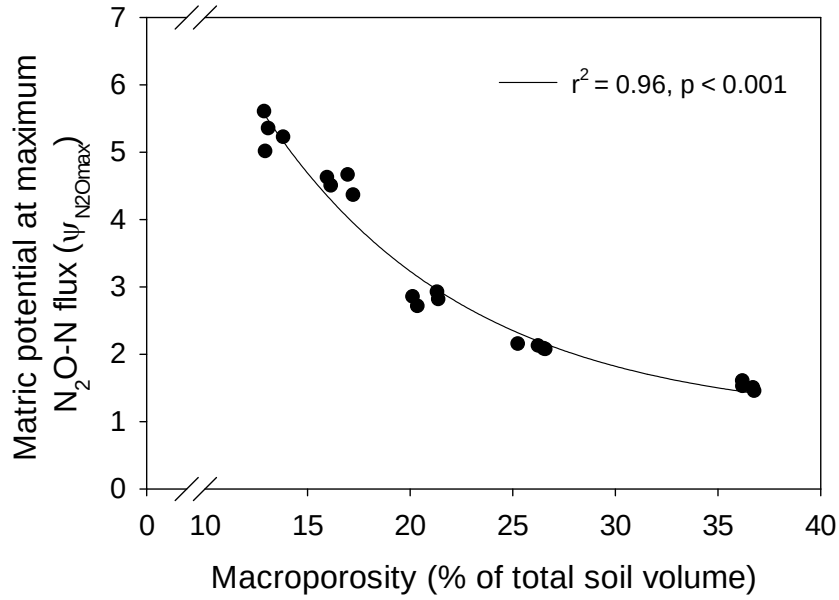

Figure 7.30 Relationship between ψ_{N2Omax} (-kPa) and macroporosity (% of total soil volume). Values represent individual replicates.

7.4.2.5 Entrapped N_2O in soil cores

In the +N soil cores, mean concentrations of N_2O entrapped in the soil water ranged from 1328 and 8209 µL L^{-1} H_2O at -1.0 kPa while at -10 kPa mean concentrations ranged from 5.9 to 4.2 µL L^{-1} H_2O (Fig. 7.31). There was a significant effect ($p < 0.01$) of soil ρ_b on entrapped N_2O between -1.0 to -6.0 kPa in the +N treated cores with higher entrapped N_2O at higher ρ_b treatments. The entrapped N_2O concentrations decreased significantly at -2.0 kPa at 1.1 and 1.2 Mg m^{-3} while they decreased gradually till -7.0 kPa in other ρ_b treatments which resulted in a significant interaction ($p < 0.01$) between ρ_b and ψ.

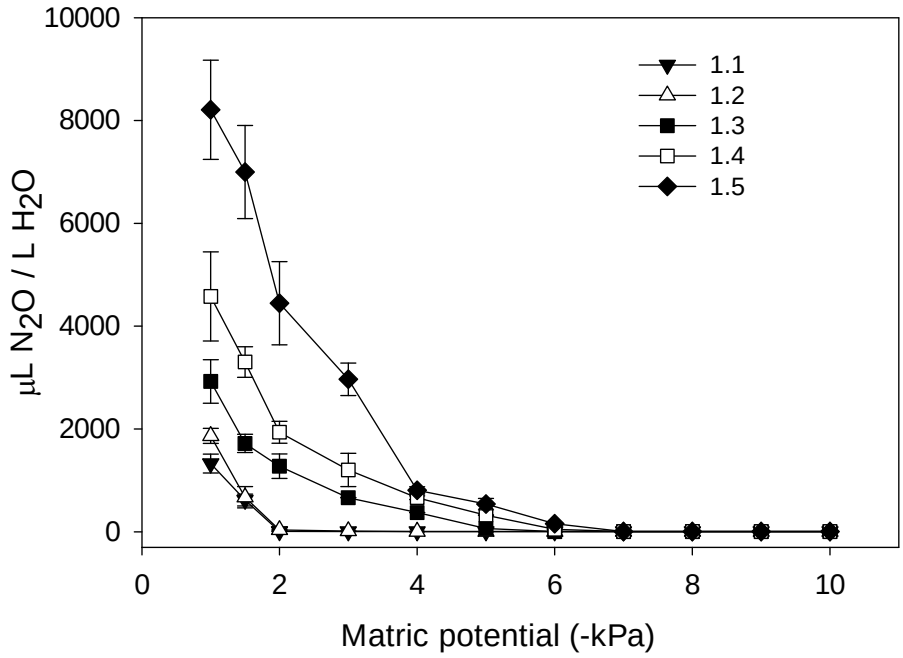

Figure 7.31 Mean N_2O entrapped in soil water from +N soil cores at varying ψ. Numerals in the legend indicate ρ_b (Mg m^{-3}) treatments applied. Error bars = s.e.m, n = 3.

7.4.2.6 N_2O-N fluxes after further substrate addition

Addition of 1 mL carbon as glucose and 1 mL of solution 2 (KNO_3, 600 µg ml^{-1} NO_3^--N, 40 atom % ^{15}N) to the soil cores produced mean N_2O-N fluxes ranging from 0.004 to 27 mg m^{-2} h^{-1} (Fig. 7.32). When log-transformed N_2O-N fluxes from these soil cores were analysed, higher ($p < 0.01$) N_2O-N fluxes occurred at $\rho_b \geq 1.3$ Mg m^{-3} at -3.0, - 4.0, -5.0, and -9.0 kPa while no interaction occurred between ρ_b and ψ. The N_2O-N fluxes decreased exponentially with decreases in ψ at each ρ_b level (Fig. 7.32). When WFPS, *Dp*/*Do* and θ_v were related with these N_2O-N fluxes, it was observed that *Dp*/*Do* showed the best relationship (Fig. 7.33).

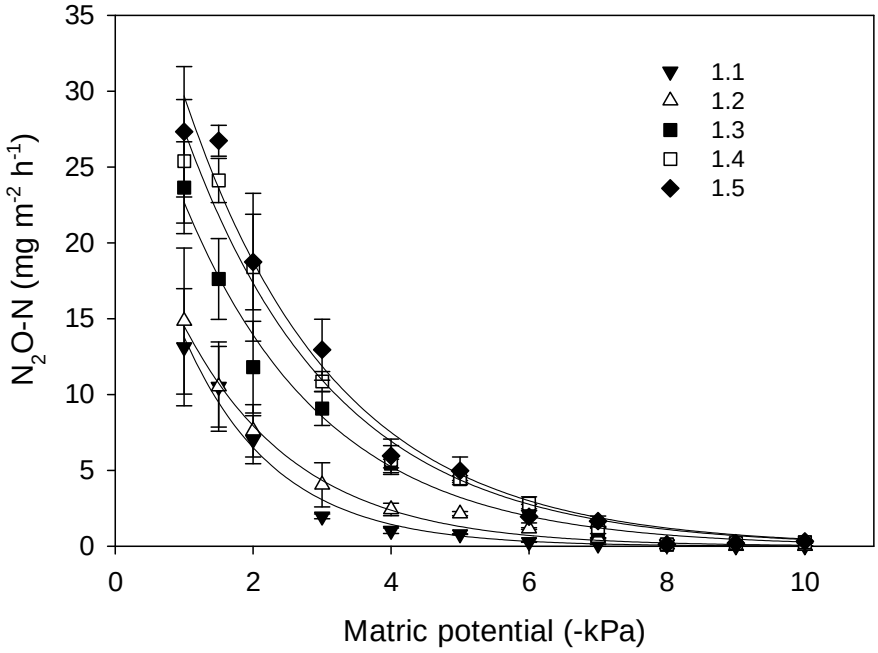

Figure 7.32 Mean soil N_2O-N fluxes from +N soil cores at varying matric potential (-kPa) measured 6 h after the addition of 1 mL NO_3^- (solution 2) and 1 mL carbon (glucose). Numerals in the legend indicate ρ_b (Mg m^{-3}) treatments applied. Error bars = s.e.m, n = 4. A two parameter exponential curve was fitted to the N_2O-N and ψ data for each ρ_b level.

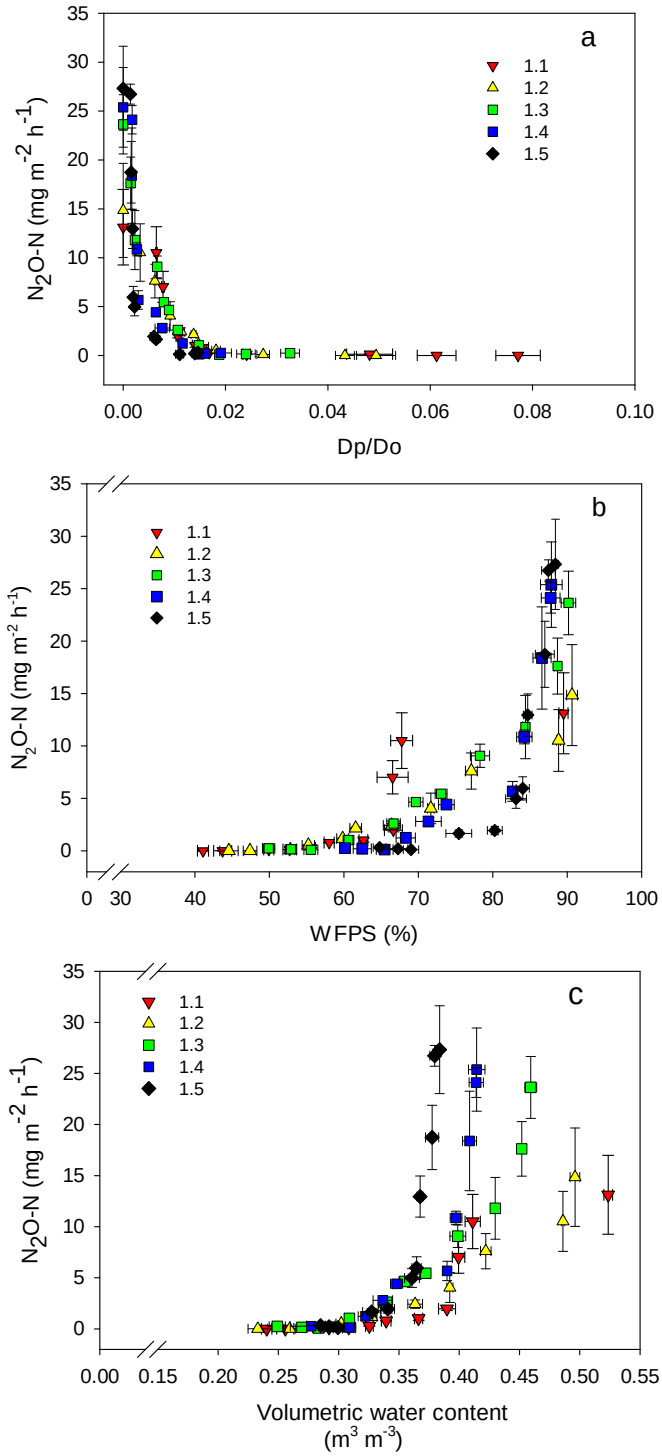

Figure 7.33 The relationship of N_2O-N obtained after further substrate addition and (a) Relative gas diffusivity (*Dp*/*Do*) (b) Water-filled pore space (WFPS) (c) Volumetric water content (m^3 m^{-3}). Numerals in the legend indicate ρ_b (Mg m^{-3}) treatments applied. Error bars = s.e.m, n = 4.

7.4.2.7 N_2O-N ^{15}N enrichment after further substrate addition

The addition of 1 mL of labelled NO_3^- at a ^{15}N enrichment of 40 atom % along with 1 mL of carbon (glucose) to the 1.5 and 1.1 Mg m^{-3} treatments did not result in corresponding ^{15}N enrichment of the N_2O-N fluxes. The range of ^{15}N atom % in the N_2O-N was relatively low and was in the range of 0.3 to 0.44 at 1.1 Mg m^{-3} and 2.96 to 1.86 for 1.5 Mg m^{-3} (Table 7.10). However, ^{15}N atom % enrichment of N_2O-N at 1.5 Mg m^{-3} was significantly ($p < 0.01$) higher than at 1.1 Mg m^{-3} for all levels of ψ. Due to the low ^{15}N enrichment, no N_2-N fluxes were detectable.

Table 7.10 The values are ^{15}N atom % enrichment of N_2O-N. Values are the averages of 4 replicates and standard deviations are in brackets.

	Soil bulk density (Mg m^{-3})	
Matric potential (-kPa)	**1.1**	**1.5**
1.0	0.32 (0.096)	2.96 (0.218)
1.5	0.61 (0.150)	2.24 (0.321)
2.0	0.33 (0.088)	2.81 (0.417)
3.0	0.55 (0.124)	1.24 (0.650)
4.0	0.43 (0.118)	1.36 (0.774)
5.0	0.41 (0.085)	1.98 (1.142)
6.0	0.52 (0.157)	1.53 (1.160)
7.0	0.41 (0.139)	1.64 (0.625)
8.0	0.41 (0.113)	1.62 (0.759)
9.0	0.42 (0.211)	1.96 (0.836)
10	0.44 (0.168)	1.86 (0.698)

7.4.2.8 Comparisions between predictive *Dp*/*Do* models

The results from this experiment showed that the occurrence of maximum N_2O-N flux via denitrification was controlled by the interaction between ψ and soil ρ_b. Soil *Dp*/*Do* was the variable which best predicted this maximum N_2O-N flux regardless of the effect of ρ_b and ψ. Thus *Dp*/*Do* has potential to be used in future studies as a predictor of N_2O via denitrification from a soil differing in ρ_b at varying ψ. Predictive models have been used to predict *Dp*/*Do* (section 2.6.3) instead of directly measuring it. Only recently has the need to incorporate the soil ρ_b effect into *Dp*/*Do* models been suggested (Chamindu Deepagoda et al., 2011b). Thus this data collected in this experiment provides an opportunity to develop a model to predict *Dp*/*Do* and to compare it with other predictive *Dp*/*Do* models.

The relationship between measured *Dp*/*Do* values and ε/ϕ (Fig. 7.34) was used to derive an equation for *Dp*/*Do* prediction by fitting a power function to the data (equation 7.7). A three parameter power function was the best fit to the data. The regression does not include the ε values where measured *Dp*/*Do* values were zero, i.e. at -1.0 kPa.

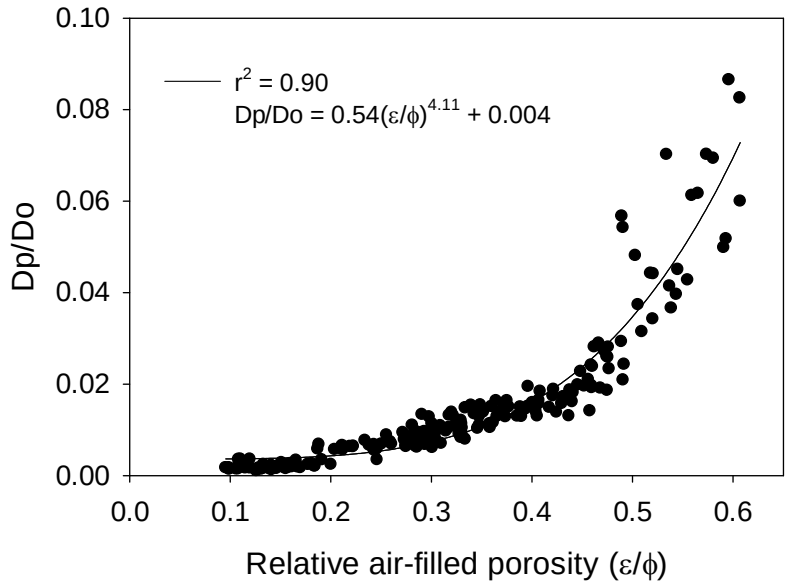

Figure 7.34 Relationship between relative gas diffusivity (*Dp*/*Do*) and relative air-filled porosity. Data points are individual replicates.

The values of *Dp*/*Do* measured in this experiment were then compared with the predicted *Dp*/*Do* values using 5 different models including the one developed in this study in order to compare model estimates with the measured *Dp*/*Do* values (section 7.3.5). Since soil cores were both repacked and compacted, the first model for *Dp*/*Do* prediction was chosen based on its capability to predict *Dp*/*Do* in wet and repacked soil cores (Moldrup et al., 2000b) and the second was a density corrected model (Chamindu Deepagoda et al., 2011b). The other two models used were the modified BBC model (Buckingham-Burdine-Campbell) (Moldrup et al., 2000a) and the TPM (Three-porosity model) (Moldrup et al., 2004) (section 2.6.3).

The density corrected model developed by Chamindu Deepagoda et al. (2011b) performed better, RMSE = 0.007, than the WLR (Penman model) (section 2.6.3), RMSE = 0.033. However, neither model performed well in predicting the measured *Dp*/*Do* values (Fig. 7.35). The density corrected model under estimated the measured *Dp*/*Do* values as depicted by a negative bias (-0.003) while the WLR (Penman model) over predicted the measured *Dp*/*Do* values as shown by a positive bias (0.025) (Fig. 7.35). The performance of the modified BBC model and the TPM (section 2.6.3) in predicting *Dp*/*Do* was better than WLR (Penman model) but both of these models also over predicted *Dp*/*Do* values at lower ρ_b levels (Fig. 7.36, 7.37). The three parameter power equation developed in this study was the best at predicting *Dp*/*Do* with the lowest RMSE and bias values of 0.005 and 0.0008 (Fig. 7.38). However, the data are not truly independent and require a separate data set for proper validation. Notably, at complete air saturation ($\varepsilon/\phi = 1$), the three parameter power model developed in this study reduces to a constant (0.544) irrespective of ρ_b or ψ while at complete water saturation ($\varepsilon = 0$), it reduces to a constant value of 0.004. Table 7.11 compares the values of Dp/Do_{N2Omax} obtained in this experiment by direct measurements (Table 7.8) and by predictive models using the density-corrected model and the three parameter power equation (this study). When comparisons using RMSE and bias were made between these predicted values of Dp/Do_{N2Omax} (Table 7.11) at each level of ρ_b, it was found that the three parameter equation developed in this study was better at predicting Dp/Do_{N2Omax}.

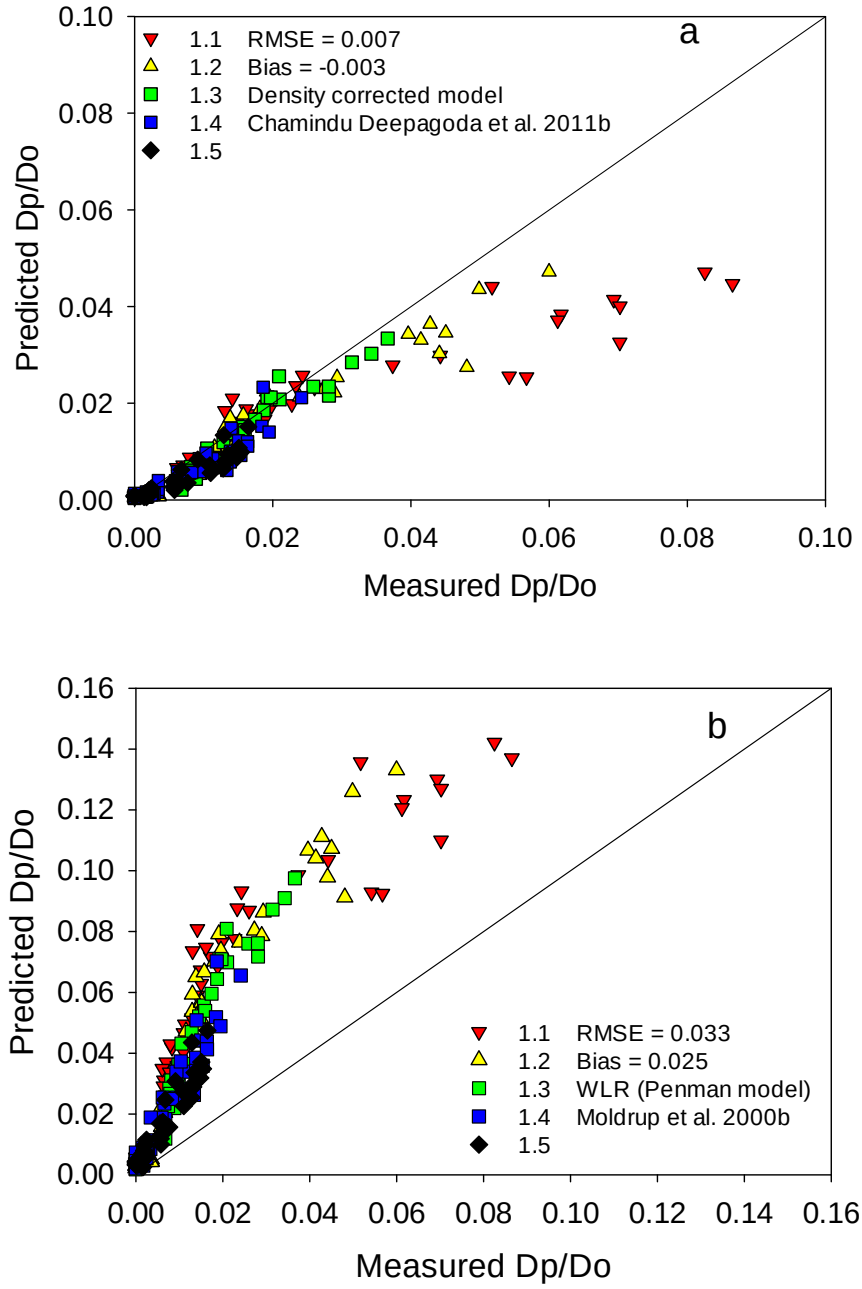

Figure 7.35 Scatter-plot comparison of model performance (a) density corrected model (b) WLR (Penman model) when tested against *Dp/Do* values (n = 220) measured at varying ρ_b over a range of ψ applied.

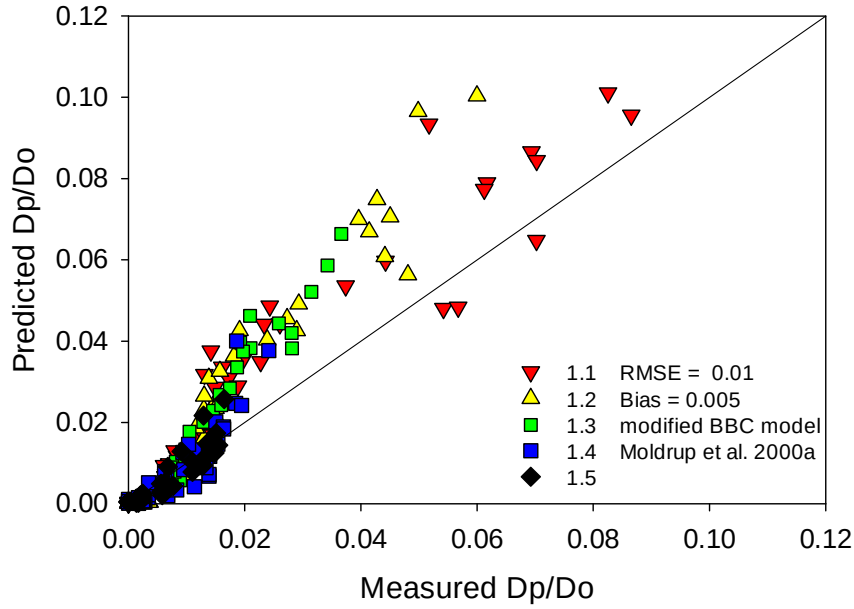

Figure 7.36 Scatter-plot comparison of model performance using the modified BBC model when tested against *Dp/Do* values (n = 220) measured at varying ρ_b over a range of ψ applied.

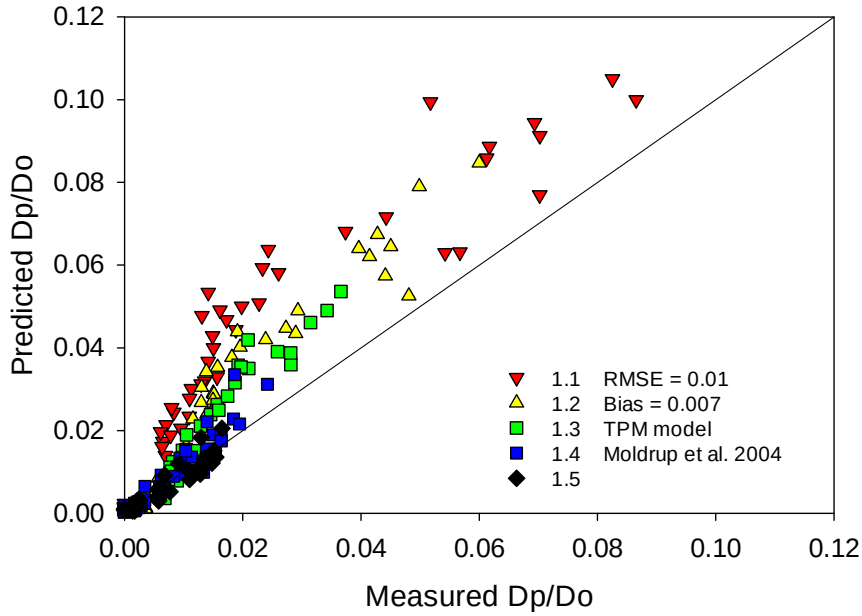

Figure 7.37 Scatter-plot comparison of model performance using the TPM model when tested against *Dp/Do* values (n = 220) measured at varying ρ_b over a range of ψ applied.

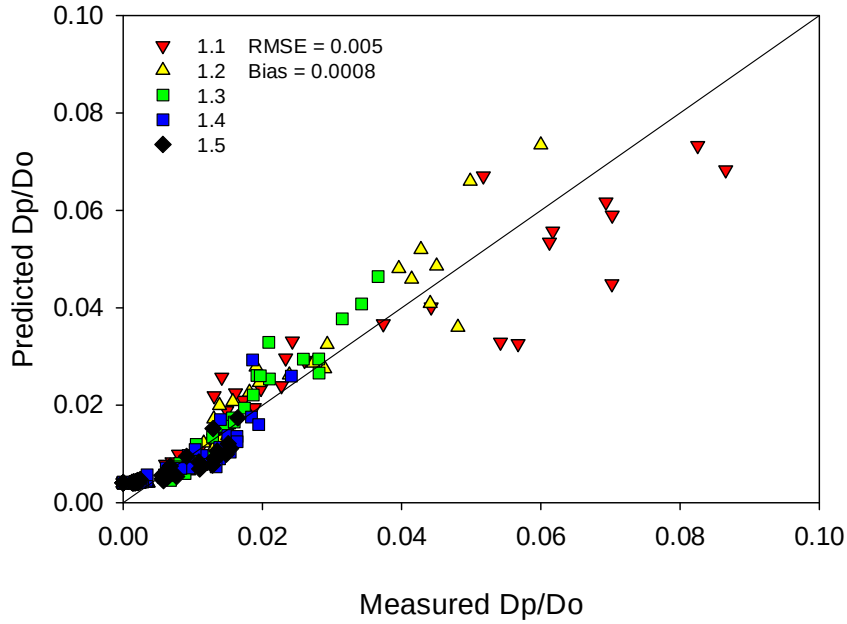

Figure 7.38 **Scatter-plot comparison of model performance using the equation developed in this study when tested against *Dp/Do* values (n = 220) measured at varying ρ_b over a range of ψ applied.**

Table 7.11 **Mean values of Dp/Do_{N2Omax} (*Dp/Do* where N_2O-N flux was at maximum) measured and obtained by fitting a density-corrected model (Chamindu Deepagoda et al., 2011b) and the equation from this study. Standard deviations are in brackets.**

Bulk density (Mg m^{-3})	Measured Dp/Do_{N2Omax}	Predicted Dp/Do_{N2Omax} using the density-corrected model by Deepagoda et al. (2011)	Predicted Dp/Do_{N2Omax} using the three parameter power equation developed in this study
1.1	0.0065 (0.0003)	0.0055 (0.0008)	0.0069 (0.0007)
1.2	0.0062 (0.0004)	0.0033 (0.0005)	0.0055 (0.0003)
1.3	0.0067 (0.0002)	0.0029 (0.0008)	0.0050 (0.0005)
1.4	0.0064 (0.0003)	0.0047 (0.0009)	0.0063 (0.0007)
1.5	0.0060 (0.0003)	0.0029 (0.0008)	0.0050 (0.0005)
		RMSE = 0.003, Bias = -0.002	RMSE = 0.001, Bias = -0.0006

7.5 Discussion

7.5.1 Requirement for non-limiting substrates

In the preliminary tests the soil NO_3^--N concentrations (505-657 µg g^{-1} soil) obtained following 2 days of saturation with a NO_3^--N solution were higher than the maximum NO_3^--N concentrations obtained in the previous experiments 1 (Chapter 4), 2a and 2b (Chapter 5). These results from the preliminary test showed that the NO_3^--N and DOC concentrations (113-158 µg C g^{-1} soil) obtained upon saturation with a NO_3^--N solution were high enough to provide non-limiting substrate conditions for denitrification to take place. Burford and Bremner (1975) previously demonstrated a linear relationship between water soluble organic C and denitrification activities of 17 different soils. Beauchamp et al. (1980) showed in a study that a minimum of 40 µg C g^{-1} soil of water extractable C was required before denitrification could occur while Burton and Beauchamp (1985) found that the concentrations of soluble organic C required to promote and sustain denitrification was in the range of 60-80 µg C g^{-1} soil.

7.5.2 Soil chemical characteristics

The decline in both soil NO_3^--N and DOC, observed in this study, with both increasing ρ_b and ψ showed denitrification increased as both these variables were manipulated to impose increasingly anaerobic conditions, as evidenced by the *Dp*/*Do* measurements. The mean bulk soil pH in +N soil cores from -1.0 to -7.0 kPa was in the range of 6.60 to 5.45 and 6.97 to 5.89 for 1.1 and 1.5 Mg m^{-3}, respectively. The mean bulk soil pH in -N soil cores from -1.0 to -7.0 kPa was in the range of 6.04 to 5.32 and 6.13 to 5.67 for 1.1 and 1.5 Mg m^{-3}, respectively while the mean pH of the NO_3^- solutions 1 and 2 was 5.5. This suggests that this increase in bulk soil pH in +N soil cores from -1.0 to -7.0 kPa was the result of denitrification, a process which results in the net release of OH^- ions during denitrification (Wrage et al., 2001). Glinski et al. (1992) showed that the reduction of NO_3^- in soil was accompanied by an increase in pH of 2.5 units, in a soil amended with a 2% NO_3^- concentration. The higher soil pH, lower NO_3^--N and lower DOC concentrations in the higher ρ_b treatments in +N soil cores indicate that denitrification increased with increasing ρ_b and increasing ψ. Further supporting this result was the higher DOC concentrations in -N soil cores in all the ρ_b treatments from -1.0 to -9.0 kPa, indicating that DOC utilisation was lower due to a lack of N substrate for denitrification.

The variation in the rate of change in NO_3^--N and DOC concentrations over ψ with soil ρ_b was likely the result of the varying utilization of DOC and NO_3^--N in denitrification since all the cores were saturated with the same KNO_3 solution at the start of the experiment.

7.5.3 Soil physical characteristics

The changes observed in soil physical characters (ε, ϕ, WFPS, *Dp*/*Do*, *C*), due to decreasing ψ, were similar to changes reported in previous studies (Petersen et al., 2008; van der Weerden et al., 2012). However, these previous studies did not mutually examine the effect of soil compaction on soil physical parameters in conjunction with decreasing ψ. Soil water retention parameters, (-*b*) and ψ_a were derived from the WRC measured in the experiment 2c (Chapter 5) using the Campbell equation. The values of *b* were similar to previous values derived for a silt loam soil using water retention modelling by Sommer and Stockle (2010). Soil *Dp*/*Do* values were also in the range expected based on previous studies performed on soil cores at different ρ_b (Fujikawa and Miyazaki, 2005; Hamamoto et al., 2011) and values were again comparable with values from earlier chapters in this thesis. The fact that ε still ranged from 5-6% when *Dp*/*Do* values, measured at -1.0 kPa, equalled zero was most likely due to the presence of blocked pores and entrapped air space in the soil, which does not contribute to gas diffusion (Ball et al., 1988; Xu et al., 1992).

It is known that increases in ρ_b reduce ϕ and that *Dp*/*Do* is strongly dependent on ε. The values of *Dp*/*Do* were higher in the highest soil ρ_b treatments when ε was < 0.3 m^3 m^{-3} (Fig. 7.5). This observed effect may have been due to relative changes in effective pore space. For a given value of ε it has been observed that more compacted soils may have higher values of *Dp*/*Do* as a consequence of a decrease in the volume of ineffective pore space (pores not involved in gas transport) and a relative increase in the effective pore space (Fujikawa and Miyazaki, 2005). Further supporting this theory was the decrease in the soil water blockage factor (*X*) with the increase in soil ρ_b, (Fig. 7.6b), indicating that the water blockage effects were reduced at higher ρ_b levels (Hamamoto et al., 2011) resulting in increased *Dp*/*Do* when ε was < 0.3 m^3 m^{-3}. The pore connectivity factor (*A*) also decreased with an increase in soil ρ_b which indicates a reduction of large pore networks at higher ρ_b, which results in reduced gas diffusion (Hamamoto et al., 2011). The increase in *Dp*/*Do* at ε < 0.3, under high ρ_b levels indicates that the net effect of decreases in water blockage and pore connectivity favoured water blockage because *Dp*/*Do* increased.

Both ρ_b and ψ affect Dp/Do. Overall, the effect of increasing compaction at any given level of ψ was to progressively decrease Dp/Do (Fig. 7.3). This decrease in Dp/Do results from the reduction in ε due to greater water retention at higher ρ_b (Chamindu Deepagoda et al., 2011b; Hamamoto et al., 2011).

The data collected in this chapter also provided the opportunity to assess the relative effects of either ρ_b or ψ on the relationship between Dp/Do and ε. Initially Dp/Do was assessed against ε for each level of ρ_b (with ψ pooled across levels of ρ_b) as shown in Fig. 7.5 and a two parameter power function (Equation 7.9) was fitted to each ρ_b data set to determine values of two parameters, X and A. It was found that X decreased exponentially with increasing ρ_b (Fig. 7.6a). This is in contrast to the findings of Hamamoto et al. (2011) who found a linear decrease in X with increasing ρ_b for varying compacted soils. The linear trend found in their study may have been a consequence of limited data points (4), over the ρ_b range studied or due to comparing differently compacted soils. The decrease in X with increasing ρ_b is a result of increasing volumetric soil surface area reducing the water-blockage effect. The parameter A was also shown to decrease in an exponential manner in this current study (Fig. 7.6b). Hamamoto et al. (2011) again found a linear decrease of A with increasing ρ_b which was explained as being due to the reduction of larger pore size networks as a result of soil compaction. Again the reason for a linear fit, as opposed to the exponential fit found in this current study, may have been a consequence of only 4 data points being available.

When Dp/Do was assessed against ε for each level of ψ (with ρ_b pooled across levels of ψ) as shown in Fig. 7.8 and a two parameter power function (Equation 7.10) was fitted to each ψ data set to determine values of X and A, referred to as X' and A', it was found that the relationships between ψ and either X' or A' were again non-linear in nature. The values of X' remained relatively constant with decreasing ψ until -7.0 kPa where upon X' increased at a linear rate. This distribution of X' with changing ψ has been previously observed by Resurreccion et al. (2008) who found that X' was dependent on ψ, with each soil type studied displaying a unique X'- ψ relationship. They termed X' a pore connectivity-tortuosity factor and used a four parameter symmetrical function which included ψ^*, a reference soil matric potential, which divided the inter- and intra-aggregate pore space regions at a point where X' was assumed to have a minimum value and therefore a minimum water blocking effect within the air-filled (inter-aggregate) pore space.

Thus at values of $\psi > \psi^*$ inter-aggregate pores drain as ψ approaches ψ^* (X' decreases) and then as ψ becomes $< \psi^*$ the intra-aggregate pore space starts to drain, which creates more tortuous air-filled pore space within the aggregates which is remote and separate from the main diffusion pathways and so *X*' increases (Resurreccion et al., 2008). Furthermore, Resurreccion et al. (2008) went on to link *X*' and ψ with the Buckingham gas diffusivity model to develop a two-region soil water retention model to describe the bimodal pore size distribution which satisfactorily explained gas diffusivity behaviour as a function of both ψ and ε.

More recently, when comparing *X*' against ψ for three different size fractions of a sieved and re-packed volcanic ash soil, Chamindu Deepagoda et al. (2012) found the variation in *X*' with ψ was linear and symmetric, with values of *X*' decreasing from -1.0 kPa to -310 kPa but then increasing with a further decrease in ψ. The rationale given for the results was the previous explanation noted by Resurreccion et al. (2008). Schjønning et al. (2011) applied a two parameter power function to *Dp*/*Do* and ε data measured at different ψ and suggested that parameter '*n*' (equal to water blockage factor) was an expression of the rate of opening up of new pores for diffusion with decreasing ψ. This seems a more plausible and logical explanation than that of Resurreccion et al. (2008).

The increase in *A*' from -7.0 to -10.0 kPa was likely the result of increased pore continuity and in fact a comparison of *A*' versus ψ (Fig. 7.9b) with pore continuity (C) versus ψ, as seen in Fig. 7.12, shows very similar trends with both A' and C increasing at -7.0 kPa.

The fact that water blockage factors and pore connectivity factors do not remain constant with changes in ρ_b or ψ obviously has implications for accurately predicting *Dp*/*Do* under varying conditions of ρ_b or ψ since they are the key parameters in the two parameter power models commonly used to predict *Dp*/*Do*. Further studies are required to look at the effects of changes in soil conditions on these factors.

7.5.4 Relationship of N_2O-N fluxes with ψ, WFPS and *Dp*/*Do*

Nitrous oxide fluxes measured in this experiment were of a comparable magnitude to those measured under urea applications in Chapters 4 and 5. Clearly, the N_2O fluxes were stimulated by the addition of KNO_3 and affected by the interaction of ρ_b and ψ (section 7.4.2.3). The effect of increasing both ρ_b and ψ lead to a decrease in *Dp*/*Do* and hence a decrease in the availability of oxygen in the soil profile. This created conditions conducive to denitrification and N_2O fluxes increased as a result.

However, the decline in N_2O fluxes at the higher values of ψ within each ρ_b treatment was not a result of declining rates of denitrification but rather the result of (i) the conversion of N_2O to N_2 as demonstrated in the earlier Chapters (4 and 5), and (ii) N_2O becoming entrapped in the soil cores. In fact, the release of entrapped N_2O became more significant as anaerobic conditions increased (i.e. as ψ and ρ_b increased), as demonstrated in Fig. 7.31. No data are available on the N_2: N_2O ratio in this experiment despite trying to add further ^{15}N enriched substrate along with glucose, since the resulting mixed NO_3^- pool was not sufficiently enriched in ^{15}N to detect N_2 fluxes as indicated by the low N_2O ^{15}N atom % values that resulted (Table 7.10).

Few studies have assessed the relationship between N_2O produced via denitrification and ψ. Castellano et al. (2010) demonstrated, using different soils, that maximum N_2O emissions occurred at a consistent mean ψ value of -3.75 kPa that was independent of the effect of soil texture, structure and ρ_b, however, no attempt was made to examine *Dp*/*Do*. In that particular study, N_2O fluxes were measured from three different soils, where two soils had similar ρ_b (1.2 Mg m^{-3}) while the third soil had a lower ρ_b (0.69 Mg m^{-3}) and NO_3^- was injected into the top 15 cm of each column at the rate of 100 Kg N ha^{-1} after water saturating the columns. The soil columns were then allowed to drain freely and N_2O and ψ were measured over a period of 96 h. They also suggested that ψ was a better predictor of the maximum N_2O fluxes than WFPS for soils differing in texture and ρ_b. The current study differs from that of Castellano et al. (2010) in that only a single soil, compacted to varying levels of ρ_b with no variation due to soil textural effects, was used and soil cores were saturated with the NO_3^- solution.

In a more recent study by Van der Weerden et al. (2012), it was shown that log N_2O flux was linearly related with ψ. However, this study differed from this current study in three ways (i) NO_3^- solution was surface applied to the soil cores before draining to specific ψ while in the current study soil cores were saturated with NO_3^- solution and then drained to designated ψ levels, (ii) the same soil cores were stepwise drained to -10 kPa while in this study a new set of soil cores was made for each level of ψ applied, (iii) two different soils with nearly similar ρ_b were used, while in this study one soil was compacted to different levels of ρ_b. They also used a fungicide to restrict the growth of fungi in the soil cores. These contrasting experimental conditions might have been the reason for getting differing results from this study.

In the current study, when plotting the measured N_2O fluxes against other measured variables it was observed that neither water-filled pore space (WFPS), θ_v, ψ or ε produced good relationships, with peak N_2O fluxes at each level of soil ρ_b occurring at differing values of either WFPS, ψ, θ_v, or ε. It has been previously shown that soil N_2O flux may be described by a Gaussian function of WFPS (Davidson, 1991; Jambert et al., 1997; Veldkamp et al., 1998; Vilain et al., 2010; Rafique et al., 2011). Some studies have also shown N_2O flux to be exponentially related to WFPS (Smith et al., 1998; Clough et al., 2004; Beare et al., 2009). But Farquharson and Baldock (2008) note WFPS defines the fraction of the total pore space that is water-filled and thus it is not proportional to the actual diffusion of gases and thus is an inappropriate measure to use when comparing soils of varying ρ_b. Instead, Farquharson and Baldock (2008) suggested the use of θ_v and ε when estimating emissions of N_2O via denitrification and nitrification, respectively across soils varying in ρ_b. However, under the conditions employed in this study, where both ψ and ρ_b varied, θ_v was not a good predictor of maximum N_2O flux.

The term, θ_v, is a measure of the m^3 of water per m^3 of soil and thus while it tells us something about the relative water content, and by default perhaps the degree of aeration, it does not relate directly to the diffusion of gas, which is very much dependent on air-filled pore space.

The measure of relative gas diffusivity (Dp/Do) in this current study was the best variable for determining when maximum N_2O fluxes occurred under varying levels of ρ_b and ψ (Fig. 7.23). This is because denitrification of NO_3^-, requires a low oxygen concentration (Russow et al., 2009) and this is directly proportional to the rate of oxygen diffusion into the soil.

When $WFPS_{N2Omax}$, $Dp/Do_{N2O\ max}$, $\varepsilon_{N2O\ max}$ and C_{N2Omax} (values of measured variables at which the maximum N_2O-N flux occurred), were analysed, it was found that only Dp/Do_{N2Omax} did not differ with soil ρ_b or ψ. This indicates Dp/Do_{N2Omax} was independent of the effect of ρ_b or ψ. The Dp/Do_{N2Omax} values were in the range of 0.0060 to 0.0067 which is near the lower limit of the Dp/Do range (0.005-0.02) observed by Stepniewski (1981), when soil starts to get anaerobic. Studies by Petersen et al. (2008) and Andersen and Petersen (2009) have also shown that Dp/Do was better than WFPS in predicting N_2O emissions from either intact or repacked soils, respectively, while soil cores were maintained at different ψ levels.

In this current study N_2O-N fluxes at each level of ρ_b showed a Gaussian relationship with ψ (Fig. 7.19) while maximum N_2O-N fluxes appeared at distinct values of ψ (ψ_{N2Omax}). When values of ψ_a (-kPa) and ψ_{N2Omax} (-kPa) were plotted against each other, a very strong linear relationship emerged which indicated that the likely reason for the maximum N_2O flux occurring at a given ψ_{N2Omax} value was that ψ_{N2Omax} was actually equal to the ψ_a. There has been no previous study which has shown similar results from a soil varying in ρ_b, so the results could not be compared. Furthermore, the strong relationships between ψ_a and ψ_{N2Omax} with soil macroporosity (pores with diameter < 30 µm) indicated that the decrease in macroporosity due to increased soil compaction caused the observed decreases in ψ_a which was the likely cause of the peak N_2O fluxes occurring at specific ψ_{N2Omax}. As ψ decreases, ψ_a is reached and macropores are drained permitting greater diffusion of N_2O from the soil. However, further studies are needed to confirm whether these relationships hold true for other soils with different textures and structure.

7.5.5 Entrapped N_2O in soil

Clough et al. (1998) showed that 5.7% of the applied ^{15}N was entrapped in drained soil columns as N_2O after 38 days. The entrapped N_2O in soil is generally measured by the physical destruction of the soil to release the denitrification gases, as demonstrated by Clough et al. (2000). The results observed in this current study demonstrated the effect of soil compaction on the entrapped N_2O concentrations measured at -1.0 to -10 kPa. The amount of entrapped N_2O was increased at higher ψ levels in more compacted soils and was negligible from -7.0 to -10 kPa. Compacted soil has a high potential to entrap N_2O in soil water due to high water retention. Generally it is not accounted for in N_2O studies. It is possible that this entrapped N_2O might get released into the atmosphere when the soil is disturbed which has significant implications in the determination of the fate of N in soil and greenhouse gas budgeting (Clough et al., 2005).

7.5.6 N_2O-N fluxes after further substrate addition

The addition of further substrate showed that N_2O-N fluxes were proportional to the degree of anaerobicity with fluxes higher with increasing ψ and ρ_b (Fig. 7.26). The N_2O fluxes didn't decline at maximum values of ψ and ρ_b as was previously seen following 4 days equilibration on tension tables. This may have been because the substrate was surface applied, with denitrification happening closer to the more aerobic surface, or because the 6 h period between further substrate addition and N_2O sampling was insufficient to allow equilibration at the designated ψ values.

Again *Dp*/*Do* resulted in a better relationship with the N_2O-N fluxes measured after further substrate addition (Fig. 7.33a), which further suggests that *Dp*/*Do* could be used in predicting N_2O-N fluxes from soil under varying ρ_b and ψ.

7.5.7 *Dp*/*Do* predictive equation and comparisons with other predictive models

The measurement of *Dp*/*Do* is relatively time consuming, so the predictive models are often used to estimate *Dp*/*Do* in various studies. However, few studies have been performed to examine ρ_b effects when predicting *Dp*/*Do* with soil gas diffusivity models. The data collected in this study provided an opportunity to develop a predictive equation for *Dp*/*Do* albeit based on the one soil. However, in future the validity of this model should be confirmed on an independent data set. The result of scatter plot comparisons performed using four pre-existing models showed that none of these could estimate the measured *Dp*/*Do* values. However, the density-corrected model (Chamindu Deepagoda et al., 2011b) performed better. More work is required in this direction and for that *Dp*/*Do* should also be measured from soils varying in texture, ψ and ρ_b.

This study suggests that models not corrected for ρ_b may erroneously over or under predict *Dp*/*Do* and that relating these predicted *Dp*/*Do* values with soil gas fluxes from compacted soil might result in dubious relationships. Future work is required to incorporate soil ρ_b effects on *Dp*/*Do* predicted through experimental and modelling approaches. It was also observed in this study that the values of A and X changed with both soil ρ_b and ψ. Thus, it is necessary to determine these values under varying soil conditions in order to correctly predict *Dp*/*Do* as they both are key parameters in the models generally used to predict *Dp*/*Do*.

7.6 Conclusions

This study has shown that under non-limiting substrate conditions for denitrification, there was a significant effect of soil ρ_b on the N_2O fluxes derived via denitrification. Maximum fluxes of N_2O-N occurred at a specific value of ψ (ψ_{N2Omax}) for each ρ_b treatment which corresponded to ψ_a. The ψ_{N2Omax} values were significantly related with ψ_a demonstrating that ψ_a acts as a critical determinant of maximum N_2O flux. Soil macroporosity was able to explain 99% of the variance in ψ_a due to soil ρ_b. Maximum N_2O-N fluxes occurred at a narrow range of *Dp*/*Do* (0.006-0.0067) independent of the effects of soil ρ_b and ψ. These results have implications for modelling N_2O fluxes.

The differences in the relationship between N_2O-N and ψ obtained from soils cores saturated with NO_3^- solution and when NO_3^- was surface applied indicates the importance of the methodology used and its subsequent effects on the ensuing N_2O-N fluxes. Previous models for predicting *Dp*/*Do* fared poorly when applied to the data set produced here and while an empirical equation was developed using the current data, it needs further independent data sets for validation. Until a robust soil ρ_b corrected *Dp*/*Do* model is developed, it is suggested that *Dp*/*Do* should not be predicted but measured from compacted soils before using it as a predictive tool for N_2O fluxes.

Chapter 8

Summary and Conclusions

8.1 Introduction

All the experiments conducted in this study were performed under controlled conditions and were described in detail in the previous chapters. This Chapter synthesizes my research and identifies areas or opportunities for future research.

8.2 Why N_2O emissions and relative gas diffusivity?

In New Zealand, agricultural N_2O emissions contributed almost 95% of the total N_2O emissions in 2010 (Ministry for the Environment New Zealand, 2012) and 85% of agricultural soils are grazed by livestock (Clark et al., 2001). Soil compaction, especially under winter grazed forages, has the potential to produce high N_2O emissions (Thomas et al., 2008). This is because of increased soil bulk density (ρ_b) and water-filled pore space (WFPS) and reduced gas diffusivity creating anaerobic conditions in the soil as a consequence of soil compaction. Farquharson and Baldock (2008) clearly justified why WFPS should not be used to predict N_2O emissions from a soil varying in ρ_b and only few studies have examined relative gas diffusivity (*Dp*/*Do*) as a predictor of N_2O fluxes (section 2.6.3.2). Thus this work was planned to study the relationship of *Dp*/*Do* with N_2O-N and N_2-N fluxes to understand its potential for predicting N_2O emissions from soil. Since it is known that gas (e.g. N_2O) transport in and out of soil occurs by diffusion and *Dp*/*Do* takes into account both air-filled porosity (ε) and pore connectivity, it was hypothesized that *Dp*/*Do* would be a better predictor of urea/nitrate derived N_2O-N fluxes. However, variability of relative gas diffusivity (*Dp*/*Do*) in soil is not well studied (Lange et al., 2009) and it has been shown that it is affected by changes in ρ_b and matric potential (ψ) (Resurreccion et al., 2008; Hamamoto et al., 2011). Moreover, there is a complete dearth of studies that have measured urea/nitrate-derived N_2O and N_2 fluxes from a compacted soil maintained at different ψ with the simultaneous measurement of *Dp*/*Do*.

8.3 Summary and conclusions

- A main focus of this study was to determine the impact of soil compaction on *Dp*/*Do* at varying levels of ψ, and to consequently measure urea/nitrate-derived N_2O-N and N_2-N fluxes in the absence of plants or pasture. In this current study, repacked soil cores were used to reduce the variability of measured variables. Another aim of the study was to determine which variable, WFPS or *Dp*/*Do* was a better predictor of N_2O emissions from a variably compacted soil maintained at different ψ. According to Clark et al. (2001) one of the proposed methods to mitigate N_2O emissions was to ensure that N from denitrification is emitted as N_2 rather than N_2O. To achieve this, the knowledge of soil's potential to reduce N_2O to N_2 under various physical conditions is necessary, especially in the presence of ruminant urine. Other mitigation strategies proposed by Clark et al. (2001) were optimisation of the soil's drainage conditions and prevention of soil compaction. This is the first time that data relating to these proposed mitigation means has been collected in detail.

- In Chapter 4, a controlled laboratory experiment was conducted where urea-derived N_2O-N and N_2-N fluxes were measured from a soil compacted at varying ρ_b while being maintained at a constant ψ of -10 kPa. Net NH_4^+-N depletion and NO_3^--N accumulation rates were lowest at the highest ρ_b treatment. Soil *Dp*/*Do* and ε decreased while WFPS increased with increases in soil ρ_b. The mean cumulative N_2O-N emissions, as a percentage of urea-N applied, ranged from 0.05 to 2.14% while the mean cumulative N_2-N emissions, as a percentage of urea-N applied ranged from 0.06 to 4.97%. Both cumulative N_2O-N and N_2-N fluxes increased with the increase in soil ρ_b and the decrease in *Dp*/*Do*. There was a threshold *Dp*/*Do* value of 0.038 below which cumulative N_2-N fluxes increased significantly. It was also observed that both WFPS and *Dp*/*Do* had similar relationships with the cumulative N_2O-N and N_2-N fluxes measured.

The dye test performed in the experiment showed that the vertical depth of dye penetration in soil decreased with increase in soil ρ_b. This explained the lower DOC concentrations observed at the highest ρ_b treatments. This may happen in the field where urine deposited on the compacted soil may distribute horizontally rather than vertically.

- In Chapter 5, two identical experiments were conducted at two levels of ψ, -6.0 and -0.2 kPa in order to increase the range of matric potential from chapter 4. This experiment again gathered N_2O, N_2 and *Dp*/*Do* data at less negative levels of ψ (wetter soil). Inorganic N and DOC data were similar to those obtained in chapter 4. The flux data showed that cumulative N_2O fluxes at -6.0 kPa decreased and cumulative N_2-N fluxes increased with the increase in soil ρ_b. At -0.2 kPa, cumulative N_2O-N fluxes were relatively lower than at -6.0 kPa at 1.1, 1.2 and 1.3 Mg m^{-3}. The maximum cumulative N_2O-N flux measured as a % of applied N was 16%, at -6.0 kPa in the 1.3 Mg m^{-3} ρ_b treatment and decreased with further increases in soil ρ_b. This reiterates the potential for soil compaction to increase N_2O emissions in grazed soils particularly in the presence of ruminant urine. The high cumulative N_2-N:N_2O-N ratios with increasing soil ρ_b specifically at higher ψ values has both negative and positive consequences as soil ρ_b has a huge potential to increase N_2O fluxes as well the capability to reduce N_2O to N_2 specifically at higher ψ levels. This experiment also showed that soil ρ_b affected the soil's water retention properties and pore size distribution.

- In Chapter 6 data from Chapters 4 and 5 were compiled. The reason to do so was to assess the change in N_2O-N and N_2-N fluxes under the varying physical treatments applied (ψ and ρ_b) and their relationships with WFPS and *Dp*/*Do*. The combined results showed that higher urea-derived cumulative N_2O-N fluxes occurred at -6.0 kPa at ≤ 1.3 Mg m^{-3}. This suggests reducing compaction might actually result in increasing N_2O fluxes from soil. This result does not suggest that soil compaction should be increased in order to reduce N_2O emissions as it is also known that plant growth is reduced in compacted soils. However, it definitely indicates that ψ should also be carefully adjusted with simultaneous reductions in soil ρ_b in order to minimise N_2O emissions from soil. Moreover, the variable, *Dp*/*Do* produced least scatter with cumulative N_2O-N, N_2-N fluxes and cumulative N_2-N: N_2O-N ratios. It was also observed that urea-derived cumulative N_2O-N fluxes peaked at a mean *Dp*/*Do* value of 0.005 which is almost identical to the value of *Dp*/*Do* where the NO_3^--derived N_2O-N fluxes peaked in Chapter 7.

- Knowledge around the effects of ρ_b on soil water retention properties and its associated effects on N_2O fluxes from soil is scarce. Only recently some studies have tried to relate N_2O emissions from different soils with changing ψ. Thus in Chapter 7, another controlled experiment was performed. Soil cores were saturated with a NO_3^- solution and then desaturated to designated ψ levels. This experiment showed that at ψ_a there was a critical *Dp*/*Do* value which resulted in a maximum N_2O flux from a soil under varying ρ_b. At $\psi > \psi_a$ N_2O-N was probably either entrapped in soil (Chapter 7) or was reduced to N_2 (Chapter 6) while at $\psi < \psi_a$, N_2O-N fluxes decreased, presumably due to soil conditions becoming aerobic. However, this N_2O-N maximum value occurred at different ψ_a as a consequence of increases in soil ρ_b changing soil macroporosity, which ultimately decreased the air entry potential (ψ_a). Thus N_2O-N maximum values for different ρ_b treatments occurred at different ψ referred to as ψ_{N2Omax}. This study shows, for the first time, that *Dp*/*Do* proved to be a consistent determinant of this maximum N_2O-N flux from a soil varying both in ψ and ρ_b. No previous study has shown the importance of both ψ_a and *Dp*/*Do* to be critical in predicting peak N_2O fluxes under variably compacted soil. In this experiment it was also shown that large amounts of N_2O can remain entrapped in soils even 6 days after saturating the soil cores which suggests that entrapped N_2O also has implications for greenhouse gas budgeting.

- Numerical modelling approaches and experimental data go hand in hand. Most of the models for predicting *Dp*/*Do* are based on ε and this study has shown that the relationship between *Dp*/*Do* and ε varies with both, soil ρ_b and ψ. As measurement of *Dp*/*Do* is relatively time consuming, predictive models are often used to estimate *Dp*/*Do* in various studies. However, little work has been performed in incorporating ρ_b effects in predicting *Dp*/*Do* in soil gas diffusivity models. The *Dp*/*Do* data collected in chapter 7 was used to develop an equation for predicting *Dp*/*Do* using the easily available parameters, ε and ϕ. The empirical equation developed in Chapter 7 was a better predictor of *Dp*/*Do* across soil differing in ρ_b and ψ levels when compared with other *Dp*/*Do* models. However, independent validation is required. In addition, the work in Chapter 7 showed that the parameters, water blockage factor (X) and pore connectivity factor (A) were not constant and changed with both ρ_b and ψ. Both, X and A, are the key parameters for predicting *Dp*/*Do*.

8.4 Recommendations for future research

- Plants or pasture are known to affect N_2O emissions as dynamics of C and N in the presence of plants are different from the areas without plants, even when soil physical conditions are similar. Thus it would be interesting to repeat this experiment in the presence of plants. Soil DOC concentrations in this current study increased immediately after urea application due to high pH and decreased thereafter. However, in the presence of plants, DOC concentrations would have persisted for a longer time as plants add carbon to the soil in the form of plant residues and root exudates. Plants also respire and consume O_2 which might have created anaerobic conditions (Mahmood et al., 1997) conducive for N_2O production at relatively lower ψ levels (more negative).

- In the Chapter 7, N_2O-N fluxes were measured after equilibrating the cores for 4 days at a designated ψ level. Similar experiments should be performed to measure the N_2O-N fluxes over time, in order to calculate the cumulative N_2O-N fluxes. This would provide further insight into the changes in these fluxes along with substrate supply.

- It was also observed in Chapter 7 that both X and A varied with soil ρ_b and ψ. These factors are important in predicting *Dp*/*Do*. Thus, it becomes necessary in future to determine these factors experimentally by measuring *Dp*/*Do* from soils with different textures at varying ρ_b, in order to precisely predict *Dp*/*Do.*

- Chamindu Deepagoda et al. (2011a) showed that decreases in *Dp*/*Do* with increases in soil ρ_b varied with soil texture. Only one soil type (silt loam) was used in this current study. It is also known that soil texture affects WRC and the pore size distribution. Moldrup et al. (2000b) showed that *Dp*/*Do* measured using intact soil cores differ from those measured using repacked soil cores. They also showed *Dp*/*Do* measured using repacked cores was independent of the effect of soil texture. So further research should use intact soil cores to perform similar experiments to assess the effect of soil texture and soil ρ_b on N_2O and N_2 fluxes after urea/urine application.

- The soil used in this study was air-dried and sieved to < 2 mm. Uchida et al. (2008) reported that N_2O emissions were higher from the smaller aggregate sizes and from the most compacted soil following urine application. However, they did not measure N_2 emissions. Thus it would be interesting to compact soils of different aggregate sizes and measure both N_2O and N_2 fluxes to determine N_2: N_2O ratios in conjunction with *Dp*/*Do* to gain an insight into how aggregates affect the relationship of *Dp*/*Do* with N_2O and N_2 fluxes.

- Only one soil type used in this study meant that there was no variation in the soil's native organic carbon. Measurements of N_2O, N_2 fluxes and *Dp*/*Do* from soils similar in texture but varying in organic carbon could reveal the impact of organic carbon on *Dp*/*Do* and N_2O fluxes as organic carbon also has a potential to affect soil pore structure functions and soil ρ_b which ultimately influence gas transport parameters in soil (Ruehlmann and Körschens, 2009; Hamamoto et al., 2012).

- There has been very little previous work performed on the effect of soil compaction on microbial populations related to N_2O production and N_2O reduction. Thus, this study should be extended to evaluate microbial activity using the latest molecular techniques to determine gene copy numbers to assess the stress caused by changing ρ_b and ψ on the respective nitrifying and denitrifying populations. Furthermore, such changes in soil microbial communities should be related to *Dp*/*Do* and N_2O, N_2 fluxes.

Appendix A

Results from -N soil cores (controls)

A 1 **The N_2O-N fluxes (mg m^{-2} h^{-1}) measured from -N soil cores at varying bulk density (Mg m^{-3}) and matric potential (-kPa) levels in chapter 7. The values are means of 4 replicates and standard deviations are in brackets.**

Matric potential (-kPa)	Soil bulk density (Mg m^{-3})				
	1.1	**1.2**	**1.3**	**1.4**	**1.5**
1.0	0.033 (0.028)	0.024 (0.012)	0.027 (0.022)	0.03 (0.024)	0.026 (0.008)
1.5	0.032 (0.013)	0.033 (0.023)	0.019 (0.008)	0.027 (0.011)	0.036 (0.013)
2.0	0.011 (0.006)	0.006 (0.005)	0.007 (0.004)	0.006 (0.007)	0.011 (0.010)
3.0	0.006 (0.005)	0.013 (0.006)	0.017 (0.02)	0.009 (0.006)	0.011 (0.004)
4.0	0.007 (0.006)	0.008 (0.003)	0.006 (0.004)	0.01 (0.003)	0.007 (0.006)
5.0	0.008 (0.006)	0.008 (0.007)	0.010 (0.007)	0.011 (0.008)	0.007 (0.010)
6.0	0.005 (0.003)	0.005 (0.003)	0.005 (0.005)	0.012 (0.011)	0.009 (0.004)
7.0	0.007 (0.004)	0.008 (0.009)	0.014 (0.011)	0.004 (0.003)	0.007 (0.006)
8.0	0.004 (0.002)	0.009 (0.005)	0.009 (0.005)	0.007 (0.004)	0.008 (0.004)
9.0	0.007 (0.005)	0.006 0.004)	0.007 (0.006)	0.004 (0.003)	0.009 (0.005)
10	0.002 (0.0005)	0.009 (0.007)	0.004 (0.003)	0.005 (0.002)	0.011 (0.006)

A 2 **Bulk soil pH measured from -N soil cores at varying bulk density (Mg m^{-3}) and matric potential (-kPa) levels in chapter 7. The values are means of 3 replicates and standard deviations are in brackets.**

Matric potential (-kPa)	Soil bulk density (Mg m^{-3})				
	1.1	**1.2**	**1.3**	**1.4**	**1.5**
1.0	6.04 (0.055)	6.09 (0.07)	6.09 (0.09)	6.18 (0.06)	6.13 (0.03)
1.5	6.06 (0.05)	6.07 (0.03)	6.08 (0.09)	6.11 (0.09)	6.10 (0.05)
2.0	5.96 (0.04)	5.84 (0.05)	5.88 (0.10)	5.81 (0.07)	5.96 (0.03)
3.0	5.81 (0.06)	5.70 (0.04)	5.68 (0.06)	5.73 (0.09)	5.81 (0.11)
4.0	5.56 (0.09)	5.64 (0.04)	5.60 (0.07)	5.68 (0.13)	5.80 (0.09)
5.0	5.42 (0.11)	5.56 (0.04)	5.53 (0.09)	5.64 (0.13)	5.76 (0.05)
6.0	5.44 (0.12)	5.60 (0.09)	5.73 (0.07)	5.60 (0.36)	5.65 (0.08)
7.0	5.32 (0.11)	5.56 (0.05)	5.60 (0.06)	5.53 (0.29)	5.67 (0.22)
8.0	5.39 (0.07)	5.5 (0.07)	5.50 (0.14)	5.63 (0.18)	5.60 (0.18)
9.0	5.32 (0.08)	5.5 (0.11)	5.48 (0.13)	5.61 (0.02)	5.60 (0.03)
10	5.36 (0.15)	5.3 (0.10)	5.40 (0.15)	5.50 (0.13)	5.55 (0.06)

A 3 **Soil NO_3^--N concentrations (µg g^{-1} soil) measured from -N soil cores at varying bulk density (Mg m^{-3}) and matric potential (-kPa) levels in chapter 7. The values are means of 3 replicates and standard deviations are in brackets.**

Matric potential (-kPa)	Soil bulk density (Mg m^{-3})				
	1.1	**1.2**	**1.3**	**1.4**	**1.5**
1.0	0.32 (0.04)	0.32 (0.52)	0.30 (0.04)	0.40 (0.12)	0.29 (0.26)
1.5	1.19 (0.25)	1.24 (0.12)	1.21 (0.24)	1.13 (0.19)	1.02 (0.09)
2.0	15.3 (0.50)	16.0 (1.47)	16.2 (0.89)	14.3 (1.49)	14.6 (0.69)
3.0	1.82 (2.09)	1.83 (2.07)	2.50 (3.03)	4.83 (2.09)	1.05 (1.01)
4.0	2.26 (0.99)	3.68 (0.84)	3.58 (2.23)	6.32 (1.61)	5.81 (0.91)
5.0	5.40 (0.52)	1.92 (1.19)	5.61 (1.51)	10.5 (3.81)	11.2 (3.29)
6.0	8.64 (1.84)	9.75 (3.78)	12.0 (1.62)	12.0 (4.92)	14.9 (0.96)
7.0	12.9 (0.84)	11.5 (3.49)	13.2 (1.20)	15.1 (0.31)	13.4 (3.24)
8.0	16.1 (2.84)	13.4 (2.54)	16.9 (0.68)	15.4 (2.99)	15.1 (0.58)
9.0	3.30 (0.30)	3.40 (0.50)	3.28 (0.54)	2.84 (0.38)	2.97 (0.16)
10	18.0 (0.80)	16.5 (0.55)	15.1 (1.06)	17.9 (0.46)	16.86 (0.65)

A 4 **Soil NH_4^+-N concentrations (µg g^{-1} soil) measured from -N soil cores at varying bulk density (Mg m^{-3}) and matric potential (-kPa) levels in chapter 7. The values are means of 3 replicates and standard deviations are in brackets.**

Matric potential (-kPa)	Soil bulk density (Mg m^{-3})				
	1.1	**1.2**	**1.3**	**1.4**	**1.5**
1.0	15.2 (1.42)	17.8 (6.68)	19.7 (1.44)	19.9 (4.37)	18.5 (4.38)
1.5	12.1 (1.12)	13.2 (1.56)	15.6 (2.93)	20.6 (3.55)	19.4 (1.98)
2.0	10.9 (1.27)	12.1 (3.81)	13.6 (4.01)	14.5 (1.85)	17.1 (2.03)
3.0	12.4 (0.88)	12.4 (0.69)	12.4 (0.95)	11.9 (1.30)	12.2 (1.76)
4.0	11.3 (0.41)	12.2 (1.50)	11.08 (0.30)	11.5 (0.76)	11.4 (2.23)
5.0	7.84 (1.31)	6.89 (1.10)	5.42 (2.53)	5.32 (1.50)	5.57 (1.73)
6.0	4.80 (2.11)	5.59 (0.99)	5.80 (1.45)	3.82 (1.58)	4.28 (0.77)
7.0	4.01 (2.07)	2.80 (2.16)	2.99 (2.00)	3.38 (2.19)	3.25 (1.35)
8.0	2.96 (0.48)	2.85 (0.27)	2.41 (1.16)	4.21 (1.96)	3.97 (2.27)
9.0	1.85 (0.41)	3.33 (0.10)	3.16 (0.82)	4.25 (0.85)	3.09 (1.39)
10	2.17 (0.93)	1.14 (0.21)	1.01 (0.08)	0.84 (0.33)	0.95 (0.07)

References

Abbasi, M.K., Adams, W.A., 2000. Gaseous N emission during simultaneous nitrification-denitrification associated with mineral N fertilization to a grassland soil under field conditions. Soil Biology & Biochemistry, 32, 1251-1259.

Allaire, S.E., Roulier, S., Cessna, A.J., 2009. Quantifying preferential flow in soils: A review of different techniques. Journal of Hydrology, 378, 179-204.

Allison, S.M., Prosser, J.I., 1993. Ammonia oxidation at low pH by attached populations of nitrifying bacteria. Soil Biology & Biochemistry, 25, 935-941.

Ambus, P., Petersen, S.O., Soussana, J.F., 2007. Short-term carbon and nitrogen cycling in urine patches assessed by combined carbon-13 and nitrogen-15 labelling. Agriculture, Ecosystems & Environment, 121, 84-92.

Andersen, A.J., Petersen, S.O., 2009. Effects of C and N availability and soil-water potential interactions on N_2O evolution and PLFA composition. Soil Biology & Biochemistry, 41, 1726-1733.

Anderson, T.W., Darling, D.A., 1952. Asymptotic theory of certain "Goodness of Fit" criteria based on stochastic processes. The Annals of Mathematical Statistics, 23, 193-212.

Arah, J.R.M., Smith, K.A., 1990. Factors influencing the fraction of the gaseous products of soil denitrification evolved to the atmosphere as nitrous oxide. In: Bouwman, A.F. (Ed.), Soils and the greenhouse effect. Wiley, Chichester, pp. 475-480.

Ardakani, M.S., Rehbock, J.T., McLaren, A.D., 1973. Oxidation of nitrite to nitrate in a soil column. Soil Science Society of America Journal, 37, 53-56.

Arthur, E., Moldrup, P., Schjønning, P., de Jonge, L.W., 2012. Linking particle and pore size distribution paramters to soil gas transport properties. Soil Science Society of America Journal, 76, 18-27.

Assouline, S., 2006. Modeling the relationship between soil bulk density and the water retention curve. Vadose Zone Journal, 5, 554-563.

Aulakh, M.S., Doran, J.W., Walters, D.T., Power, J.F., 1991a. Legume residue and soil water effects on denitrification in soils of different textures. Soil Biology & Biochemistry, 23, 1161-1167.

Aulakh, M.S., Walters, D.T., Doran, J.W., Francis, D.D., Mosier, A.R., 1991b. Crop residue type and placement effects on denitrification and mineralization. Soil Science Society of America Journal, 55, 1020-1025.

Avnimelech, Y., Laher, M., 1977. Ammonia volatilization from soils: equilibrium considerations. Soil Science Society of America Journal, 41, 1080-1084.

Azam, F.A., Müller, C.M., Weiske, A.W., Benckiser, G.B., Ottow, J.O., 2002. Nitrification and denitrification as sources of atmospheric nitrous oxide-role of oxidizable carbon and applied nitrogen. Biology and Fertility of Soils, 35, 54-61.

Ball, B.C., 1981. Modelling of soil pores as tubes using gas permeabilties, gas diffusivities and water release. Journal of Soil Science, 32, 465-481.

Ball, B.C., Ritchie, R.M., 1999. Soil and residue management effects on arable cropping conditions and nitrous oxide fluxes under controlled traffic in Scotland: 1. Soil and crop responses. Soil and Tillage Research, 52, 177-189.

Ball, B.C., Schjønning, P., 2002. Air Permeability. In: Dane, J.H., Topp, G.C. (Eds.), Methods of Soil Analysis, Part 4, Physical methods. Soil Science Society of America, Madison, WI, pp. 1141-1158.

Ball, B.C., Harris, W., Burford, J.R., 1981. A laboratory method to measure gas diffusion and flow in soil and other porous materials. Journal of Soil Science, 32, 323-334.

Ball, B.C., O'Sullivan, M.F., Hunter, R., 1988. Gas diffusion, fluid flow and derived pore continuity indices in relation to vehicle traffic and tillage. Journal of Soil Science, 39, 327-339.

Ball, B.C., Parker, J.P., Scott, A., 1999a. Soil and residue management effects on cropping conditions and nitrous oxide fluxes under controlled traffic in Scotland: 2. Nitrous oxide, soil N status and weather. Soil and Tillage Research, 52, 191-201.

Ball, B.C., Scott, A., Parker, J.P., 1999b. Field N_2O, CO_2 and CH_4 fluxes in relation to tillage, compaction and soil quality in Scotland. Soil and Tillage Research, 53, 29-39.
Ball, B.C., Crichton, I., Horgan, G.W., 2008. Dynamics of upward and downward N_2O and CO_2 fluxes in ploughed or no-tilled soils in relation to water-filled pore space, compaction and crop presence. Soil and Tillage Research, 101, 20-30.
Bathurst, N.O., 1952. The amino-acids of sheep and cow urine. The Journal of Agricultural Science, 42, 476-478.
Beare, M., White, S., Wilson, D., 2006. Managing winter forage crops sustainably. Proceedings of the South Isand Dairy Event, 35-41.
Beare, M.H., Gregorich, E.G., St-Georges, P., 2009. Compaction effects on CO_2 and N_2O production during drying and rewetting of soil. Soil Biology & Biochemistry, 41, 611-621.
Beauchamp, E.G., Gale, C., Yeomans, J.C., 1980. Organic matter availability for denitrification in soils of different textures and drainage classes. Communications in Soil Science and Plant Analysis, 11, 1221-1233.
Bertram, J.E., Clough, T.J., Sherlock, R.R., Condron, L.M., O'Callaghan, M., Wells, N.S., Ray, J.L., 2009. Hippuric acid and benzoic acid inhibition of urine derived N_2O emissions from soil. Global Change Biology, 15, 2067-2077.
Bhandral, R., Saggar, S., Bolan, N.S., Hedley, M.J., 2007. Transformation of nitrogen and nitrous oxide emission from grassland soils as affected by compaction. Soil and Tillage Research, 94, 482-492.
Blackmer, A.M., Bremner, J.M., 1978. Inhibitory effect of nitrate on reduction of N_2O to N_2 by soil microorganisms. Soil Biology & Biochemistry, 10, 187-191.
Blackmer, A.M., Bremner, J.M., 1979. Stimulatory effect of nitrate on reduction of N_2O to N_2 by soil microorganisms. Soil Biology & Biochemistry, 11, 313-315.
Blackmer, A.M., Cerrato, M.E., 1986. Soil Properties Affecting Formation of Nitric Oxide by Chemical Reactions of Nitrite. Soil Science Society of America Journal, 50, 1215-1218.
Blakemore, L.C., Searle, P.L., Daly, B.K., 1987. Methods for Chemical Analysis of Soils. NZ Soil Bureau, Lower Hutt.
Bremner, J.M., Blackmer, A.M., 1981. Terrestrial nitrification as a source of atmospheric nitrous oxide. In: Delwiche, C.C. (Ed.), Denitrification, nitrification and atmospheric nitrous oxide. Wiley, New York, pp. 76-84.
Brooks, R.H., Corey, A.T., 1964. Hydraulic properties of porous media, Hydrology Paper no. 3, Colorado State University, Fort Collins, CO.
Buckingham, E., 1904. Contributions to our knowledge of the aeration of soils, vol. 25. United States Dept of Agriculture, Bureau of Soil Bulletin, Washington, DC. Retrieved from http://hdl.handle.net/2027/uc1.b3044430.
Burford, J.R., Bremner, J.M., 1975. Relationships between the denitrification capacities of soils and total, water-soluble and readily decomposable soil organic matter. Soil Biology & Biochemistry, 7, 389-394.
Burton, D.L., Beauchamp, E.G., 1985. Denitrification rate relationships with soil parameters in the field. Communications in Soil Science and Plant Analysis, 16, 539-549.
Campbell, G.S., 1974. A simple method for determining unsaturated conductivity from moisture retention data. Soil Science, 117, 311-314.
Carslaw, H.S., Jaeger, J.C., 1959. Conduction of heat in solids., 2nd ed. Claredon Press, Oxford.
Carter, M., Klumpp, K., Le Roux, X., 2006. Lack of increased availability of root-derived C may explain the low N_2O emission from low N-urine patches. Nutrient Cycling in Agroecosystems, 75, 91-100.
Castellano, M.J., Schmidt, J.P., Kaye, J.P., Walker, C., Graham, C.B., Lin, H., Dell, C.J., 2010. Hydrological and biogeochemical controls on the timing and magnitude of nitrous oxide flux across an agricultural landscape. Global Change Biology, 16, 2711-2720.
Cavigelli, M.A., Robertson, G.P., 2001. Role of denitrifier diversity in rates of nitrous oxide consumption in a terrestrial ecosystem. Soil Biology & Biochemistry, 33, 297-310.

Chalk, P.M., Smith, C.J., 1983. Chemodenitrification. In: Freney, J.R., Simpson, J.R. (Eds.), Gaseous loss of nitrogen from plant–soil systems. Martinus Nijhoff Publications, Dordrecht, the Netherlands, pp. 65–89.

Chamindu Deepagoda, T.K.K., Moldrup, P., Schjønning, P., Kawamoto, K., Komatsu, T., Wollesen de Jonge, L., 2011a. Generalized density-corrected model for gas diffusivity in variably saturated soils. Soil Science Society of America Journal, 75, 1315-1329.

Chamindu Deepagoda, T.K.K., Moldrup, P., Schjønning, P., Jonge, L.W.d., Kawamoto, K., Komatsu, T., 2011b. Density-corrected models for gas diffusivity and air permeability in unsaturated soil. Vadose Zone Journal, 10, 226-238.

Chamindu Deepagoda, T.K.K., Moldrup, P., Schjønning, P., Kawamoto, K., Komatsu, T., de Jonge, L.W., 2012. Variable pore connectivity model linking gas diffusivity and air-phase tortuosity to soil matric potential. Vadose Zone Journal, 11.

Chapuis-Lardy, L., Wrage, N., Metay, A., Chotte, J.-L., Bernoux, M., 2007. Soils, a sink for N_2O? A review. Global Change Biology, 13, 1-17.

Cicerone, R.J., 1987. Changes in stratospheric ozone. Science, 237, 35-42.

Clark, H., de Klein, C.A.M., Newton, P., 2001. "Potential management practices and technologies to reduce nitrous oxide, methane and carbon dioxide emissions from New Zealand agriculture". Wellington , New Zealand: Ministry of the Agriculture and Forestry, MAF Report.

Clough, T.J., 1994. Fate of urine nitrogen applied to peat and mineral soils from grazed pastures. Ph.D. Thesis, Department of Soil Science. Lincoln University, Lincoln, New Zealand.

Clough, T.J., Sherlock, R.R., Cameron, K.C., 2000. Entrapment and displacement of nitrous oxide in a drained pasture soil. Nutrient Cycling in Agroecosystems, 57, 191-193.

Clough, T.J., Sherlock, R.R., Rolston, D.E., 2005. A review of the movement and fate of N_2O in the subsoil. Nutrient Cycling in Agroecosystems, 72, 3-11.

Clough, T.J., Sherlock, R.R., Cameron, K.C., Ledgard, S.F., 1996. Fate of urine nitrogen on mineral and peat soils in New Zealand. Plant and Soil, 178, 141-152.

Clough, T.J., Kelliher, F.M., Sherlock, R.R., Ford, C.D., 2004. Lime and soil moisture effects on nitrous oxide emissions from a urine patch. Soil Science Society of America Journal, 68, 1600-1609.

Clough, T.J., Kelliher, F.M., Wang, Y.P., Sherlock, R.R., 2006. Diffusion of ^{15}N-labelled N_2O into soil columns: a promising method to examine the fate of N_2O in subsoils. Soil Biology & Biochemistry, 38, 1462-1468.

Clough, T.J., Jarvis, S.C., Dixon, E.R., Stevens, R.J., Laughlin, R.J., Hatch, D.J., 1998. Carbon induced subsoil denitrification of ^{15}N-labelled nitrate in 1 m deep soil columns. Soil Biology & Biochemistry, 31, 31-41.

Clough, T.J., Sherlock, R.R., Cameron, K.C., Stevens, R.J., Laughlin, R.J., Muller, C., 2001. Resolution of the ^{15}N balance enigma? Australian Journal of Soil Research, 39, 1419-1431.

Clough, T.J., Ray, J.L., Buckthought, L.E., Calder, J., Baird, D., O'Callaghan, M., Sherlock, R.R., Condron, L.M., 2009. The mitigation potential of hippuric acid on N_2O emissions from urine patches: An in situ determination of its effect. Soil Biology & Biochemistry, 41, 2222-2229.

Cresswell, H.P., Paydar, Z., 1996. Water retention in Australian soils. I. Description and prediction using parametric functions. Soil Research, 34, 195-212.

Crutzen, P.J., 1981. Atmospheric chemical processes of the oxides of nitrogen, including nitrous oxide. In: Delwiche, C.C. (Ed.), Denitrification, nitrification and nitrous oxide. Wiley, New York, pp. 17–44.

Cui, K., Défossez, P., Cui, Y.J., Richard, G., 2010. Soil compaction by wheeling: changes in soil suction caused by compression. European Journal of Soil Science, 61, 599-608.

Currie, J.A., 1960. Gaseous diffusion in porous media. Part1. A non-steady state method. British Journal of Applied Physics, 11, 314-317.

Currie, J.A., 1983. Gas diffusion through soil crumbs: the effects of wetting and swelling. Journal of Soil Science, 34, 217-232.

Currie, J.A., 1984. Gas diffusion through soil crumbs: the effects of compaction and wetting. Journal of Soil Science, 35, 1-10.

Daum, D., Schenk, M.K., 1998. Influence of nutrient solution pH on N_2O and N_2 emissions from a soilless culture system. Plant and Soil, 203, 279-288.

Davidson, E.A., 1991. Fluxes of nitrous oxide and nitric oxide from terrestrial ecosystems. In: Rojers, J.E., Whitman, W.B (Ed.), Microbial Production and Consumption of Greenhouse Gases: Methane, Nitrogen oxides and Halomethanes. American Society for Microbiology, Washington DC, pp. 219-236.

Davidson, E.A., Firestone, M.K., 1988. Measurement of nitrous oxide dissolved in soil solution. Soil Science Society of America Journal, 52, 1201-1203.

Davidson, E.A., Schimel, J.P., 1995. Microbial processes of production and consumption of nitric oxide, nitrous oxide, and methane. In: Matson, P.A., Harriss, R.C. (Eds.), Biogenic Trace Gases: Measuring Emissions from Soil and Water Blackwell Science, New York, pp. 327-357.

Davidson, E.A., Seitzinger, S., 2006. The enigma of progress in denitrification research. Ecological Applications, 16, 2057–2063.

de Klein, C.A.M., Barton, L., Sherlock, R.R., Li, Z., Littlejohn, R.P., 2003. Estimating a nitrous oxide emission factor for animal urine from some New Zealand pastoral soils. Soil Research, 41, 381-399.

Dendooven, L., Anderson, J.M., 1994. Dynamics of reduction enzymes involved in the denitrification process in pasture soil. Soil Biology & Biochemistry, 26, 1501-1506.

Denman, K.L., Brasseur, G., Chidthaisong, A., Ciais, P., Cox, P.M., Dickinson, R.E., Hauglustaine, D., Heinze, C., Holland, E., Jacob, D., Lohmann, U., Ramachandran, S., da Silva Dias, P.L., Wofsy, S.C., Zhang, X., Solomon, S., Qin, D., Manning, M., Chen, Z., Marquis, M., Averyt, K.B., Tignor, M., Miller, H.L., 2007. Couplings between changes in the climate system and biogeochemistry. In: Climate Change 2007: The Physical Science Basis. Contribution of Working Group I to the Fourth Assessment Report of the Intergovernmental Panel on Climate Change. Cambridge University Press, Cambridge, United Kingdom and New York, NY, USA

Di, H.J., Cameron, K.C., Shen, J.P., Winefield, C.S., O'Callaghan, M., Bowatte, S., He, J.Z., 2009. Nitrification driven by bacteria and not archaea in nitrogen-rich grassland soils. Nature Geoscience, 2, 621-624.

Di, H.J., Cameron, K.C., Milne, J., Drewry, J.J., Smith, N.P., Hendry, T., Moore, S., Reijnen, B., 2001. A mechanical hoof for simulating animal treading under controlled conditions. New Zealand Journal of Agricultural Research, 44, 111-116.

Doak, B.W., 1952. Some chemical changes in the nitrogenous constituents of urine when voided on pasture. The Journal of Agricultural Science, 42, 162-171.

Dobbie, K.E., Smith, K.A., 2001. The effects of temperature, water-filled pore space and land use on N_2O emissions from an imperfectly drained gleysol. European Journal of Soil Science, 52, 667-673.

Dobbie, K.E., Smith, K.A., 2006. The effect of water table depth on emissions of N_2O from a grassland soil. Soil Use and Management, 22, 22-28.

Dobbie, K.E., McTaggart, I.P., Smith, K.A., 1999. Nitrous oxide emissions from intensive agricultural systems: Variations between crops and seasons, key driving variables, and mean emission factors. Journal of Geophysical Research, 104, 26891-26899.

Drewry, J.J., Paton, R.J., 2005. Soil physical quality under cattle grazing of a winter-fed brassica crop. Soil Research, 43, 525-531.

Drewry, J.J., Cameron, K.C., Buchan, G.D., 2001. Effect of simulated dairy cow treading on soil physical properties and ryegrass pasture yield. New Zealand Journal of Agricultural Research, 44, 181 - 190.

Farquharson, R., Baldock, J., 2008. Concepts in modelling N_2O emissions from land use. Plant and Soil, 309, 147-167.

Firestone, M.K., 1982. Biological Denitrification. In: Stevenson, F.J. (Ed.), Nitrogen in Agricultural Soils. American society of Agronomy, Inc., Soil Science Society of America, Inc., Madison, WI, USA., pp. 289-326.

Firestone, M.K., Davidson, E.A., 1989. Microbiological basis of NO and N_2O production and consumption in soil. In: Andreae, M.O., Schimel, D.S. (Eds.), Exchange of Trace gases between terrestrial Ecosystems and the Atmosphere. John Wiley & Sons, Chichester, pp. 7-21.

Flury, M., Fluhler, H., 1994. Brilliant blue FCF as a dye tracer for solute transport studies - A toxicological overview. Journal of Environmental Quality, 23, 1108-1112.

Focht, D.D., 1974. The effect of temperature, pH and aeration on the production of nitrous oxide and gaseous nitrogen- A zero-order kinetic model. Soil Science, 118, 173-179.

Forster, P., Ramaswamy,V., P. Artaxo, T. Berntsen, R. Betts, D.W. Fahey, J., Haywood, J.L., D.C. Lowe, G. Myhre, J. Nganga, R.G. Prinn, G., Raga, M.S., and R. Van Dorland, 2007. Changes in atmospheric constituents and in radiative forcing. In: S.Soloman, D.Qin, M.Manning, Z.Che, M.Marquis, K.B. Averyt, M. Tignor, H.L. Miller (Eds.), Climate Change 2007: The Physical Science Basis. Contribution of Working Group I to the Fourth Assessment Report of the Intergovernmental Panel on Climate Change. Cambridge University Press, Cambridge, United Kingdom, pp. 129-234.

Freijer, J.I., 1994. Calibration of jointed tube model for the gas diffusion coefficient in soils. Soil Sci. Soc. Am. J., 58, 1067-1076.

Fujikawa, T., Miyazaki, T., 2005. Effects of bulk density and soil type on the gas diffusion coefficient in repacked and undisturbed soils. Soil Science, 170, 892-901

Galbally, I.E., Roy, C.R., 1983. The fate of nitrogen compounds in the atmosphere. In: Freney, J.R., Simpson, J.R. (Eds.), Gaseous loss of nitrogen from plant-soil systems. Dr. W. Junk, The Hague, The Netherlands, pp. 265-284.

Galloway, J.N., Aber, J.D., Erisman, J.W., Seitzinger, S.P., Howarth, R.W., Cowling, E.B., Cosby, B.J., 2003. The Nitrogen Cascade. BioScience, 53, 341-356.

Ghani, A., Dexter, M., Perrott, K.W., 2003. Hot-water extractable carbon in soils: a sensitive measurement for determining impacts of fertilisation, grazing and cultivation. Soil Biology & Biochemistry, 35, 1231-1243.

Glinski, J., Stahr, K., Stepniewska, Z., Brzezinska, M., 1992. Changes of redox and pH conditions in a flooded soil amended with glucose and nitrate under laboratory conditions. Zeitschrift für Pflanzenernährung und Bodenkunde, 155, 13-17.

Grable, A.R., Siemer, E.G., 1968. Effects of bulk density, aggregate size, and soil water suction on oxygen diffusion, redox potentials, and elongation of corn roots. Soil Sci. Soc. Am. J., 32, 180-186.

Greenwood, K.L., McKenzie, B.M., 2001. Grazing effects on soil physical properties and the consequences for pastures: a review. Australian Journal of Experimental Agriculture, 41, 1231-1250.

Greenwood, K.L., MacLeod, D.A., Hutchinson, K.J., 1997. Long-term stocking rate effects on soil physical properties. Australian Journal of Experimental Agriculture, 37, 413-419.

Hamamoto, S., Moldrup, P., Kawamoto, K., Komatsu, T., 2012. Organic Matter Fraction Dependent Model for Predicting the Gas Diffusion Coefficient in Variably Saturated Soils. Vadose Zone Journal, 11.

Hamamoto, S., Moldrup, P., Kawamoto, K., Wickramarachchi, P., Nagamori, M., Komatsu, T., 2011. Extreme compaction effects on gas transport parameters and estimated climate gas exchange for a landfill final cover soil. Journal of Geotechnical and Geoenvironmental Engineering, 137, 653-662.

Haynes, R.J., 1986. Nitrification. In: Haynes, R.J. (Ed.), Mineral Nitrogen in the Plant-Soil System. Academic Press, Inc., Orlando, FL, pp. 127-165.

Haynes, R.J., Sherlock, R.R., 1986. Gaseous loss of nitrogen. In: Haynes, R. (Ed.), Mineral nitrogen in plant -soil systems. Academic Press Inc., Boca Raton, FL., pp. 242-302.

Haynes, R.J., Williams, P.H., 1992. Changes in soil solution composition and pH in urine-affected areas of pasture. Journal of Soil Science, 43, 323-334.

Haynes, R.J., Williams, P.H., 1993. Nutrient cycling and soil fertility in the grazed pasture ecosystem. Advances in Agronomy, 49, 119-199.

Hewitt, A.E., 1998. New Zealand Soil Classification. Landcare Research Science Series, No.1. 2nd ed. Manaaki Whenua Press, Lincoln, NZ.

Hill, J.N.S., Sumner, M.E., 1967. Effect of bulk density on moisture characteristics of soils. Soil Science, 103, 234-238.

Hillel, D., 1998. Environmental Soil Physics. Academic Press, San Diego, CA.

Hillel, D., 2004. Introduction to Environmental Soil Physics. Academic Press, San Diego.

Houlbrooke, D.J., Paton, R.J., Morton, J.D., Littlejohn, R.P., 2009. Soil quality and plant yield under dryland and irrigated winter forage crops grazed by sheep or cattle. Soil Research, 47, 470-477.

Huang, Y., Zou, J., Zheng, X., Wang, Y., Xu, X., 2004. Nitrous oxide emissions as influenced by amendment of plant residues with different C:N ratios. Soil Biology & Biochemistry, 36, 973-981.

Hutchinson, G.L., Mosier, A.R., 1981. Improved soil cover method for field measurement of nitrous oxide fluxes. Soil Science Society of America Journal, 45, 311-316.

Jambert, C., Delmas, R., Serça, D., Thouron, L., Labroue, L., Delprat, L., 1997. N_2O and CH_4 emissions from fertilized agricultural soils in southwest France. Nutrient Cycling in Agroecosystems, 48, 105-114.

Khan, S., Clough, T.J., Goh, K.M., Sherlock, R.R., 2011. Influence of soil pH on NOx and N_2O emissions from bovine urine applied to soil columns. New Zealand Journal of Agricultural Research, 54, 285-301.

Khdyer, I.I., Cho, C.M., 1983. Nitrification and denitrification of nitrogen fertilizers in a soil column[1]. Soil Sci. Soc. Am. J., 47, 1134-1139.

Klute, A., 1986. Water retention: Laboratory methods. In: Klute, A. (Ed.), Methods of soil analysis: Part I. Physical and mineralogical methods. ASA, Madison, WI

Knowles, R., 1982. Denitrification. Microbiological reviews, 46, 43-70.

Kool, D.M., Hoffland, E., Abrahamse, S., van Groenigen, J.W., 2006. What artificial urine composition is adequate for simulating soil N_2O fluxes and mineral N dynamics? Soil Biology & Biochemistry, 38, 1757-1763.

Kool, D.M., Dolfing, J., Wrage, N., Van Groenigen, J.W., 2011. Nitrifier denitrification as a distinct and significant source of nitrous oxide from soil. Soil Biology & Biochemistry, 43, 174-178.

Koops, J.G., van Beusichem, M.L., Oenema, O., 1997. Nitrous oxide production, its source and distribution in urine patches on grassland on peat soil. Plant and Soil, 191, 57-65.

Kremen, A., Bear, J., Shavit, U., Shaviv, A., 2005. Model demonstrating the potential for coupled nitrification denitrification in soil aggregates. Environmental Science & Technology, 39, 4180-4188.

Kuai, L., Verstraete, W., 1998. Ammonium removal by the oxygen-limited autotrophic nitrification-denitrification system. Applied and Environmental Microbiology, 64, 4500-4506.

Lange, S.F., Allaire, S.E., Rolston, D.E., 2009. Soil-gas diffusivity in large soil monoliths. European Journal of Soil Science, 60, 1065-1077.

Langlands, J.P., Bennett, I.L., 1973. Stocking intensity and pastoral production: I. Changes in the soil and vegetation of a sown pasture grazed by sheep at different stocking rates. The Journal of Agricultural Science, 81, 193-204.

Ledgard, S.F., Sprosen, M.S., Brier, G.J., Nemaia, E.K.K., Clark, D.A., 1996. Nitrogen inputs and losses from New Zealand dairy farmlets, as affected by nitrogen fertilizer application: year one. Plant and Soil, 181, 65-69.

Leininger, S., Urich, T., Schloter, M., Schwark, L., Qi, J., Nicol, G.W., Prosser, J.I., Schuster, S.C., Schleper, C., 2006. Archaea predominate among ammonia-oxidizing prokaryotes in soils. Nature, 442, 806-809.

Letey, J., Jury, W.A., Hadas, A., Valoras, N., 1980. Gas diffusion as a factor in laboratory incubation studies on denitrification. Journal of Environmental Quality, 9, 223-227.

Linn, D.M., Doran, J.W., 1984. Effect of water-filled pore space on carbon dioxide and nitrous oxide production in tilled and nontilled soils. Soil Science Society of America Journal, 48, 1267-1272.

Luo, J., Tillman, R.W., Ball, P.R., 1999. Factors regulating denitrification in a soil under pasture. Soil Biology & Biochemistry, 31, 913-927.

Luxmoore, R., 1981. Micro-, meso-, and macroporosity of soil. Soil Science Society of America Journal, 45, 671-672.

Mahmood, T., Ali, R., Malik, K.A., Shamsi, S.R.A., 1997. Denitrification with and without maize plants (*Zea mays L.*) under irrigated field conditions. Biology and Fertility of Soils, 24, 323-328.

Malhi, S.S., McGill, W.B., 1982. Nitrification in three Alberta soils: Effect of temperature, moisture and substrate concentration. Soil Biology & Biochemistry, 14, 393-399.
Marshall, T.J., 1959. The diffusion of gases through porous media. Journal of Soil Science, 10, 79-82.
McTaggart, I.P., Akiyama, H., Tsuruta, H., Ball, B.C., 2002. Influence of soil physical properties, fertiliser type and moisture tension on N_2O and NO emissions from nearly saturated Japanese upland soils. Nutrient Cycling in Agroecosystems, 63, 207-217.
Menneer, J.C., Ledgard, S.F., McLay, C.D.A., Silvester, W.B., 2005a. The effects of treading by dairy cows during wet soil conditions on white clover productivity, growth and morphology in a white clover-perennial ryegrass pasture. Grass and Forage Science, 60, 46-58.
Menneer, J.C., Ledgard, S., McLay, C., Silvester, W., 2005b. Animal treading stimulates denitrification in soil under pasture. Soil Biology & Biochemistry, 37, 1625-1629.
Miller, C., Yesiller, N., Yaldo, K., Merayyan, S., 2002. Impact of Soil Type and Compaction Conditions on Soil Water Characteristic. Journal of Geotechnical and Geoenvironmental Engineering, 128, 733-742.
Millington, R.J., Quirk, J.P., 1961. Permeability of porous solids. Transactions of the Faraday Society, 57, 1200-1207.
Ministry for the Environment New Zealand, 2012. New Zealand's Greenhouse Gas Inventory 1990-2010. Wellington, New Zealand: Ministry for the Environment New Zealand.
Moldrup, P., Kruse, C.W., Rolston, D.E., Yamaguchi, T., 1996. Modeling diffusion and reaction in soils: III. predicting gas diffusivity from the Campbell soil-water retention model. Soil Science, 161, 366-375.
Moldrup, P., Olesen, T., Yamaguchi, T., Schjønning, P., Rolston, D.E., 1999. Modeling diffusion and reaction in soils: IX. the Buckingham-Burdine-Campbell equation for gas diffusivity in undisturbed soil. Soil Science, 164, 542-551.
Moldrup, P., Olesen, T., Schjønning, P., Yamaguchi, T., Rolston, D.E., 2000a. Predicting the gas diffusion coefficient in undisturbed soil from soil water characteristics. Soil Science Society of America Journal, 64, 94-100.
Moldrup, P., Olesen, T., Yoshikawa, S., Komatsu, T., Rolston, D.E., 2004. Three-porosity model for predicting the gas diffusion coefficient in undisturbed soil. Soil Science Society of America Journal, 68, 750-759.
Moldrup, P., Olesen, T., Gamst, J., Schjønning, P., Yamaguchi, T., Rolston, D.E., 2000b. Predicting the gas diffusion coefficient in repacked soil water-induced linear reduction model. Soil Science Society of America Journal, 64, 1588-1594.
Moldrup, P., Olesen, T., Yoshikawa, S., Komatsu, T., McDonald, A.M., Rolston, D.E., 2005. Predictive-descriptive models for gas and solute diffusion coefficients in variably saturated porous media coupled to pore-size distribution: III. inactive pore space interpretations of gas diffusivity. Soil Science, 170, 867-880
Monaghan, R., Barraclough, D., 1992. Some chemical and physical factors affecting the rate and dynamics of nitrification in urine-affected soil. Plant and Soil, 143, 11-18.
Monaghan, R.M., Barraclough, D., 1993. Nitrous oxide and dinitrogen emissions from urine-affected soil under controlled conditions. Plant and Soil, 151, 127-138.
Mulholland, B., Fullen, M.A., 1991. Cattle trampling and soil compaction on loamy sands. Soil Use and Management, 7, 189-193.
Müller, C., Stevens, R.J., Laughlin, R.J., Jäger, H.J., 2004. Microbial processes and the site of N_2O production in a temperate grassland soil. Soil Biology & Biochemistry, 36, 453-461.
Mulvaney, R.L., Boast, C.W., 1986. Equations for determination of nitrogen-15 labelled dinitrogen and nitrous oxide by mass spectrometry. Soil Science Society of America Journal, 50, 360-363.
Murray, P.J., Hatch, D.J., Dixon, E.R., Stevens, R.J., Laughlin, R.J., Jarvis, S.C., 2004. Denitrification potential in a grassland subsoil: effect of carbon substrates. Soil Biology & Biochemistry, 36, 545-547.
Murray, R.E., Knowles, R., 2003. Production of NO and N_2O in the presence and absence of C_2H_2 by soil slurries and batch cultures of denitrifying bacteria. Soil Biology & Biochemistry, 35, 1115-1122.

Nelson, D.W., 1982. Gaseous losses of nitrogen other than through denitrification. In: Stevenson, F.J. (Ed.), Nitrogen in Agricultural soils. Agronomy., pp. 327-363.
Nelson, D.W., Bremner, J.M., 1970. Role of soil minerals and metallic cations in nitrite decomposition and chemodenitrification in soils. Soil Biology & Biochemistry, 2, 1-8.
Oenema, O., Velthof, G.L., Yamulki, S., Jarvis, S.C., 1997. Nitrous oxide emissions from grazed grassland. Soil Use and Management, 13, 288-295.
Oenema, O., Wrage, N., Velthof, G., Groenigen, J.W., Dolfing, J., Kuikman, P., 2005. Trends in global nitrous oxide emissions from animal production systems. Nutrient Cycling in Agroecosystems, 72, 51-65.
Park, S., Bae, W., Chung, J., Baek, S.-C., 2007. Empirical model of the pH dependence of the maximum specific nitrification rate. Process Biochemistry, 42, 1671-1676.
Penman, H.L., 1940. Gas and vapour movements in the soil: I. The diffusion of vapours through porous solids. The Journal of Agricultural Science, 30, 437-462.
Petersen, S.O., Schjønning, P., Thomsen, I.K., Christensen, B.T., 2008. Nitrous oxide evolution from structurally intact soil as influenced by tillage and soil water content. Soil Biology & Biochemistry, 40, 967-977.
Pilot, L.U.C., Patrick, W.H.J., 1972. Nitrate reduction in soils: effect of soil moisture tension. Soil Science, 114, 312-316.
Poth, M., Focht, D.D., 1985. ^{15}N kinetic analysis of N_2O production by *Nitrosomonas europaea*: an examination of nitrifier denitrification. Applied and Environmental Microbiology, 49, 1134-1141.
Rafique, R., Hennessy, D., Kiely, G., 2011. Nitrous oxide emission from grazed grassland under different management systems. Ecosystems, 14, 563-582.
Ravishankara, A.R., Daniel, J.S., Portmann, R.W., 2009. Nitrous Oxide (N_2O): The dominant ozone-depleting substance emitted in the 21st century. Science, 326, 123-125.
Resurreccion, A.C., Moldrup, P., Kawamoto, K., Yoshikawa, S., Rolston, D.E., Komatsu, T., 2008. Variable pore connectivity factor model for gas diffusivity in unsaturated, aggregated Soil. Vadose Zone Journal, 7, 397-405.
Reuss, J.O., Smith, R.L., 1965. Chemical Reactions of Nitrites in Acid Soils. Soil Science Society of America Journal, 29, 267-270.
Richard, G., Cousin, I., Sillon, J.F., Bruand, A., Guérif, J., 2001. Effect of compaction on the porosity of a silty soil: influence on unsaturated hydraulic properties. European Journal of Soil Science, 52, 49-58.
Robertson, G.P., Tiedje, J.M., 1987. Nitrous oxide sources in aerobic soils: Nitrification, denitrification and other biological processes. Soil Biology & Biochemistry, 19, 187-193.
Rolston , D.E., 1986. Gas diffusivity. In: Klute, A. (Ed.), Methods of soil analysis, Part 1. Physical and Mineralogical Methods - Agrononomy Monograph no.9 (2nd Edition). Agronomy society of America, Madison, WI, pp. 1089-1102.
Rolston, D.E., Moldrup, P., 2002. Gas diffusivity. In: Topp, G.C., Dane, J.H. (Eds.), Methods of Soil Analysis, Part 4, Physical methods. Soil Science Society of America, Madison, WI, pp. 1113-1139.
Rolston, D.E., Hoffman, D.L., Toy, D.W., 1978. Field Measurement of Denitrification: I. Flux of N_2 and N_2O. Soil Sci. Soc. Am. J., 42, 863-869.
Rudaz, A.O., Wälti, E., Kyburz, G., Lehmann, P., Fuhrer, J., 1999. Temporal variation in N_2O and N_2 fluxes from a permanent pasture in Switzerland in relation to management, soil water content and soil temperature. Agriculture, Ecosystems & Environment, 73, 83-91.
Ruehlmann, J., Körschens, M., 2009. Calculating the effect of soil organic matter concentration on soil bulk density. Soil Science Society of America Journal, 73, 876-885.
Ruser, R., Flessa, H., Russow, R., Schmidt, G., Buegger, F., Munch, J.C., 2006. Emission of N_2O, N_2 and CO_2 from soil fertilized with nitrate: effect of compaction, soil moisture and rewetting. Soil Biology & Biochemistry, 38, 263-274.
Russow, R., Stange, C.F., Neue, H.U., 2009. Role of nitrite and nitric oxide in the processes of nitrification and denitrification in soil: Results from ^{15}N tracer experiments. Soil Biology & Biochemistry, 41, 785-795.

Ryden, J.C., 1982. Effects of acetylene on nitrification and denitrification in two soils during incubation with ammonium nitrate. Journal of Soil Science, 33, 263-270.
Ryden, J.C., 1983. Denitrification loss from a grassland soil in the field receiving different rates of nitrogen as ammonium nitrate. Journal of Soil Science, 34, 355-365.
Schjønning, P., Thomsen, I.K., Moldrup, P., Christensen, B.T., 2003. Linking Soil Microbial Activity to Water- and Air-Phase Contents and Diffusivities. Soil Science Society of America Journal, 67, 156-165.
Schjønning, P., Thomsen, I.K., Petersen, S.O., Kristensen, K., Christensen, B.T., 2011. Relating soil microbial activity to water content and tillage-induced differences in soil structure. Geoderma, 163, 256-264.
Schmidt, E.L., 1982. Nitrification in soil. In: Stevenson, F.J. (Ed.), Nitrogen in agricultural soils. Agron. Monogr. 22. ASA, Madison, WI., pp. 253-288.
Scott, H.D., 2000. Soil Physics: Agriculture and Environmental Applications. Iowa State University Press., Ames, Iowa
Shand, C.A., Williams, B.L., Smith, S., Young, M.E., 2000. Temporal changes in C, P and N concentrations in soil solution following application of synthetic sheep urine to a soil under grass. Plant and Soil, 222, 1-13.
Shand, C.A., Williams, B.L., Dawson, L.A., Smith, S., Young, M.E., 2002. Sheep urine affects soil solution nutrient composition and roots: differences between field and sward box soils and the effects of synthetic and natural sheep urine. Soil Biology & Biochemistry, 34, 163-171.
Sherlock, R.R., 1984. Ammonia volatilisation and nitrous oxide production from urine patches in grazed pastures. Ph.D. Thesis, Department of Soil Science. Lincoln University, Christchurch, New Zealand
Sherlock, R.R., Goh, K.M., 1984. Dynamics of ammonia volatilization from simulated urine patches and aqueous urea applied to pasture I. Field experiments. Nutrient Cycling in Agroecosystems, 5, 181-195.
Shestak, C.J., Busse, M.D., 2005. Compaction alters physical but not biological indices of soil health. Soil Sci. Soc. Am. J., 69, 236-246.
Simek, M., Jisova, L., Hopkins, D.W., 2002. What is the so-called optimum pH for denitrification in soil? Soil Biology & Biochemistry, 34, 1227-1234.
Simpson, J.R., Steele, K.W., 1983. Gaseous nitrogen exchange in grazed pastures. In: Freney, J.R., Simpson, J.R. (Eds.), Gaseous losses of Nitrogen from Plant-Soil Systems. Nijhoff, The Hague, pp. 215-236.
Singleton, P.L., Addison, B., 1999. Effects of cattle treading on physical properties of three soils used for dairy farming in the Waikato, North Island, New Zealand. Soil Research, 37, 891-902.
Sitaula, B.K., Hansen, S., Sitaula, J.I.B., Bakken, L.R., 2000. Effects of soil compaction on N_2O emission in agricultural soil. Chemosphere - Global Change Science, 2, 367-371.
Smith, C.J., Chalk, P.M., 1980. Fixation and loss of nitrogen during transformations of nitrite in soils. Soil Science Society of America Journal, 44, 288-291.
Smith, K.A., Thomson, P.E., Clayton, H., McTaggart, I.P., Conen, F., 1998. Effects of temperature, water content and nitrogen fertilisation on emissions of nitrous oxide by soils. Atmospheric Environment, 32, 3301-3309.
Smith, K.A., Ball, T., Conen, F., Dobbie, K.E., Massheder, J., Rey, A., 2003. Exchange of greenhouse gases between soil and atmosphere: interactions of soil physical factors and biological processes. European Journal of Soil Science, 54, 779-791.
Smith, M.S., Tiedje, J.M., 1979. Phases of denitrification following oxygen depletion in soil. Soil Biology & Biochemistry, 11, 261-267.
Sommer, R., Stöckle, C., 2010. Correspondence between the Campbell and van Genuchten soil-water-retention models. Journal of Irrigation and Drainage Engineering, 136, 559-562.
Stepniewski, W., 1981. Oxygen diffusion and the strength as related to soil compaction. II Oxygen diffusion coefficient. Polish Journal of Soil Science, 14, 3-13.
Stevens, R.J., Laughlin, R.J., 1998. Measurement of nitrous oxide and di-nitrogen emissions from agricultural soils. Nutrient Cycling in Agroecosystems, 52, 131-139.

Stevens, R.J., Laughlin, R.J., Malone, J.P., 1998. Soil pH affects the processes reducing nitrate to nitrous oxide and di-nitrogen. Soil Biology & Biochemistry, 30, 1119-1126.
Suzuki, I., Dular, U., Kwok, S.C., 1974. Ammonia or ammonium ion as substrate for oxidation by nitrosomonas europaea cells and extracts. Journal of Bacteriology, 120, 556-558.
Taylor, S.A., 1949. Oxygen diffusion in porous media as a measure of soil aeration. Proceedings. Soil Science Society of America, 14, 55-61.
Thomas, S., Beare, M., Francis, G., Barlow, H., Hedderley, D., 2008. Effects of tillage, simulated cattle grazing and soil moisture on N_2O emissions from a winter forage crop. Plant and Soil, 309, 131-145.
Tiedje, J., 1988. Ecology of denitrification and dissimilatory nitrate reduction to ammonium. In: Zehnder, A.J.B. (Ed.), Biology of Anaerobic Microorganisms, Wiley, New York, pp. 179-244.
Tiedje, J., Simkins, S., Groffman, P., 1989. Perspectives on measurement of denitrification in the field including recommended protocols for acetylene based methods. Plant and Soil, 115, 261-284.
Torbert, H.A., Wood, C.W., 1992. Effects of soil compaction and water-filled pore space on soil microbial activity and N losses. Communications in Soil Science and Plant Analysis 23, 1321-1331.
Troeh, F.R., Jabro, J.D., Kirkham, D., 1982. Gaseous diffusion equations for porous materials. Geoderma, 27, 239-253.
Uchida, Y., Clough, T.J., Kelliher, F.M., Sherlock, R.R., 2008. Effects of aggregate size, soil compaction, and bovine urine on N_2O emissions from a pasture soil. Soil Biology & Biochemistry, 40, 924-931.
van Cleemput, O., 1998. Subsoils: chemo-and biological denitrification, N_2O and N_2 emissions. Nutrient Cycling in Agroecosystems, 52, 187-194.
Van Cleemput, O., Patrick Jr, W.H., 1974. Nitrate and nitrite reduction in flooded gamma-irradiated soil under controlled pH and redox potential conditions. Soil Biology and Biochemistry, 6, 85-88.
Van Cleemput, O., Samater, A.H., 1995. Nitrite in soils: accumulation and role in the formation of gaseous N compounds. Nutrient Cycling in Agroecosystems, 45, 81-89.
van der Weerden, T.J., Kelliher, F.M., de Klein, C.A.M., 2012. Influence of pore size distribution and soil water content on nitrous oxide emissions. Soil Research, 50, 125-135.
van Genuchten, M.T., 1980. A closed-form equation for predicting the hydraulic conductivity of unsaturated soils. Soil Science Society of America Journal, 44, 892-898.
van Groenigen, J.W., Kuikman, P.J., de Groot, W.J.M., Velthof, G.L., 2005. Nitrous oxide emission from urine-treated soil as influenced by urine composition and soil physical conditions. Soil Biology & Biochemistry, 37, 463-473.
Van Slyke, D.D., 1911. A method for quantitative determination of aliphatic amino groups. Applications to the study of proteolysis and proteolytic products. Journal of Biological Chemistry ASBMB, 185-205.
Veldkamp, E., Keller, M., Nuñez, M., 1998. Effects of pasture management on N_2O and NO emissions from soils in the humid tropics of Costa Rica. Global Biogeochem. Cycles, 12, 71-79.
Venterea, R.T., 2007. Nitrite-driven nitrous oxide production under aerobic soil conditions: kinetics and biochemical controls. Global Change Biology, 13, 1798-1809.
Venterea, R.T., Rolston, D.E., 2000. Mechanisms and kinetics of nitric and nitrous oxide production during nitrification in agricultural soil. Global Change Biology, 6, 303-316.
Vilain, G., Garnier, J., Tallec, G., Cellier, P., 2010. Effect of slope position and land use on nitrous oxide (N_2O) emissions (Seine Basin, France). Agricultural and Forest Meteorology, 150, 1192-1202.
Villaverde, S., García-Encina, P.A., Fdz-Polanco, F., 1997. Influence of pH over nitrifying biofilm activity in submerged biofilters. Water Research, 31, 1180-1186.
Walczak, R., Rovdan, E., Witkowska-Walczak, B., 2002. Water retention characteristics of peat and sand mixtures. Int. Agrophysics, 16, 161-165.
Webster, F.A., Hopkins, D.W., 1996. Contributions from different microbial processes to N_2O emission from soil under different moisture regimes. Biology and Fertility of Soils, 22, 331-335.

Weier, K.L., Doran, J.W., Power, J.F., Walters, D.T., 1993. Denitrification and the dinitrogen/nitrous oxide ratio as affected by soil water, available carbon, and nitrate. Soil Science Society of America Journal, 57, 66-72.

Williams, D.L., Ineson, P., Coward, P.A., 1999. Temporal variations in nitrous oxide fluxes from urine-affected grassland. Soil Biology & Biochemistry, 31, 779-788.

Wrage, N., Velthof, G.L., van Beusichem, M.L., Oenema, O., 2001. Role of nitrifier denitrification in the production of nitrous oxide. Soil Biology & Biochemistry, 33, 1723-1732.

Wrage, N., Groenigen, J.W.v., Oenema, O., Baggs, E.M., 2005. A novel dual-isotope labelling method for distinguishing between soil sources of N_2O. Rapid Communications in Mass Spectrometry, 19, 3298-3306.

Xu, X., Nieber, J.L., Gupta, S.C., 1992. Compaction effect on the gas diffusion coefficient in soils. Soil Science Society of America Journal, 56, 1743-1750.

Yamulki, S., Jarvis, S.C., Owen, P., 1998. Nitrous oxide emissions from excreta applied in a simulated grazing pattern. Soil Biology & Biochemistry, 30, 491-500.

Zumft, W.G., 1997. Cell biology and molecular basis of denitrification. Microbiology and Molecular Biology Reviews, 61, 533-616.